Theory of Diffraction and Scattering from Periodic Surfaces with Binary Fluctuations

Kazuhiro Hattori

March 2008

Graduate School of Engineering and Design

Kyoto Institute of Technology

Acknowlegdment

I wish to express herewith my appreciation to many people for their contribution on this dissertation. I am grateful beyond words to my family for their support and encouragement over many years.

My sincere gratitude goes to Professor Junichi Nakayama for his invaluable guidance, continuous encouragement and generous support throughout my doctoral work.

I would like to thank Professor Masahiro Akiyama, Professor Hisamitsu Endo and Professor Nobuyuki Nakamori for their helpful comments and suggestions for the thesis.

I am very grateful to Dr. Yasuhiko Tamura for his effective advices, fruitful discussions and comments. Special gratitude is expressed to Dr. Lan Gao for many comments. My appreciation extends to each member of Nakayama Laboratory at Kyoto Institute of Technology for his/her favorable support. I am especially grateful to Mr. Hiroshi Matsuoka for his approval of using the collaborating work to accomplish this dissertation.

Also, I would like to thank the Radiation Science Society of Japan for the research subsidies.

Finally, special thanks are extended to Mayekawa MFG. Co.,Ltd. and the members of the Research and Development Center for their generous support and understanding.

Contents

Chapter 1

Introduction

In electronics, there are several devices with periodic structure such as metal parallel lines on the integrated circuits and LCD(liquid crystal displays) electrodes. However, such periodic structure often has defects due to inaccurate fabrications. Therefore, measurement and inspection of defects are essential to control manufacturing processes. To develop a real-time non-destructive measurement, optical methods making use of the scattering from defects are important. These periodic structures of electronic devices mentioned above can be modelled as rectangular grooves formed on the surface and defects where grooves are not formed. However, there has not been studied the scattering from a periodic structure with defects. From a standpoint of analysis, a single groove or a finite number of grooves can be considered as a finite number of scatterers. Further, a periodic structure has an infinite number of scatterers, however, diffraction from a periodic structure results in a problem of a single scatterer by use of describing the wavefield in the Floquet form of solution. Thus, numerical analysis is available as a single scattering problem. On the other hand, when there are defects in periodic structure, it is necessary to take an infinite number of scatterers into account. Due to this aspect, numerical approaches may have difficulties. Therefore, this thesis proposes a new theory of analysis on diffraction and scattering from a periodic surface with defects.

On another front, recent digital recording devices, such as CD (compact discs) and DVD (digital versatile discs), have been widely used. Such devices store binary random data by periodically located surface deformations, which can be modelled as periodic surfaces with binary fluctuations. Since such a binary random surface is manufactured by known binary data, its surface profile is known, while it is difficult to know statistical properties of natural random surfaces exactly. Such manufactured periodic random surfaces may be used as a 'standard scatterer' with known statistical properties of fluctuations. Thus, analysis of diffraction and scattering from such binary periodic random surfaces has been an important subject. They are theoretically interesting because the diffraction due to the periodicity, the incoherent scattering due to the fluctuation and the interaction between such diffraction and scattering may occur. Also, because of binary fluctuations, the properties of the scattering may differ from the Gaussian fluctuation case. Moreover, it is necessary to study such optical properties of such binary periodic random surfaces for higher density storage on recording devices. There have been some works on diffraction and scattering from periodic random surfaces [1–8], however, only a few studies on such binary fluctuations of periodic random surfaces have been carried out by a single scattering approximation. Thus, this thesis proposes a theoretical approach involving effects of multiple scattering.

Under these circumstances, this thesis theoretically studies diffraction and scattering from

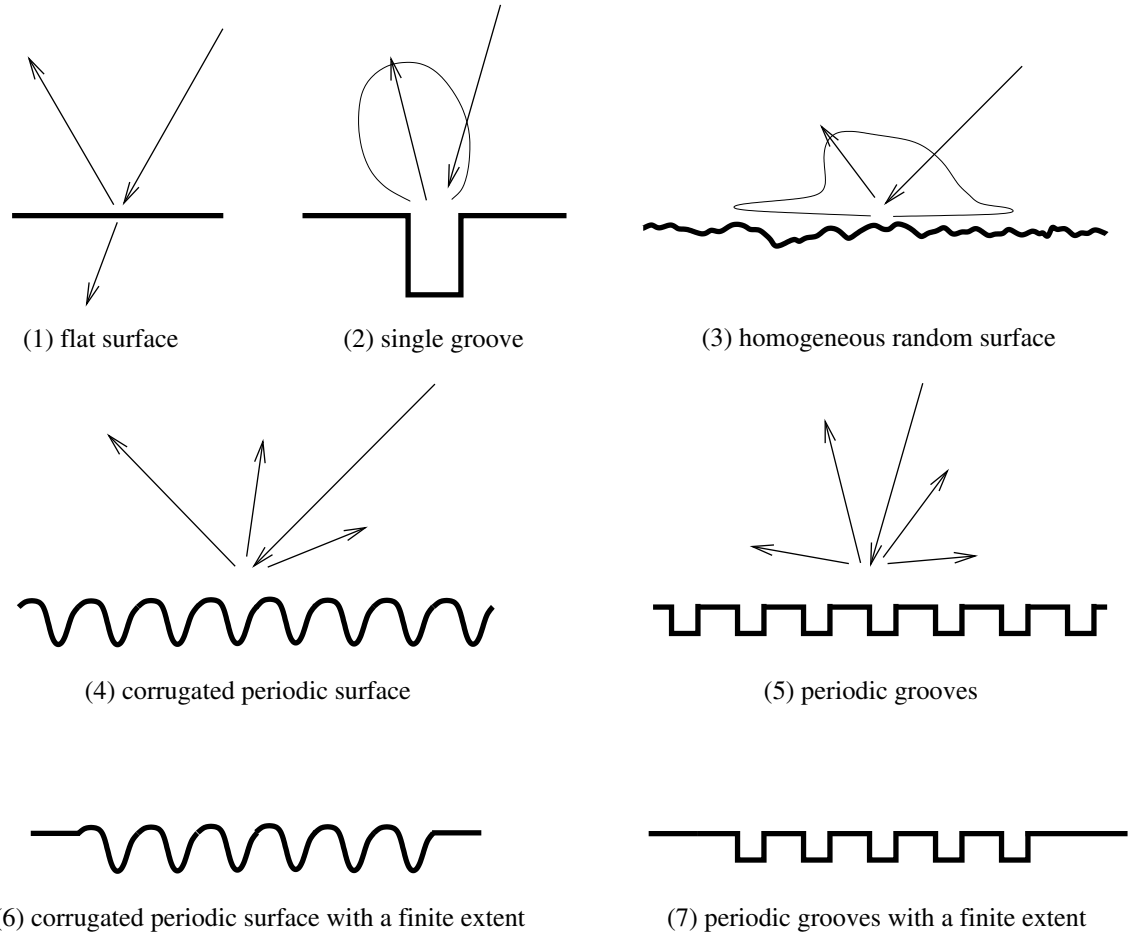

Figure 1.1 Types of surfaces: (1) flat surface, (2) single groove, (3) homogeneous random surface, (4) corrugated periodic surface, (5) periodic grooves, (6) corrugated periodic surface with a finite extent, (7) periodic grooves with a finite extent.

periodic surfaces with binary fluctuations aiming at developing methods of optical measurement and inspection of defects in the periodic structure. We study two types of binary fluctuations: one is the case of single defect in the perfectly periodic array of rectangular grooves. This can be considered as the simplest case of defects in the periodic structure. We discuss it from a standpoint of the electromagnetic theory. The other is the case of binary fluctuations on the height parameter, that is, a boss and pit appear randomly with equal probability. To clarify effects of these binary fluctuations on the optical properties of the diffraction and scattering, we treat two-dimensional problems and take a plane wave incidence. Then, several numerical results of these problems are described and illustrated in figures.

1.1 Diffraction and scattering by rough surfaces: A brief review

In this section, we briefly review the preceding studies on wave diffraction and scattering from rough surfaces. Some types of rough surfaces are drawn in Figure 1.1.

When a plane wave is incident on a flat surface or a flat boundary between two media, reflection and refraction take place following the law of reflection and Snell's law(See Figure 1.1(1)). When the surface is perfectly conductive and flat, only the specular reflection takes

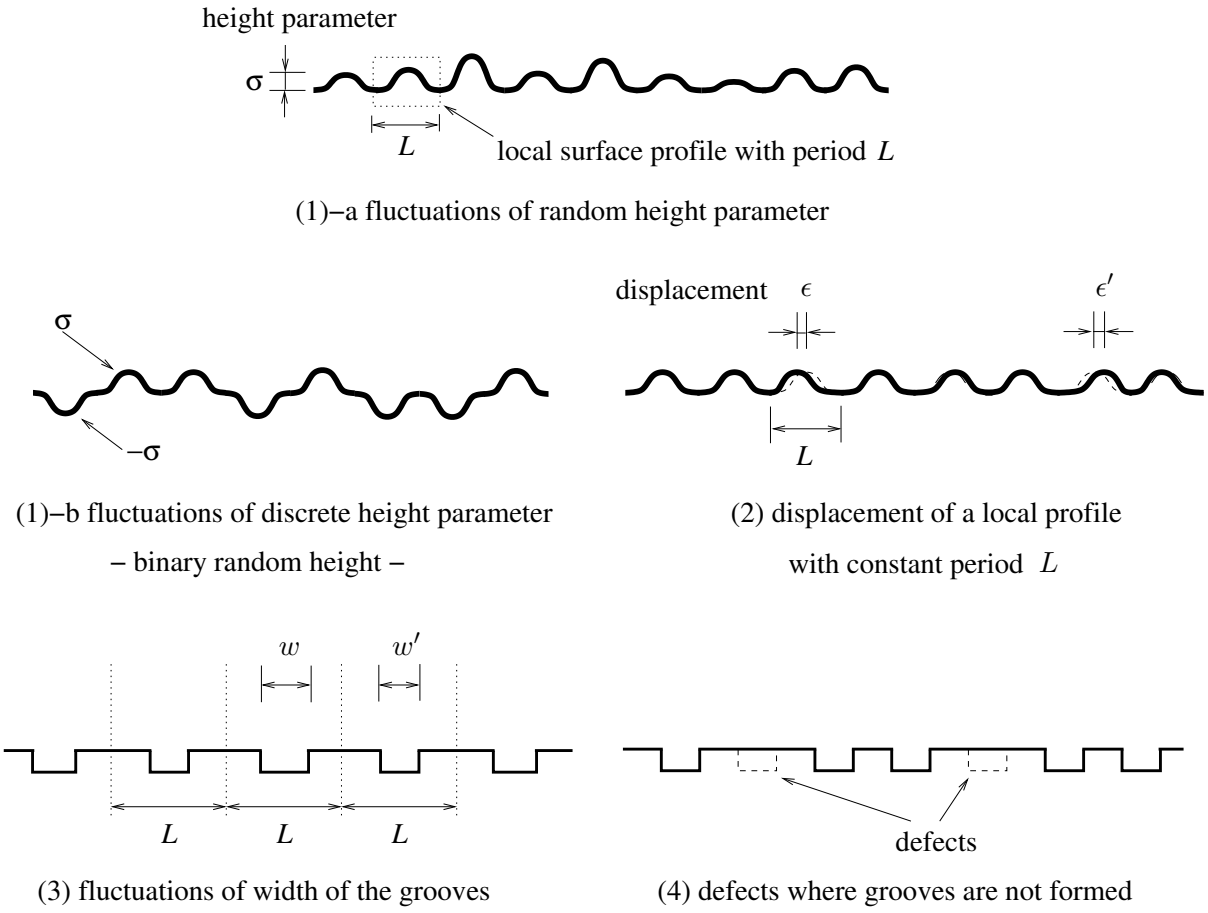

Figure 1.2 Types of fluctuations of periodic surfaces: (1)-a fluctuations of random height parameter, (1)-b fluctuations of discrete height parameter (binary random height), (2) fluctuations of period of the surface, (3) fluctuations of width of the groove, (4) defects where gooves are not formed.

place. If a single groove is formed on the flat surface, the groove generates scattering to all directions(See Figure 1.1(2)). Such a scattering has been analyzed by several authors [9–12] for estimation of crack depth and other aims. There are also works on scattering from a finite number of rectangular grooves [13, 14].

On the other hand, scattering from homogeneous random surfaces(See Figure 1.1(3)) has been studied by many authors, since sea and land surfaces are randomly rough. For analysis, the Kirchhoff approximation, the perturbation method, the multiple scattering approach among others [15–18] have been developed. Ogura and Nakayama developed a probabilistic method called the stochastic functional approach [19–25], in which the scattered wave is assumed to be a functional of a random surface.

As another type of rough surface, however, periodic surfaces have attracted interests of the researchers [27–34], because periodic surfaces work as diffraction gratings. When a corrugation of surface appears repeatedly(See Figure 1.1(4)) or grooves are formed with an equal interval(See Figure 1.1(5)), such surfaces can be assumed to have periodicity. We may call such deformation of the surface for one period 'a local profile'. From such a periodic surface, the incident wave may be

diffracted into discrete directions. Further, Nakayama *et al.* have been studied periodic surfaces with a finite extent (See Figure 1.1(6) and (7)) by use of periodic Fourier transform [35–42], and an expression of the scattered wavefield from such surfaces with a finite extent is obtained. Due to the finite extension of the local surface profile, the incident wave is scattered to all directions, however, the scattered wave becomes strong into the directions of diffraction with the period as the extension of the local profile spreads.

These types of rough surfaces mentioned above have been extensively studied. Actually, real periodic surfaces are not ideal and imperfect, and there often have fluctuations due to inaccurate manufacturing or varying conditions in manufacturing processes. Thus, it becomes necessary to study diffraction and scattering from such periodic surfaces with fluctuations, however, there has not been many works on analysis of diffraction and scattering from periodic surfaces with fluctuations.

Fluctuations of the periodic surfaces could be classified into several types:

(1) height or depth of the local profile
  a. fluctuations of random height parameter
  b. fluctuations of discrete height parameter such as binary random height
(2) displacement of a local profile
(3) width of the groove or boss
(4) defect where a local profile is not formed

among others. These types are illustrated in Figure 1.2. Studies on fluctuations of random height parameter of the surface, (1)-a in Figure 1.2, have been reported in the case of Gaussian random fluctuations by J.Nakayama and L.Gao [7,8], and those on fluctuations of displacement of a local profile, (2) in Figure 1.2, for a volume disorder (dislocations of periodically located many particles in a dielectric medium) by M.Tateiba [43]. However, there are few works on binary fluctuations in the height parameter and studies on defects in the periodic structure have been accomplished.

A periodic random surface with binary random height, (1)-b in Figure 1.2, has binary fluctuations, which we call a binary periodic random surface. We assume that a binary periodic random surface is generated by a stationary binary sequence and obtain the wavefield from such a periodic random surface by use of a probabilistic approach. From a viewpoint of analysis, it is essentially important to distinguish the cases whether the ensemble average of the periodic random surface is periodic or becomes flat with zero average. A binary periodic random surface was first studied by Gao *et al.* [44], however, the discussion was limited to the case where the ensemble average of the periodic random surface is periodic and to the TE incidence. When the average surface is flat, the first-order scattered wave diverges unphysically for the TM incidence, if multiple scattering effects are not taken into account [44]. This thesis overcomes this divergence problem, and the representation of the wavefield for the TM incidence.

Among these types of fluctuations, defects in the periodic structure, (4) in Figure 1.2, could be also considered as a type of binary fluctuations, because a local profile is not formed at the positions of the defect. From a standpoint of electromagnetic theory, it is a new problem to obtain an representation of the scattered wavefield due to the defect. In this thesis, we study a deterministic case of single defect in the periodic array of rectangular grooves, of which position is known. It can be considered as the simplest case of defects in the periodic structure.

In this thesis, we will study these two types of binary fluctuations in the periodic structure.

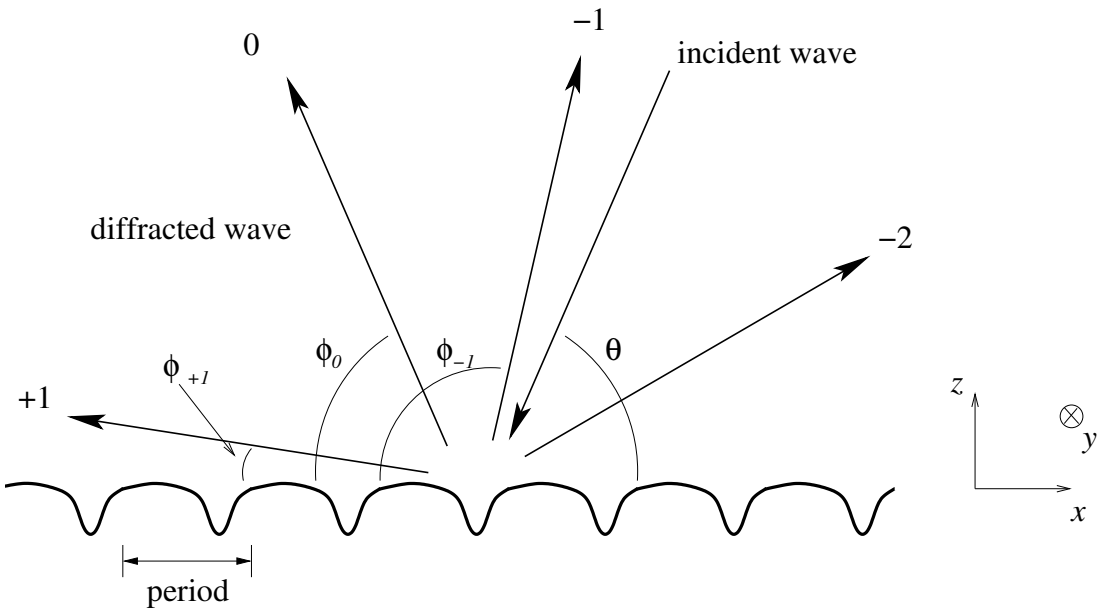

Figure 1.3 Diffraction from a periodic surface with the period L. The incident wave the angle of incidence θ is diffracted into discrete directions ϕ_n ($n = 0, \pm1, \pm2, \cdots$), which is determined by wavelength and the period.

1.1.1 Diffraction by perfectly periodic structure

In this thesis, we consider two-dimensional problems, where the geometry and wavefield are uniform in the y direction. In the two-dimensional cases, incident waves can be decomposed into two plane waves: a transverse electric wave (TE plane wave), the electric field with only the y component, and a transverse magnetic wave (TM plane wave), the magnetic field with only the y component. When a wavefield in free space is a function of x and z and constant in the y direction, the Maxwell equations, which the wavefield satisfies, are separated into two sets:

$$\text{TE}: \begin{cases} \left[\dfrac{\partial^2}{\partial x^2}+\dfrac{\partial^2}{\partial z^2}+k^2\right] E_y(x,z) = 0, \\ \dfrac{\partial}{\partial y} E_y(x,z) = 0, \end{cases} \qquad \text{TM}: \begin{cases} \left[\dfrac{\partial^2}{\partial x^2}+\dfrac{\partial^2}{\partial z^2}+k^2\right] H_y(x,z) = 0, \\ \dfrac{\partial}{\partial y} H_y(x,z) = 0, \end{cases} \tag{1.1}$$

where E_y and H_y denotes the y component of the electric and magnetic fields, and k is wavenumber in free space. On the perfectly conductive surface $z = f(x)$, TE and TM plane waves satisfies Dirichlet and Neumann conditions because the electric field vanishes on the surface:

$$\text{TE}: \ E_y(x,z)\Big|_{z=f(x)} = 0, \qquad \text{TE}: \ \frac{\partial}{\partial n} H_y(x,z)\Big|_{z=f(x)} = 0, \tag{1.2}$$

where n is the normal to the surface.

When the surface has perfectly periodic structure [†] such as a periodically corrugated surface (see Figure 1.3), the incident plane wave $e^{ipx}e^{-i\beta_0(p)z}$ may be diffracted into discrete directions

[†]Since we consider a periodic surface with single defect or with binary fluctuations on the height parameter of such a local profile in what follows, we utilize the word 'perfectly periodic' for the classical periodic surfaces without fluctuations even though the word 'periodic' implies periodicity without any fluctuation.

and the total wavefield $\Psi(x,z)$ can be considered to have the well known Floquet form

$$\Psi(x,z) = e^{ipx}\left[e^{-i\beta_0(p)z} + \sum_{n=-\infty}^{\infty} A_n(p)e^{ink_Lx+i\beta_n(p)z}\right], \tag{1.3}$$

$$p = -k\cos\theta, \quad k_L = \frac{2\pi}{L}, \quad \beta_n(p) = \sqrt{k^2-(p+nk_L)^2}, \tag{1.4}$$

where the second term of the right-hand side in (1.3) is a sum of the diffracted waves with the diffraction amplitude $A_n(p)$, which are diffracted into discrete directions of the grating orders [30] as

$$\phi_n = \cos^{-1}\left(\cos\theta + \frac{n\lambda}{L}\right), \tag{1.5}$$

where λ is wavelength, L is the period of the surface, θ is the angle of incidence and ϕ_n is the angle of diffraction with nth-order of the grating (see Figure 1.3).

However, real gratings are not ideally periodic and there may be some degree of fluctuations in the periodic structures. Such fluctuations generate scattering to all directions with continuous wavenumbers. In this thesis, diffractions due to the periodicity and scattering due to the fluctuations are analyzed, and properties of such diffractions and scattering are numerically calculated and illustrated in figures.

1.1.2 Wood's anomaly and incoherent Wood's anomaly

In the cases of classical random surfaces [15, 45], which have random fluctuations of height parameter and do not have periodicity, several phenomena in the scattering such as anomalous scattering [19,20], which can be observed as a peak of the radar cross section (an average power flux per unit aperture length) to the low grazing angles, and backscattering enhancement [21–23], have been reported for the incidence of TM plane wave or vertically polarized wave.

On the other hand, in the cases of periodic structure, rapid variations in the intensity of the diffracted spectral orders against the observation angles found in experiments on a reflection grating by R.W.Wood in 1902 [28], which is well known as Wood's anomaly. Hessel and Olinear classified such anomalies into two types [29]: one is a resonance behavior in the amplitudes and the other is a rapid variation of the amplitudes corresponding to the Rayleigh wavenumber k.

The latter phenomenon appears for specific angles of incidence $\theta_W^{[n]}$, which are determined only with the wavelength λ and the period of the surface L as

$$k^2 - \left(-k\cos\theta_W^{[n]} - n\frac{k\lambda}{L}\right)^2 = 0, \quad (n = \pm1, \pm2, \cdots), \tag{1.6}$$

where λ is wavelength and k is wavenumber in free space.

The latter type of Wood's anomaly has been reported to occur in the diffraction from a periodic random surface with random height fluctuations which is periodic on average [8]. However, we newly find that this anomaly appears in the diffraction from periodic grooves with single defect and a binary periodic random surface with zero average.

On the other hand, due to the fluctuations, random height or binary height parameters, scattered wave can be generated from periodic random surfaces. Recently, another anomaly similar to Wood's anomalies, which appears as rapid variations in the angular distribution of the scattering, have been found in cases of random surfaces that are periodic on average [6,8]. We

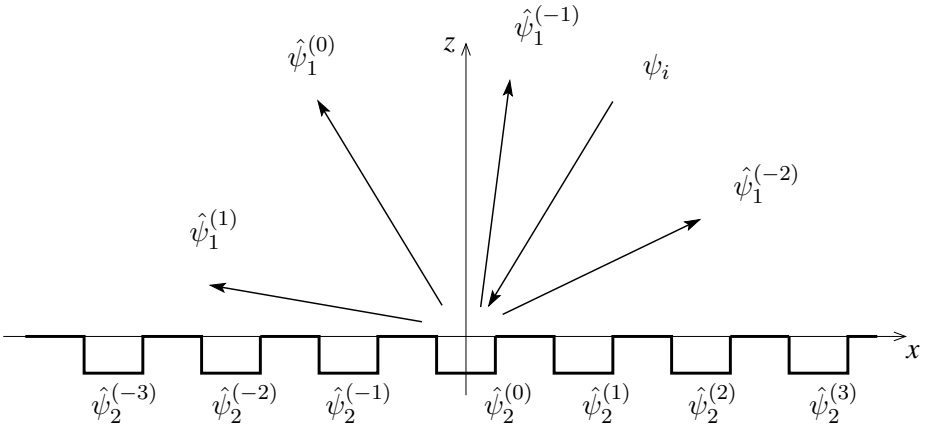

(a) diffraction from periodic grating

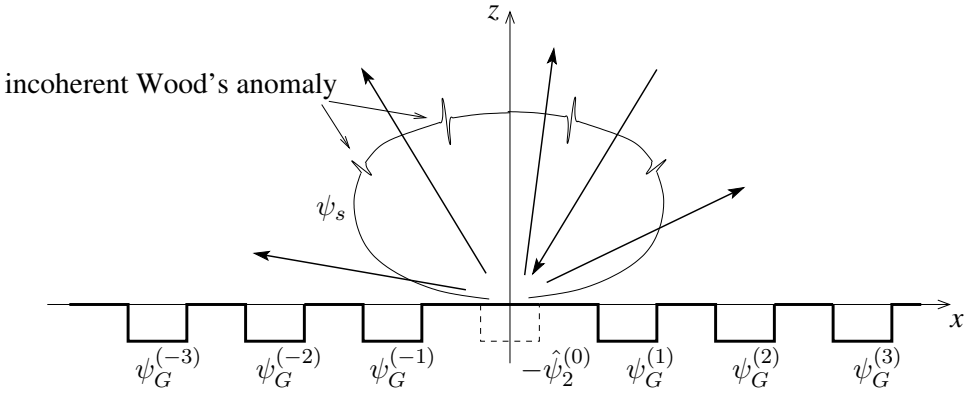

(b) scattering as perturbation from perfectly periodic grating

Figure 1.4 Diffraction and scattering from periodic grating with single defect. Scattered wave is determined by two steps: (a) The first step determines the diffracted wave by the perfectly periodic grating. (b) The second step determines the scattered wave as variation from perfectly periodic grating due to single defect. ψ_i is the incident wave, $\hat{\psi}_1^{(n)}$ is the nth-order diffracted wave, $\hat{\psi}_2^{(m)}$ is the wavefield inside the mth groove for the perfectly periodic grating, ψ_s is the scattered wave and $\psi_G^{(m)}$ is the perturbed wavefield inside the mth groove due to single defect. When a TM plane wave is incident, incoherent Wood's anomaly appears in the scattering, however, it does not occur for a TE case.

call that anomaly "incoherent Wood's anomaly". In this thesis, we newly show that incoherent Wood's anomaly appears in a deterministic case of periodic grooves with single defect [46] and a case of a binary periodic random surface even when it has zero average. Further, we discuss the physical mechanisms of Wood's anomaly and incoherent Wood's anomaly.

1.2 Methods of analysis

1.2.1 Periodic grooves with single defect

Scattering as variation from perfectly periodic case Let us consider periodic rectangular grooves with single defect of which position is known. This type may be the simplest case among various types of binary fluctuations.

In such a case, the surface is almost periodic but single defect generates scattering. This thesis presents a new idea of analysis, where the scattering is considered as a variation from the perfectly periodic case [27,30] †. Therefore, the total wavefield above the surface $\Psi_1(x,z)$ is expressed as a sum of the diffracted waves $\hat{\Psi}_1(x,z)$ and the scattered wave $\psi_s(x,z)$ as

$$\Psi_1(x,z) = \hat{\Psi}_1(x,z) + \psi_s(x,z), \tag{1.7}$$

$$\hat{\Psi}_1(x,z) = \psi_i(x,z) + \sum_{n=-\infty}^{\infty} \hat{\psi}_1^{(n)}(x,z), \tag{1.8}$$

where ψ_i is the incident wave, $\hat{\psi}_1^{(n)}$ is the nth-order diffracted wave for the perfectly periodic grating. On the other hand, the wavefield inside the grooves $\Psi_2(x,z)$ as a sum of the wavefield which consists of base components $\hat{\Psi}_2(x,z)$ and perturbed components $\psi_G(x,z)$ due to the defect as

$$\Psi_2(x,z) = \hat{\Psi}_2(x,z) + \psi_G(x,z), \tag{1.9}$$

$$\hat{\Psi}_2(x,z) = \sum_{m=-\infty}^{\infty} \hat{\psi}_2^{(m)}(x,z) = \sum_{m=-\infty}^{\infty} e^{ipmL} \hat{\psi}_2^{(0)}(x-mL,z), \tag{1.10}$$

$$\psi_G(x,z) = \sum_{m=-\infty}^{\infty} \psi_G^{(m)}(x,z), \tag{1.11}$$

where $\hat{\psi}_2^{(m)}(x,z)$ is the wavefield inside the mth groove for the perfectly periodic grating and e^{ipmL} is a phase factor for the mth groove to the x direction with $p = k\cos\theta$, and $\psi_G^{(m)}$ is the perturbed wavefield inside the mth groove due to single defect.

The wavefield can be obtained in two steps (See Figure 1.4). First, $\hat{\Psi}_1(x,z)$ and $\hat{\Psi}_2(x,z)$ are determined as the wavefields for the perfectly periodic case. Then, equations to obtain the scattered wave $\psi_s(x,z)$ and the perturbed components of the wavefield inside grooves $\psi_G(x,z)$ are derived from the boundary condition.

Boundary conditions For the case of periodic grooves with single defect, it is possible to treat the boundary conditions without approximation, since the analysis is based on the mode-matching method and the position of defect is known. Boundary conditions are specified at $z = 0$ both on the apertures of the grooves and upon the flat part outside the grooves.

1.2.2 Binary periodic random surfaces

Stochastic functional approach The other type of the surface studied in this thesis is binary periodic random surfaces shown in Figure 1.5. We will make use of a concept of stochastic processes to formulate the problem and to express the scattered wave. It is a known concept, however, we explain it to make our approach understood easily.

Let us consider a binary sequence $\{b_m(\omega)\}$ in the sample space Ω, which is of function space type [47] and is the ensemble of such stationary binary sequences. ω is a sample point in Ω and is an infinite-dimensional vector as

$$\omega = (\cdots, \omega_{-1}, \omega_0, \omega_1, \cdots), \quad \omega_m = b_m(\omega), \tag{1.12}$$

† In this thesis, we take the "mode-matching method" in a wide sense, that is, we determine wavefields from the conditions of the continuity of both electric and magnetic fields. Thus, it does not exactly mean so-called mode-matching method proposed in [32].

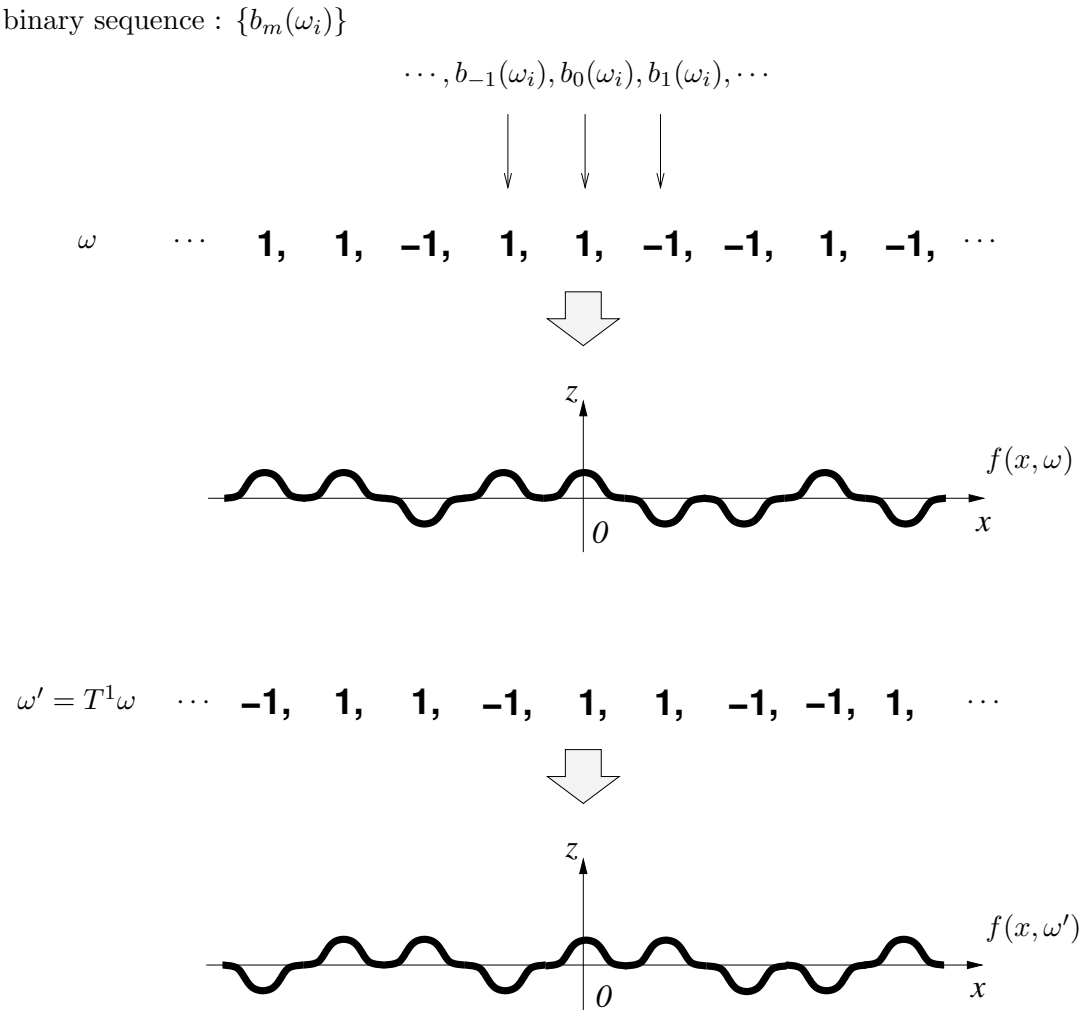

Figure 1.5 Generation of a binary periodic random surface from a stationary binary sequence $\{b_m(\omega)\}$ (average height $\sigma_0 = 0$). A local surface becomes a boss when $b_m(\omega) = 1$, while it becomes a pit when $b_m(\omega) = -1$. In this case, $\omega' = T^1\omega$ is obtained by shifting ω with T^1.

where ω_m is the nth component of ω. Each component $b_m(\omega)$ takes the value $+1$ or -1. Physically, $b_m(\omega) = +1$ or -1 becomes a boss or a pit. Then, we write a binary periodic random surface $f(x, \omega)$

$$z = f(x,\omega) = \sum_{m=-\infty}^{\infty} g(x - mL)[\sigma_0 + \sigma_1 b_m(\omega)], \tag{1.13}$$

where L is the period of the surface, $g(x)$ is a local surface profile defined in $|x| \leq L/2$, m is integer and σ_0 and σ_1 are an average component and a fluctuating component of the height parameter, respectively. When ω changes, the height of the corresponding local surface changes. Therefore, the scattered wave from such a periodic random surface can be expressed as a functional of the stationary binary sequence. On the other hand, a binary sequence which corresponds to any realization of a binary periodic random surface exists in such Ω. A translation by n of a binary sequence $\{b_m(\omega)\}$: $b_m(\omega) \rightarrow b_{m+n}(\omega)$ can be regarded as a shift of a sample point $\omega \rightarrow \omega'$

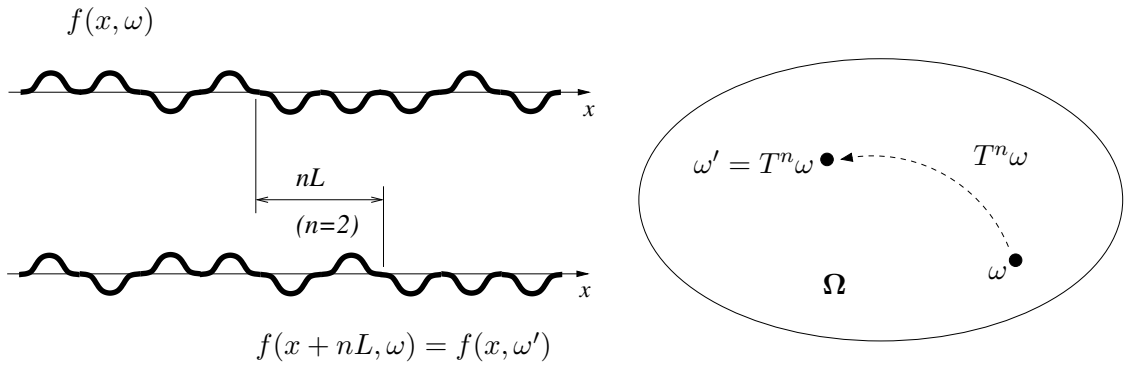

Figure 1.6 Shift of binary periodic random surface $f(x,\omega)$ by nL along x-axis : $f(x,\omega) \to f(x+nL,\omega)$, and shift in sample space Ω : $\omega \to T^n\omega$.

in sample space Ω (See Figure 1.6). which is represented by shift operator T as $\omega' = T^n\omega$, where the shift T is a measure-preserving transformation with $P(\omega) = P(T^n\omega)$, and has a group properties: $T^0 \equiv 1$ (identity); $T^{m+n} = T^m T^n$ [7]. Such a shift corresponds to a shift of the surface along the x-axis by mL as $f(x,\omega) \to f(x+mL,\omega)$. Thus, we find that the surface $f(x,\omega)$ is invariant under the translation $(x,\omega) \to (x+nL, T^{-n}\omega)$

$$f(x,\omega) = f(x+nL, T^{-n}\omega). \tag{1.14}$$

Let us consider the scattered wave $\Psi_s(x,z,\omega)$ under a plane wave incidence $\Psi_i(x,z) = e^{ipx-i\beta_0(p)z}$, where $\beta_0(p)$ is often called a propagator defined as $\beta_0(p) = \sqrt{k^2-p^2}$, and p is wavenumber in the x direction. Such a scattered wave $\Psi_s(x,z,\omega)$ can be considered as a response from a periodic random surface. To determine a form of $\Psi_s(x,z,\omega)$, we define a translation operator D acting on the wave function $\Psi_s(x,z,\omega)$ by

$$D^m\Psi_s(x,z,\omega) = \Psi_s(x+mL,z,T^{-m}\omega), \quad (m=0,\pm1,\pm2,\cdots). \tag{1.15}$$

Since $f(x,\omega)$ is invariant under D^m by (1.14), if $\Psi_i(x,z)+\Psi_s(x,z,\omega)$ satisfies the wave equation $[\partial^2/\partial x^2+\partial^2/\partial z^2+k^2]\Psi(x,z,\omega)=0$ and the boundary condition, then $D^m\Psi_s(x,z,\omega) = \Psi_s(x+mL,z,T^{-m}\omega)$ becomes a solution for the incident plane wave $D^m\Psi_i(x,z) = e^{ipmL}e^{ipx-i\beta_0(p)z}$. Thus, we get

$$D^m\Psi_s(x,z,\omega) = \Psi_s(x+mL,z,T^{-m}\omega) = e^{ipmL}\Psi_s(x,z,\omega). \tag{1.16}$$

If we put

$$\Psi_s(x,z,\omega) = e^{ipx}U(x,z,\omega), \tag{1.17}$$

then from (1.16) we find that $U(x,z,\omega)$ satisfies the shift invariance property :

$$\begin{aligned} D^mU(x,z,\omega) &= U(x+mL,z,T^{-m}\omega) \\ &= U(x,z,\omega). \end{aligned} \tag{1.18}$$

This and (1.14) mean that $U(x,z,\omega)$ is a periodic stationary process of x. If $U(x,z,\omega)$ is a deterministic periodic function, (1.17) is the Floquet form for periodic gratings. However, in

our case, $U(x,z,\omega)$ is not periodic, but the ensemble average $\langle U(x,z,\omega)\rangle$ over the sample space Ω becomes periodic, since $U(x,z,\omega)$ is periodic stationary:

$$\langle U(x+mL,z,\omega)\rangle = \langle U(x,z,T^m\omega)\rangle = \langle U(x,z,\omega)\rangle. \tag{1.19}$$

Thus, (1.17) is considered as an extension of the Floquet form, which we call the stochastic Floquet form [7]. Note that the wavefield $\Psi_s(x,z,\omega)$ itself is not shift-invariant.

Because of this shift invariant property, $U(x,z,\omega)$, which is a response from a binary periodic random surface, could be considered to belong to a translation-invariant system on $(R\times\Omega)$ [†], that is, the ensemble average over the sample space Ω becomes periodic. Thus, it is constant in sampling by any integer multiple of the period L. On the other hand, the periodic grating with single defect does not belong to such translation-invariant systems.

Periodic stationary process, binary expansion and harmonic series representation By the stochastic Floquet form (1.17), the problem to obtain the scattered wave $\Psi_s(x,z,\omega)$ is reduced to determine the periodic stationary process $U(x,z,\omega)$.

Since the scattered wave is a response from a binary periodic random surface and such a binary periodic random surface is generated by the stationary binary sequence of binary random variables $b_m(\omega)$ [‡], the scattered wave is regarded as a functional of binary random variables. Such a functional can be represented in the binary orthogonal expansion with binary polynomials. Binary orthogonal expansion was given by J.Nakayama and L.Gao [49] with multivariate orthogonal polynomials, recurrence formulae and generating function in explicit form [50].

By use of the binary orthogonal expansion, the periodic stationary process of the scattered wavefield can be written as

$$U(x,z,\omega)=C_0(x,z)+\sum_{n=1}^{\infty}\sum_{\substack{m_l=-\infty\\ l=1,\cdots,n}}^{\infty} B_n[b_{m_1}(\omega),\cdots,b_{m_n}(\omega)]C_n(x-m_1L,\cdots,x-m_nL,z), \tag{1.20}$$

where $B_n[\cdot]$ is the binary polynomial defined in Appendix A and coefficients of the nth-order polynomials $C_n(x_1,\cdots,x_n,z)$ $(n=0,1,2,\cdots)$ are deterministic functions called binary kernels. However, it is necessary to rewrite (1.20) so that $e^{ipx}U(x,z,\omega)$ satisfies the Helmholtz equation (1.1). Representing the binary kernels by multiple Fourier integrals, we write

$$\begin{aligned} U(x,z,\omega) = &\sum_{q=-\infty}^{\infty} C_0^{(q)}(p)e^{ik_Lqx}e^{i\beta_0(p)z} \\ &+\sum_{n=1}^{\infty}\sum_{\substack{m_l=-\infty\\ l=1,\cdots,n}}^{\infty} B_n[b_{m_1}(\omega),\cdots,b_{m_n}(\omega)]\int\cdots\int_{-\infty}^{\infty} C_n(\lambda_1,\cdots,\lambda_{n-1},\lambda_s|p)e^{i\beta_0(p+\lambda_s)z} \\ &\times e^{i\lambda_1(x-m_1L)+\cdots+i\lambda_{n-1}(x-m_{n-1}L)+i(\lambda_s-(\lambda_1+\cdots+\lambda_{n-1}))(x-m_nL)}d\lambda_1\cdots\lambda_{n-1}d\lambda_s. \end{aligned} \tag{1.21}$$

[†]Translation-invariant systems can be classified into several types: (1) constant systems such as flat boundary between two media, (2) periodic systems such as periodic grating, (3) random system such as Gaussian random surfaces, (4) periodic random systems such as Gaussian periodic random surfaces and binary periodic random surfaces among others [48].

[‡]If the fluctuations are given by the Gaussian random variables such as the classical random surfaces and random media, another stochastic approach the Wiener analysis, which is another stochastic approach, is used to obtain the wavefield [7,8].

Although the expression (1.21) satisfies (1.1), it is still redundant and is not possible to determine binary kernels $C_n(\lambda_1, \cdots, \lambda_{n-1}, \lambda_s|p)$ uniquely. Thus, we write (1.21) in the harmonic series representation [51, 52] dividing the integral intervals of $\lambda_1, \cdots, \lambda_{n-1}, \lambda_s$ into bands with equal width $[-k_L/2, k_L/2]$ as

$$U(x,z,\omega) = \sum_{q=-\infty}^{\infty} e^{ik_L qx} U^{(q)}(x,z,\omega) \tag{1.22}$$

$$\begin{aligned} U^{(q)}(x,z,\omega) &= C_0^{(q)}(p) e^{i\beta_q(p)z} \\ &+ \sum_{n=1}^{\infty} \sum_{\substack{m_l=-\infty \\ l=1,\cdots,n}}^{\infty} B_n[b_{m_1}(\omega), \cdots, b_{m_n}(\omega)] \int \cdots \int_{-k_L/2}^{k_L/2} C_n^{(q)}(\lambda_1, \cdots, \lambda_{n-1}, \lambda_s|p) \\ &\times e^{i\lambda_1(x-m_1L)+\cdots+i\lambda_{n-1}(x-m_{n-1}L)+i\lambda_s(x-m_nL)+i\beta_0(p+\lambda_s)z} d\lambda_1 \cdots \lambda_{n-1} d\lambda_s, \end{aligned} \tag{1.23}$$

where k_L is defined in (1.4). To obtain the scattered wavefield, we should determine the band-limited binary kernels $C_n^{(q)}(\lambda_1, \cdots, \lambda_{n-1}, \lambda_s|p)$ from the boundary conditions. Substituting the expressions of the scattered wave (1.22) and (1.23) into the boundary conditions, hierarchical equations for such band-limited binary kernels are derived, which continue to the infinite order of n. The n-th order hierarchical equation for the n-th order binary kernel $C_n^{(q)}$ describes relations both with the $(n-1)$-th order binary kernel $C_{n-1}^{(q)}$ and with integrations of the $(n+1)$-th order binary kernel $C_{n+1}^{(q)}$, which are called ascending and descending couplings, respectively [53,54]. In this thesis, we solve such hierarchical equations by use of truncation and diagonal approximation [53] in Chapters 4 and 5.

Boundary conditions In the binary random case, as is mentioned above, it is necessary to determine the band-limited binary kernels to obtain the diffracted and scattered wave form the boundary condition.

For a periodic stationary process $\Phi(x,\omega)$, we introduce the norm $\| \Phi(x,\omega) \|$, which is defined as an ensemble average of a space average of $|\Phi(x,\omega)|^2$ over one period [†] :

$$\| \Phi(x,\omega) \|^2 = \left\langle \frac{1}{L} \int_{-L/2}^{L/2} |\Phi(x,\omega)|^2 \, dx \right\rangle, \tag{1.24}$$

and we assume that the wavefield $\Psi(x,z,\omega)$ satisfies the boundary condition in the norm sense (1.24).

Generally, in the boundary value problems of random surfaces, it is extremely difficult to evaluate boundary conditions rigorously, so that boundary conditions have been often approximated [19–22]. In the scattering problem for perfectly conductive surfaces, so-called effective boundary conditions [18], which are Taylor's expansion of the wavefield in terms of $z = f(x,\omega)$ at $z = 0$ and their higher order terms are neglected, as

$$\text{Dirichlet} \quad (\text{TE}) \quad : \quad \Psi(x,z,\omega) + f(x,\omega) \frac{\partial \Psi(x,z,\omega)}{\partial z} = 0, \qquad (z=0), \tag{1.25}$$

$$\text{Neumann} \quad (\text{TM}) \quad : \quad -\frac{df(x,\omega)}{dx} \frac{\partial \Psi(x,z,\omega)}{\partial x} + \frac{\partial \Psi(x,z,\omega)}{\partial z} + \frac{\partial^2 \Psi(x,z,\omega)}{\partial z^2} = 0, \qquad (z=0), \tag{1.26}$$

[†] In [59], the norm was defined as a space average of $\langle |\Phi(x,\omega)|^2 \rangle$ over one period, however, it should be modified as is defined in (1.24), when the boundary condition is not approximated and is taken along the binary periodic random surface.

(a) binary periodic random surface
– average surface is periodic –

(b) binary periodic random surface
– average surface is flat –

Figure 1.7 Binary periodic random surfaces: (a) average surface is periodic (thin solid line is an average surface), (b) average surface is flat.

are often used [7, 8, 19, 20, 44, 53].

On the other hand, we may employ the Dirichlet and Neumann conditions without approximation in the binary case.

Since the boundary conditions are related to the value of the incident wave $e^{ipx-i\beta_0(p)z}$ upon the surface $z = f(x,\omega)$, the z-dependency of the scattered wavefield generally appears as $e^{i\beta_0(\lambda')z}$. By substituting $z = f(x,\omega)$ and using the special property $b_m(\omega) = \pm 1$, we get an identity as

$$\begin{aligned} e^{i\beta_0(\lambda')f(x,\omega)} &= e^{i\beta_0(\lambda')g(x)\{\sigma_0+\sigma_1 b_0(\omega)\}} \\ &= e^{i\sigma_0\beta_0(\lambda')g(x)} \left\{\cos[\sigma_1\beta_0(\lambda')g(x)] + i\sin[\sigma_1\beta_0(\lambda')g(x)]b_0(\omega)\right\} \end{aligned} \tag{1.27}$$

for $|x| \le L/2$ $(m = 0)$. With this property, the binary random variable $b_m(\omega)$ comes out of the exponential phase factor. Thus, the boundary conditions can be evaluated without approximation.

Effects of multiple scattering From the viewpoint of analysis, it is essentially important to distinguish that the ensemble average of the surface is periodic or flat.

In [44], the binary periodic random surface, of which ensemble average is a periodic surface, was studied(See Figure 1.7(a)). Similarly in [7] and [8], the Gaussian periodic random surfaces, of which ensemble average are periodic, were discussed. On the other hand, this thesis deals with the binary periodic random surface, of which ensemble average is a flat plane(See Figure 1.7(b)). When the ensemble average of the periodic surface is flat, it is necessary to evaluate effects of multiple scattering much strictly for the TM plane wave incidence.

In the stochastic functional approach, the random scattering problem is reduced to obtain deterministic kernel functions from hierarchical equations. To solve the hierarchical equations [†], Ref [7] and [44] employ truncation in the first order hierarchical equation and the diagonal approximation, and then effects of multiple scattering are involved with the iterative mass operator [54, 55] for TE incidence. Further, Ref [8] determines the wavefield by use of what we call a single scattering approximation, which neglects the integration of descending coupling. These approaches are valid even for TM incidence as far as the ensemble average of the periodic

[†]The hierarchical equations in [7] and [8] are for unknown Wiener kernels since the fluctuation of the height parameter is describes as a Gaussian random variable and the wavefield is expressed in the Wiener expansion with Wiener kernels.

random surface is periodic. However, when the average surface becomes flat, the scattered wave obtained by these methods diverges unphysically.

In Chapter 5, we overcome such divergence difficulties for TM incidence by use of multiply renormalizing approximation [53]. After obtaining the binary kernels by use of truncation and diagonal approximation with the iterative mass operator, we consider a limit where the truncation number goes to infinity. In terms of such a limit, we may obtain an approximate solution by the multiply renormalizing approximation.

1.3 Compositions of the thesis

This thesis consists of six chapters and several appendices.

Chapter 2 and Chapter 3 deal with the scattering from a periodic grating with single defect, of which position is known. The surface is perfectly conductive and made up with a periodic array of rectangular grooves and a defect where a groove is not formed. Scattering from such a periodic surface with single defect is analyzed from a standpoint of the electromagnetic theory and a new formulation of the problem is proposed, which is made up of two steps. First, we obtain the diffracted wave and the guided modes inside the grooves by use of the modal expansion method for the perfectly periodic case. Then, assuming that such diffracted wave is scattered by the single defect, we derive a set of infinite-dimensional equations for the scattered wave and the perturbed component of the guided modes inside the grooves due to the defect. Such a set of equation could be considered to involve effects of multiple scattering. We then obtain a new representation of the optical theorem, relating total scattering cross section with reduction of the scattering amplitude, and also propose an analytical expression of a single scattering approximation. In Chapter 2, an infinite-dimensional equation for unknown amplitudes of the perturbed component of the guided modes is newly derived from the set of equations for the TE case. By use of truncation, we numerically obtain the perturbed component, in terms of which the total scattering cross section and the differential scattering cross section are calculated and illustrated in figures. It is found that effects of multiple scattering is small in the TE incident case, so that the single scattering approximation can describe the scattered wave for the shallow case. Chapter 3 studies the TM incident case. From the set of equations, an integral equation for an unknown amplitude of the scattered wave in the spectral domain is derived, since the scattered wave may decay slowly along the surface and affect the guided modes in the grooves far from the defect. Then, such an integral equation is solved numerically by use of truncation and the iteration method. The differential scattering cross section and the optical theorem are calculated in terms of the scattering amplitude and are illustrated in figures. It is found that effects of multiple scattering should be involved to describe the wavefield for TM incidence. It is also shown that incoherent Wood's anomaly appears as steep peaks and dips at critical scattering angles. The physical mechanisms of Wood's anomaly and incoherent Wood's anomaly are discussed in relation to the guided surface wave excited by the incident plane wave. It is concluded that incoherent Wood's anomaly is caused by the coupling between the scattered wave and the guided surface wave along the surface.

Chapter 4 and Chapter 5 deal with the diffraction and scattering from a periodic random surface generated by a stochastic binary sequence, of which ensemble average is a flat surface, using a stochastic functional approach. The surface is periodically modulated in amplitude, forming a boss and a pit corresponding to the binary random variable. Such a periodic random surface has been known to become a periodic stationary process, and the diffracted and scattered

waves from such a surface are also written as a periodic stationary process and can be expanded with orthogonal binary polynomials. In the preceding work [44], the first-order scattered wave was determined from the effective boundary condition. However, when the ensemble average of the binary periodic random surface is a flat plane, an unphysical divergence problem arises in the scattered wave in case of the TM incidence. This thesis provides methods to avoid such a divergence problem involving effects of multiple scattering in the scattered wave.

The scattered wave is first expressed by a product of an exponential phase factor and a periodic stationary process. The periodic stationary process is then expressed by "Fourier series", where "Fourier coefficients" are mutually correlated stationary processes. These stationary processes are regarded as stochastic functionals of the binary sequence and they are represented by orthogonal binary functional expansions with band-limited binary kernels. In Chapter 4, the binary kernels are determined up to the second order from the Dirichlet boundary condition without approximation. Then, several statistical properties of the scattering are numerically calculated and illustrated in figures. It is found that the diffracted wave to discrete directions is generated even when the periodic random surface has zero average, and in the binary case, the second order scattering cross section has a subtractive part and becomes much smaller than the first order one. Chapter 5 studies the case of TM incidence. With the representation of the scattered wave by the orthogonal binary functional expansion with band-limited binary kernels, hierarchical equations for the binary kernels are derived from the Neumann boundary condition without approximation. The expressions of such binary kernels are then obtained by use of the multiply renormalizing approximation, which involves effects of multiple scattering. Statistical properties such as differential scattering cross section and optical theorem are numerically calculated with first two order binary kernels and illustrated in figures. It is found that Wood's anomaly appears for critical angles of incidence and incoherent Wood's anomaly appears in the angular distribution of scattering, even when the surface has zero average. It is also found that the power of diffracted wave increases for critical angles of incidence, while the power of scattered wave decreases contrarily and the scattered wave becomes small around the direction of specular reflection except for the critical scattering angles.

Chapter 6 is the conclusion of this thesis. We will give some problems which are left for the future study.

In Appendix A, we summarize definitions of multi-variate binary polynomials and several formulae on such binary polynomials and binary expansion, which are used in Chapter 4 and Chapter 5. Moreover, in these chapters, we have represented the wavefield in the harmonic series representation of the periodic stationary process, which can be considered as "Fourier series" with "Fourier coefficients". Such "Fourier coefficients" are given by stationary processes, which are written with band-limited binary kernels. In Appendix B, we discuss properties of such band-limited binary kernels and the stationary processes. Appendix C summarizes the derivation of the optical theorem both for the single defect case and the binary random case. In Appendix D, we derive expressions of the binary kernels by the multiply renormalizing approximation for TE incidence in the same manner as chapter 5.

The time dependence $e^{-i2\pi f_0 t}$ with the frequency f_0 is assumed and suppressed throughout the thesis.

Chapter 2

Scattering of TE plane wave from periodic grating with single defect

2.1 Introduction

In electronics, many devices such as memory chips and LCD electrodes have periodic structure with rectangular parallel lines. Defects in such periodic structure due to the imperfection in the manufacturing processes have been a serious problem for years. It is practically important to study the possibility of optical detection of such defects and to develop a method of measurement and inspection. Theoretically, such defects in the periodic structure could be modelled as defects in the periodic gratings with rectangular grooves.

Lately, there have been many works [9–14, 34] on the scattering and diffraction by a single groove, a finite number of grooves and a periodic array of grooves without any defects. However, there has not been studied the scattering from a periodic grating with defects. From a standpoint of analysis, a single groove or a finite number of grooves can be considered as a finite number of scatterer, which determine the wavefield. Further, a periodic surface has an infinite number of scatterers, however, it results in problems of a single scatterer by the Floquet form. On the other hand, when there are defects in periodic structure, it is necessary to take an infinite number of scatterers into account. Thus, we newly present a theoretical formulation on the scattering from a periodic gratings with defects.

As a simple model of such a periodic grating with defect, this chapter studies TE wave scattering from a periodic array of rectangular grooves with single defect shown in Figure 2.1. Since there is only one defect in the periodic grating, we consider that the diffracted wave for the periodic grating is scattered by a single defect. Therefore, we obtain the scattered wave as a variation from the diffracted wave. The wavefield above the surface is written as a sum of the incident wave, diffracted wave and the scattered wave due to the defect, while the wavefield inside the grooves is expressed as a sum of guided modes with unknown mode amplitudes by use of the modal expansion method [30]. The mode amplitudes are regarded as a sum of base components and perturbed components due to the defect, where the base component is the solution in case of the perfectly periodic grating without any defect.

We introduce a two-step method to determine the wavefield. In the first step, an equation for the diffracted wave and the base component of the guided modes is obtained for the periodic case without any defect. Then, by use of the base component and the diffracted wave, a new equation for the scattered wave and the perturbed component of the guided modes is derived in

the second step.

We begin in Section 2.2 with the mathematical formulation of the periodic grating with single defect. We assume that the surface is perfectly conductive and made up with a periodic array of rectangular grooves and a defect where a groove is not formed. In Section 2.3, the diffracted wave and the base component of the guided modes are obtained for the perfectly periodic grating. In Section 2.4, the scattered wave and the perturbed component of the guided mode are represented in terms of the base component of the guided modes obtained in Section 2.3. We give a new representation of the optical theorem, which relates the total scattering cross section with the reduction of the scattering amplitude. To determined the scattered wave, we derive an equation for the perturbed component of the guided modes in the grooves, including an integral part for the coupling between different guided modes. We find that such an integral part is independent of the angle of incidence and is determined only by the geometry of the surface. To evaluate the scattering property approximately, we introduce a single scattering approximation, which is written only by the base component of the guided modes. In Section 2.5, we obtain a numerical solution of the perturbed component by use of truncation, in terms of which the amplitude of the scattered wave is described. The optical theorem and the differential scattering cross section are calculated with such an amplitude of the scattered wave and are illustrated in figures.

Then, we find that the optical theorem for the periodic grating with single defect holds within an accuracy of 0.5% for most angles of incidence both in the shallow and resonant cases of the groove depth, but the accuracy decreases for low grazing angles of incidence and angles corresponding to the entry of a new spectral order. For the shallow cases, scattering is relatively strong in the direction of specular reflection, however, for the resonant case, the differential scattering cross section seems symmetric with respect to the normal scattering angle. It is also found that the single scattering approximation almost agrees with the numerical solution, which suggests that the single scattering approximation is valid for a TE incidence when the depth of the groove is shallow.

2.2 Periodic grating with single defect

Let us consider a periodic array of rectangular grooves with a single defect at $x = 0$ (See figure 2.1). We write such an array as

$$z = f(x) = -d\left[\sum_{g=-\infty}^{\infty} u(x-gL|w) - u(x|w)\right], \tag{2.1}$$

where L is the period, w and d are the width and the depth of the groove. Here, $u(x|w)$ is a rectangular groove defined as

$$u(x|w) = \begin{cases} 1, & |x| \le w/2, \\ 0, & |x| > w/2. \end{cases} \tag{2.2}$$

It has the orthogonal property such that

$$u(x - gL|w)u(x - g'L|w) = \delta_{gg'}u(x - gL|w), \quad (g, g' = 0, \pm1, \pm2, \cdots), \tag{2.3}$$

where $\delta_{gg'}$ is Kronecker's delta. The Fourier transform of $u(x|w)$ is calculated as

$$U(q) = \int_{-\infty}^{\infty} u(x|w)e^{-iqx}dx = 2\frac{\sin(qw/2)}{qw}w, \tag{2.4}$$

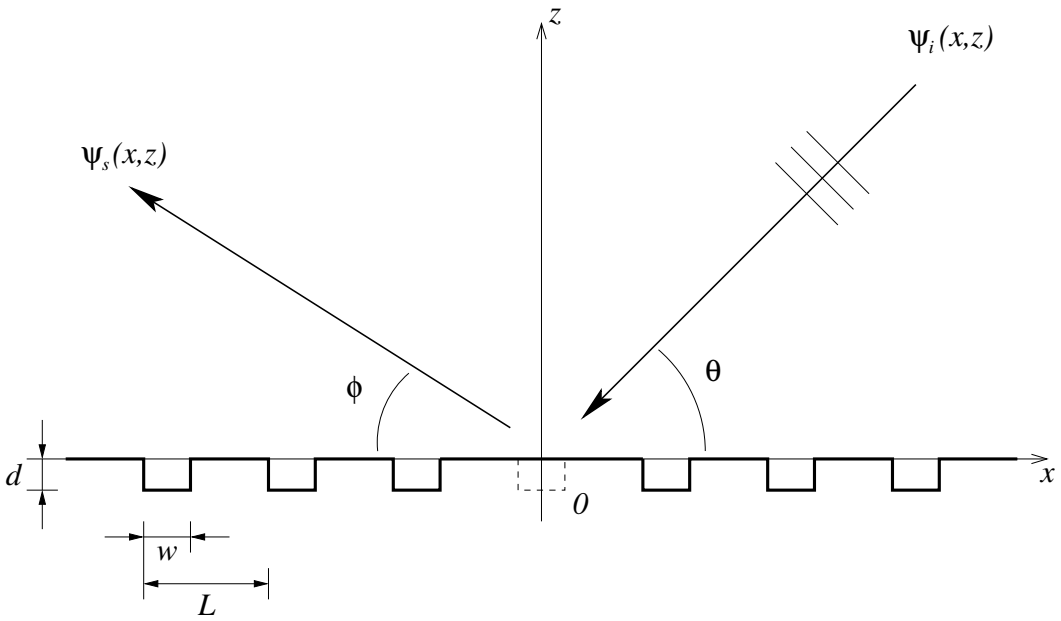

Figure 2.1 Scattering of TE plane wave from a periodic grating with single defect. The surface is a periodic array of rectangular grooves and has a defect where a groove is not formed. $\psi_i(x,z)$ is the incident wave and $\psi_s(x,z)$ is the scattered wave. θ is the angle of incidence, ϕ is the scattering angle, L is the period of surface, w and d are the width and the depth of groove.

which will be used later to obtain the scattered field.

For convenience, we put k_L and k_w as

$$k_w = \frac{\pi}{w}, \quad k_L = \frac{2\pi}{L}, \tag{2.5}$$

and we define an auxiliary function $s_m(q)$ as follows.

$$s_m(q) = \int_{-\infty}^{\infty} u(x|w)\sin(mk_w(x+w/2))e^{-iqx}dx \tag{2.6}$$

$$= \frac{1}{2i}\left[U(q-mk_w)e^{im\pi/2} - U(q+mk_w)e^{-im\pi/2}\right], \tag{2.7}$$

where m is integer. Figure 2.2 illustrates $s_m(q)$ for $m = 1, 4, 7$ with width the $w = 1.3\lambda$, where λ is wavelength. $s_m(q)$ becomes a real even function for odd integer m, and an imaginary odd function for even integer m. Note that $s_m(q) \sim 1/q^2$ when $|q|$ becomes large. This auxiliary function $s_m(q)$ takes the phase shift by e^{-iqmL} with the shift of x by mL.

$$\int_{-\infty}^{\infty} u(x-mL|w)\sin(mk_w(x+w/2-mL))e^{-iqx}dx = e^{-iqmL}s_m(q). \tag{2.8}$$

We denote the y component of the electric field by $\Psi(x,z)$, which satisfies the Helmholtz equation

$$\left[\frac{\partial^2}{\partial x^2} + \frac{\partial^2}{\partial z^2} + k^2\right]\Psi(x,z) = 0, \tag{2.9}$$

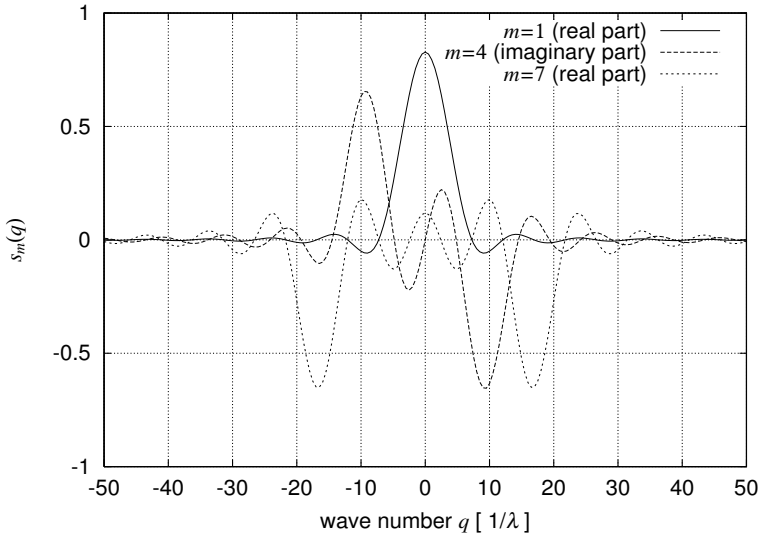

Figure 2.2 Auxiliary function $s_m(q)$ against wave number q for $m = 1, 4, 7$ with width $w = 1.3\lambda$, λ is wavelength.

in the region $z > f(x)$. Here, $k = 2\pi/\lambda$ is wavenumber. We consider that the surface is perfectly conductive. On the surface $z = f(x)$, the wavefield $\Psi(x, z)$ satisfies the Dirichlet condition,

$$\Psi(x, z)|_{z=f(x)} = 0. \tag{2.10}$$

We write the incident plane wave $\psi_i(x, z)$ as

$$\psi_i(x, z) = e^{ipx} e^{-i\beta_0(p)z}, \quad p = -k\cos\theta, \tag{2.11}$$

$$\beta_n(p) = \beta_0(p + nk_L) = \sqrt{k^2 - (p + nk_L)^2}, \tag{2.12}$$

$$\mathrm{Im}[\beta_n(p)] \geq 0, \quad (n = 0, \pm 1, \pm 2, \cdots), \tag{2.13}$$

where θ is the angle of incidence (See Figure 2.1) and Im stands for imaginary part.

2.3 Diffraction from a perfectly periodic grating

First, we consider a perfectly periodic case without defect. We write such a perfectly periodic surface $f_p(x)$ as

$$z = f_p(x) = -d \sum_{g=-\infty}^{\infty} u(x - gL|w). \tag{2.14}$$

For the region $z \geq 0$, we put the y component of the electric field $\hat{\Psi}_1(x, z)$ as a sum of the incident wave $\psi_i(x, z)$ and the diffracted wave $\psi_d(x, z)$ due to the periodicity of the surface,

$$\hat{\Psi}_1(x, z) = e^{ipx} e^{-i\beta_0(p)z} + \psi_d(x, z), \tag{2.15}$$

$$\psi_d(x, z) = e^{ipx} \sum_{n=-\infty}^{\infty} A_n(p) e^{ink_L x + i\beta_n(p)z}. \tag{2.16}$$

Here, $A_n(p)$ is the amplitude of the mth order diffracted wave. On the other hand, by use of the modal expansion method [30], we write the y component of the electric field inside the grooves $\hat{\Psi}_2(x,z)$ as a sum of the guided modes,

$$\hat{\Psi}_2(x,z) = \sum_{g=-\infty}^{\infty} u(x-gL|w)e^{ipgL} \times \left[\sum_{m=1}^{\infty} Q_m^s(p)\sin(mk_w(x+w/2-gL))\frac{\sin(\gamma_m(z+d))}{\gamma_m}\right], \tag{2.17}$$

$$\gamma_m = \sqrt{k^2-(mk_w)^2}, \tag{2.18}$$

where $Q_m^s(p)$ is the amplitude of the guided mode which we call the base component, and γ_m is the propagation constant of the mth guided mode. Note that the number of the guided modes starts from $m=1$ since there is no constant mode for TE case.

Energy conservation relation Let us obtain the energy conservation relation for the perfectly periodic case. Using the identity $\mathrm{Im}[\mathrm{div}\hat{\Psi}_1\mathrm{grad}\hat{\Psi}_1^*]=0$ and the fact that $\hat{\Psi}_1\mathrm{grad}\hat{\Psi}_1^*$ is a periodic function with the period L, we obtain after some manipulation,

$$\mathrm{Im}\left[\int_{-L/2}^{L/2}\hat{\Psi}_1(x,z)\frac{\partial}{\partial z}\hat{\Psi}_1^*(x,z)dx\right]=0, \tag{2.19}$$

where $z>0$. Substituting (2.15) into (2.19), we get

$$\beta_0(p) = \sum_{n=-\infty}^{\infty}\mathrm{Re}[\beta_n(p)]|A_n(p)|^2, \tag{2.20}$$

which is the well known energy conservation relation. Here, Re stands for the real part, $\beta_0(p)$ is the power of the incident wave per unit length, and $\mathrm{Re}[\beta_n(p)]|A_n(p)|^2$ is the mth order diffraction power. The normalized energy conservation relation and energy error due to the appoximation Err^{energy} are written as follows.

$$1 = \sum_{n=-\infty}^{\infty}\mathrm{Re}[\beta_n(p)]|A_n(p)|^2/\beta_0(p), \tag{2.21}$$

$$Err^{energy} = \left|1-\sum_{n=-N_d}^{N_d}\mathrm{Re}[\beta_n(p)]|A_n(p)|^2/\beta_0(p)\right|, \tag{2.22}$$

where N_d is the number of the diffracted modes considered in the numerical calculation. The normalized energy conservation relation will be illustrated in Figure 2.3.

Solution for a perfectly periodic grating Let us determine $A_n(p)$ and $Q_m^s(p)$ from the continuity of both the electric field and the magnetic field at $z=0$.

From $\hat{\Psi}_1(x,0)=\hat{\Psi}_2(x,0)$, we get

$$e^{ipx}\left[1+\sum_{n=-\infty}^{\infty}A_n(p)e^{ink_Lx}\right] = \sum_{g=-\infty}^{\infty}u(x-gL|w)e^{ipgL}\left[\sum_{m=1}^{\infty}Q_m^s(p)\sin(mk_w(x+w/2-gL))\frac{\sin(\gamma_m d)}{\gamma_m}\right]. \tag{2.23}$$

Multiplying e^{-ink_Lx} and integrating over one period L, we get

$$A_n(p) = -\delta_{n0} + \frac{1}{L}\sum_{m=1}^{\infty} Q_m^s(p)\frac{\sin(\gamma_m d)}{\gamma_m} s_m(p+nk_L). \tag{2.24}$$

Next, from $\sum_{g\neq 0} u(x-gL|w)[\partial\hat{\Psi}_1/\partial z - \partial\hat{\Psi}_2/\partial z]_{z=0} = 0$, we get

$$\begin{aligned}\sum_{g=-\infty}^{\infty} u(x-gL|w)e^{ipx}&\left[-i\beta_0(p) + i\sum_{n=-\infty}^{\infty}\beta_n(p)A_n(p)e^{ink_Lx}\right]\\ &= \sum_{g=-\infty}^{\infty} u(x-gL|w)e^{ipgL}\sum_{m=1}^{\infty} Q_m^s(p)\sin(mk_w(x+w/2-gL))\cos(\gamma_m d).\end{aligned} \tag{2.25}$$

Taking Fourier transform after multiplying $u(x-mL|w)\times\sin(mk_w(x+w/2-mL))$, we obtain

$$i\sum_{n=-\infty}^{\infty}\beta_n(p)A_n(p)s_m(-p-nk_L) = i\beta_0(p)s_m(-p) + \frac{wQ_m^s(p)}{2}\cos(\gamma_m d). \tag{2.26}$$

From (2.24) and (2.26), $A_n(p)$ and $Q_m^s(p)$ can be determined. Note that for the normal incidence $\theta = 90^\circ$ $(p=0)$, $Q_m^s(p)$ vanishes for even numbers $m = 2,4,6,\cdots$ since $s_m(0)$ in the right hand side of (2.26) becomes 0 for even m and $\beta_n(0)A_n(0)s_m(-mk_L)$ and $\beta_{-n}(0)A_{-n}(0)s_m(mk_L)$ cancel each other. This will be discussed later.

In the following section, we will obtain the scattered wave by using $\hat{\Psi}_1(x,z)$ and $\hat{\Psi}_2(x,z)$.

2.4 Scattering from a periodic grating with single defect

A single defect in a periodic grating generates the scattering. We express such scattering as a perturbation from the diffracted wave for the perfectly periodic case. Thus, we write for $z>0$,

$$\Psi_1(x,z) = \hat{\Psi}_1(x,z) + \psi_s(x,z), \tag{2.27}$$

$$\psi_s(x,z) = \int_{-\infty}^{\infty} a(s|p)e^{i(p+s)x+i\beta_0(p+s)z}ds, \tag{2.28}$$

where $\psi_s(x,z)$ is the scattered wave due to the defect, which is described as a sum of plane waves with a continuous spectrum into the $+z$ direction, and $a(s|p)$ is the amplitude of the scattered wave. Since $\psi_s(x,z)$ is scattered from the single defect, $\psi_s(x,z)$ is an outgoing cylindrical wave and satisfies the radiation condition, that is, $\psi_s(r\cos\theta, r\sin\theta) \sim f(\theta)e^{ikr}/\sqrt{kr}$ $(r=\sqrt{x^2+z^2})$ and decays at $kr\to\infty$. This property will be used below. $a(s|p)e^{i(p+s)x+i\beta_0(p+s)z}$ is a component of the scattered wave with the scattering angle $\phi(p+s)$ given by

$$\phi(p+s) = \cos^{-1}\left[-\frac{p+s}{k}\right]. \tag{2.29}$$

On the other hand, we write the wavefield inside the grooves $\Psi_2(x,z)$ as a sum of the wavefield for the perfectly periodic grating and the fluctuated term $\psi_G(x,z)$ due to the defect.

$$\begin{aligned}&\Psi_2(x,z) = \hat{\Psi}_2(x,z) + \psi_G(x,z),\\ &\psi_G(x,z) = \sum_{g=-\infty}^{\infty} u(x-gL|w)e^{ipgL}\sum_{m=1}^{\infty} q_m^{(g)}(p)\sin(mk_w(x+w/2-gL))\frac{\sin(\gamma_m(z+d))}{\gamma_m}\\ &\qquad\qquad - u(x|w)\sum_{m=1}^{\infty} Q_m^s(p)\sin(mk_w(x+w/2))\frac{\sin(\gamma_m(z+d))}{\gamma_m}.\end{aligned} \tag{2.30}$$

Here, $q_m^{(g)}(p)$ is the perturbed amplitude of the mth guided mode in the nth groove. Note that

$$q_m^{(0)}(p) \equiv 0 \tag{2.31}$$

for all m since a groove is not formed at $g = 0$.

Optical theorem and scattering cross section Let us obtain the optical theorem for the single defect case. Since $\psi_s(x,z)$ decays proportional to $(x^2+z^2)^{-1/4}$, $\hat{\Psi}_1 \mathrm{grad}\psi_s^*$, $\psi_s \mathrm{grad}\hat{\Psi}_1^*$ and $\psi_s \mathrm{grad}\psi_s^*$ vanish at $|x| \to \infty$. Further, $\hat{\Psi}_1 \mathrm{grad}\hat{\Psi}_1^*$ is a periodic function of x with the period L. Using these facts and the identity $\mathrm{Im}[\mathrm{div}(\hat{\Psi}_1+\psi_s)\mathrm{grad}(\hat{\Psi}_1+\psi_s)^*] = 0$, we obtain after some manipulation,

$$\begin{aligned}
&\lim_{N\to\infty} \mathrm{Im}\left[\int_{-(N+\frac{1}{2})L}^{(N+\frac{1}{2})L} \Psi_1(x,z)\frac{\partial}{\partial z}\Psi_1^*(x,z)dx\right] \\
&\quad = \lim_{N\to\infty} \mathrm{Im}\left[\int_{-(N+\frac{1}{2})L}^{(N+\frac{1}{2})L} \hat{\Psi}_1(x,z)\frac{\partial}{\partial z}\psi_s^*(x,z)\right. \\
&\qquad\qquad \left. + \psi_s(x,z)\frac{\partial}{\partial z}\hat{\Psi}_1^*(x,z) + \psi_s(x,z)\frac{\partial}{\partial z}\psi_s^*(x,z)dx\right] = 0,
\end{aligned} \tag{2.32}$$

where $z > 0$. Here, we have applied (2.19).

Substituting (2.15), (2.16) and (2.28) into (2.32), we get a new representation of the optical theorem, which is written as

$$P_c = \Phi_s, \tag{2.33}$$

$$P_c = -\frac{2}{k}\sum_{n=-\infty}^{\infty} \mathrm{Re}[\beta_n^*(p)]\mathrm{Re}[a(k_L m|p)A_n^*(p)], \tag{2.34}$$

$$\Phi_s = \frac{1}{k}\int_{-\infty}^{\infty} \mathrm{Re}[\beta_0(p+s)]|a(s|p)|^2 ds. \tag{2.35}$$

Here, P_c is related to the reduction of the scattering amplitude and Φ_s expresses the total scattering cross section. The optical theorem (2.33) can be used to estimate accuracy of a numerical calculation. It is an extension of the forward scattering theorem [15, 57]. The total scattering cross section can be rewritten as

$$\frac{1}{k}\int_{-\infty}^{\infty} \mathrm{Re}[\beta_0(p+s)]|a(s|p)|^2 ds = \frac{L}{2\pi}\int_0^{\pi} \sigma(\phi|\theta)d\phi, \tag{2.36}$$

where ϕ is the scattering angle and $\sigma(\phi|\theta)$ is the differential scattering cross section per period,

$$\sigma(\phi|\theta) = \frac{2\pi k \sin^2\phi\,|a(-k\cos\phi - p)|^2}{L}, \tag{2.37}$$

which has no dimension.

$$Err^{opt} = \left|1 - \frac{\Phi_s}{P_c}\right| \tag{2.38}$$

Scattered wavefield and single scattering approximation In this section, we determine $a(s|p)$ and $q_m^{(g)}(p)$ to solve the single defect case. From the continuity of both the electric field and the magnetic field, the equations to obtain $a(s|p)$ and $q_m^{(g)}(p)$ are derived.

Since $\Psi_1(x,0) = \Psi_2(x,0)$ means $\psi_s(x,0) = \psi_G(x,0)$, we get

$$\int_{-\infty}^{\infty} a(s|p)e^{i(p+s)x}ds = \sum_{g=-\infty}^{\infty} u(x-gL|w)e^{ipgL} \sum_{m=1}^{\infty} q_m^{(g)}(p)\sin(mk_w(x+w/2-gL))\frac{\sin(\gamma_m d)}{\gamma_m} - u(x|w)\sum_{m=1}^{\infty} Q_m^s(p)\sin(mk_w(x+w/2))\frac{\sin(\gamma_m d)}{\gamma_m}. \quad (2.39)$$

Taking Fourier transform after multiplying $e^{-i(p+s)x}/2\pi$, we obtain the amplitude of the scattered wave $a(s|p)$ as

$$a(s|p) = \frac{1}{2\pi}\sum_{m=1}^{\infty} s_m(p+s)\frac{\sin(\gamma_m d)}{\gamma_m}\left[\sum_{g=-\infty}^{\infty} e^{-isgL}q_m^{(g)}(p) - Q_m^s(p)\right]. \quad (2.40)$$

When the depth d is not so large that the resonance does not occur in the grooves of the grating, the term related to the first order guided mode $m = 1$ may become large. However, when the resonance occurs in the grooves, that is, the value of the depth d satisfies $\sin(\gamma_1 d) = 0$, the summation on m starts from $m = 2$, so the property of the scattering may become different. In such a case, the term related to the second order guided mode $m = 2$ may give large effect in the scattering. This will be discussed later.

On the other hand, from $\sum_{n\neq 0} u(x-gL|w)[\partial\Psi_1/\partial z - \partial\Psi_2/\partial z]_{z=0} = 0$, we obtain $\sum_{n\neq 0} u(x-gL|w)[\partial\psi_s/\partial z - \partial\psi_G/\partial z]_{z=0} = 0$. Then, we get

$$\sum_{g=-\infty}^{\infty} u(x-gL|w)\int_{-\infty}^{\infty} i\beta_0(p+s)a(s|p)e^{i(p+s)x}ds - u(x|w)\int_{-\infty}^{\infty} i\beta_0(p+s)a(s|p)e^{i(p+s)x}ds = \sum_{g=-\infty}^{\infty} u(x-gL|w)e^{ipgL}\sum_{m=1}^{\infty} q_m^{(g)}(p)\sin(mk_w(x+w/2-gL))\cos(\gamma_m d). \quad (2.41)$$

Taking Fourier transform after multiplying $u(x-gL|w) \times \sin(mk_w(x+w/2-gL))$, we obtain

$$i\,(1-\delta_{g0})\int_{-\infty}^{\infty}\beta_0(p+s)s_m(-p-s)e^{isgL}a(s|p)ds = \frac{w}{2}\cos(\gamma_m d)q_m^{(g)}. \quad (2.42)$$

Substituting (2.40) into (2.42), we get the equation for the perturbed component $q_m^{(g)}(p)$ as

$$\sum_{m'=1}^{\infty}\sum_{g'=-\infty}^{\infty} C_{mg}(m',g')q_{m'}^{(g')}(p) = \sum_{m'=1}^{\infty} Q_{m'}^s(p)\left[C_{mg}(m',0) + \delta_{g0}\delta_{mm'}\frac{w}{2}\cos(\gamma_m d)\right]. \quad (2.43)$$

Here, $Q_{m'}^s(p)$ is the base component obtained from (2.24) and (2.26), and $C_{mg}(m',g')$ is given as

$$C_{mg}(m',g') = (1-\delta_{g0})\frac{i}{2\pi}\frac{\sin(\gamma_{m'}d)}{\gamma_{m'}}e^{-ip(g-g')L}\int_{-\infty}^{\infty}\beta_0(s')s_m(-s')s_{m'}(s')e^{is'(g-g')L}ds' - \delta_{gg'}\delta_{mm'}\frac{w}{2}\cos(\gamma_m d), \quad (2.44)$$

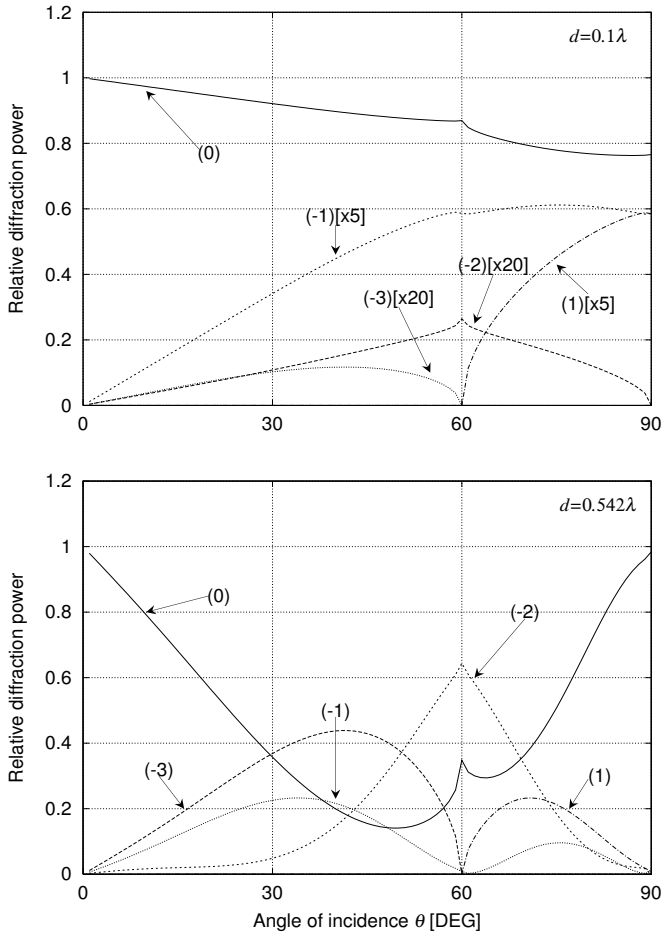

Figure 2.3 Relative diffraction power against the angle of incidence θ for depths $d = 0.1\lambda$(upper figure), 0.542λ(lower figure) with period $L = 2\lambda$ and width $w = 1.3\lambda$, λ is wavelength. Power of incident wave is normalized to 1. The line '(0)' means the relative power of the 0th order Floquet mode, i.e, $\mathrm{Re}[\beta_0(p)]|A_0|^2/\beta_0(p)$, and the line '(1)' that of the 1st order Floquet mode, and so on. In the upper figure for $d = 0.1\lambda$, '[x5]' means that values are multiplied by 5 and '[x20]' means that values are multiplied by 20.

where the integral can be easily evaluated numerically because the integrand decays proportional to $1/s'^3$ when $|s'| \to \infty$. Here, $C_{mg}(m', g')$ represents coupling between the m'th guided mode at the g'th groove and the mth guided mode at the gth groove. Note that the integral part of $C_{mg}(m', g')$ is independent of p. which means that properties of such coupling are determined only by the geometry of the grooves. We will calculate $C_{mg}(m', g')$ numerically to solve (2.43) for the perturbed component $q_m^{(g)}(p)$, in terms of which $a(s|p)$ is calculated.

Single scattering approximation On the other hand, if $q_m^{(g)}(p)$ is small, the approximated amplitude of the scattered wave $\hat{a}(s|p)$ could be calculated from (2.40) only with $Q_m^s(p)$ as

$$\hat{a}(s|p) = -\frac{1}{2\pi} \sum_{m=1}^{\infty} s_m(p+s) \frac{\sin(\gamma_m d)}{\gamma_m} Q_m^s(p), \tag{2.45}$$

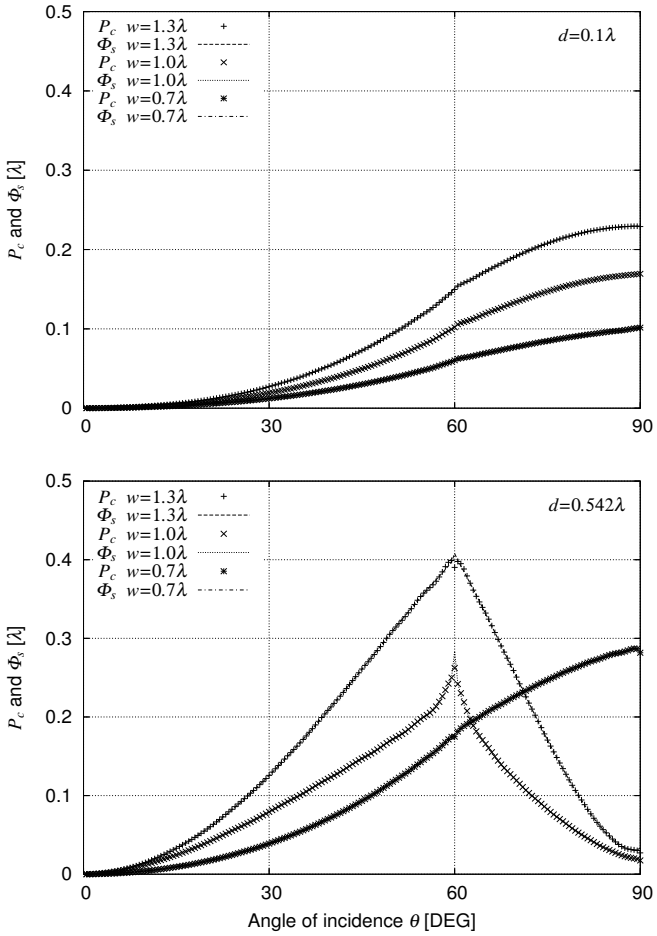

Figure 2.4 Optical theorem against the angle of incidence θ for widths $w = 0.7\lambda$, 1.0λ, 1.3λ with period $L = 2\lambda$, depth $d = 0.1\lambda$(upper figure) and $d = 0.542\lambda$(lower figure), λ is wavelength. Total scattering cross section Φ_s is drawn with line, while the reduction of scattering amplitude P_c is shown with dots.

which we call the single scattering approximation. $\hat{a}(s|p)$ is written only by the base component $Q_m^s(p)$ neglecting $q_m^{(g)}(p)$, which is the effect of coupling between neighboring grooves. We will compare this single scattering approximation $\hat{a}(s|p)$ with numerical solution $a(s|p)$ in what follows.

2.5 Numerical examples

Let us obtain some numerical examples for $L = 2\lambda$.

Since (2.43) is a linear equation for infinitely many unknown $q_m^{(g)}(p)$, it is still an open question how to solve (2.43). However, we attempt to solve this by use of truncation. We introduce the truncation number N_d of the diffraction orders, the truncation number N_m of the

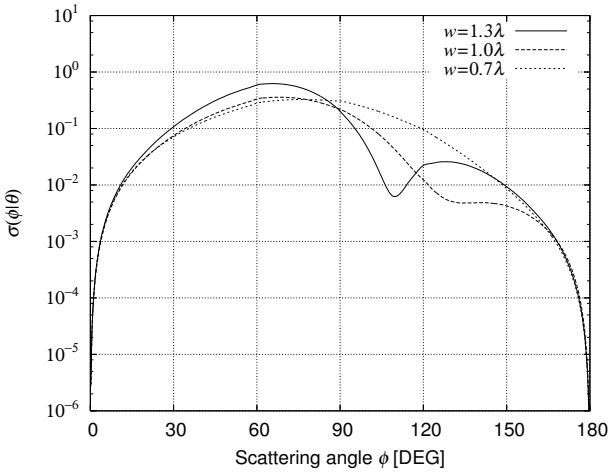

Figure 2.5 Differential scattering cross section $\sigma(\phi|\theta)$ for widths $w = 0.7\lambda$, 1.0λ, 1.3λ with period $L = 2\lambda$, and depth $d = 0.1\lambda$, angle of incidence $\theta = 60°$, λ is wavelength. Note that $\sigma(\phi|\theta)$, which is devided by the period L, has no dimension, since the amplitude of the scattering $a(s|p)$ and k has the dimension of $[m]$ and $[m^{-1}]$, respectively (See eq. (2.37)).

guided modes inside the groove and the number of the grooves N_g. This means that we assume

$$\begin{array}{ll} A_n(p) = 0, & |n| > N_d, \\ Q_m^s(p) \ = 0, & m \ > N_m, \\ q_m^{(g)}(p) = 0, & |g| > N_g, \quad m > N_m, \end{array} \tag{2.46}$$

in the summation (2.24) and (2.26) and we take into account the perturbed effect in the grooves between $g = -N_g$ and N_g, In this case, we set

$$N_d = 7, \quad N_m = 15, \quad N_g = 7. \tag{2.47}$$

Thus, $[A_n(p)]$ becomes a $(2N_d{+}1)$ vector, $[Q_m^s(p)]$ becomes an N_m vector and $[q_m^{(g)}(p)]$ becomes an $(N_m) \times (2N_g + 1)$ matrix in the calculation below. We numerically calculate the base component $Q_m^s(p)$ and $C_{mg}(m', g')$ to solve (2.43) for the perturbed component $q_m^{(g)}(p)$. Then, we obtain a numerical solution $a(s|p)$ to calculate the optical theorem and the scattering cross section.

First, we consider the perfectly periodic case. Figure 2.3 illustrates the relative diffraction power against the angle of incidence θ for the depths $d = 0.1\lambda$ (upper figure) and $d = 0.542\lambda$ (lower figure) with the width $w = 1.3\lambda$. Note that with the depth $d = 0.542\lambda$ the lowest guided mode $l = 1$ becomes resonant, that is, $\sin(\gamma_1 d) = 0$. The power of incident wave is normalized to 1. The line '(0)' means the relative power of the 0th order Floquet mode, i.e, $\mathrm{Re}[\beta_0(p)]|A_0|^2/\beta_0(p)$, and the line '(1)' that of the 1st order Floquet mode, and so on. The energy error is always less than 10^{-14} in these cases. It suggests that the truncation numbers N_d and N_m are sufficient for the perfectly periodic case. For $d = 0.1\lambda$, the power of the 0th mode is quite large. However, for $d = 0.542\lambda$, the powers of the $-$2nd mode and the $-$3rd mode become large and that of the 0th mode decreases when the angle of incidence is between 30° and 70°.

For the case with single defect, we calculate the optical theorem by truncating the number of the grooves with N_g. Figure 2.4 illustrates the total scattering cross section Φ_s and the reduction of the scattering amplitude P_c against the angle of incidence θ for the widths $w = 0.7\lambda$, 1.0λ,

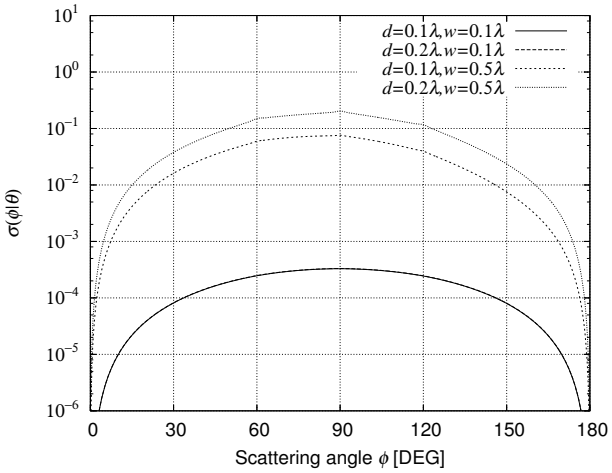

Figure 2.6 Differential scattering cross section $\sigma(\phi|\theta)$ when the widths of the groove are relatively small($w = 0.1\lambda$ and 0.5λ) with period $L = 2\lambda$, angle of incidence $\theta = 60^\circ$ and depths $d = 0.1\lambda$ and 0.2λ, λ is wavelength.

1.3λ with the depths $d = 0.1\lambda$ (upper figure) and 0.542λ (lower figure). The total scattering cross section is drawn with lines, while the reduction of scattering amplitude is shown with dots. In both figures, the total scattering cross section Φ_s almost agrees with the reduction of the scattering amplitude P_c in three cases of w. However, there are some cases in which relative error $Err^{opt} = |(\Psi_s - P_c)/P_c|$ becomes large. For $d = 0.1\lambda$, Err^{opt} is less than 0.01, but, it becomes approximately 0.02 when θ is close to 60° where the 1st mode appears and the -3th mode disappears. For $d = 0.542\lambda$, Err^{opt} is less than 0.02, but, it becomes approximately 0.1 when θ is close to 60°, and becomes approximately 0.2 when θ is close to 90° where the 2nd mode appears and the -2nd mode disappears. When $\theta < 20^\circ$, Err^{opt} increases up to 0.1 for both cases of d. These facts suggest that the truncation in (2.43) gives a reasonable solution in general, but is not good enough for several cases. Thus, practical methods of approximation must be studied to solve (2.43).

Figure 2.5 illustrates the differential scattering cross section $\sigma(\phi|\theta)$ for the widths $w = 0.7\lambda$, 1.0λ, 1.3λ with the depth $d = 0.1\lambda$ and the angle of incidence $\theta = 60^\circ$. The differential scattering cross section is determined by $s_m(q)$ in (2.40), which is the spectrum of the groove with the width w. Figure 2.6 illustrates $\sigma(\phi|\theta)$ when the widths of the groove are relatively small ($w = 0.1\lambda$ and $w = 0.5\lambda$) with the angle of incidence $\theta = 60^\circ$. Calculations are done for two cases of the depths $d = 0.1\lambda$ and 0.2λ. For $w = 0.1\lambda$, which is much smaller than the half wavelength, all order guided modes inside the grooves become cutoff. This makes little difference in the differential scattering cross section for different values of the depth d. Figure 2.7 illustrates $\sigma(\phi|\theta)$ for the angles of incidence $\theta = 90^\circ$, 60°, 30° with the width $w = 1.3\lambda$ and the depths $d = 0.1\lambda$ (upper figure) and 0.542λ (lower figure). It is found that for $d = 0.1\lambda$, scattering is relatively strong in the direction of specular reflection. However, for $d = 0.542\lambda$, the differential scattering cross section seems symmetric with respect to $\phi = 90^\circ$. It may be due to the fact that the resonance inside the grooves depends on the depth d and the width w, but is independent of the angle of incidence θ. In these cases, the term related to the second order guided mode (mainly $s_2(p+s)$) in (2.40) becomes large. For $\theta = 90^\circ$, the scattering amplitude becomes small due to the fact that Q_2^s vanishes for the normal incidence and the term related to the third order guided mode determines the scattering property. Figure 2.8 illustrates $\sigma(\phi|\theta)$ for the depths $d = 0.1\lambda$, 0.271λ,

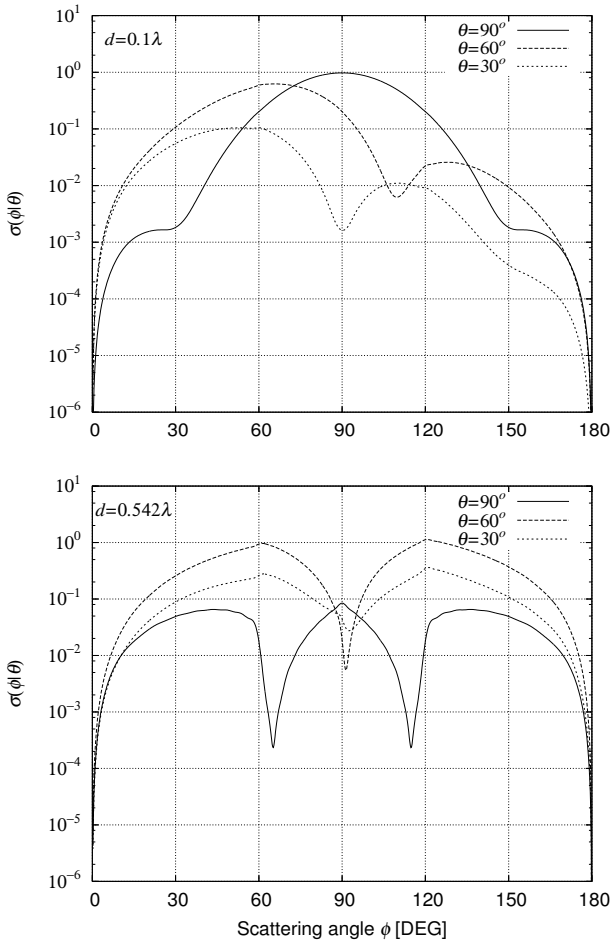

Figure 2.7 Differential scattering cross section $\sigma(\phi|\theta)$ for angles of incidence $\theta = 90°, 60°, 30°$ with period $L = 2\lambda$, width $w = 1.3\lambda$, depth $d = 0.1\lambda$(upper figure) and 0.542λ(lower figure), λ is wavelength.

0.542λ with $w = 1.3\lambda$ and $\theta = 60°$. For $d = 0.1\lambda$ and 0.271λ, the differential scattering cross section increases as the depth d becomes large and the forward scattering around the direction of the specular reflection is relatively strong. However, for $d = 0.542\lambda$, the differential scattering cross section is smaller than that for $d = 0.271\lambda$ around the direction of specular reflection.

Figure 2.9 examines the single scattering approximation (2.45). Comparison of the numerical solution with the single scattering approximation is illustrated for the depths $d = 0.1\lambda$ (upper figure) and 0.542λ (lower figure) with the width $w = 1.3\lambda$ and $\theta = 60°$. For $d = 0.1\lambda$, the single scattering approximation (2.45) almost agrees with the numerical solution, which takes $q_m^{(g)}(p)$ into account. However, for $d = 0.542\lambda$, the agreement becomes worse since some ripples appear in the scattering cross section due to the effect of the perturbed component $q_m^{(g)}$. This may suggest that when the depth of the grooves is not large the interaction between neighboring grooves may be small for TE incidence.

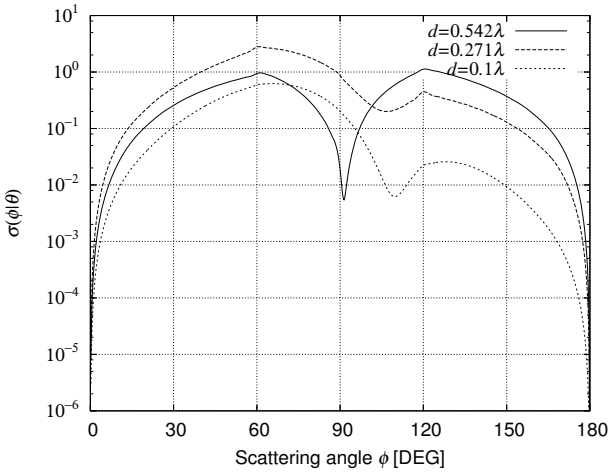

Figure 2.8 Differential scattering cross section $\sigma(\phi|\theta)$ for depths $d = 0.1\lambda$, 0.271λ, 0.542λ with period $L = 2\lambda$, and width $w = 1.3\lambda$ and angle of incidence $\theta = 60°$, λ is wavelength.

2.6 Conclusions

We considered a one-dimensional periodic grating with single defect, of which position is known. We took TE plane wave as an incidence, wrote the wavefield above the grooves as a perturbation from the diffracted wave for the perfectly periodic case. We derived two sets of equations to determine the wavefield from the boundary condition, and we obtained a new representation of the optical theorem, which relates the total scattering cross section with the reduction of the scattering amplitude. Further, we proposed the single scattering approximation given only by the base components for the perfectly periodic grating.

We found that the differential scattering cross section is determined by the spectrum of the groove. This property may be applicable to the measurement of the condition of surfaces combining with the other polarization. We found that when a guided mode in the grooves becomes resonant, the differential scattering cross section becomes almost symmetric even for oblique incidence. We found the single scattering approximation is useful when the depth of the groove is small.

We obtained the scattered wave by use of truncation, and there are several cases in which relative error with respect to the optical theorem becomes large. This means that our truncation method is not good enough and practical methods of approximation must be studied to obtain a highly accurate solution.

Our discussion was limited to the case of TE incidence. It can be extended to TM case, which will be studied in the following chapter.

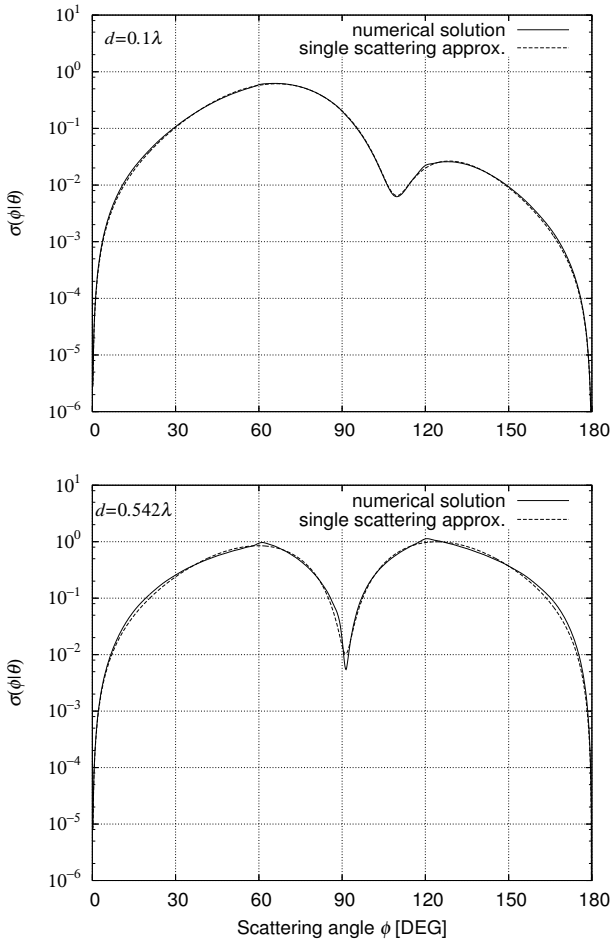

Figure 2.9 Comparison of numerical solution with the single scattering approximation for depths $d = 0.1\lambda$(upper figure) and 0.542λ(lower figure), for period $L = 2\lambda$, width $w = 1.3\lambda$ and angle of incidence $\theta = 60°$, λ is wavelength. The approximation is shown in dotted lines.

Chapter 3

Scattering of TM plane wave from periodic grating with single defect

3.1 Introduction

In the previous chapter, we have discussed the properties of diffraction and scattering of TE plane wave from periodic rectangular grooves with single defect. We successfully obtained the scattered wave as variation from the perfectly periodic case. In this chapter, we will study the TM case.

When a TE plane wave is incident, the scattered wave from a single defect may decay rapidly along the surface. This means that the scattered wave does not affect the distant grooves, thus we have solved an equation for the perturbed component of the guided modes inside the grooves. However, when a TM plane wave is incident, the scattered wave may decay slowly for $|x| \to \infty$ and affect the guided modes in the grooves far from the defect. Therefore, for the TM case, we will solve an integral equation for the scattered wave in the spectral domain by use of the Fourier transform. This point is different from the solution in Chapter 2.

We write the wavefield both above the surface and inside the grooves as a variation from the perfectly periodic case, and obtain a set of equations for the scattered wave and the perturbed component of the guided modes from the Neumann boundary condition. Then, we derive an integral equation for the scattering amplitude in the spectral domain. Then, we numerically obtain the scattering amplitude by use of truncation and the iteration method starting from the diagonal approximation solution as an initial value of the integral. The differential scattering cross section and the optical theorem are calculated in terms of the scattering amplitude and are illustrated in figures.

We begin in Section 3.2 with the mathematical formulation of the perfectly conductive periodic grating with single defect, which is made up with a periodic array of rectangular grooves and a defect where a groove is not formed. In Section 3.3, the diffracted wave and the base component of the guided modes are obtained for the perfectly periodic grating. In Section 3.4, the scattered wave and the perturbed component of the guided mode are represented in terms of the base component of the guided modes obtained in Section 3.3. To determine the scattered wave, we derive an integral equation for the scattered wave, which is solved by the iteration method. Section 3.5 discusses the physical mechanisms of Wood's anomaly and incoherent Wood's anomaly. In Section 3.6, we obtain a numerical solution of the scattered wave by use of iteration method employing the diagonal approximation solution as an initial guess, in terms of

which the optical theorem and the differential scattering cross section are calculated with such an amplitude of the scattered wave and are illustrated in figures. As is well known, in the perfectly periodic case, Wood's anomaly appears for critical angles of incidence as rapid variations of the diffraction powers. In the case of a periodic grating with defect, however, another anomaly, which we call incoherent Wood's anomaly, appears at critical angles of scattering as rapid variations in the angular distribution of the scattering. In this chapter, we discuss the physical mechanisms of Wood's anomaly and incoherent Wood's anomaly. Incoherent Wood's anomaly has been found in cases of periodic random surfaces [6, 8]. However, we newly find that such anomaly appears in the case of a periodic surface with single defect.

3.2 Periodic grating with single defect

Let us consider a periodic array of rectangular grooves with single defect at $x = 0$ (See figure 3.1). We write such an array as

$$z = f(x) = f_p(x) + d \cdot u(x|w), \tag{3.1}$$

$$f_p(x) = -d \sum_{g=-\infty}^{\infty} u(x - gL|w), \tag{3.2}$$

where L is the period, w and d are the width and the depth of a groove. $f_p(x)$ is a perfectly periodic surface without defect and the second term in (3.1) expresses the defect. Here, $u(x|w)$ is a rectangular groove defined as

$$u(x|w) = \begin{cases} 1, & |x| \le w/2, \\ 0, & |x| > w/2. \end{cases} \tag{3.3}$$

It has the orthogonal property such that

$$u(x - gL|w)u(x - g'L|w) = \delta_{gg'}u(x - gL|w), \quad (g, g' = 0, \pm 1, \pm 2, \cdots), \tag{3.4}$$

where $\delta_{gg'}$ is Kronecker's delta. For convenience, we put k_L and k_w as

$$k_w = \pi/w, \quad k_L = 2\pi/L, \tag{3.5}$$

and we define an auxiliary function $c_m(q)$ as follows.

$$c_m(q) \;=\; \int_{-\infty}^{\infty} u(x|w) \cos(mk_w(x + w/2))e^{-iqx}dx, \tag{3.6}$$

where m is integer. Note that $c_m(q) \sim 1/q$ when $|q|$ becomes large.

We denote the y component of the magnetic field by $\Psi(x, z)$, which satisfies the Helmholtz equation

$$\left[\frac{\partial^2}{\partial x^2} + \frac{\partial^2}{\partial z^2} + k^2\right] \Psi(x, z) = 0, \tag{3.7}$$

in the region $z > f(x)$. Here, $k = 2\pi/\lambda$ is wavenumber and λ is wavelength. On the surface $z = f(x)$, the wavefield $\Psi(x, z)$ satisfies the Neumann condition,

$$\left.\frac{\partial \Psi(x, z)}{\partial n}\right|_{z=f(x)} = 0. \tag{3.8}$$

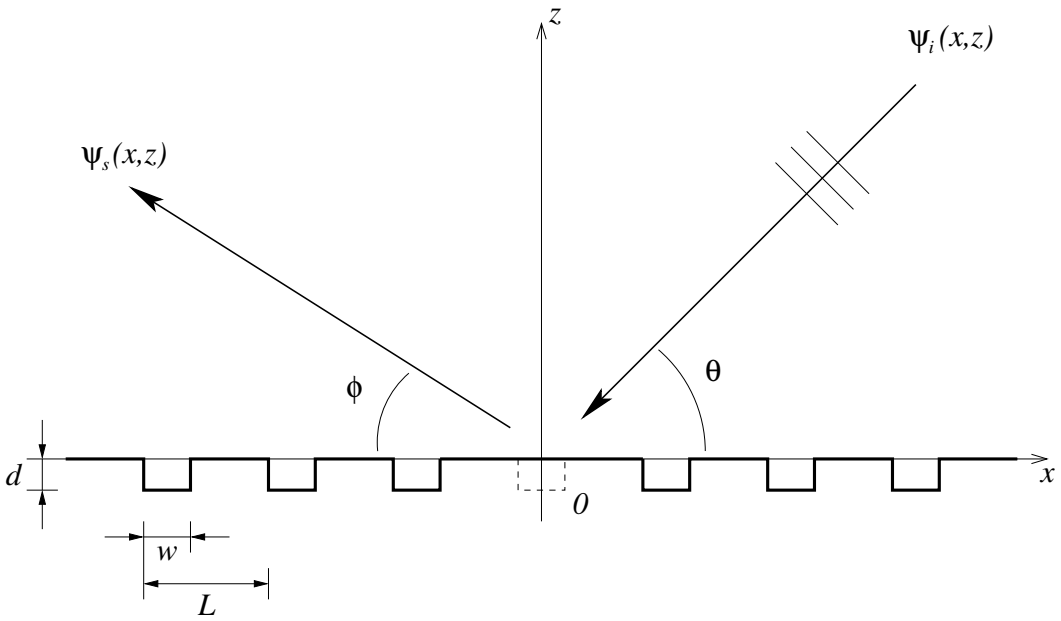

Figure 3.1 Scattering of TM plane wave from a periodic grating with single defect. The surface is a periodic array of rectangular grooves and has a defect where a groove is not formed. $\psi_i(x,z)$ is the incident wave and $\psi_s(x,z)$ is the scattered wave. θ is the angle of incidence, ϕ is the scattering angle, L is the period of surface, w and d are the width and the depth of groove.

We write the incident plane wave $\psi_i(x,z)$ as

$$\psi_i(x,z) = e^{ipx}e^{-i\beta_0(p)z}, \quad p = -k\cos\theta, \tag{3.9}$$

$$\beta_n(p) = \beta_0(p+nk_L) = \sqrt{k^2-(p+nk_L)^2}, \tag{3.10}$$

$$\mathrm{Im}[\beta_n(p)] \geq 0, \quad (n = 0, \pm1, \pm2, \cdots), \tag{3.11}$$

where θ is the angle of incidence (See Figure3.1) and Im stands for the imaginary part.

3.3 Diffraction by a perfectly periodic grating

First, we consider a perfectly periodic case. For the region $z \geq 0$, we write the y component of the magnetic field $\hat{\Psi}_1(x,z)$ as a sum of the incident wave $\psi_i(x,z)$ and the diffracted wave $\psi_d(x,z)$ due to the periodicity of the surface,

$$\hat{\Psi}_1(x,z) = e^{ipx}e^{-i\beta_0(p)z} + \psi_d(x,z), \tag{3.12}$$

$$\psi_d(x,z) = e^{ipx}\sum_{n=-\infty}^{\infty} A_n(p)e^{ink_Lx+i\beta_n(p)z}. \tag{3.13}$$

Here, $A_n(p)$ is the amplitude of the nth order Floquet mode. On the other hand, by use of the modal expansion method [30], we write the y component of the magnetic field inside the grooves $\hat{\Psi}_2(x,z)$ as a sum of the guided modes,

$$\hat{\Psi}_2(x,z) = \sum_{g=-\infty}^{\infty} u(x-gL|w)e^{ipgL}\sum_{m=0}^{\infty} Q_m^c(p)$$

$$\times \cos(mk_w(x+w/2-gL))\cos(\gamma_m(z+d)), \tag{3.14}$$

$$\gamma_m = \sqrt{k^2-(mk_w)^2}, \tag{3.15}$$

where $Q_m^c(p)$ is the amplitude of the guided mode which we call the base component, and γ_m is the propagation constant of the mth guided mode. Note that the guided mode number starts from $m=0$ in the TM case.

The normalized energy conservation relation for the perfectly periodic case can be obtained as

$$1 = \sum_{n=-\infty}^{\infty} \mathrm{Re}[\beta_n(p)]|A_n(p)|^2/\beta_0(p), \tag{3.16}$$

which is same as (2.21) for the TE case. Re denotes the real part and $\mathrm{Re}[\beta_n(p)]|A_n(p)|^2/\beta_0(p)$ is the nth order relative diffraction power. The normalized energy conservation relation will be illustrated below.

Solution for a perfectly periodic grating Let us determine $A_n(p)$ and $Q_m^c(p)$ from the continuity of both the magnetic field and the electric field at $z=0$.

We start with a boundary condition $[\partial\hat{\Psi}_1/\partial z - \partial\hat{\Psi}_2/\partial z]|_{z=0} = 0$. Multiplying this by $e^{-i(p+nk_L)x}$ and integrating over one period L, we get

$$i\beta_n(p)LA_n(p) - i\beta_0(p)L\delta_{n0} = -\sum_{m=0}^{\infty} \gamma_m Q_m^c(p)\sin(\gamma_m d)c_m(p+nk_L). \tag{3.17}$$

Next, we have another boundary condition $\sum_{g=-\infty}^{\infty} u(x-gL|w)[\hat{\Psi}_1(x,0)-\hat{\Psi}_2(x,0)]=0$. Taking Fourier transform of this after multiplying $u(x-gL|w)\times\cos(mk_w(x+w/2-gL))$, we obtain

$$\sum_{n=-\infty}^{\infty} A_n(p)c_m(-p-nk_L) + c_m(-p) = \frac{wQ_m^c(p)}{2}\cos(\gamma_m d)(1+\delta_{m0}). \tag{3.18}$$

Here, (3.17) and (3.18) are infinitely dimensional equations. By use of truncation [29, 30], we will numerically solve (3.17) and (3.18) to obtain $A_n(p)$ and $Q_m^c(p)$.

In what follows, we always consider a non-resonance case, that is, $\cos(\gamma_m d)\neq 0$ for any m. Eliminating $Q_m^c(p)$ from (3.17) and (3.18), we get an equation for $A_n(p)$ as

$$\sum_{l=-\infty}^{\infty} [i\beta_n(p)\delta_{nl} + k_L M(p+nk_L, p+lk_L)]A_l(p) = i\beta_0(p)\delta_{n0} - k_L M(p+nk_L, p), \tag{3.19}$$

where k_L is defined in (3.5), $i\beta_0(p)\delta_{n0}$ is an excitation by the incident wave. and $M(s,s')$ is a coupling factor defined as

$$M(s,s') = \sum_{m=0}^{\infty} \frac{\gamma_m \tan(\gamma_m d)}{\pi w(1+\delta_{m0})} c_m(s)c_m(-s'), \tag{3.20}$$

where the difference $s-s'$ works as a Bragg vector. When the depth of the grooves d is small, $M(s,s')$ becomes small. We regard (3.19) as an infinitely dimensional matrix equation for $A_n(p)$. Thus, the inverse matrix of $[i\beta_n(p)\delta_{nl}+k_L M(p+nk_L, p+lk_L)]$ can be considered as Green's function of the periodic grating in the spectral domain. Since the periodic surface $f_p(x)$ has a discrete spectrum, $M(p+nk_L, p+lk_L)$ represents the discrete Bragg coupling from $A_l(p)$

to $A_n(p)$, where $(p+nk_l)-(p+lk_L) = (n-l)k_L$ is the Bragg vector transforming the wave vector $p+lk_L$ of $A_l(p)$ to $p+nk_L$ of $A_n(p)$. When $p = -k\cos\theta \approx \pm k + lk_L$ $(l = \pm 1, \pm 2, \cdots)$ holds, i.e., $\theta \approx \cos^{-1}(\mp 1 - lk_L/k)$, a well-known phenomenon, so-called Wood's anomaly [28,29], occurs as a rapid variation of the diffraction amplitude. However, as far as the author knows, there have been few discussions on the physical mechanism of Wood's anomaly in the periodic cases. We will point out that such an anomaly is caused by a coupling with guided surface waves [8] in what follows.

In the single defect case, however, the surface $f(x)$ has a continuous component in the spectrum. Thus, a continuous Bragg coupling appears in the case with defect, as is discussed below.

3.4 Scattering from a periodic grating with single defect

The single defect in a periodic grating generates the scattering. We express such scattering as a variation from the diffracted wave for the perfectly periodic case. Thus, we write for $z > 0$,

$$\Psi_1(x,z) = \hat{\Psi}_1(x,z) + \psi_s(x,z), \tag{3.21}$$

$$\psi_s(x,z) = \int_{-\infty}^{\infty} a(s|p) e^{i(p+s)x + i\beta_0(p+s)z} ds, \tag{3.22}$$

where $\psi_s(x,z)$ is the scattered wave due to the defect and $a(s|p)$ is the scattering amplitude. Since $\psi_s(x,z)$ is scattered from the single defect, we assume that $\psi_s(x,z)$ satisfies Sommerfeld's radiation condition, that is, $\psi_s(r\cos\theta, r\sin\theta) \sim f(\theta)e^{ikr}/\sqrt{kr}$ $(r = \sqrt{x^2+z^2})$ and is expected to decay at $kr \to \infty$.

On the other hand, we write the wavefield inside the grooves $\Psi_2(x,z)$ as a sum of the wavefield for the perfectly periodic grating and the fluctuated term $\psi_G(x,z)$ due to the defect.

$$\Psi_2(x,z) = \hat{\Psi}_2(x,z) + \psi_G(x,z), \tag{3.23}$$

$$\psi_G(x,z) = \sum_{g=-\infty}^{\infty} u(x-gL|w) e^{ipgL} \sum_{m=0}^{\infty} q_m^{(g)}(p) \cos(mk_w(x+w/2-gL)) \cos(\gamma_m(z+d)) - u(x|w) \sum_{m=0}^{\infty} Q_m^c(p) \cos(mk_w(x+w/2)) \cos(\gamma_m(z+d)). \tag{3.24}$$

Here, $q_m^{(g)}(p)$ is the perturbed amplitude of the mth guided mode in the gth groove. Note that $q_m^{(0)}(p) \equiv 0$ for all m since a groove is not formed at $g = 0$.

Optical theorem and scattering cross section The optical theorem for the single defect case can be obtained from the identity $\mathrm{Im}[\mathrm{div}\Psi_1 \mathrm{grad}\Psi_1^*] = 0$ as [56]

$$P_c = \Phi_s, \tag{3.25}$$

$$P_c = -\frac{2}{k} \sum_{n=-\infty}^{\infty} \mathrm{Re}[\beta_n^*(p)] \mathrm{Re}[a(k_L n|p) A_n^*(p)], \tag{3.26}$$

$$\Phi_s = \frac{1}{k} \int_{-\infty}^{\infty} \mathrm{Re}[\beta_0(p+s)] |a(s|p)|^2 ds = \frac{L}{2\pi} \int_0^{\pi} \sigma(\phi|\theta) d\phi, \tag{3.27}$$

which is an extension of the forward scattering theorem [15, 57]. Here, the asterisk denotes the complex conjugate, P_c is related to the reduction of the scattering amplitude, Φ_s expresses the total scattering cross section and $\sigma(\phi|\theta)$ is the differential scattering cross section per period

$$\sigma(\phi|\theta) = \frac{2\pi k \sin^2\phi\,|a(-k\cos\phi - p|p)|^2}{L}, \tag{3.28}$$

where $\phi = \cos^{-1}(-(p+s)/k)$ is a scattering angle (See Fig. 1). Note that $\sigma(\phi|\theta)$ has no dimension. The optical theorem (3.25) can be used to estimate accuracy of a numerical solution.

Scattered wavefield by single defect Let us obtain equations for $a(s|p)$ and $q_m^{(g)}(p)$ from the continuity of both the magnetic field and the electric field. From $[\partial\Psi_1/\partial z - \partial\Psi_2/\partial z]|_{z=0} = 0$, we have $[\partial\psi_s/\partial z - \partial\psi_G/\partial z]|_{z=0} = 0$. Taking Fourier transform of this relation and multiplying $e^{-i(p+s)x}/2\pi$, we obtain an equation for $a(s|p)$ and $q_m^{(g)}(p)$ as

$$i\beta_0(p+s)a(s|p) = \frac{1}{2\pi}\sum_{m=0}^{\infty}\gamma_m c_m(p+s)\sin(\gamma_m d)\left[Q_m^c(p) - \sum_{g=-\infty}^{\infty} e^{-isgL} q_m^{(g)}(p)\right]. \tag{3.29}$$

On the other hand, from $\sum_{g\neq 0} u(x-gL|w)[\Psi_1(x,0) - \Psi_2(x,0)] = 0$, we obtain $\sum_{g\neq 0} u(x - gL|w)[\psi_s(x,0) - \psi_G(x,0)] = 0$. Then, taking Fourier transform of this after multiplying $u(x - gL|w) \times \cos(mk_w(x + w/2 - gL))$, we obtain

$$(1-\delta_{g0})\int_{-\infty}^{\infty} c_m(-p-s)e^{isgL}a(s|p)ds = \frac{w}{2}q_m^{(g)}(p)\cos(\gamma_m d)(1+\delta_{m0}). \tag{3.30}$$

Here, (3.29) and (3.30) are infinitely dimensional. However, these equations can be solved approximately by use of truncation.

Substituting (3.30) into (3.29), we get

$$\begin{aligned} i\beta_0(p+s)a(s|p) = &\frac{1}{2\pi}\sum_{m=0}^{\infty}\gamma_m c_m(p+s)\sin(\gamma_m d) \\ &\times\left(Q_m^c(p) - \sum_{g=-\infty}^{\infty} e^{-isgL}\frac{1-\delta_{g0}}{\frac{w}{2}\cos(\gamma_m d)(1+\delta_{m0})}\int_{-\infty}^{\infty} c_m(-p-s')e^{is'gL}a(s|p)ds'\right). \end{aligned} \tag{3.31}$$

Taking the sum on g and using the Fourier series representation of delta pulse series

$$\sum_{g=-\infty}^{\infty} e^{isgL} = k_L\sum_{l=-\infty}^{\infty}\delta(s - lk_L), \tag{3.32}$$

then we get an integral equation for the scattering amplitude $a(s|p)$ as

$$\begin{aligned} &\sum_{l=-\infty}^{\infty}[i\beta_0(p+s)\delta_{l0} + k_L M(p+s, p+s+lk_L)]a(s+lk_L|p) \\ &\qquad = \sum_{m=0}^{\infty}\frac{\gamma_m}{2\pi}c_m(p+s)\sin(\gamma_m d)Q_m^c(p) + \int_{-\infty}^{\infty} M(p+s, p+s')a(s'|p)ds', \end{aligned} \tag{3.33}$$

which is analogous in form with (3.19). Here, $M(p+s, p+s+lk_L)$ on the left-hand side represents a discrete Bragg coupling due to the surface periodicity, whereas $M(p+s, p+s')$ on the right-hand side is a continuous coupling due to the single defect.

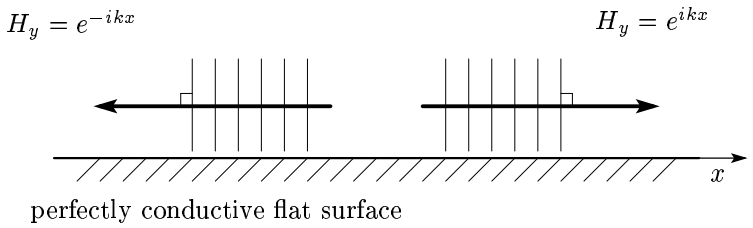

(a) free guided waves along a flat surface

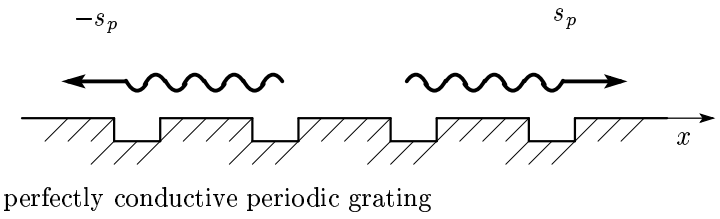

(b) guided surface waves on a periodic grating

Figure 3.2 (a) Free guided waves propagating into the x direction along a perfectly conductive flat surface without any roughness. Such free guided waves have the Rayleigh wavenumber $+k$ and $-k$, and satisfy the Helmholtz equation (3.7) and the Neumann boundary condition $\partial H_y/\partial z = 0$ at $z = 0$. (b) Guided surface waves propagating along the perfectly conductive grating. Guided surface waves have complex propagation constants $\pm s_p$ into the x direction.

We regard (3.33) as an infinitely dimensional matrix equation for $a(s|p)$. Thus, the inverse matrix of $[i\beta_0(p+s)\delta_{l0} + k_L M(p+s, p+s+lk_L)]$ may be considered as Green's function of the periodic grating with single defect. When $p + s = -k\cos\phi \approx \pm k + lk_L$ $(l = \pm 1, \pm 2, \cdots)$ holds, the amplitude of the scattered wave into the direction $\phi \approx \cos^{-1}(\mp 1 - lk_L/k)$ changes rapidly as a function of the scattering angle ϕ, which we call incoherent Wood's anomaly. Such an anomaly may occur due to a strong coupling of the scattered wave with guided surface waves. We will discuss the physical mechanism of incoherent Wood's anomaly and show numerical examples of the anomaly in the angular distribution of the scattering below.

In what follows, we solve (3.33) by iteration.

3.5 Wood's anomaly and Incoherent Wood's anomaly

When $\beta_n(p)$ in (3.19) vanishes, the diffraction amplitude $A_n(p)$ may become large in a shallow case with $d \ll \lambda$. As is well known, this causes Wood's anomaly, which appears at critical angles of incidence as rapid variations of the diffraction powers against the angle of incidence.

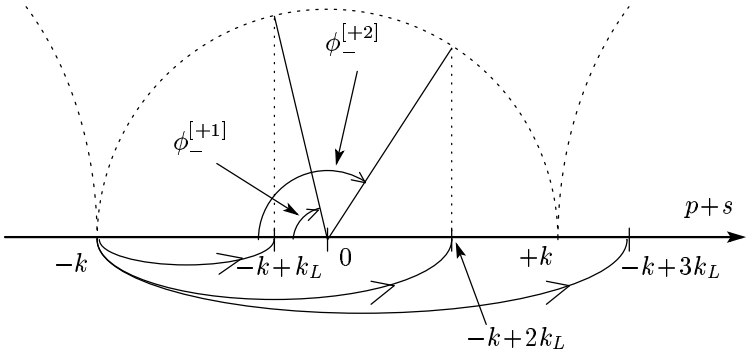

(a) diffraction of the guided surface wave
with the wavenumber near $-k$

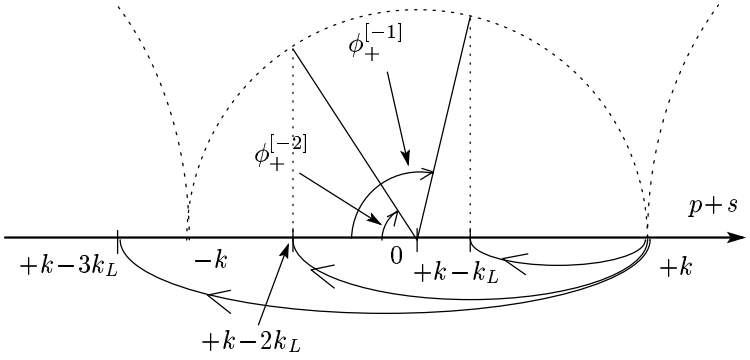

(b) diffraction of the guided surface wave
with the wavenumber near $+k$

Figure 3.3 Incoherent Wood's anomaly at critical angles of scattering (a) $\phi_-^{[+1]}$ and $\phi_-^{[+2]}$ and (b) $\phi_+^{[-1]}$ and $\phi_+^{[-2]}$ for $L = 1.3\lambda$. (a) Guided surface wave with the wavenumber near $-k$ is diffracted into $-k+k_L$ and $-k+2k_L$ by the periodic grating. It is also diffracted to $-k+3k_L$ in the evanescent region. (b) Guided surface wave with the wavenumber near $+k$ is diffracted into $+k-k_L$ and $+k-2k_L$ by the periodic grating. It is also diffracted to $+k-3k_L$ in the evanescent region.

First, we point out a mathematical fact. In a flat surface case without any roughness, TM plane waves with the Rayleigh wavenumber $+k$ and $-k$ are the exact solutions of the Helmholtz equation (3.7) and satisfy the Neumann boundary condition on the surface (See figure 3.2 (a)):

$$H_y = e^{\pm ikx \pm i\beta_0(\pm k)z} = e^{\pm ikx} \tag{3.34}$$

$$\frac{\partial H_y}{\partial z} = 0 \quad (z = 0) \tag{3.35}$$

Therefore, a plane wave with the Rayleigh wavenumber $+k$ or $-k$ is a free guided wave propagating along the flat surface [20, 58]. Such a free guided wave does not exist in the TE case. When the surface has a periodic structure, such a free guided wave is scattered by the surface roughness and decays exponentially with propagation distance. As a result, it becomes a guided surface wave with a complex propagation constant $+s_p$ or $-s_p$ into the x direction (See figure 3.2 (b)). Mathematically, such $\pm s_p$ are given as complex roots of the determinant of $[i\beta_n(p)\delta_{nl} + k_L M(p+nk_L, p+lk_L)]$. When the surface roughness is sufficiently small, however, we may expect that the complex propagation constant s_p exists very close to the Rayleigh wavenumber k [†]. In the case of a perfectly periodic surface, the surface has a discrete spectrum, and such a guided surface wave is excited by the incident wave due to the discrete Bragg coupling. Therefore, such excitation takes place only for the critical angles of incidence $\theta_W^{[l]}$, which are determined by

$$k^2 - (-k\cos\theta_W^{[l]} - lk_L)^2 = 0, \quad (l = \pm 1, \pm 2, \cdots). \tag{3.36}$$

When the angle of incidence θ is critical, such a guided surface wave is excited and may have a large amplitude. Then, it is scattered by the periodic surface again. Thus, the multiple scattering takes place for a critical angle of incidence, which causes Wood's anomaly. As a result, Wood's anomaly appears as rapid variations of the diffraction powers. Note that, at $\theta = \theta_W^{[l]}$, the lth order Floquet mode becomes cutoff.

In the case of a periodic grating with single defect, another anomaly, which we call incoherent Wood's anomaly, appears at several angles of scattering as rapid variations in the angular distribution of the scattering. The surface spectrum has a discrete component due to the periodicity and a continuous component due to the defect. Because of the scattering by the continuous component, such a guided surface wave is always excited by the incident plane wave with any angle of incidence and then diffracted into discrete directions by the discrete component. To describe these processes, we introduce a critical wavenumber $s_\pm^{[l]}$ as

$$s_\pm^{[l]} = \pm k - p + lk_L, \quad (l = 0, \pm 1, \pm 2, \cdots). \tag{3.37}$$

Let us consider the solution $a(s|p)$ of (32). When $\beta_0(p+s) = 0$ and $s = s_\pm^{[0]} = \pm k - p$, the solution $a(s|p) = a(s_\pm^{[0]}|p)$ has a large amplitude, because $M(p+s, p+s+lk_L)$ is small in the shallow case. We regard $a(s_\pm^{[0]}|p)$ as the amplitude of the guided surface wave, which is diffracted into discrete directions. This means that $a(s_\pm^{[l]}|p) = a(\pm k - p + lk_L|p)$ could have a large amplitude for any integer l, due to the discrete Bragg coupling from $s_\pm^{[0]} = (\pm k - p)$ to $s_\pm^{[l]} = (\pm k - p + lk_L)$. Thus, we may observe incoherent Wood's anomaly at a critical angle of

[†]Since this complex propagation constant s_p should exist very close to the Rayleigh wavenumber k in the shallow case, we assume $\mathrm{Re}(s_p) \approx k$ and put such complex s_p as real k in the following discussion for simplicity.

scattering $\phi_{\pm}^{[l]}$ (See figure 3.3),

$$p + s_{\pm}^{[l]} = \pm k + lk_L = -k\cos\phi_{\pm}^{[l]}, \tag{3.38}$$

$$\phi_{\pm}^{[l]} = \cos^{-1}\left(\mp 1 - l\frac{\lambda}{L}\right), \quad (l = \pm 1, \pm 2, \cdots), \tag{3.39}$$

where the signs $\pm$ and $\mp$ go together in (5.65). In the numerical results below, we will see that $|a(s|p)|$ has a steep peak or dip at $s = s_{\pm}^{[l]} = \pm k + lk_L$. Note that $s_{\pm}^{[l]}$ and $\phi_{\pm}^{[l]}$ only depend on the period L and the wavelength λ and are independent of the angle of incidence θ.

Incoherent Wood's anomaly has been found in cases of periodic random surfaces [6,8]. However, we newly show that it takes place in such a deterministic case as a periodic surface with single defect. We also note that incoherent Wood's anomaly appears in the TM case but does not occur in the TE case [56].

3.6 Numerical examples

3.6.1 Perfectly periodic case

Here, we obtain some numerical examples for the perfectly periodic case. We determine the diffraction amplitude $A_n(p)$ and the base component $Q_m^c(p)$ by introducing the truncation numbers N_d and N_m. N_d is the truncation number of the diffraction orders and N_m is that of the guided modes inside the groove in the summation (3.17) and (3.18), which means that we assume

$$\begin{array}{ll} A_n(p) = 0, & |n| > N_d, \\ Q_m^c(p) = 0, & m > N_m. \end{array} \tag{3.40}$$

In this paper, we set

$$N_d = 10, \quad N_m = 20. \tag{3.41}$$

Thus, $[A_n(p)]$ becomes a $(2N_d{+}1)$-vector, $[Q_m^c(p)]$ becomes an $(N_m{+}1)$-vector in the calculation below.

Figure 3.4 illustrates the relative diffraction power against the angle of incidence θ for the periods $L = 1.3\lambda$ (upper figure) and $L = 1.7\lambda$ (lower figure) with the width $w = 0.7\lambda$ and the depth $d = 0.1\lambda$. The incident power is normalized to 1. The line '(0)' means the relative power of the 0th order Floquet mode, i.e, $\mathrm{Re}[\beta_0(p)]|A_0|^2/\beta_0(p)$, and the line '(1)' that of the 1st order Floquet mode, and so on. The energy error defined in (2.22) is always less than 10^{-10}, which suggests that the truncation numbers N_d and N_m in (3.41) are sufficient for the perfectly periodic case. For $L = 1.3\lambda$, the diffraction power changes rapidly near the critical angles $\theta_W^{[-2]} = 57.42^\circ$ and $\theta_W^{[1]} = 76.66^\circ$ given by (3.36). For $L = 1.7\lambda$, Wood's anomaly appears at critical angles $\theta_W^{[-3]} = 40.12^\circ$, $\theta_W^{[1]} = 65.68^\circ$ and $\theta_W^{[-2]} = 79.84^\circ$.

3.6.2 Single defect case

Let us solve the integral equation (3.33) to obtain numerical examples for the single defect case. Here, we only consider the case with $w = 0.7\lambda$.

Since (3.33) is an equation for infinitely many unknowns and has an integral term including $a(s'|p)$, it is still an open question how to solve (3.33). In this paper, we attempt to solve (3.33) approximately by the iteration method. However, we introduce a single scattering approximation and a diagonal approximation.

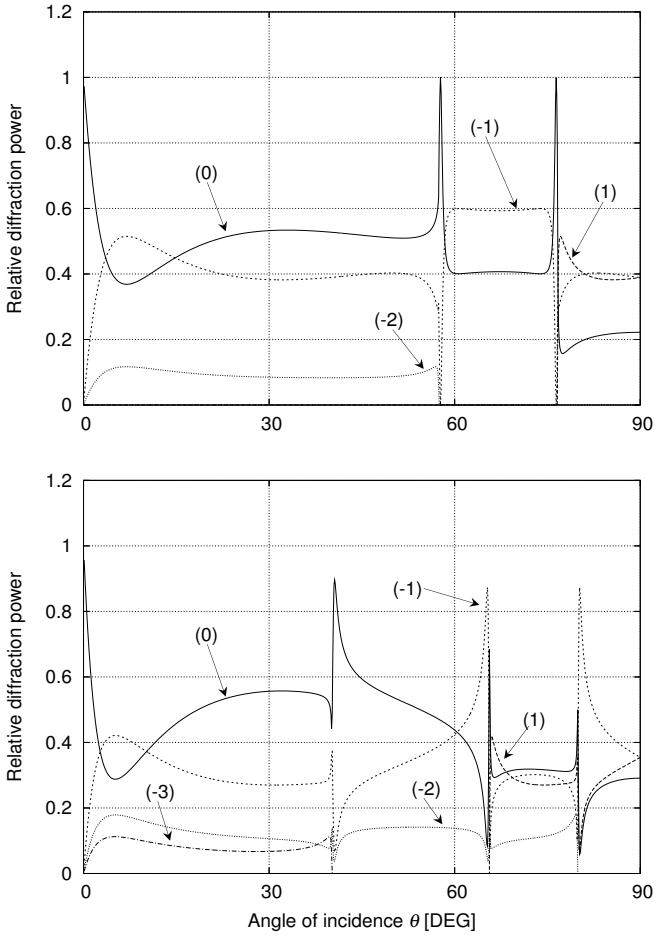

Figure 3.4 Relative diffraction power against the angle of incidence θ for periods $L = 1.3\lambda$(upper figure), 1.7λ(lower figure) with depth $d = 0.1\lambda$ and width $w = 0.7\lambda$. The line '(0)' means the relative power of the 0th order Floquet mode, i.e, $\mathrm{Re}[\beta_0(p)]|A_0|^2/\beta_0(p)$, and the line '(1)' that of the 1st order Floquet mode, and so on. Wood's anomaly occurs at angles where one particular diffraction mode disappears.

Single scattering approximation First, neglecting $M(p+s, p+s+lk_L)$ and the integral term in (3.33), we obtain a single scattering solution $a^S(s|p)$ as

$$a^S(s|p) = \frac{1}{2\pi} \sum_{m=0}^{N_m} \frac{\gamma_m c_m(p+s) \sin(\gamma_m d) Q_m^c(p)}{i\beta_0(p+s)}, \tag{3.42}$$

where $\sum_{m=0}^{N_m} \gamma_m c_m(p+s) \sin(\gamma_m d) Q_m^c(p)$ represents the effect of the single defect, however, the discrete Bragg coupling and the continuous Bragg coupling are neglected. Since the factor $1/\beta_0(p+s)$ is the free space Green's function in the spectral domain, the single scattering approximation gives non-vanishing amplitudes for the grazing limit of the scattering angles and no peaks nor dips appear in the differential scattering cross section, as is illustrated in Figure 3.6. It is due to the fact that (3.42) does not involve effects of the diffraction by the periodic surface.

Diagonal approximation Next, neglecting the integral term in (3.33), we obtain an equation for the diagonal approximation $a^D(s|p)$ with the truncation numbers N_l and N_m as

$$\sum_{l=-N_l}^{N_l} \left[i\beta_0(p+s)\delta_{l0} + k_L M(p+s, p+s+lk_L) \right] a^D(s+lk_L|p)$$
$$= \sum_{m=0}^{N_m} \frac{\gamma_m}{2\pi} c_m(p+s) \sin(\gamma_m d) Q_m^c(p), \tag{3.43}$$

which is solved numerically. Such the diagonal approximation is analogous to the Gaussian random rough case discussed in [53]. The diagonal approximation $a^D(s|p)$ is then used as an initial guess of the iterative solution below.

Numerical calculation by iteration To solve (3.33), however, we rewrite (3.33) as an iterative form,

$$\sum_{l=-N_l}^{N_l} \left[i\beta_0(p+s)\delta_{l0} + k_L M(p+s, p+s+lk_L) \right] a^{(N)}(s+lk_L|p)$$
$$= \sum_{m=0}^{N_m} \frac{\gamma_m}{2\pi} c_m(p+s) \sin(\gamma_m d) Q_m^c(p) + \int_{-\xi-p}^{\xi-p} M(p+s, p+s') a^{(N-1)}(s'|p) ds', \tag{3.44}$$

where $^{(N)}$ is the iteration number and ξ is the truncated bandwidth of $a(s|p)$. We set the initial value as $a^{(0)}(s|p) = a^D(s|p)$ and iteration is repeated until $N = N_{ite}$. In this paper, we set N_l, ξ and N_{ite} as

$$N_l = 11, \quad \xi = 3k, \quad N_{ite} = \begin{cases} 21, & (d = 0.05\lambda), \\ 31, & (d = 0.1\lambda), \\ 51, & (d = 0.125\lambda,\ 0.15\lambda). \end{cases} \tag{3.45}$$

Figure 3.5 illustrates the diagonal approximation $a^D(s|p)$ against wavenumber s with $L = 1.3\lambda$, $d = 0.1\lambda$, $\theta = 90^\circ$ ($p = -k\cos\theta = 0$). As is discussed above, $a^D(s|p)$ becomes large at

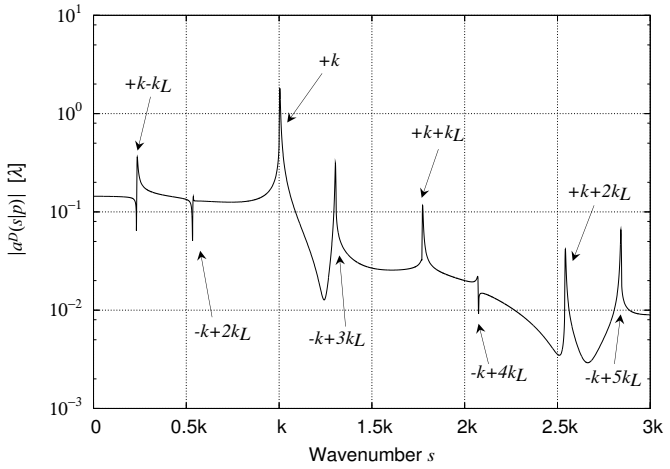

Figure 3.5 Diagonal approximation $a^D(s|p)$ with $L = 1.3\lambda$, $d = 0.1\lambda$, $w = 0.7\lambda$ and $\theta = 90°$ ($p = 0$). $a^D(s|p)$ has steep peaks and dips at $s \approx +k$ and $s \approx s_{\pm}^{[l]} = \pm k + lk_L$ ($l = \pm 1, \pm 2, \cdots$).

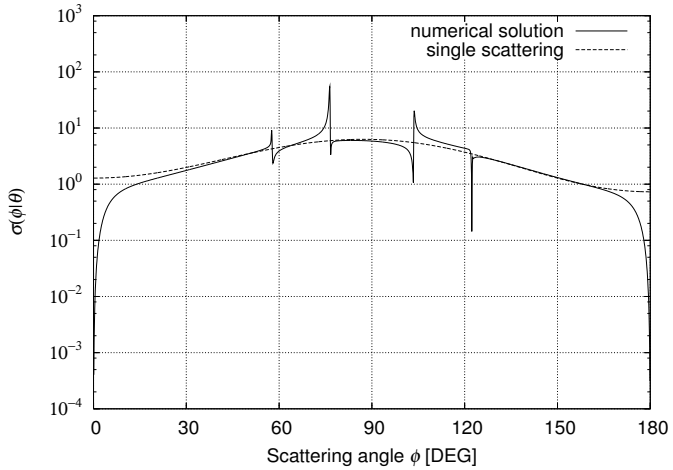

Figure 3.6 Comparison of differential scattering cross section $\sigma(\phi|\theta)$ by numerical solution and single scattering approximation with $L = 1.3\lambda$, $d = 0.1\lambda$ and $w = 0.7\lambda$ and $\theta = 60°$. Note that $\sigma(\phi|\theta)$, which is devided by the period L, has no dimension, since the amplitude of the scattering $a(s|p)$ and k has the dimension of $[m]$ and $[m^{-1}]$ respectively (See eq. (3.28)).

$s \approx -p + k = +k$, which means the guided surface wave propagating along the surface has a large amplitude at the Rayleigh wavenumber $\beta_0(p+s) = 0$. Such the guided surface wave is diffracted by the periodic surface. As a result, $a^D(s|p)$ has several steep peaks and dips at $s \approx s_{\pm}^{[l]} = \pm k + lk_L$ $(l = \pm 1, \pm 2, \cdots)$ given by (3.38), and incoherent Wood's anomaly appears in the differential cross section at $\phi \approx \phi_{\pm}^{[l]}$.

Figure 3.6 illustrates the differential scattering cross section $\sigma(\phi|\theta)$ with $L = 1.3\lambda$, $d = 0.1\lambda$ and $\theta = 60°$. Here, the iterative solution by (3.44) is compared with the single scattering solution (3.42). We see that, in the differential scattering cross section $\sigma(\phi|\theta)$ by the iterative solution, incoherent Wood's anomaly appears near the critical angles of scattering, which are calculated by (5.65) with $L = 1.3\lambda$ as $\phi_+^{[-2]} = 57.42°$, $\phi_-^{[1]} = 76.66°$, $\phi_+^{[-1]} = 103.34°$ and $\phi_-^{[2]} = 122.58°$. It is important to note that the iterative solution $a^{(N)}(s|p)$ gives $\sigma(\pi|\theta) = 0$ and $\sigma(0|\theta) = 0$, which mean that no scattering takes place into grazing directions due to the periodic surface. On the other hand, the single scattering approximation $a^S(s|p)$ yields no peaks and dips in the differential scattering cross section $\sigma(\phi|\theta)$. But it gives non-vanishing amplitudes for $\sigma(\pi|\theta)$ and $\sigma(0|\theta)$. This is because the single scattering approximation neglects the scattering by the periodic surface. In the following calculation, the iterative solution $a^{(N)}(s|p)$ is used to evaluate $\sigma(\phi|\theta)$. Figure 3.7 illustrates $\sigma(\phi|\theta)$ for $\theta = 76°$ and $60°$ with $L = 1.3\lambda$ and $d = 0.1\lambda$. This figure shows that the critical scattering angles at which incoherent Wood's anomaly appears are independent of the incident angles θ. For $\theta = 76°$, however, the total scattering cross section becomes much larger than that with $\theta = 60°$. This is because $\theta = 76°$ is close to a critical angle of incidence $\theta_W^{[1]} = 76.66°$. This point will be shown later. Figure 3.8 illustrates $\sigma(\phi|\theta)$ for $L = 1.3\lambda$ and $L = 1.7\lambda$ with $d = 0.1\lambda$ and $\theta = 60°$. It can be seen that scattering angles at which incoherent Wood's anomaly appears depend on the period L and the wavelength λ. This is because $\phi_{\pm}^{[l]}$ is dependent on the period. Figure 3.9 illustrates $\sigma(\phi|\theta)$ for $d = 0.1\lambda$ and $d = 0.05\lambda$ with $L = 1.3\lambda$ and $\theta = 60°$. Behavior of $\sigma(\phi|\theta)$ near $\phi_+^{[-2]}$ and $\phi_-^{[1]}$ is shown in the lower figure. It is found that, in the shallow case with $d = 0.05\lambda$, anomalous peaks and dips become narrow and steep.

Figure 3.10 illustrates the total scattering cross section Φ_s and the reduction of the scattering amplitude P_c against θ for $L = 1.3\lambda$, $d = 0.1\lambda$. The total scattering cross section Φ_s is drawn with dots, while the reduction of scattering amplitude P_c is shown with line. P_c and Φ_s becomes large when the angle of incidence θ is close to one of the critical angles of incidence $\theta_W^{[1]} = 76.66°$. Figure 3.11 shows the normalized optical theorem P_c/Φ_s for $d = 0.05\lambda$, 0.1λ, 0.125λ and 0.15λ with $w = 0.7\lambda$ and $L = 1.3\lambda$ in the upper figure. Behavior of P_c/Φ_s between $\theta = 73°$ and $\theta = 79°$ is shown in the lower figure. From figure 3.11, it is found that error $|1 - P_c/\Phi_s|$ is less than 0.1 for any angles of incidence except for ones close to the critical angle of incidence $\theta_W^{[l]}$ and grazing angle incidence smaller than 10°. For the incident angles close to $\theta_W^{[l]}$, error become large, which suggests that the iterative solution of the integral equation has limitation to apply and other approaches might be necessary to obtain a highly accurate solution.

3.7 Conclusions

We have considered the scattering of a TM plane wave from a periodic grating with single defect. We wrote the scattered wave above the grooves as a variation from the diffracted wave for the perfectly periodic case. Then, we obtained an integral equation for the scattering amplitude,

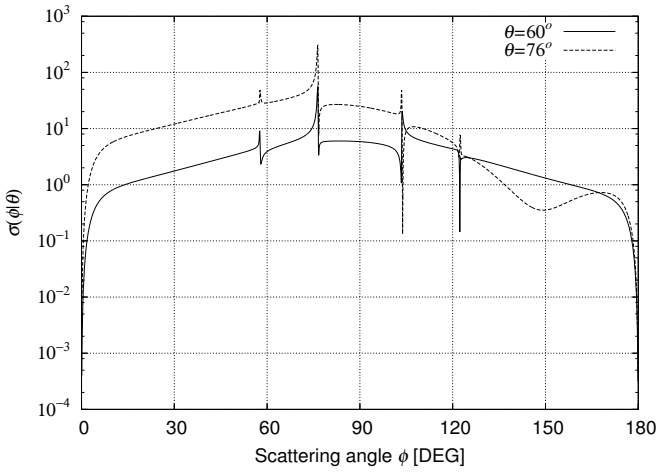

Figure 3.7 Differential scattering cross section $\sigma(\phi|\theta)$ for $\theta = 60^\circ$ and 76° with $L = 1.3\lambda$, $d = 0.1\lambda$ and $w = 0.7\lambda$.

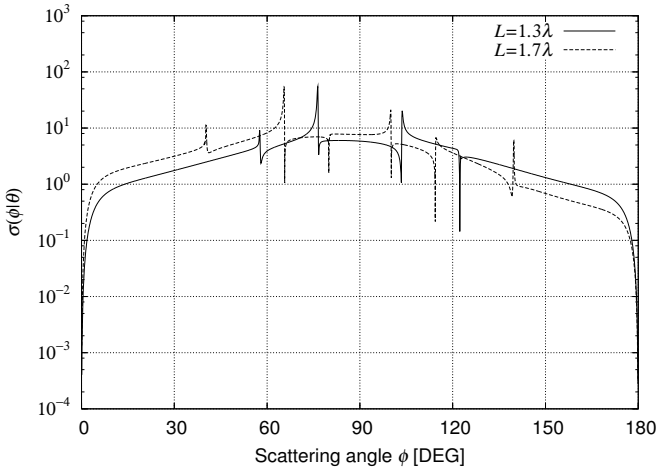

Figure 3.8 Differential scattering cross section $\sigma(\phi|\theta)$ for $L = 1.3\lambda$ and 1.7λ with $w = 0.7\lambda$, $d = 0.1\lambda$ and $\theta = 60^\circ$.

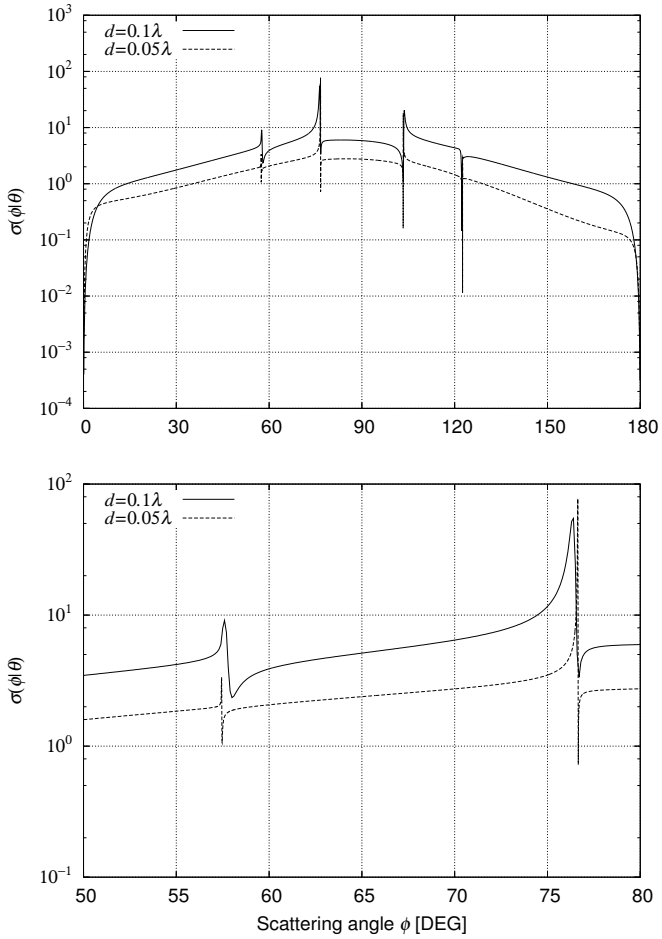

Figure 3.9 Differential scattering cross section $\sigma(\phi|\theta)$ for $d = 0.1\lambda$ and $d = 0.05\lambda$ with $L = 1.3\lambda$, and $\theta = 60°$(upper figure), and the behavior of $\sigma(\phi|\theta)$ near $\phi_W^{[l]}$ (lower figure). Widths of the peaks and dips are smaller for $d = 0.05\lambda$.

which is solved by the iteration method using the diagonal approximation solution as an initial guess.

We found that incoherent Wood's anomaly appears in the differential scattering cross section for the periodic grating with single defect. The critical angles of scattering where incoherent Wood's anomaly appears only depend on the period of the grating and the wavelength, and are independent of the angle of incidence. We pointed out that incoherent Wood's anomaly is caused by the diffraction of the guided surface waves.

When the angle of incidence becomes close to one of the critical angles of incidence or close to a low grazing angle, error with respect to the optical theorem becomes large. This means that our iterative solution is not good enough for such angles of incidence. Therefore, practical methods of approximation must be studied to obtain a highly accurate solution.

Our discussion in Chapter 2 and Chapter 3 was limited to the single defect case in the periodic grating. However, there are other mathematical models of periodic grating with defects: one is a case with double or finite number of defects of which positions are known. Another model is a case with random defects, that is, the defect probability is known but their positions are unknown. It is theoretically interesting to study such periodic gratings with defects. Although it is practically important to consider a metallic or dielectric grating with single defect for the optical measurement or inspection, it is still difficult to treat the cases with defects for such materials. However, these problems are left for the future studies.

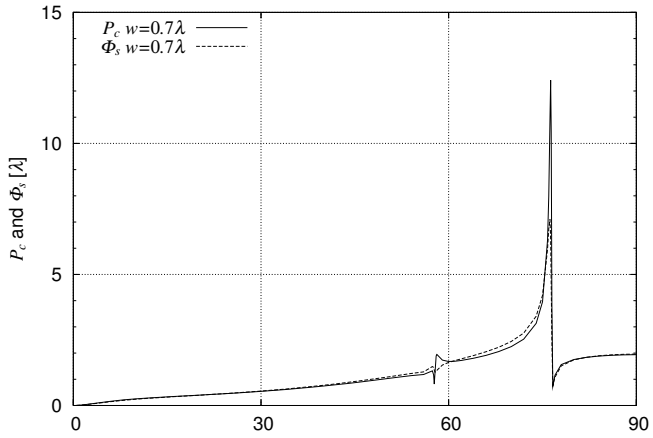

Figure 3.10 Optical theorem against θ for $w = 0.7\lambda$ with $L = 1.3\lambda$, $d = 0.1\lambda$. P_c and Φ_s are shown in the figure.

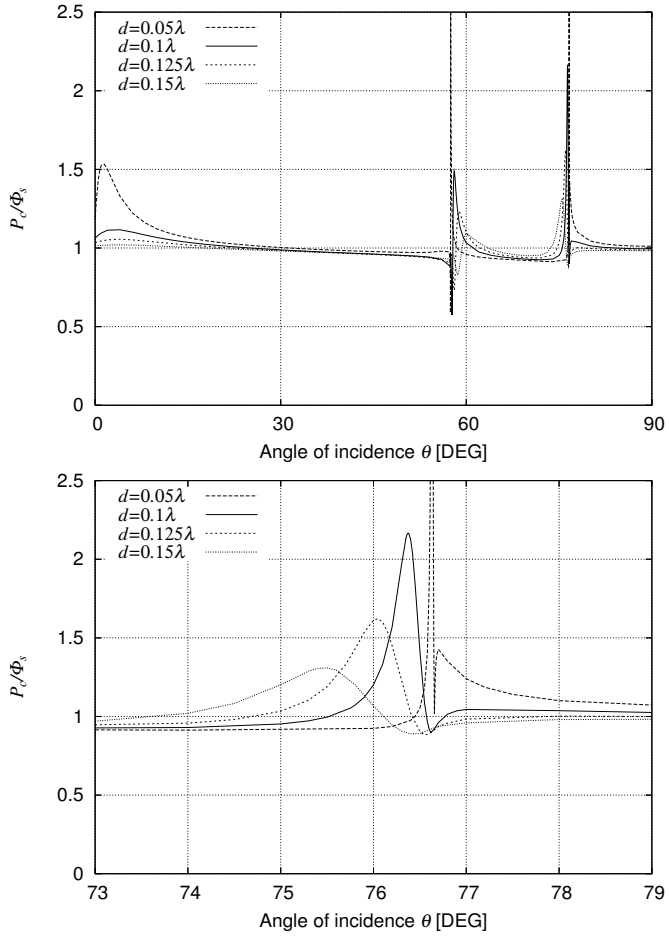

Figure 3.11 Normalized optical theorem P_c/Φ_s against θ for $d = 0.05\lambda$, 0.1λ, 0.125λ and 0.15λ with $w = 0.7\lambda$ and $L = 1.3\lambda$. Behavior of P_c/Φ_s between $\theta = 73°$ and $\theta = 79°$ is shown in the lower figure.

Chapter 4

Diffraction and scattering of TE plane wave from a binary periodic random surface

4.1 Introduction

Natural and artificial periodic surfaces often have randomly fluctuating components. For example, real gratings are not ideally periodic but have fluctuations due to inaccurate fabrications [1–4]. Other examples are ocean surfaces which are sometimes modeled by a sinusoidal surface superimposed with random ripples of small amplitude [61]. Recently, digital recording devices which store binary random data are widely used. These devices usually record data by periodically located binary surface deformations, and it has been required higher density integration of devices and more accuracy in manufacturing processes. Therefore, it has been an important problem to study the diffraction and scattering from such periodic random surfaces with binary deformation. Although they are theoretically interesting and practically important [5, 6], diffraction and scattering from such a binary periodic random surface have not been extensively studied.

This and the following chapters deal with the scattering of plane waves from a binary periodic random surface making use of the concept of periodic stationary processes in the probability theory. This chapter studies the case of TE plane wave incidence. A periodic stationary process is a non-stationary process [51, 65], of which ensemble average and correlation function are periodic. We assume that the binary periodic random surface is generated by a stochastic binary sequence taking only ± 1 with equal probability, shown in figure 4.1. Since such a binary periodic random surface is simple in structure, it may be easy to fabricate and may be applicable as a standard random surface with known statistical properties. For analysis, we employ by the stochastic functional approach [7, 8, 44, 59], which is made up of several steps. First, by use of the shift invariance property of the periodic random surface, the scattered wave is shown to become a product of an exponential phase factor and an unknown periodic stationary process of which average and correlation functions are periodic. We regard such periodic stationary processes as stochastic functionals of the binary sequence [49,60] generating the periodic random surface and they are represented by a sum of orthogonal binary functional series with unknown binary kernels. We write such binary kernels by multiple Fourier integrals. Dividing such Fourier integrals into bands with equal band width, we then find that the unknown periodic

stationary process is reduced to a sum of mutually correlated stationary processes given by binary functionals with band-limited binary kernels, which can be considered as "Fourier series", where "Fourier coefficients" are the mutually correlated stationary processes. Such binary functionals were studied in [44] to calculate properties of the scattering and diffraction from a binary periodic random surface. However, only the first order binary kernels were obtained from an approximate boundary condition for a sufficiently small surface roughness. No mathematical discussions were given for higher order binary functionals representing mutually correlated stationary processes. Thus, this chapter discusses such binary functionals representing the stationary processes to obtain the second order scattering.

Hierarchical equations for such unknown binary kernels are derived from the Dirichlet boundary condition without approximation. We then determine the band-limited binary kernels up to the second order, from which several statistical properties of the scattering, such as scattering cross section and optical theorem, are numerically calculated and illustrated in figures. It is found that the second order incoherent scattering has dips in the diffraction direction of the coherent Floquet modes.

We find that the binary and Gaussian cases become essentially different in the second order. It is shown that, in the binary case, the second order scattering cross section has a subtractive term and becomes much smaller than the first order one. This is mathematically caused by a fact that, for a binary random variable b taking $\pm$ 1, b^2 always becomes a constant equal to 1, whereas ϵ^2 remains random when ϵ is a Gaussian random variable.

4.2 Probabilistic formulation of the problem

Let us consider a periodic random surface, shown in figure 4.1, where the surface deformations are expressed by a periodic stationary process $f(x,\omega)$ generated by a binary sequence :

$$z = f(x,\omega) = \sigma \sum_{m=-\infty}^{\infty} g(x-mL) b_m(\omega), \qquad (-\infty < x < \infty), \tag{4.1}$$

$$= \sigma g(x) b_0(\omega), \qquad (-L/2 < x < L/2). \tag{4.2}$$

Here, L is the period, $g(x)$ is the local surface profile with $g(x) = 0$ for $|x| \geq L/2$ under which (4.2) holds. The $b_m(\omega)$ is an independent stationary binary sequence taking ± 1 with equal probability : $P(b_m = 1) = P(b_m = -1) = 1/2$. Then, $b_m(\omega)$ has zero average and orthogonal correlation,

$$\langle b_m(\omega) \rangle = 0, \qquad \langle b_m(\omega) b_n(\omega) \rangle = \delta(m,n), \tag{4.3}$$

where ω is a probability parameter denoting a sample point in the sample space Ω, the angular brackets $\langle \cdot \rangle$ denote the ensemble average over Ω, and $\delta(m,n)$ is the Kronecker delta. Furthermore, it is important to notice that $b_m(\omega)$ is random, but $b_m^2(\omega)$ takes the deterministic value 1 :

$$b_m^2(\omega) = 1. \tag{4.4}$$

When $\epsilon_m(\omega)$ is a Gaussian random variable, $\epsilon_m^2(\omega)$ is also random. Thus, (4.4) is the special property of the binary random variable $b_m(\omega)$, which may lead an essential difference between Gaussian and binary cases in the statistical properties of the scattering.

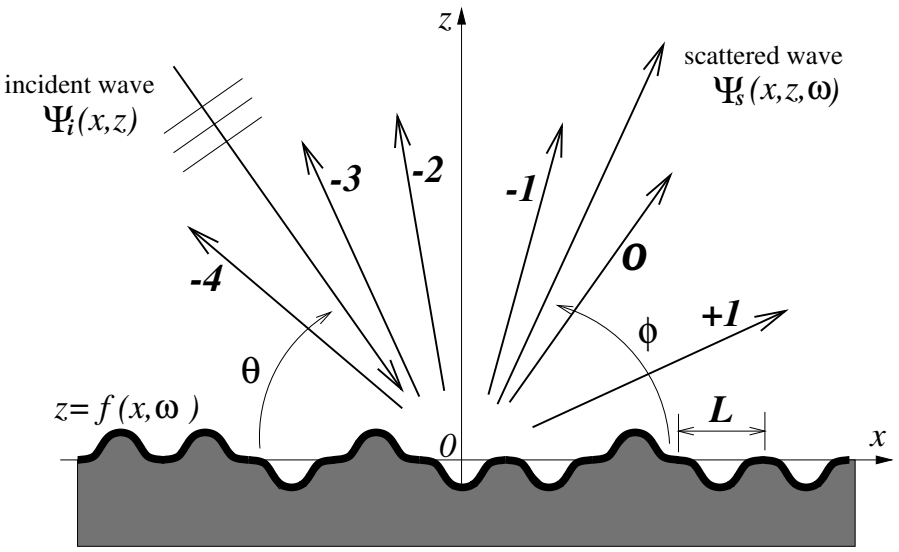

Figure 4.1 Wave scattering and diffraction from a periodic random surface generated by a binary sequence. L is the period, θ is the angle of incidence, ϕ is a scattering angle. Coherently diffracted waves are denoted by numbers.

From (4.1) and (4.3), one easily finds the average and the correlation function of $f(x,\omega)$ as

$$\langle f(x,\omega)\rangle = \langle \sigma \sum_{m=-\infty}^{\infty} g(x-mL) b_m(\omega)\rangle = 0, \tag{4.5}$$

$$\begin{aligned} R_f(x,x') &= \langle f(x,\omega) f(x',\omega)\rangle = \sigma^2 \sum_{m=-\infty}^{\infty} g(x-mL) g(x'-mL) \\ &= R_f(x+nL, x'+nL) \end{aligned} \tag{4.6}$$

where n is any integer and $R_f(x,x')$ is periodic in the direction of $x = x'$ in the x-x' plane. Figure 4.2 shows $R_f(x,x')$ with $L = 3.0\lambda$, $a_0 = 0.5\lambda$ and $\kappa = 0.18\lambda$ in the $x - x'$ plane. From (4.5) and (4.6), it is found that the periodic random surface is a periodic stationary process with the period L [7].

We assume that the sample space Ω is of function space type [47], where Ω is regarded as an infinite-dimensional Euclidean space and a sample point ω is an infinite-dimensional vector in Ω given by a sample sequence :

$$\omega = (\cdots, \omega_{-1}, \omega_0, \omega_1, \cdots), \qquad \omega_n = b_n(\omega) \tag{4.7}$$

where ω_n is the n-th component of ω. Under this assumption, a translation by m : $b_n(\omega) \rightarrow b_{n+m}(\omega)$, generates a shift from ω to another sample point $\omega' = (\cdots, \omega_{m-1}, \omega_m, \omega_{m+1}, \cdots)$. Such a shift in the sample space Ω is represented as $\omega' = T^m\omega$ with a shift operator T. Since $b_m(\omega)$ is independent and stationary, the shift T becomes a measure-preserving transformation with $P(\omega) = P(T^m\omega)$, and has group properties : $T^0 \equiv 1$ (identity) ; $T^{m+n} = T^m T^n$ [7]. Thus, we may write,

$$b_n(\omega) = b_0(T^n\omega). \tag{4.8}$$

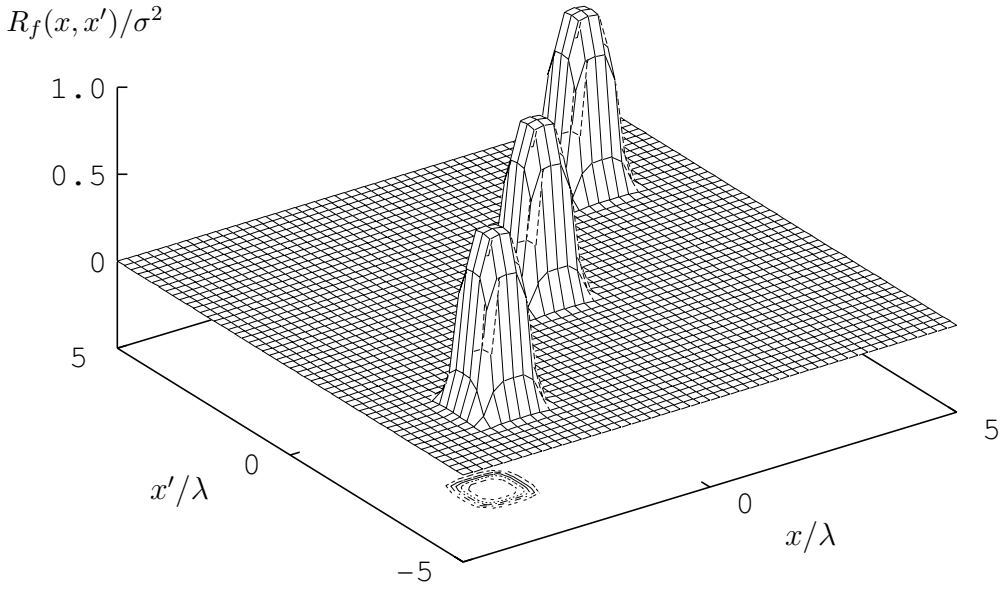

Figure 4.2 Correlation function of the binary periodic random surface $R_f(x,x')$ with $L = 3.0\lambda$, $a_0 = 0.5\lambda$ and $\kappa = 0.18\lambda$ ($R_f(x,x')$ is divided by σ^2), λ being wavelength. $R_f(x,x')$ is periodic with the period L in the direction of $x = x'$ in the $x - x'$ plane.

Using this property, we find that $f(x,\omega)$ is invariant under the translation $(x,\omega) \rightarrow (x + nL, T^{-n}\omega)$

$$f(x,\omega) = f(x + nL, T^{-n}\omega). \tag{4.9}$$

On the other hand, from (4.9) and the measure-preserving property : $P(\omega) = P(T^n\omega)$, we obtain

$$\begin{aligned}\langle f(x,\omega)\rangle &= \int_\Omega f(x,\omega)dP(\omega) = \int_\Omega f(x+nL, T^{-n}\omega)dP(\omega) \\ &= \int_\Omega f(x+nL,\omega')dP(T^n\omega') = \int_\Omega f(x+nL,\omega')dP(\omega') = \langle f(x+nL,\omega)\rangle. \end{aligned} \tag{4.10}$$

If we replace $f(x,\omega)$ with $f(x,\omega)f(x',\omega)$ in (4.10), we find that $R_f(x,x') = R_f(x+nL, x'+nL)$ holds for any integer n. Therefore, if $f(x,\omega)$ has the shift invariance property (4.9), $f(x,\omega)$ becomes a periodic stationary process. This fact will be used later.

Let us denote the y component of the TE electric field by $\Psi(x,z,\omega)$, which satisfies the wave equation in free space,

$$\left[\frac{\partial^2}{\partial x^2} + \frac{\partial^2}{\partial z^2} + k^2\right]\Psi(x,z,\omega) = 0, \tag{4.11}$$

where k is the wave number. For a periodic stationary process $\Phi(x,\omega)$, we introduce the norm $\parallel \Phi(x,\omega) \parallel$, which is defined as an ensemble average of a space average of $|\Phi(x,\omega)|^2$ over one period :

$$\parallel \Phi(x,\omega) \parallel^2 = \left\langle \frac{1}{L}\int_{-L/2}^{L/2} |\Phi(x,\omega)|^2\, dx \right\rangle. \tag{4.12}$$

On a perfectly conductive random surface $z = f(x, \omega)$, the wave function satisfies the Dirichlet condition :

$$\Psi(x, z, \omega)\Big|_{z=f(x,\omega)} = 0. \tag{4.13}$$

We write the wave field as a sum of the incident plane wave $\Psi_i(x, z)$ and the scattered wave $\Psi_s(x, z, \omega)$, which is a functional of a binary sequence $\{b_n(\omega)\}$,

$$\Psi(x, z, \omega) = \Psi_i(x, z) + \Psi_s(x, z, \omega), \tag{4.14}$$

$$\Psi_i(x, z) = e^{ipx - i\beta_0(p)z}, \tag{4.15}$$

$$p = k\cos\theta, \quad \beta_n(\lambda') = \sqrt{k^2 - \left(\lambda' + \frac{2\pi n}{L}\right)^2} = \beta_{n+q}\left(\lambda' - k_L q\right), \tag{4.16}$$

$$\mathrm{Im}[\beta_n(\lambda')] \geq 0, \quad (n = 0, \pm 1, \pm 2, \cdots), \quad k_L = \frac{2\pi}{L},$$

where θ is the angle of incidence, k_L is the spatial angular frequency of the period L and Im denotes the imaginary part.

To determine a form of the scattered wave $\Psi_s(x, z, \omega)$, we define a translation operator D acting on the wave function $\Psi_s(x, z, \omega)$ by

$$D^m \Psi_s(x, z, \omega) = \Psi_s(x + mL, z, T^{-m}\omega), \quad (m = 0, \pm 1, \pm 2, \cdots). \tag{4.17}$$

Since $f(x, \omega)$ is invariant under D^m by (4.9), if $\Psi_s(x, z, \omega)$ is a solution of the wave equation (4.11) and the boundary condition (4.13), then $D^m\Psi_s(x, z, \omega) = \Psi_s(x + mL, z, T^{-m}\omega)$ becomes a solution for the incident plane wave $D^m\Psi_i(x, z) = e^{ipmL}e^{ipx - i\beta_0(p)z}$. Thus we get

$$D^m \Psi_s(x, z, \omega) = \Psi_s(x + mL, z, T^{-m}\omega) = e^{ipmL}\Psi_s(x, z, \omega). \tag{4.18}$$

If we put

$$\Psi_s(x, z, \omega) = e^{ipx}U(x, z, \omega), \tag{4.19}$$

then from (4.18) we find that $U(x, z, \omega)$ satisfies the shift invariance property :

$$\begin{aligned} D^m U(x, z, \omega) &= U(x + mL, z, T^{-m}\omega) \\ &= U(x, z, \omega). \end{aligned} \tag{4.20}$$

This and (4.9) mean that $U(x, z, \omega)$ is a periodic stationary process of x. If $U(x, z, \omega)$ is a deterministic periodic function, (4.19) is the Floquet form for periodic gratings. However, in our case, $U(x, z, \omega)$ is not periodic, but $\langle U(x, z, \omega)\rangle$ becomes periodic. Thus, (4.19) is considered as an extension of the Floquet form, which we call the stochastic Floquet form [7].

4.3 Representations of periodic stationary processes

This section discusses a harmonic series representation of the periodic stationary process $U(x, z, \omega)$ as a stochastic functional of the binary sequence. Such a harmonic series representation was first discussed in [44]. However, the discussion was limited to the fist order functional and was incomplete for higher order functionals. Thus, we here reconsider such a harmonic series representation to get an expression for the second order functional.

Since $U(x,z,\omega)$ is a stochastic functional of the binary sequence $\{b_n(\omega)\}$, it can be represented by a binary functional expansion (A.13) for each value of (x,z). Making such an expansion to satisfy $U(x,z,\omega)=U(x+mL,z,T^{-m}\omega)$, however, we write

$$U(x,z,\omega)=C_0(x,z)+\sum_{m=-\infty}^{\infty}C_1(x-mL,z)B_1[b_m] + \sum_{m,n=-\infty}^{\infty}C_2(x-mL,x-nL,z)B_2[b_m,b_n]+\cdots. \tag{4.21}$$

Here, $B_n[\cdot]$ is the binary polynomial defined in appendix A, and $C_0(x,z),C_1(x,z),\cdots$ are the deterministic functions called binary kernels. When $n\geq 2$, $C_n(x_1,x_2,\cdots,x_n,z)$ is symmetrical with respect to its arguments x_n's. From (4.20), (4.21) and (A.6), we find that $C_0(x,z)$ is a periodic function.

Next, we modify the expression (4.21) to make $e^{ipx}U(x,z,\omega)$ satisfy the wave equation (4.11) and the radiation condition for $z\to\infty$. Representing the binary kernels by multiple Fourier integrals, we put

$$U(x,z,\omega)=\sum_{q=-\infty}^{\infty}C_0^{(q)}(p)e^{ik_Lqx}e^{i\beta_0(p)z}+\sum_{m=-\infty}^{\infty}B_1[b_m]\int_{-\infty}^{\infty}C_1(\lambda'|p)e^{i\lambda'(x-mL)+i\beta_0(p+\lambda')z}d\lambda' + \sum_{m,n=-\infty}^{\infty}B_2[b_m,b_n]\iint_{-\infty}^{\infty}C_2(\lambda_1,\lambda_2|p)e^{i\lambda_1(x-nL)+i\lambda_2(x-mL)+i\beta_0(p+\lambda_1+\lambda_2)z}d\lambda_1d\lambda_2+\cdots, \tag{4.22}$$

where $C_0(p),C_1(\lambda'|p),C_2(\lambda_1,\lambda_2|p),\cdots$ are the binary kernels in the spectral domain. This expansion is physically written as a sum of outgoing waves and surface waves $e^{i(\lambda_1+\cdots+\lambda_n)x+i\beta_0(p+\lambda_1+\cdots+\lambda_n)z}$. Taking the Rayleigh hypothesis, we assume that (4.22) is valid even in the region $z\leq z_d=\max\{f(x,\omega)\}$. However, the expression (4.22) is redundant, and the kernel functions cannot be determined uniquely.

On the other hand, it is known that a periodic stationary process has a harmonic series representation [51, 52], which is a "Fourier series" with "Fourier coefficients" that are band-limited stationary processes. Taking the fact that $e^{i(\lambda_1+\cdots+\lambda_n)x+i\beta_0(p+\lambda_1+\cdots+\lambda_n)z}$ is determined by $\lambda_s=\lambda_1+\cdots+\lambda_n$, we divide the integral interval of λ_s into bands with equal width $[-k_L/2,k_L/2]$. Defining a gate function $S(\lambda')$ as

$$S(\lambda')=\begin{cases}1, & (|\lambda'|\leq k_L/2)\\ 0, & (|\lambda'|>k_L/2)\end{cases},\qquad \sum_{l=-\infty}^{\infty}S(\lambda'+k_Ll)\equiv 1, \tag{4.23}$$

we rewrite, for example, the second order integral of $U(x,z,\omega)$ as :

$$\begin{aligned}&\iint_{-\infty}^{\infty}C_2(\lambda_1,\lambda_2|p)e^{i\lambda_1(x-nL)+i\lambda_2(x-mL)+i\beta_0(p+\lambda_1+\lambda_2)z}d\lambda_1d\lambda_2\\ &\quad=\sum_{q,l=-\infty}^{\infty}\iint_{-\infty}^{\infty}S(\lambda_s-k_Lq)S(\lambda_1-k_Ll)C_2(\lambda_1,\lambda_s-\lambda_1|p)\\ &\qquad\qquad\times e^{i(\lambda_s-\lambda_1)(x-mL)+i\lambda_1(x-nL)+i\beta_0(p+\lambda_s)z}d\lambda_1d\lambda_s\\ &\quad=\sum_{q=-\infty}^{\infty}e^{ik_Lqx}\iint_{-\infty}^{\infty}S(\Lambda_s)S(\Lambda_1)C_2^{(q)}(\Lambda_1,\Lambda_s-\Lambda_1|p)\\ &\qquad\qquad\times e^{i(\Lambda_s-\Lambda_1)(x-mL)+i\Lambda_1(x-nL)+i\beta_q(p+\Lambda_s)z}d\Lambda_1d\Lambda_s,\end{aligned} \tag{4.24}$$

where $C_2^{(q)}(\lambda_1, \lambda_s - \lambda_1)$ is the second order band-limited kernel

$$C_2^{(q)}(\lambda_1, \lambda_s - \lambda_1 | p) = \sum_{l=-\infty}^{\infty} C_2(\lambda_1 + k_L l, \lambda_s - \lambda_1 + k_L(q-l)|p), \quad (\lambda_1, \lambda_s \le |k_L/2|). \tag{4.25}$$

Repeating this procedure for higher order integrals, we finally obtain the harmonic series representation for $U(x, z, \omega)$,

$$U(x, z, \omega) = \sum_{q=-\infty}^{\infty} e^{ik_L q x} U^{(q)}(x, z, \omega) \tag{4.26}$$

$$\begin{aligned} U^{(q)}(x, z, \omega) = C_0^{(q)}(p) e^{i\beta_q(p)z} &+ \sum_{m=-\infty}^{\infty} B_1[b_m] \int_{-k_L/2}^{k_L/2} C_1^{(q)}(\lambda_s|p) e^{i\lambda_s(x-mL)+i\beta_q(p+\lambda_s)z} d\lambda_s \\ &+ \sum_{m,n=-\infty}^{\infty} B_2[b_m, b_n] \int_{-k_L/2}^{k_L/2} \int_{-k_L/2}^{k_L/2} C_2^{(q)}(\lambda_1, \lambda_s - \lambda_1|p) \\ &\times e^{i(\lambda_s-\lambda_1)(x-mL)+i\lambda_1(x-nL)+i\beta_q(p+\lambda_s)z} d\lambda_1 d\lambda_s + \cdots, \end{aligned} \tag{4.27}$$

where $C_1^{(q)}(\lambda_s)$ is the first order band-limited kernel given as

$$C_1^{(q)}(\lambda_s|p) = C_1(\lambda_s + k_L q|p). \tag{4.28}$$

By (4.27), $U^{(q)}(x, z, \omega)$ becomes wide sense stationary, that is, the ensemble average $\left\langle U^{(q)}(x, z, \omega) \right\rangle$ is constant and independent of x, and its two-point correlation function is a function of the difference of the two point $x - x'$(See appendix B). The expression (4.27) is not a power series of the roughness parameter σ but is an orthogonal expansion. The band limited kernel functions can be uniquely determined, as will be shown later.

Since $e^{i(p+k_L q)x} U^{(q)}(x, z, \omega)$ is a component of the scattered wave, $C_1^{(q)}(\lambda_s|p), C_2^{(q)}(\lambda_s - \lambda_1, \lambda_1|p), \cdots$ are amplitude factors of the plane wave with the scattering angle $\phi_q(p + \lambda_s)$ given by

$$\phi_q(p + \lambda') = \cos^{-1}\left[\frac{1}{k}\left(p + k_L q + \lambda'\right)\right], \tag{4.29}$$

which is measured from the x-axis. (See figure 4.1.)

Since $B_m[\cdot]$ has zero average for $m \ge 1$ by (A.6), we obtain the coherent wave (average wave) from (4.14), (4.19), (4.26) and (4.27)

$$\langle \Psi(x, z, \omega) \rangle = e^{ipx}\left[e^{-i\beta_0(p)z} + \sum_{q=-\infty}^{\infty} C_0^{(q)}(p) e^{ik_L q x} e^{i\beta_q(p)z}\right]. \tag{4.30}$$

This is exactly the Floquet solution for a periodic grating, where $C_0^{(q)}(p)$ is an amplitude factor of the q-th Floquet mode. It means that the periodic binary random surface acts as a periodic surface and the coherent wave is diffracted into discrete directions $\phi_q(p)$.

From (4.26) and (4.27), we obtain the optical theorem [50]

$$\frac{\beta_0(p)}{k} = \frac{1}{k} \sum_{q=-\infty}^{\infty} \mathrm{Re}\left[\beta_q(p)\right] \left|C_0^{(q)}(p)\right|^2 + \frac{1}{2\pi} \int_0^{\pi} \sigma(\phi|\theta) d\phi, \tag{4.31}$$

where Re denotes the real part. The left-hand side is the incident power per unit length, the first term and the integral in the right-hand side are the sum of the coherently diffracted power

and the incoherent scattered power, respectively. $\sigma(\phi|\theta)$ is the scattering cross section per unit length to the scattering angle ϕ

$$\sigma(\phi|\theta) = \sigma_1(\phi|\theta) + \sigma_2(\phi|\theta) + \cdots, \tag{4.32}$$

where $\sigma_1(\phi|\theta)$ is the contribution from the first-order binary kernels

$$\sigma_1(\phi|\theta) = 2\pi k \sin^2\phi \sum_{q=-\infty}^{\infty} k_L \left| C_1^{(q)}(k\cos\phi - p - k_L q|p) \right|^2 S(k\cos\phi - p - k_L q), \tag{4.33}$$

and $\sigma_2(\phi|\theta)$ is the contribution from the second-order binary kernels

$$\begin{aligned}\sigma_2(\phi|\theta) = 4\pi k \sin^2\phi \sum_{q=-\infty}^{\infty} \Bigg[& k_L^2 \int_{-k_L/2}^{k_L/2} \left| C_2^{(q)}(\lambda_1, k\cos\phi - p - k_L q - \lambda_1|p) \right|^2 S(k\cos\phi - p - k_L q) d\lambda_1 \\ & - k_L \left| \int_{-k_L/2}^{k_L/2} C_2^{(q)}(\lambda_1, k\cos\phi - p - k_L q - \lambda_1|p) S(k\cos\phi - p - k_L q) d\lambda_1 \right|^2 \Bigg],\end{aligned} \tag{4.34}$$

where $S(\lambda)$ is the gate function (4.23). The first term in the right hand side is the main part denoted by $\sigma_2(\phi|\theta)_m$. The second term is the subtractive part denoted by $\sigma_2(\phi|\theta)_d$, which comes from the special property (4.4) of $b_m(\omega)$. When one only considers the first order scattering, no significant difference exists between the binary case and the Gaussian case. Since such a subtractive term in $\sigma_2(\phi|\theta)$ does not exist in the Gaussian case [8], it is concluded that the difference between two cases appears in the second or higher order scattering. Later, we see this difference in numerical calculations.

The band-limited binary kernel $C_1^{(q)}(\cdot)$ is expected to satisfy

$$C_1^{(q)}(k_L/2 - p|p) = C_1^{(q+1)}(-k_L/2 - p|p) \tag{4.35}$$

at the band edge.

4.4 Hierarchical equations and an approximate solution

4.4.1 Derivation of hierarchical equations

On a perfectly conductive random surface $z = f(x,\omega)$, the wave function $\Psi(x,z,\omega)$ satisfies the Dirichlet condition (4.13). Even though $\Psi(x,z,\omega)$ itself is not periodic stationary, $|\Psi(x,z,\omega)|$ becomes a periodic stationary process by (4.19). Thus, we assume that the boundary condition (4.13) holds in the norm sense (4.12),

$$\left\| \Psi(x,z,\omega)\Big|_{z=f(x,\omega)} \right\|^2 = \left\langle \frac{1}{L} \int_{-L/2}^{L/2} \left| \left(e^{-i\beta_0(p)z} + U(x,z,\omega) \right) \Big|_{z=f(x,\omega)} \right|^2 dx \right\rangle = 0. \tag{4.36}$$

In the previous paper [44], the boundary condition was approximated under the assumption $\sigma^2 k^2 \ll 1$ as $\Psi(x,z,\omega) + f(x,\omega)\cdot\partial\Psi(x,z,\omega)/\partial z = 0$ at $z = 0$, where σ is the surface roughness. However, this paper employs (4.13) without approximation. To calculate the norm (4.36), we substitute (4.19), (4.26) and (4.27) into (4.36) in $|x| \le L/2$. Using the identity $e^{i\beta_0(p)f(x,\omega)} = e^{i\sigma\beta_0(p)g(x)b_0(\omega)} = \cos[\sigma\beta_0(p)g(x)] + i\sin[\sigma\beta_0(p)g(x)]b_0(\omega)$, and applying the recurrence relations (A.11) and the orthogonal relation (A.7), we obtain a hierarchy of equations for the binary

kernels as a sufficient condition. Lower-order ones are
(zero order)

$$\cos[\sigma\beta_0(p)g(x)] + \sum_{q=-\infty}^{\infty} e^{ik_Lqx}\Bigg[C_0^{(q)}(p)\cos[\sigma\beta_q(p)g(x)] + i\int_{-k_L/2}^{k_L/2} C_1^{(q)}(\lambda_s|p)e^{i\lambda_s x}\sin[\sigma\beta_q(p+\lambda_s)g(x)]d\lambda_s\Bigg] = 0, \quad (4.37)$$

(first order) $(m = 0, \pm1, \pm2, \cdots)$

$$\begin{aligned} &i\delta(m,0)\Bigg(-\sin[\sigma\beta_0(p)g(x)] + \sum_{q=-\infty}^{\infty} e^{ik_Lqx}C_0^{(q)}(p)\sin[\sigma\beta_q(p)g(x)]\Bigg) \\ &+\sum_{q=-\infty}^{\infty} e^{ik_Lqx}\Bigg[\int_{-k_L/2}^{k_L/2} C_1^{(q)}(\lambda_s|p)e^{i\lambda_s(x-mL)}\cos[\sigma\beta_q(p+\lambda_s)g(x)]d\lambda_s \\ &\quad + 2i\iint_{-k_L/2}^{k_L/2} C_2^{(q)}(\lambda_s-\lambda_1,\lambda_1|p)e^{i(\lambda_s-\lambda_1)(x-mL)+i\lambda_1 x}\sin[\sigma\beta_q(p+\lambda_s)g(x)]d\lambda_1 d\lambda_s \\ &\quad - 2i\delta(m,0)\iint_{-k_L/2}^{k_L/2} C_2^{(q)}(\lambda_s-\lambda_1,\lambda_1|p)e^{i\lambda_s x}\sin[\sigma\beta_q(p+\lambda_s)g(x)]d\lambda_1 d\lambda_s\Bigg] = 0, \end{aligned} \quad (4.38)$$

(second order) $(m, n = 0, \pm1, \pm2, \cdots)$

$$\begin{aligned} &\sum_{q=-\infty}^{\infty} e^{ik_Lqx}\Bigg[\iint_{-k_L/2}^{k_L/2} C_2^{(q)}(\lambda_s-\lambda_1,\lambda_1|p)e^{i(\lambda_s-\lambda_1)(x-mL)+i\lambda_1(x-nL)}\cos[\sigma\beta_q(p+\lambda_s)g(x)]d\lambda_1 d\lambda_s \\ &\quad +\frac{i}{2}\delta(n,0)\int_{-k_L/2}^{k_L/2} C_1^{(q)}(\lambda_s-\lambda_1|p)e^{i(\lambda_s-\lambda_1)(x-mL)}\sin[\sigma\beta_q(p+\lambda_s-\lambda_1)g(x)]d\lambda_s \\ &\quad +\frac{i}{2}\delta(m,0)\int_{-k_L/2}^{k_L/2} C_1^{(q)}(\lambda_1|p)e^{i\lambda_1(x-nL)}\sin[\sigma\beta_q(p+\lambda_1)g(x)]d\lambda_1 \\ &\quad + 3i\iiint_{-k_L/2}^{k_L/2} C_3^{(q)}(\lambda_s-\lambda_1-\lambda_2,\lambda_1,\lambda_2|p)e^{i(\lambda_s-\lambda_1-\lambda_2)(x-mL)+i\lambda_1(x-nL)+i\lambda_2 x} \\ &\qquad\qquad \times\sin[\sigma\beta_q(p+\lambda_s)g(x)]d\lambda_1 d\lambda_2 d\lambda_s \\ &\quad - 6i\delta(n,0)\iiint_{-k_L/2}^{k_L/2} C_3^{(q)}(\lambda_s-\lambda_1-\lambda_2,\lambda_1,\lambda_2|p)e^{i(\lambda_s-\lambda_1-\lambda_2)(x-mL)+i\lambda_1 x+i\lambda_2 x} \\ &\qquad\qquad \times\sin[\sigma\beta_q(p+\lambda_s)g(x)]d\lambda_1 d\lambda_2 d\lambda_s\Bigg] = 0. \end{aligned} \quad (4.39)$$

Here, (4.38) and (4.39) hold for any m and n. Since (4.37), (4.38) and (4.39) hold for any x in $|x| \le L/2$, we expand the factors $e^{ik_Lqx}e^{i\lambda' x}\cos[\sigma\beta_q(p+\lambda')g(x)]$ and $e^{ik_Lqx}e^{i\lambda' x}\sin[\sigma\beta_q(p+\lambda')g(x)]$ into Fourier series as

$$e^{ik_Lqx}e^{i\lambda' x}\begin{bmatrix}\cos[\sigma\beta_q(p+\lambda')g(x)]\\ \sin[\sigma\beta_q(p+\lambda')g(x)]\end{bmatrix} = \sum_{j=-\infty}^{\infty}\begin{bmatrix}\Gamma^{\rm c}_{jq}(\lambda'|p)\\ \Gamma^{\rm s}_{jq}(\lambda'|p)\end{bmatrix}e^{ik_Ljx}. \quad (4.40)$$

Then, we get a set of hierarchical equations of Fourier coefficients for $j = 0, \pm1, \pm2, \cdots$. It is convenient to introduce infinite-dimensional matrices $\mathbf{\Gamma}^{\rm s}, \mathbf{\Gamma}^{\rm c}$ and infinite-dimensional vectors

$\mathbf{I}^0, \mathbf{C}_n(\cdot)(n = 0, 1, 2, \cdots)$ as

$$\begin{aligned}
\mathbf{\Gamma}^{\mathrm{c}}(\lambda'|p) &= [\Gamma^{\mathrm{c}}_{jq}(\lambda'|p)], && (4.41)\\
\mathbf{\Gamma}^{\mathrm{s}}(\lambda'|p) &= [\Gamma^{\mathrm{s}}_{jq}(\lambda'|p)], && (4.42)\\
\mathbf{C}_0(p) &= [\cdots, C_0^{(-1)}(p), C_0^{(0)}(p), C_0^{(1)}(p), \cdots]^t && (4.43)\\
\mathbf{C}_1(\lambda'|p) &= [\cdots, C_1^{(-1)}(\lambda'|p), C_1^{(0)}(\lambda'|p), C_1^{(1)}(\lambda'|p), \cdots]^t && (4.44)\\
\mathbf{C}_2(\lambda_1, \lambda_2|p) &= [\cdots, C_2^{(-1)}(\lambda_1, \lambda_2|p), C_2^{(0)}(\lambda_1, \lambda_2|p), C_2^{(1)}(\lambda_1, \lambda_2|p), \cdots]^t, && (4.45)\\
\mathbf{I}^0 &= [\cdots, 0, 1, 0, \cdots]^t = [\delta(m, 0)]^t. && (4.46)
\end{aligned}$$

Multiplying $e^{i\Lambda mL}$ and $e^{i\Lambda_1 mL + i\Lambda_2 nL}$ to the first and second order equations, respectively, summing up with m and n, and using the identity

$$\sum_{m=-\infty}^{\infty} e^{imL(\Lambda-\lambda')} = k_L \sum_{m=-\infty}^{\infty} \delta(\Lambda - \lambda' + k_L m), \tag{4.47}$$

we obtain the hierarchy of equations in matrix form,
(zero order)

$$\mathbf{\Gamma}^{\mathrm{c}}(0|p)\mathbf{I}^0 + \mathbf{\Gamma}^{\mathrm{c}}(0|p)\mathbf{C}_0(p) + i\int_{-k_L/2}^{k_L/2} \mathbf{\Gamma}^{\mathrm{s}}(\lambda'|p)\mathbf{C}_1(\lambda'|p)d\lambda' = 0, \tag{4.48}$$

(first order)

$$\begin{aligned}
-i\mathbf{\Gamma}^{\mathrm{s}}(0|p)\mathbf{I}^0 &+ i\mathbf{\Gamma}^{\mathrm{s}}(0|p)\mathbf{C}_0(p) + k_L\mathbf{\Gamma}^{\mathrm{c}}(\Lambda|p)\mathbf{C}_1(\Lambda|p)\\
&+ 2ik_L\int_{-k_L/2}^{k_L/2} \mathbf{\Gamma}^{\mathrm{s}}(\Lambda+\lambda_1|p)\mathbf{C}_2(\Lambda, \lambda_1|p)d\lambda_1\\
&- 2i\iint_{-k_L/2}^{k_L/2} \mathbf{\Gamma}^{\mathrm{s}}(\lambda_1+\lambda_2|p)\mathbf{C}_2(\lambda_s-\lambda_1, \lambda_1|p)d\lambda_1 d\lambda_s = 0,
\end{aligned} \tag{4.49}$$

(second order)

$$\begin{aligned}
k_L\mathbf{\Gamma}^{\mathrm{c}}&(\Lambda_1 + \Lambda_2|p)\mathbf{C}_2(\Lambda_1, \Lambda_2|p)\\
&+ \frac{i}{2}\mathbf{\Gamma}^{\mathrm{s}}(\Lambda_1|p)\mathbf{C}_1(\Lambda_1|p) + \frac{i}{2}\mathbf{\Gamma}^{\mathrm{s}}(\Lambda_2|p)\mathbf{C}_1(\Lambda_2|p)\\
&+ 3ik_L\int_{-k_L/2}^{k_L/2} \mathbf{\Gamma}^{\mathrm{c}}(\Lambda_1+\Lambda_2+\lambda_2|p)\mathbf{C}_3(\Lambda_1, \Lambda_2, \lambda_2|p)d\lambda_2\\
&- 6i\iint_{-k_L/2}^{k_L/2} \mathbf{\Gamma}^{\mathrm{c}}(\Lambda_1+\lambda_1+\lambda_2|p)\mathbf{C}_3(\Lambda_1, \lambda_1, \lambda_2|p)d\lambda_1 d\lambda_2 = 0.
\end{aligned} \tag{4.50}$$

Let us obtain the second order solution involving up to $\mathbf{C}_2(\lambda_s - \lambda_1, \lambda_1|p)$. Neglecting $\mathbf{C}_3(\cdot)$ in (4.50), substituting (4.50) into (4.49) and employing the diagonal approximation [53], we get

$$i\mathbf{\Gamma}^{\mathrm{s}}(0|p)\left(-\mathbf{I}^0 + \mathbf{C}_0(p)\right) + k_L\left[\mathbf{\Gamma}^{\mathrm{c}}(\Lambda|p) + \mathbf{M}^{(1)}(\Lambda|p)\right]\mathbf{C}_1(\Lambda|p) = 0, \tag{4.51}$$

where $\mathbf{M}^{(1)}(\Lambda|p)$ is the 1st order mass operator representing diffraction and scattering effects, defined as

$$\mathbf{M}^{(1)}(\Lambda|p) = \frac{1}{k_L}\int_{-k_L/2}^{k_L/2} \mathbf{\Gamma}^{\mathrm{s}}(\Lambda+\lambda'|p)[\mathbf{\Gamma}^{\mathrm{c}}(\Lambda+\lambda'|p)]^{-1}\mathbf{\Gamma}^{\mathrm{s}}(\Lambda|p)d\lambda', \tag{4.52}$$

which is proportional to σ^2. From (4.48), (4.50) and (4.51), we obtain

$$\mathbf{C}_0(p) = -\left[\mathbf{\Gamma}^{\mathrm{c}}(0|p)+\mathbf{M}^{(2)}(0|p)\right]^{-1}\left[\mathbf{\Gamma}^{\mathrm{c}}(0|p)-\mathbf{M}^{(2)}(0|p)\right]\mathbf{I}^0, \tag{4.53}$$

$$\mathbf{C}_1(\Lambda|p) = \frac{i}{k_L}[\mathbf{\Gamma}^{\mathrm{c}}(\Lambda|p)+\mathbf{M}^{(1)}(\Lambda|p)]^{-1}\mathbf{\Gamma}^{\mathrm{s}}(0|p)(\mathbf{I}^0-\mathbf{C}_0(p)) \tag{4.54}$$

$$= \frac{i}{k_L}[\mathbf{\Gamma}^{\mathrm{c}}(\Lambda|p)+\mathbf{M}^{(1)}(\Lambda|p)]^{-1} \times\mathbf{\Gamma}^{\mathrm{s}}(0|p)\left(\mathbf{I}-\left[\mathbf{\Gamma}^{\mathrm{c}}(0|p)+\mathbf{M}^{(2)}(0|p)\right]^{-1}\left[\mathbf{M}^{(2)}(0|p)-\mathbf{\Gamma}^{\mathrm{c}}(0|p)\right]\right)\mathbf{I}^0, \tag{4.55}$$

$$\mathbf{C}_2(\Lambda_1,\Lambda_2|p) = -\frac{i}{2k_L}[\mathbf{\Gamma}^{\mathrm{c}}(\Lambda_1+\Lambda_2|p)]^{-1} \times(\mathbf{\Gamma}^{\mathrm{s}}(\Lambda_1|p)\mathbf{C}_1(\Lambda_1|p)+\mathbf{\Gamma}^{\mathrm{s}}(\Lambda_2|p)\mathbf{C}_1(\Lambda_2|p)) \tag{4.56}$$

$$= \frac{1}{2{k_L}^2}[\mathbf{\Gamma}^{\mathrm{c}}(\Lambda_1+\Lambda_2|p)]^{-1} \times\Big(\mathbf{\Gamma}^{\mathrm{s}}(\Lambda_1|p)[\mathbf{\Gamma}^{\mathrm{c}}(\Lambda_1|p)+\mathbf{M}^{(1)}(\Lambda_1|p)]^{-1}\mathbf{\Gamma}^{\mathrm{s}}(0|p)(\mathbf{I}^0-\mathbf{C}_0(p)) +\mathbf{\Gamma}^{\mathrm{s}}(\Lambda_2|p)[\mathbf{\Gamma}^{\mathrm{c}}(\Lambda_2|p)+\mathbf{M}^{(1)}(\Lambda_2|p)]^{-1}\mathbf{\Gamma}^{\mathrm{s}}(0|p)(\mathbf{I}^0-\mathbf{C}_0(p))\Big), \tag{4.57}$$

where the 2nd order mass operator $\mathbf{M}^{(2)}(\Lambda|p)$ is defined as follows :

$$\mathbf{M}^{(2)}(\Lambda|p) = \frac{1}{k_L}\int_{-k_L/2}^{k_L/2}\mathbf{\Gamma}^{\mathrm{s}}(\Lambda+\lambda'|p) \times\left[\mathbf{\Gamma}^{\mathrm{c}}(\Lambda+\lambda'|p)+\mathbf{M}^{(1)}(\Lambda+\lambda'|p)\right]^{-1}\mathbf{\Gamma}^{\mathrm{s}}(\Lambda|p)d\lambda', \tag{4.58}$$

which is approximated by $\mathbf{M}^{(1)}(0|p)$ in the following numerical calculations.

From (4.53), one finds that the coherent Floquet mode $\mathbf{C}_0(p)$ is excited by $\mathbf{I}^0$, which denotes the incident plane wave. If we put $\mathbf{M}^{(2)}(0|p) = 0$, equation (4.53) is reduced to $\mathbf{C}_0(p) = -\mathbf{I}^0$. This means that the non-zeroth-order Floquet modes vanish and only the specular reflection exists if we neglect the multiple scattering effect. Thus, we may conclude that the non-zeroth-order Floquet modes are generated by multiple-scattering process in the case of the flat average surface with $\langle f(x,\omega)\rangle = 0$. Since (4.54) has a 'dressed' single scattering factor $[\mathbf{\Gamma}^{\mathrm{c}}(\Lambda|p)+\mathbf{M}^{(1)}(\Lambda|p)]^{-1}$, $\mathbf{C}_1(\Lambda|p)$ describes a 'dressed' single scattering excited by $\mathbf{I}^0$ the incident plane wave and $\mathbf{C}_0(p)$ the coherent Floquet mode. In addition to such a 'dressed' single scattering factor, however, equation (4.57) has an 'undressed' single scattering factor $[\mathbf{\Gamma}^{\mathrm{c}}(\Lambda_1+\Lambda_2|p)]^{-1}$. Therefore, $\mathbf{C}_2(\Lambda_1,\Lambda_2|p)$ representes a double scattering process made up of 'undressed' single scattering and 'dressed' single scattering.

4.5 Numerical examples

4.5.1 Parameters of calculation

For numerical calculations, we assume a local surface profile $g(x)$ as

$$g(x) = \frac{1}{2}\left[\mathrm{erf}\left(\frac{x+a_0}{\kappa}\right)-\mathrm{erf}\left(\frac{x-a_0}{\kappa}\right)\right], \tag{4.59}$$

$$\mathrm{erf}(x) = \frac{2}{\sqrt{\pi}}\int_0^x e^{-t^2}dt, \tag{4.60}$$

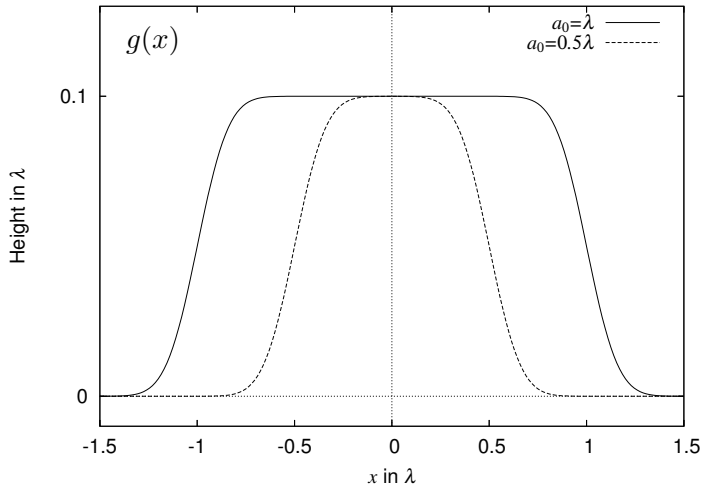

(a) local surface profile $g(x)$

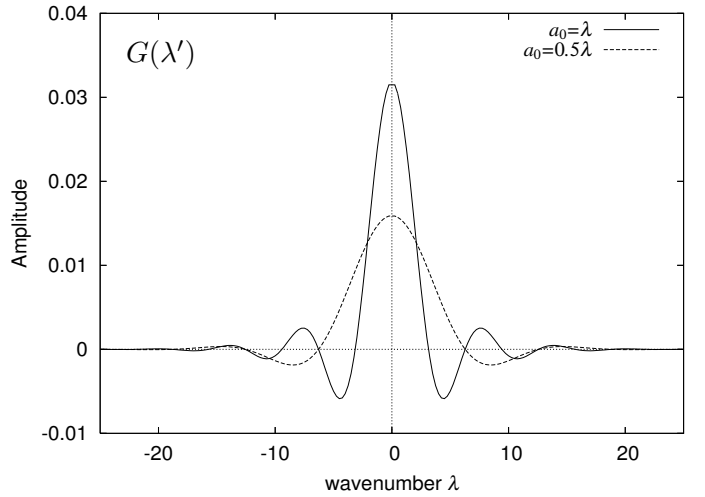

(b) spectrum of local surface profile $G(\lambda')$

Figure 4.3 Local surface profile $g(x)$, which is a rectangular boss with smooth edges (upper figure). λ is the wavelength, and spectrum of local surface profile $G(\lambda')$ (lower figure). Some ripples are seen in the spectrum when $a_0 = \lambda$.

$$G(\lambda') \quad = \quad \frac{\sin(a_0\lambda')}{\pi\lambda'}\sigma e^{-\frac{(\kappa\lambda')^2}{4}}, \tag{4.61}$$

where $\mathrm{erf}(x)$ is the error function, a_0 is a width parameter, σ is a height parameter and κ is a constant which determines the slope angle. Figure 4.3 shows $g(x)$ and $G(\lambda')$ for $a_0 = \lambda$ and 0.5λ, where λ is wavelength. $g(x)$ is a rectangular boss with smooth edges. For numerical calculations, we put $L = 3\lambda, \kappa = 0.18\lambda$. Also, we approximate infinite-dimensional matrices and vectors (4.41) - (4.46) by finite ones : 21×21 matrices and 21 dimensional vectors.

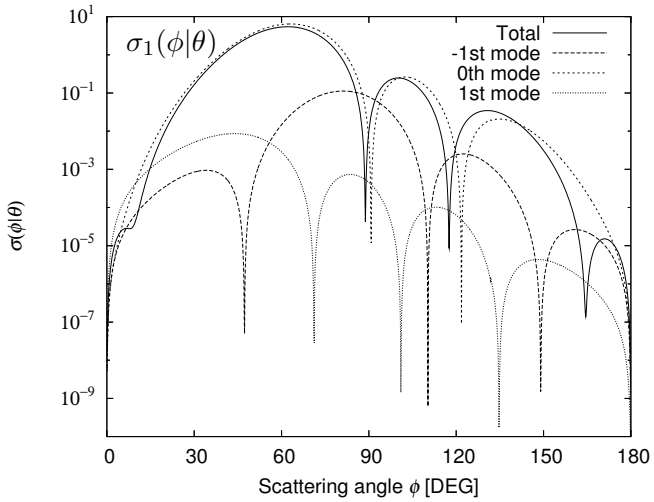

Figure 4.4 Scattering cross section $\sigma_1(\phi|\theta)$(solid line) for $L = 3\lambda$, $a_0 = \lambda$, $\theta = 60°$, $\sigma = 0.1\lambda$ and $\kappa = 0.18\lambda$, λ being the wavelength. Other curves are an incoherent scattering component excited by a coherent Floquet mode. Each component has dips due to the zeros of $G(\lambda')$ and becomes large at a scattering angle equal to the diffraction direction of the Floquet mode of excitation. The incoherent component excited by the 0th coherent mode is relatively large. Since incoherent components interfere each other, the dip angles of $\sigma_1(\phi|\theta)$(solid line) are different from those of the incoherent component excited only by the 0th coherent mode.

4.5.2 Properties of diffraction and scattering

Let us start with the incoherent scattering cross section. From (4.54) one finds that $C_1^{(q)}(\lambda_s|p)$ consists of components excited by the coherent modes $C_0^{(n)}(p)$ $(n = 0, \pm 1, \cdots)$. Figure 4.4 shows $\sigma_1(\phi|\theta)$ for $a_0 = \lambda, \theta = 60°$ and $\sigma = 0.1\lambda$, where the components excited by the 0th, 1st, -1st order coherent modes are illustrated separately. Each component becomes relatively large in the diffraction direction of the exciting Floquet modes, and has dips due to the zeros of $G(\lambda')$. When σ is small, the component excited by the 0th Floquet mode is relatively large and mainly determines $\sigma_1(\phi|\theta)$, while the contribution from non-zero-order coherent modes increases as σ becomes large.

Figure 4.5 illustrates $\sigma_1(\phi|\theta)$ for several width parameters. When a_0 is small, no dip appears. Figure 4.6 illustrates $\sigma_1(\phi|\theta)$ for several angles of incidence. The amplitude of scattering is relatively large in the direction of specular reflection, i.e. the diffraction direction of the 0th Floquet mode. Figure 4.7 shows $\sigma_1(\phi|\theta)$ for several height parameters. $\sigma_1(\phi|\theta)$ increases when σ is large. The directions where the dips appear depend on the height parameter σ. It is due to the interference among the incoherent components excited by different order Floquet modes, since the scattered wave excited by non-zero-order Floquet modes increase when σ is large. Figure 4.8 illustrates $\sigma_2(\phi|\theta)$, its main part $\sigma_2(\phi|\theta)_m$ and subtractive part $\sigma_2(\phi|\theta)_d$ for $\sigma = 0.05\lambda, a_0 = \lambda, \theta = 80°$. This figure shows that $\sigma_2(\phi|\theta)_m$ and $\sigma_2(\phi|\theta)_d$ are approximately same in amplitude, so that $\sigma_2(\phi|\theta)$ becomes much smaller than $\sigma_2(\phi|\theta)_m$. We see that $\sigma_2(\phi|\theta)$ has some dips in the diffraction directions of the Floquet modes. Such dips appear in the binary case, but they do not exist in the Gaussian case [8]. It is due to the fact that the subtractive part $\sigma_2(\phi|\theta)_d$ becomes relatively large in such directions. Figure 4.9 illustrates $\sigma(\phi|\theta) = \sigma_1(\phi|\theta) + \sigma_2(\phi|\theta)$ for $\sigma = 0.05\lambda, \theta = 60°, a_0 = \lambda$. $\sigma_2(\phi|\theta)$ is much smaller than $\sigma_1(\phi|\theta)$,

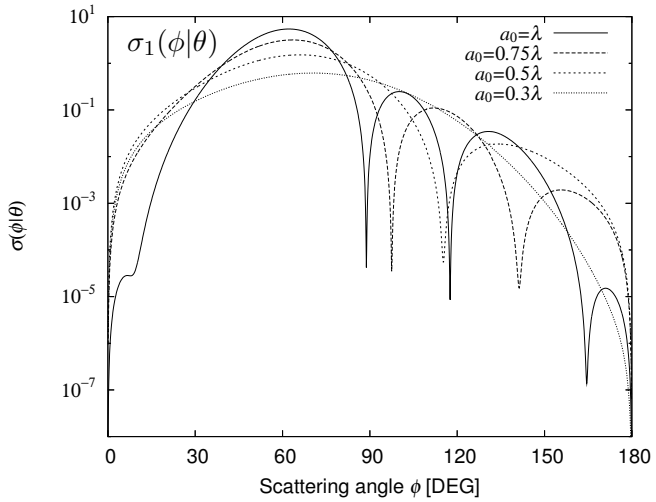

Figure 4.5 Scattering cross section $\sigma_1(\phi|\theta)$ for several width parameter a_0. $L = 3\lambda$, $\sigma = 0.1\lambda$, $\theta = 60^\circ$ and $\kappa = 0.18\lambda$. When a_0 is large, the number of dips increases. No dip appears when a_0 is 0.3λ.

so that $\sigma_2(\phi|\theta)$ contributes to $\sigma(\phi|\theta)$ only when $\sigma_1(\phi|\theta)$ is very small.

Figure 4.10 shows the optical theorem calculated by the zero and first order binary kernels against the surface height parameter σ. Total power is normalized as unity. As the surface height becomes large, approximately up to 0.15λ, the incoherent scattering and non-zero-order coherent modes increase, while the zero-order coherent mode and total coherent scattering decrease instead. However, when σ becomes larger than 0.15λ, the incoherent power decreases. It may be due to $\mathbf{M}^{(1)}(p)$, which represents the diffraction and multiple scattering effects. Total power including coherent modes and incoherent scattering is almost constant, approximately equal to the incident power. Figure 4.11 illustrates the optical theorem against the angle of incidence θ, where the 1st and -1st order coherent powers are enlarged 10 times. Since $L = 3\lambda$, the 1st order coherent power becomes radiating when $\theta \geq 48.19^\circ$. When the angle of incidence is close to 90°, the zero-order coherent power decreases.

4.6 Conclusion

We have studied the diffraction and scattering of a TE plane wave from a binary periodic random surface generated by a binary sequence using the stochastic functional approach. Assuming that such a periodic random surface is mathematically modeled by a periodic stationary process, we have pointed out that the scattered wave has a stochastic Floquet form, which is a product of an exponential phase factor and a periodic stationary process. We reconsidered the harmonic series representation used in [44] for such a periodic stationary process. We wrote such a periodic stationary process by orthogonal binary functionals with binary kernels given by multiple Fourier integrals. We have then found that for the binary case it is necessary to divide such Fourier integrals into bands with equal band width. Then, such a periodic stationary process was represented by a harmonic series, of which coefficients are mutually correlated wide sense stationary processes given by binary functionals with band-limited binary kernels. Using the Dirichlet boundary condition without approximation, we have determined the band-limited

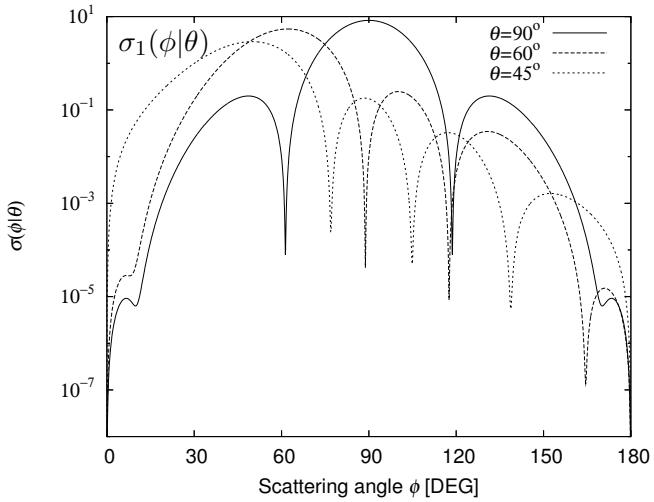

Figure 4.6 Scattering cross section $\sigma_1(\phi|\theta)$ for several angles of incidence θ. $L = 3\lambda$, $\sigma = 0.1\lambda$, $a_0 = \lambda$ and $\kappa = 0.18\lambda$. Incoherent scattering is relatively strong in the direction of specular reflection, i.e. the diffraction direction of the 0th Floquet mode.

binary kernels up to the second order, from which several statistical properties of the scattering were calculated. It is found that the components of the first order incoherent scattering are relatively large in the diffraction directions of the exciting Floquet modes and have some dips corresponding to the zeros of spectrum of the local profile. We find that, due to the special property of the binary random variable, the second order scattering cross section has a subtractive term and becomes much smaller than the first order one. The second order scattering cross section has dips in the diffraction directions of the Floquet modes. It is also found that the incoherent power begins to decrease when the height parameter gets large, possibly due to the diffraction and multiple scattering effects by the mass operator.

The discussion in this chapter was limited to the TE case. However, this approach can be extended without any difficulties to TM wave scattering from a binary periodic random surface. The TM case is discussed in the following chapter.

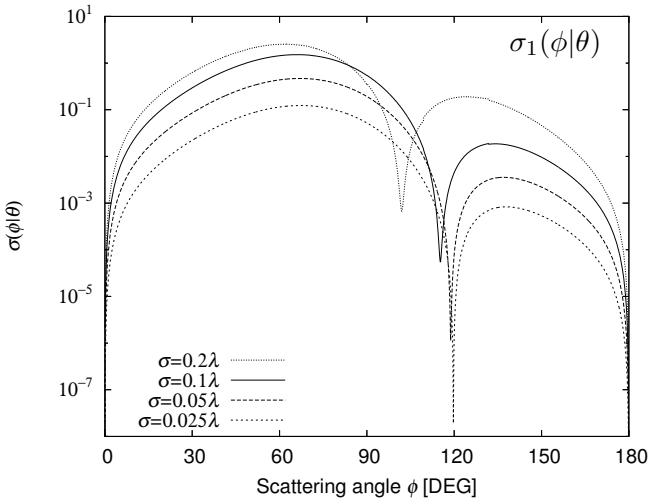

Figure 4.7 Scattering cross section $\sigma_1(\phi|\theta)$ for several height parameter σ. $L = 3\lambda$, $\theta = 60°$, $a_0 = 0.5\lambda$ and $\kappa = 0.18\lambda$. Incoherent scattering becomes large when σ is large. The dip angle changes with σ because incoherent scattering components excited by different order Floquet modes interfere.

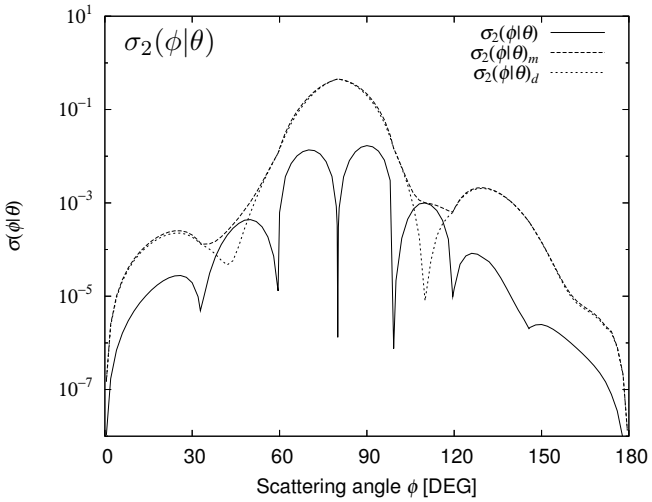

Figure 4.8 Scattering cross section $\sigma_2(\phi|\theta)$, its main part $\sigma_2(\phi|\theta)_m$ and subtractive part $\sigma_2(\phi|\theta)_d$. $L = 3\lambda$, $\sigma = 0.05\lambda$, $\theta = 80°$, $a_0 = \lambda$ and $\kappa = 0.18\lambda$. $\sigma_2(\phi|\theta)_m$ and $\sigma_2(\phi|\theta)_d$ are approximately same in amplitude, so that $\sigma_2(\phi|\theta)$ becomes much smaller than $\sigma_2(\phi|\theta)_m$. There are some dips in $\sigma_2(\phi|\theta)$, which correspond to the diffraction directions of Floquet modes. It is due to the fact that $\sigma_2(\phi|\theta)_d$ becomes relatively large in such directions.

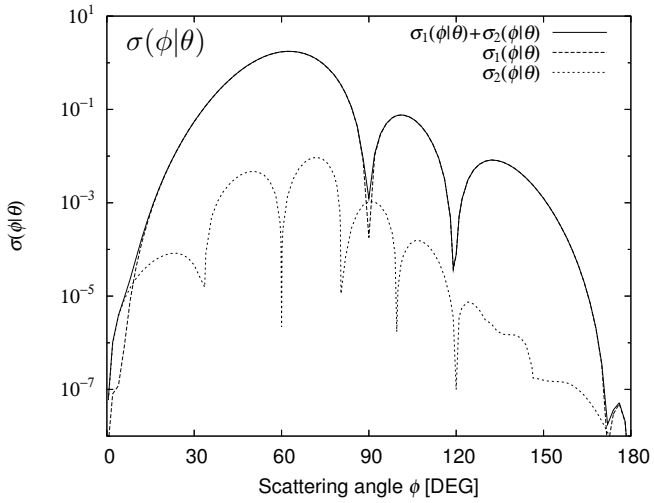

Figure 4.9 Scattering cross section $\sigma(\phi|\theta) = \sigma_1(\phi|\theta) + \sigma_2(\phi|\theta)$. $L = 3\lambda$, $\sigma = 0.05\lambda$, $\theta = 60°$, $a_0 = \lambda$ and $\kappa = 0.18\lambda$. $\sigma_2(\phi|\theta)$ is much smaller than $\sigma_1(\phi|\theta)$, so that $\sigma_2(\phi|\theta)$ contributes to $\sigma(\phi|\theta)$ only when $\sigma_1(\phi|\theta)$ is very small.

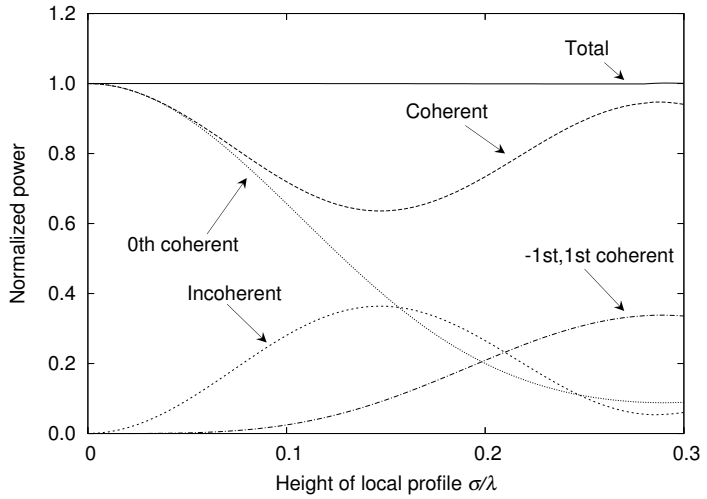

Figure 4.10 Optical theorem vs. height parameter σ. $L = 3\lambda$, $a_0 = 0.5\lambda$, $\kappa = 0.18\lambda$ and $\theta = 90°$. The 0th coherent power decreases when the height parameter σ is large, while $\pm$1st coherent power increases. Incoherent power increases proportionally to σ for $\sigma < 0.15\lambda$, but decreases when σ is large. Total power is almost equal to the incident power that is normalized as unity.

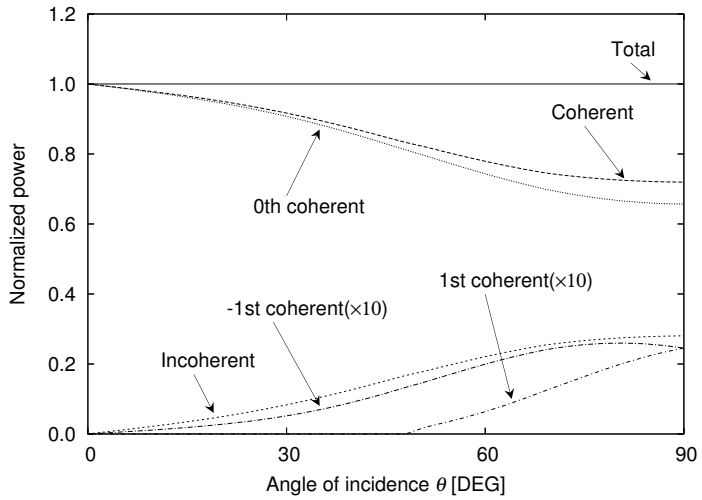

Figure 4.11 Optical theorem vs. angle of incidence. $L = 3\lambda$, $a_0 = 0.5\lambda$, $\sigma = 0.1\lambda$ and $\kappa = 0.18\lambda$. The $\pm$1st coherent powers are enlarged 10 times. Incoherent power increases when θ is near 90°, while 0th coherent power decreases. The 1st coherent mode becomes radiating when $\theta \geq 48.19°$. Total power is almost equal to the incident power that is normalized as unity.

Chapter 5

Diffraction and scattering of TM plane wave from a binary periodic random surface

5.1 Introduction

In the previous chapter, we have studied the diffraction and scattering from a binary periodic random surface generated by a stationary binary sequence. But the discussions were limited to TE wave case.

This chapter deals with the diffraction and scattering of a TM plane wave from a perfectly conductive periodic random surface shown in figure 5.1, following the same manner as the previous chapter in the formulation of the problem. We again employ the stochastic functional approach [7, 8, 44, 59], and hierarchical equations for the TM case are derived to determine such band-limited binary kernels are derived from the Neumann boundary condition without approximation.

When the periodic random surface is periodic with average height, binary kernels can be obtained by a single scattering approximation in Ref [8]. However, when the periodic random surface is zero on average, such binary kernels by a single scattering approximation diverge unphysically for critical wavenumbers. To obtain a physically meaningful(appropriate) solution, effects of multiple scattering should be taken into account. Thus, to determine the band-limited binary kernels, this chapter employs the multiply renormalizing approximation [53]. Then, we obtain a new solution without such divergence difficulties. In terms of the new solution, several statistical properties of the diffraction and scattering, such as differential scattering cross section and optical theorem, are numerically calculated in terms of such binary kernels and illustrated in figures.

As is well known, Wood's anomaly occurs for critical angles of incidence as rapid variations in the diffraction powers in the perfectly periodic case [†] [28, 29], however, we find that Wood's anomaly appears in the diffraction from such a binary periodic random surface with zero average. It is because the periodic random surface with binary fluctuations acts as a periodic surface in an average sense. Furthermore, incoherent Wood's anomaly appears as rapid variations in the

[†]Since we consider a surface obtained by displacing the local profile with constant period, and binary fluctuations on the height parameter of such a local profile, we utilize the word 'perfectly periodic' for the classical periodic surfaces without fluctuations.

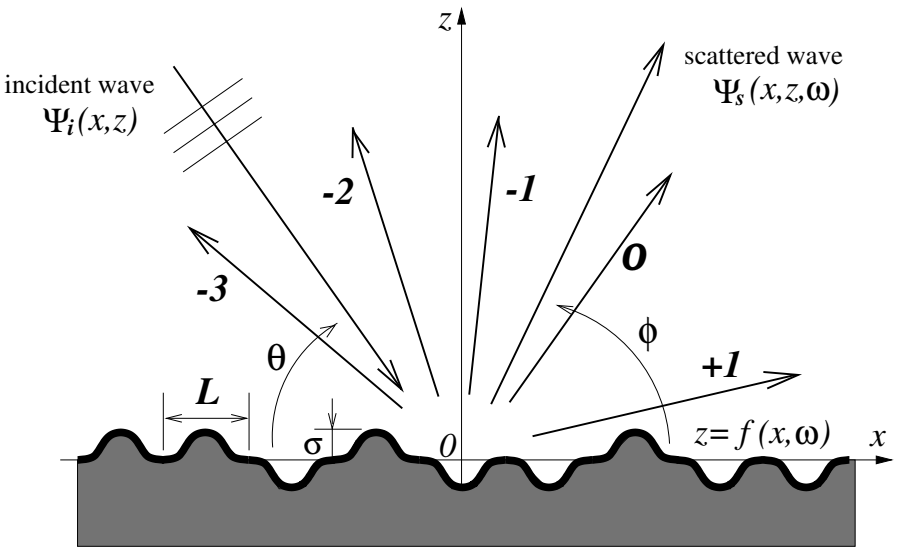

Figure 5.1 Geometry of the problem. Incident wave is diffracted and scattered by a periodic random surface generated by a binary sequence. L and σ are the period and the height parameter of the surface, θ is the angle of incidence and ϕ is a scattering angle. The orders of the coherently diffracted waves are denoted by numbers.

angular distribution of the scattering. In this chapter, we discuss the physical mechanisms of Wood's anomaly and incoherent Wood's anomaly, which is a similar discussion to Chapter 3. Incoherent Wood's anomaly has been found in cases of random surfaces that are periodic on average [6, 8] and in a deterministic case of a periodic grooves with single defect [46]. However, we newly show that incoherent Wood's anomaly appears even when a binary periodic random surface has zero average.

5.2 Probabilistic formulation of the problem

5.2.1 Properties of binary periodic random surfaces

Following the same manner as the previous chapter, let us consider a periodic random surface with binary fluctuations, shown in figure 5.1, where the surface deformations are expressed by a periodic stationary process $f(x,\omega)$ generated by a binary sequence :

$$z = f(x,\omega) = \sigma \sum_{m=-\infty}^{\infty} g(x-mL) b_m(\omega), \quad (-\infty < x < \infty), \tag{5.1}$$

$$= \sigma g(x) b_0(\omega), \quad (-L/2 < x < L/2). \tag{5.2}$$

Here, σ is a parameter representing surface height, L is the period of the surface, and $g(x)$ is the local surface profile with $g(x) = 0$ for $|x| \geq L/2$ under which (5.2) holds. $g(x)$ has no dimension. $\{b_m(\omega)\}$ is an independent binary random sequence taking ± 1 with equal probability : $P(b_m(\omega) = 1) = P(b_m(\omega) = -1) = 1/2$, where ω is a probability parameter denoting a sample point in the sample space Ω.

Here, $P(\cdot)$ is the probability measure [24]. Then, $b_m(\omega)$ has zero average and orthogonal correlation,

$$\langle b_m(\omega)\rangle = 0, \qquad \langle b_m(\omega)b_n(\omega)\rangle = \delta(m,n), \tag{5.3}$$

where the angular brackets $\langle\cdot\rangle$ denote the ensemble average over Ω, and $\delta(m,n)$ is the Kronecker delta. Furthermore, it is important to notice that $b_m(\omega)$ is random but $b_m^2(\omega)$ always becomes deterministic, namely,

$$b_m^2(\omega) = 1. \tag{5.4}$$

This is a special property[‡] for the binary random variable taking ± 1. As is pointed out in the previous chapter, however, this simple property makes it complicated to treat its functionals, compared with the Gaussian random cases [7, 8].

From (5.1) and (5.3), the average and the correlation function of $f(x,\omega)$ become

$$\langle f(x,\omega)\rangle = 0, \tag{5.5}$$

$$R_f(x,x') = \langle f(x,\omega)f(x',\omega)\rangle = \sigma^2 \sum_{m=-\infty}^{\infty} g(x-mL)g(x'-mL)$$
$$= R_f(x+L,x'+L). \tag{5.6}$$

Here, $R_f(x,x')$ is periodic in the direction of $x = x'$ in the x-x' plane (See figure 4.2). By (5.5) and (5.6), the binary periodic random surface $f(x,\omega)$ becomes a periodic stationary process with the period L. It should be noted that any realization $f(x,\omega)$ has no periodicity, however, its correlation function is a periodic function with the period L. Furthermore, one easily finds that $R_f(x,x) = \{f(x,\omega)\}^2$ under the condition (5.5), which is non-random and periodic.

We assume that the sample space Ω is of function space type [47], where Ω is regarded as an infinite-dimensional Euclidean space and a sample point ω is an infinite-dimensional vector in Ω given by a sample sequence :

$$\omega = (\cdots, \omega_{-1}, \omega_0, \omega_1, \cdots), \qquad \omega_n = b_n(\omega), \tag{5.7}$$

where ω_n is the n-th component of ω. Under this assumption, we define a measure-preserving transformation in the sample space Ω by T^m, which generates a shift from ω to another sample point $\omega' = T^m\omega = (\cdots, \omega_{m-1}, \omega_m, \omega_{m+1}, \cdots)$ where $T^m\omega_n = b_{m+n}(\omega)$, and the probability measure $P(\cdot)$ is preserved, i.e. $P(\omega) = P(\omega')$. T^m has group properties : $T^0 \equiv 1$ (identity) ; $T^{m+n} = T^mT^n$ [7]. Thus, we may write,

$$b_n(\omega) = b_0(T^n\omega). \tag{5.8}$$

By this property, $f(x,\omega)$ is invariant under the translation operator D^n [7]

$$D^n f(x,\omega) = f(x+nL, T^{-n}\omega) = f(x,\omega), \tag{5.9}$$

and becomes a periodic stationary process [59].

[‡]On the other hand, if $b_m(\omega)$ is a Gaussian random variable, $b_m^2(\omega)$ remains random. Thus, here is a significant difference between binary random variables and Gaussian random variables. However, such difference becomes prominent in the properties of the scattering in the second or higher orders [59].

5.2.2 Expression of wave field

Let us denote the y component of the magnetic field by $\Psi(x,z,\omega)$, which satisfies the wave equation in free space,

$$\left[\frac{\partial^2}{\partial x^2}+\frac{\partial^2}{\partial z^2}+k^2\right]\Psi(x,z,\omega)=0, \quad z>f(x,\omega), \tag{5.10}$$

where k is the wave number. On the perfectly conductive random surface $z=f(x,\omega)$, $\Psi(x,z,\omega)$ satisfies the Neumann condition :

$$\left.\frac{\partial\Psi(x,z,\omega)}{\partial n}\right|_{z=f(x,\omega)}=\frac{1}{\sqrt{1+(df/dx)^2}}\left[-\frac{df}{dx}\frac{\partial}{\partial x}+\frac{\partial}{\partial z}\right]\Psi(x,z,\omega)\Big|_{z=f(x,\omega)}=0. \tag{5.11}$$

For a periodic stationary process $\Phi(x,\omega)$, we define a norm $\parallel \Phi(x,\omega) \parallel$ as an ensemble average of a space average of $|\Phi(x,\omega)|^2$ over one period

$$\parallel \Phi(x,\omega) \parallel^2=\left\langle \frac{1}{L}\int_{-L/2}^{L/2}|\Phi(x,\omega)|^2\,dx\right\rangle, \tag{5.12}$$

which will be used below.

When a TM plane wave $e^{ipx}e^{-i\beta_0(p)z}$ is incident on the periodic random surface, the wave field can be represented as

$$\Psi(x,z,\omega)=e^{ipx}e^{-i\beta_0(p)z}+e^{ipx}U(x,z,\omega), \quad p=k\cos\theta, \tag{5.13}$$

$$\beta_n(\lambda')=\sqrt{k^2-(\lambda'+2\pi n/L)^2}=\beta_{n+q}\left(\lambda'-k_Lq\right), \quad k_L=\frac{2\pi}{L}, \tag{5.14}$$

$$\mathrm{Im}[\beta_n(\lambda')]\geq 0, \qquad (n,q=0,\pm1,\pm2,\cdots).$$

Here, (5.13) is a 'stochastic Floquet theorem' [7]. The second term of the right-hand side of (5.13) is the scattered wave and $U(x,z,\omega)$ is a periodic stationary process. Here, θ is the angle of incidence, k_L is the spatial angular frequency of the period L, and 'Im' denotes the imaginary part.

Note that a periodic stationary process $U(x,z,\omega)$ is not periodic, but the ensemble average $\langle U(x,z,\omega)\rangle$ becomes periodic, and $U(x,z,\omega)$ satisfies the shift invariance property [59]:

$$D^mU(x,z,\omega) \;=\; U(x+mL,z,T^{-m}\omega)=U(x,z,\omega). \tag{5.15}$$

5.3 Representations of periodic stationary processes

5.3.1 Binary expansion of periodic stationary processes

To obtain the scattered wave $e^{ipx}U(x,z,\omega)$, it is necessary to determine the periodic stationary process $U(x,z,\omega)$. In previous papers [44, 59], we discussed that such a periodic stationary process can be expressed by a harmonic series representation.

Since $U(x,z,\omega)$ is a stochastic functional of the binary sequence $\{b_m(\omega)\}$, it can be represented by an orthogonal binary functional expansion for each value of (x,z), which should satisfy $U(x,z,\omega)=U(x+mL,z,T^{-m}\omega)$.

To make $e^{ipx}U(x,z,\omega)$ satisfy the wave equation (5.10), we write $U(x,z,\omega)$ as

$$U(x,z,\omega)=\sum_{q=-\infty}^{\infty}e^{ik_Lqx}U^{(q)}(x,z,\omega), \tag{5.16}$$

which is a harmonic series representation. (5.16) can be regarded as a "Fourier series" with "Fourier coefficients" given by mutually correlated stationary processes $U^{(q)}(x,z,\omega)$:

$$U^{(q)}(x,z,\omega) = C_0^{(q)}(p)\ e^{i\beta_q(p)z} + \sum_{m=-\infty}^{\infty} B_1[b_m] \int_{-k_L/2}^{k_L/2} C_1^{(q)}(\lambda_s|p) e^{i\lambda_s(x-mL)+i\beta_q(p+\lambda_s)z} d\lambda_s$$
$$+ \sum_{m,n=-\infty}^{\infty} B_2[b_m, b_n] \iint_{-k_L/2}^{k_L/2} C_2^{(q)}(\lambda_1, \lambda_s-\lambda_1|p)$$
$$\times e^{i(\lambda_s-\lambda_1)(x-mL)+i\lambda_1(x-nL)+i\beta_q(p+\lambda_s)z} d\lambda_1 d\lambda_s + \cdots. \tag{5.17}$$

Here, $B_n[\cdot]$ is the n-th order binary polynomial defined in Appendix A, and $C_0^{(q)}(p)$, $C_1^{(q)}(\lambda'|p)$, $C_2^{(q)}(\lambda_1,\lambda_2|p),\cdots$ are the band-limited binary kernels [59] in the spectral domain. Note that this expansion is physically written as a sum of outgoing plane waves and surface waves $e^{i\lambda_s x+i\beta_q(p+\lambda_s)z}$. Taking the Rayleigh hypothesis, we assume that (5.16) and (5.17) are valid even in the region $f(x,\omega) \le z \le \max\{f(x,\omega)\}$. By (5.17), $U^{(q)}(x,z,\omega)$ becomes wide sense stationary [59]. The band-limited binary kernels $C_0^{(q)}(p)$, $C_1^{(q)}(\lambda|p)$, $C_2^{(q)}(\lambda_1,\lambda_2|p),\cdots$ can be uniquely determined, as will be shown later.

Since $e^{i(p+k_Lq)x}U^{(q)}(x,z,\omega)$ is a component of the scattered wave, $C_1^{(q)}(\lambda_s|p)$, $C_2^{(q)}(\lambda_s-\lambda_1,\lambda_1|p),\cdots$ are amplitude factors of the plane wave with the scattering angle $\phi_q(p+\lambda_s)$ given by

$$\phi_q(p+\lambda_s) = \cos^{-1}\left[\frac{p+k_Lq+\lambda_s}{k}\right], \tag{5.18}$$

which is measured from the x-axis. (See figure 5.1.)

5.3.2 Statistical properties of wave field

Since $B_m[\cdot]$ has zero average for $m \ge 1$ by (A.6), we obtain the coherent wave (average wave) from (5.13), (5.16) and (5.17) as

$$\langle \Psi(x,z,\omega)\rangle = e^{ipx}\left[e^{-i\beta_0(p)z} + \sum_{q=-\infty}^{\infty} C_0^{(q)}(p) e^{ik_Lqx} e^{i\beta_q(p)z}\right]. \tag{5.19}$$

This shows exactly the Floquet solution for a periodic grating, where $C_0^{(q)}(p)$ is an amplitude factor of the q-th Floquet mode diffracted into the angle $\phi_q(p)$. It means that the binary periodic random surface which has zero average acts as a perfectly periodic surface for the coherent wave. Due to this fact, we say that the periodic random surface effectively has a discrete component of the spectrum.

From (5.13), (5.16) and (5.17), we obtain the optical theorem [50, 59]

$$\frac{\beta_0(p)}{k} = \frac{1}{k}\sum_{q=-\infty}^{\infty} \mathrm{Re}\left[\beta_q(p)\right]\left|C_0^{(q)}(p)\right|^2 + \frac{1}{2\pi}\int_0^{\pi}\sigma(\phi|\theta)d\phi, \tag{5.20}$$

where 'Re' denotes the real part. The left-hand side is the incident power per unit length, the first term and the integral in the right-hand side are the sum of the coherent diffraction power and the power of incoherent scattering, respectively. $\sigma(\phi|\theta)$ is the differential scattering cross section per unit length to the scattering angle ϕ

$$\sigma(\phi|\theta) = \sigma_1(\phi|\theta) + \sigma_2(\phi|\theta) + \cdots. \tag{5.21}$$

$\sigma_1(\phi|\theta)$ is the contribution from the first-order band-limited binary kernels

$$\sigma_1(\phi|\theta) = 2\pi k \sin^2\phi \sum_{q=-\infty}^{\infty} k_L \left| C_1^{(q)}(k\cos\phi - p - k_L q|p) \right|^2 S(k\cos\phi - p - k_L q), \tag{5.22}$$

where $S(\lambda')$ is a gate function defined as

$$S(\lambda') = \begin{cases} 1, & (|\lambda'| \le k_L/2) \\ 0, & (|\lambda'| > k_L/2) \end{cases}, \qquad \sum_{l=-\infty}^{\infty} S(\lambda' + k_L l) \equiv 1. \tag{5.23}$$

The band-limited binary kernel $C_1^{(q)}(\cdot)$ is expected to satisfy

$$C_1^{(q)}(k_L/2 - p|p) = C_1^{(q+1)}(-k_L/2 - p|p) \tag{5.24}$$

at the band edge. $\sigma_2(\phi|\theta)$ in (5.21) is the contribution from the second-order band-limited kernels, however, in this paper, only $\sigma_1(\phi|\theta)$ is calculated for $\sigma(\phi|\theta)$ and illustrated later.

5.4 Hierarchical equations and an approximate solution

5.4.1 Derivation of hierarchical equations

Even though $\Psi(x,z,\omega)$ itself is not periodic stationary, $|\Psi(x,z,\omega)| = |e^{-i\beta_0(p)z} + U(x,z,\omega)|$ becomes a periodic stationary process by (5.13). Thus, we assume that the boundary condition (5.11) holds in the norm sense (5.12) along the surface,

$$\begin{aligned} &\left\| \frac{\partial \Psi(x,z,\omega)}{\partial n}\bigg|_{z=f(x,\omega)} \right\|^2 \\ &\quad = \left\langle \frac{1}{L}\int_{-L/2}^{L/2} \frac{1}{\sqrt{1+(df/dx)^2}} \left| \left[-\frac{df}{dx}\frac{\partial}{\partial x} + \frac{\partial}{\partial z} \right] \Psi(x,z,\omega)\bigg|_{z=f(x,\omega)} \right|^2 dx \right\rangle = 0. \end{aligned} \tag{5.25}$$

For TM incidence, an approximate boundary condition, so-called effective boundary condition [18]: $-(df/dx)\partial\Psi(x,z,\omega)/\partial x + \partial\Psi(x,z,\omega)/\partial z + \partial^2\Psi(x,z,\omega)/\partial z^2 = 0$ at $z=0$, is often employed to determine the wave field under the assumptions of small roughness $\sigma^2 k^2 \ll 1$ and small slope $|df/dx| < 1$. However, this paper deals with the Neumann boundary condition (5.11) without approximation. To calculate the norm (5.25), we substitute (5.13), (5.16) and (5.17) into (5.25). For simplicity, we note that

$$\frac{d}{dx} f(x,\omega) = h(x) b_0(\omega), \qquad h(x) = \sigma \frac{d}{dx} g(x) \tag{5.26}$$

for $|x| \le L/2$. Using the identity for $b_0(\omega) = \pm 1$,

$$e^{i\beta_0(p) f(x,\omega)} = e^{i\sigma\beta_0(p) g(x) b_0(\omega)} = \cos[\sigma\beta_0(p) g(x)] + i \sin[\sigma\beta_0(p) g(x)] b_0(\omega) \tag{5.27}$$

for $|x| \le L/2$, and applying the recurrence relations (A.11) and the orthogonal relation (A.7), we obtain hierarchical equations for the binary kernels as a sufficient condition:
(zero order)

$$-i\{\beta_0(p)\cos[\sigma\beta_0(p) g(x)] - iph(x)\sin[\sigma\beta_0(p) g(x)]\}$$

$$+\sum_{q=-\infty}^{\infty} e^{ik_Lqx}\Big[i\{\beta_q(p)\cos[\sigma\beta_q(p)g(x)]-i(p+k_Lq)h(x)\sin[\sigma\beta_q(p)g(x)]\}C_0^{(q)}(p)$$
$$-\int_{-k_L/2}^{k_L/2}\{\beta_q(p+\lambda_s)\sin[\sigma\beta_q(p+\lambda_s)g(x)]$$
$$+i(p+k_Lq+\lambda_s)h(x)\cos[\sigma\beta_q(p+\lambda_s)g(x)]\}C_1^{(q)}(\lambda_s|p)e^{i\lambda_s x}d\lambda_s\Big]=0, \qquad (5.28)$$

(first order) $(m=0,\pm1,\pm2,\cdots)$

$$-\delta(m,0)\{\beta_0(p)\sin[\sigma\beta_0(p)g(x)]+iph(x)\cos[\sigma\beta_0(p)g(x)]\}$$
$$-\delta(m,0)\sum_{q=-\infty}^{\infty}e^{ik_Lqx}\{\beta_q(p)\sin[\sigma\beta_q(p)g(x)]+i(p+k_Lq)h(x)\cos[\sigma\beta_q(p)g(x)]\}C_0^{(q)}(p)$$
$$+\sum_{q=-\infty}^{\infty}e^{ik_Lqx}\Big[i\int_{-k_L/2}^{k_L/2}\{\beta_q(p+\lambda_s)\cos[\sigma\beta_q(p+\lambda_s)g(x)]$$
$$-i(p+k_Lq+\lambda_s)h(x)\sin[\sigma\beta_q(p+\lambda_s)g(x)]\}$$
$$\times e^{i\lambda_s(x-mL)}C_1^{(q)}(\lambda_s|p)d\lambda_s$$
$$-2\iint_{-k_L/2}^{k_L/2}\{\beta_q(p+\lambda_s)\sin[\sigma\beta_q(p+\lambda_s)g(x)]$$
$$+i(p+k_Lq+\lambda_s)h(x)\cos[\sigma\beta_q(p+\lambda_s)g(x)]\}$$
$$\times e^{i(\lambda_s-\lambda_1)(x-mL)+i\lambda_1x}C_2^{(q)}(\lambda_s-\lambda_1,\lambda_1|p)d\lambda_1d\lambda_s$$
$$+2\delta(m,0)\iint_{-k_L/2}^{k_L/2}\{\beta_q(p+\lambda_s)\sin[\sigma\beta_q(p+\lambda_s)g(x)]$$
$$+i(p+k_Lq+\lambda_s)h(x)\cos[\sigma\beta_q(p+\lambda_s)g(x)]\}$$
$$\times e^{i\lambda_sx}C_2^{(q)}(\lambda_s-\lambda_1,\lambda_1|p)d\lambda_1d\lambda_s\Big]=0, \qquad (5.29)$$

(second order) $(m_1,m_2=0,\pm1,\pm2,\cdots)$

$$\sum_{q=-\infty}^{\infty}e^{ik_Lqx}\Big[i\iint_{-k_L/2}^{k_L/2}\{\beta_q(p+\lambda_s)\cos[\sigma\beta_q(p+\lambda_s)g(x)]$$
$$-i(p+k_Lq+\lambda_s)h(x)\sin[\sigma\beta_q(p+\lambda_s)g(x)]\}$$
$$\times e^{i(\lambda_s-\lambda_1)(x-m_1L)+i\lambda_1(x-m_2L)}C_2^{(q)}(\lambda_s-\lambda_1,\lambda_1|p)d\lambda_1d\lambda_s$$
$$-\frac{1}{2}\delta(m_2,0)\int_{-k_L/2}^{k_L/2}\{\beta_q(p+\lambda_s-\lambda_1)\sin[\sigma\beta_q(p+\lambda_s-\lambda_1)g(x)]$$
$$+i(p+k_Lq+\lambda_s-\lambda_1)h(x)\cos[\sigma\beta_q(p+\lambda_s-\lambda_1)g(x)]\}$$
$$\times e^{i(\lambda_s-\lambda_1)(x-m_1L)}C_1^{(q)}(\lambda_s-\lambda_1|p)d\lambda_s$$
$$-\frac{1}{2}\delta(m_1,0)\int_{-k_L/2}^{k_L/2}\{\beta_q(p+\lambda_1)\sin[\sigma\beta_q(p+\lambda_1)g(x)]$$
$$+i(p+k_Lq+\lambda_1)h(x)\cos[\sigma\beta_q(p+\lambda_1)g(x)]\}$$
$$\times e^{i\lambda_1(x-m_2L)}C_1^{(q)}(\lambda_1|p)d\lambda_1$$
$$-3\iiint_{-k_L/2}^{k_L/2}\{\beta_q(p+\lambda_s)\sin[\sigma\beta_q(p+\lambda_s)g(x)]$$

$$
\begin{aligned}
&+i(p+k_Lq+\lambda_s)h(x)\cos[\sigma\beta_q(p+\lambda_s)g(x)]\}\\
&\times e^{i(\lambda_s-\lambda_1-\lambda_2)(x-m_1L)+i\lambda_1(x-m_2L)+i\lambda_2x}\\
&\times C_3^{(q)}(\lambda_s-\lambda_1-\lambda_2,\lambda_1,\lambda_2|p)d\lambda_1d\lambda_2d\lambda_s\\
+6\delta(n,0)\iiint_{-k_L/2}^{k_L/2}&\{\beta_q(p+\lambda_s)\sin[\sigma\beta_q(p+\lambda_s)g(x)]\\
&+i(p+k_Lq+\lambda_s)h(x)\cos[\sigma\beta_q(p+\lambda_s)g(x)]\}\\
&\times e^{i(\lambda_s-\lambda_1-\lambda_2)(x-m_1L)+i\lambda_1x+i\lambda_2x}\\
&\times C_3^{(q)}(\lambda_s-\lambda_1-\lambda_2,\lambda_1,\lambda_2|p)d\lambda_1d\lambda_2d\lambda_s\Big]=0, \qquad (5.30)
\end{aligned}
$$

(n-th order) $(n\geq 3)$ $\qquad (m_1,\cdots,m_n=0,\pm1,\pm2,\cdots)$

$$
\begin{aligned}
\sum_{q=-\infty}^{\infty}e^{ik_Lqx}\Big[i\int\cdots\int_{-k_L/2}^{k_L/2}&\{\beta_q(p+\lambda_s)\cos[\sigma\beta_q(p+\lambda_s)g(x)]\\
&-i(p+k_Lq+\lambda_s)h(x)\sin[\sigma\beta_q(p+\lambda_s)g(x)]\}\\
&\times e^{i(\lambda_s-(\lambda_1+\cdots+\lambda_{n-1}))(x-m_nL)+i\lambda_1(x-m_1L)+\cdots+i\lambda_{n-1}(x-m_{n-1}L)}\\
&\times C_n^{(q)}(\lambda_s-(\lambda_1+\cdots+\lambda_{n-1}),\lambda_1,\cdots,\lambda_{n-1}|p)d\lambda_1\cdots d\lambda_{n-1}d\lambda_s\\
-\frac{1}{n}\delta(m_1,0)\int\cdots\int_{-k_L/2}^{k_L/2}&\{\beta_q(p+\lambda_s-\lambda_1)\sin[\sigma\beta_q(p+\lambda_s-\lambda_1)g(x)]\\
&+i(p+k_Lq+\lambda_s-\lambda_1)h(x)\cos[\sigma\beta_q(p+\lambda_s-\lambda_1)g(x)]\}\\
&\times e^{i(\lambda_s-(\lambda_1+\cdots+\lambda_{n-1}))(x-m_nL)+i\lambda_2(x-m_2L)+\cdots+i\lambda_{n-1}(x-m_{n-1}L)}\\
&\times C_{n-1}^{(q)}(\lambda_s-(\lambda_1+\cdots+\lambda_{n-1}),\lambda_2,\cdots,\lambda_{n-1}|p)d\lambda_2\cdots d\lambda_{n-1}d\lambda_s\\
&\vdots\\
-\frac{1}{n}\delta(m_n,0)\int\cdots\int_{-k_L/2}^{k_L/2}&\{\beta_q(p+\lambda_1+\cdots+\lambda_{n-1})\sin[\sigma\beta_q(p+\lambda_1+\cdots+\lambda_{n-1})g(x)]\\
&+i(p+k_Lq+\lambda_1+\cdots+\lambda_{n-1})h(x)\cos[\sigma\beta_q(p+\lambda_1+\cdots+\lambda_{n-1})g(x)]\}\\
&\times C_{n-1}^{(q)}(\lambda_1,\cdots,\lambda_{n-1}|p)e^{i\lambda_1(x-m_1L)+\cdots+i\lambda_{n-1}(x-m_{n-1}L)}d\lambda_1\cdots d\lambda_{n-1}\\
-(n+1)\int\cdots\int_{-k_L/2}^{k_L/2}&\{\beta_q(p+\lambda_s)\sin[\sigma\beta_q(p+\lambda_s)g(x)]\\
&+i(p+k_Lq+\lambda_s)h(x)\cos[\sigma\beta_q(p+\lambda_s)g(x)]\}\\
&\times e^{i(\lambda_s-(\lambda_1+\cdots+\lambda_n))x+i\lambda_1(x-m_1L)+\cdots+i\lambda_n(x-m_nL)}\\
&\times C_{n+1}^{(q)}(\lambda_s-(\lambda_1+\cdots+\lambda_n),\lambda_1,\cdots,\lambda_n|p)d\lambda_1\cdots d\lambda_nd\lambda_s\\
+n(n+1)\delta(m_n,0)\int\cdots\int_{-k_L/2}^{k_L/2}&\{\beta_q(p+\lambda_s)\sin[\sigma\beta_q(p+\lambda_s)g(x)]\\
&+i(p+k_Lq+\lambda_s)h(x)\cos[\sigma\beta_q(p+\lambda_s)g(x)]\}\\
&\times e^{i(\lambda_s-(\lambda_1+\cdots+\lambda_n))x+i\lambda_1(x-m_1L)+\cdots+i\lambda_{n-1}(x-m_{n-1}L)+i\lambda_nx}\\
&\times C_{n+1}^{(q)}(\lambda_s-(\lambda_1+\cdots+\lambda_n),\lambda_1,\cdots,\lambda_n|p)d\lambda_1\cdots d\lambda_nd\lambda_s\Big]=0 \qquad (5.31)
\end{aligned}
$$

Here, (5.29), (5.30) and (5.31) hold for any m or m_j $(j=1,\cdots,n)$. Since (5.28)-(5.31) hold for any x in $|x|\leq L/2$, we expand the factors $\{\beta_q(p+\lambda')\cos[\sigma\beta_q(p+\lambda')g(x)]-i(p+k_Lq+\lambda')h(x)\sin[\sigma\beta_q(p+\lambda')g(x)]\}e^{ik_Lqx}e^{i\lambda'x}$ and $\{\beta_q(p+\lambda')\sin[\sigma\beta_q(p+\lambda')g(x)]+i(p+k_Lq+$

$\lambda')h(x)\cos[\sigma\beta_q(p+\lambda')g(x)]\}e^{ik_Lqx}e^{i\lambda' x}$ into Fourier series as

$$\left[\begin{array}{l}\beta_q(p+\lambda')\cos[\sigma\beta_q(p+\lambda')g(x)]-i(p+k_Lq+\lambda')h(x)\sin[\sigma\beta_q(p+\lambda')g(x)]\\ \beta_q(p+\lambda')\sin[\sigma\beta_q(p+\lambda')g(x)]+i(p+k_Lq+\lambda')h(x)\cos[\sigma\beta_q(p+\lambda')g(x)]\end{array}\right]e^{ik_Lqx}e^{i\lambda' x}$$
$$=\sum_{j=-\infty}^{\infty}\left[\begin{array}{l}H^{\rm c}_{jq}(\lambda'|p)\\ H^{\rm s}_{jq}(\lambda'|p)\end{array}\right]e^{ik_Ljx}, \tag{5.32}$$

where $H^s_{jq}(\lambda'|p)$ is at most of the order of σ^1, while $H^c_{jq}(\lambda'|p)$ is of the order of σ^0. Note that

$$H^{\rm c}_{jq}(\lambda'|p)=0,\quad (p+\lambda'=\pm k-k_Lq), \tag{5.33}$$

for all j, since $\beta_q(p+\lambda')$ vanishes for such λ', which causes anomalies in the diffraction and scattering. This will be discussed later.

Then, we introduce infinite-dimensional matrices $\mathbf{H}^{\rm s}(\lambda'|p)$, $\mathbf{H}^{\rm c}(\lambda'|p)$ and infinite-dimensional vectors $\mathbf{C}_0(p)$, $\mathbf{C}_1(\lambda'|p)$, $\mathbf{C}_n(\lambda_1,\cdots,\lambda_n|p)$ $(n\geq 2)$, $\mathbf{I}^0$ as

$$\mathbf{H}^{\rm c}(\lambda'|p) = [H^{\rm c}_{jq}(\lambda'|p)], \tag{5.34}$$
$$\mathbf{H}^{\rm s}(\lambda'|p) = [H^{\rm s}_{jq}(\lambda'|p)], \tag{5.35}$$
$$\mathbf{C}_0(p) = [\cdots,C_0^{(-1)}(p),C_0^{(0)}(p),C_0^{(1)}(p),\cdots]^t, \tag{5.36}$$
$$\mathbf{C}_1(\lambda'|p) = [\cdots,C_1^{(-1)}(\lambda'|p),C_1^{(0)}(\lambda'|p),C_1^{(1)}(\lambda'|p),\cdots]^t, \tag{5.37}$$
$$\mathbf{C}_n(\lambda_1,\cdots,\lambda_n|p) = [\cdots,C_n^{(-1)}(\lambda_1,\cdots,\lambda_n|p), C_n^{(0)}(\lambda_1,\cdots,\lambda_n|p),C_n^{(1)}(\lambda_1,\cdots,\lambda_n|p),\cdots]^t, \tag{5.38}$$
$$\mathbf{I}^0 = [\cdots,0,1,0,\cdots]^t=[\delta(m,0)]^t. \tag{5.39}$$

From (5.33),

$$\det[\mathbf{H}^{\rm c}(0|p)] = 0,\quad (p=\pm k-k_Lq), \tag{5.40}$$
$$\det\left[\mathbf{H}^{\rm c}(\lambda'|p)\right] = 0,\quad (p+\lambda'=\pm k-k_Lq), \tag{5.41}$$

for $q=0,\ \pm1,\ \pm2,\ \cdots$, where $\det[\cdot]$ is a determinant of the matrix. (5.41) means that the inverse matrix $[\mathbf{H}^c(\lambda'|p)]^{-1}$ diverges when $p+\lambda'=\pm k-k_Lq$. This fact is related to Wood's anomaly and incoherent Wood's anomaly as is discussed below.

Multiplying $e^{i\Lambda mL}$, $e^{i\Lambda_1m_1L+i\Lambda_2m_2L}$ and $e^{i\Lambda_1m_1L+\cdots+i\Lambda_nm_nL}$ to the first, second and n-th order equations, respectively, summing up with every m_j $(1\leq j\leq n)$, and using the identity

$$\sum_{m=-\infty}^{\infty}e^{imL(\Lambda-\lambda')}=k_L\sum_{m=-\infty}^{\infty}\delta(\Lambda-\lambda'+k_Lm), \tag{5.42}$$

we obtain the hierarchical equations in a matrix form,
(zero order)

$$-i\mathbf{H}^{\rm c}(0|p)\mathbf{I}^0+i\mathbf{H}^{\rm c}(0|p)\mathbf{C}_0(p)-\int_{-k_L/2}^{k_L/2}\mathbf{H}^{\rm s}(\lambda'|p)\mathbf{C}_1(\lambda'|p)d\lambda'=0, \tag{5.43}$$

(first order)

$$ik_L\mathbf{H}^{\rm c}(\Lambda|p)\mathbf{C}_1(\Lambda|p)-\mathbf{H}^{\rm s}(0|p)\left\{\mathbf{I}^0+\mathbf{C}_0(p)\right\}$$
$$-2k_L\int_{-k_L/2}^{k_L/2}\mathbf{H}^{\rm s}(\Lambda+\lambda_1|p)\mathbf{C}_2(\Lambda,\lambda_1|p)d\lambda_1$$
$$+2\iint_{-k_L/2}^{k_L/2}\mathbf{H}^{\rm s}(\lambda_s|p)\mathbf{C}_2(\lambda_s-\lambda_1,\lambda_1|p)d\lambda_1d\lambda_s=0, \tag{5.44}$$

(second order)

$$
\begin{aligned}
&ik_L\mathbf{H}^{\mathrm{c}}(\Lambda_1+\Lambda_2|p)\mathbf{C}_2(\Lambda_1,\Lambda_2|p)-\frac{1}{2}\mathbf{H}^{\mathrm{s}}(\Lambda_1|p)\mathbf{C}_1(\Lambda_1|p)-\frac{1}{2}\mathbf{H}^{\mathrm{s}}(\Lambda_2|p)\mathbf{C}_1(\Lambda_2|p)\\
&\quad-3k_L\int_{-k_L/2}^{k_L/2}\mathbf{H}^{\mathrm{s}}(\Lambda_1+\Lambda_2+\lambda_2|p)\mathbf{C}_3(\Lambda_1,\Lambda_2,\lambda_2|p)d\lambda_2\\
&\quad+3\iint_{-k_L/2}^{k_L/2}\mathbf{H}^{\mathrm{s}}(\Lambda_1+\lambda_1+\lambda_2|p)\mathbf{C}_3(\Lambda_1,\lambda_1,\lambda_2|p)d\lambda_1 d\lambda_2\\
&\quad+3\iint_{-k_L/2}^{k_L/2}\mathbf{H}^{\mathrm{s}}(\Lambda_2+\lambda_1+\lambda_2|p)\mathbf{C}_3(\Lambda_2,\lambda_1,\lambda_2|p)d\lambda_1 d\lambda_2=0, \qquad (5.45)
\end{aligned}
$$

(n-th order)

$$
\begin{aligned}
&ik_L\mathbf{H}^{\mathrm{c}}(\Lambda_1+\cdots+\Lambda_n|p)\mathbf{C}_n(\Lambda_1,\cdots,\Lambda_n|p)\\
&-\sum_{l=1}^{n}\frac{1}{n}\,\mathbf{H}^{\mathrm{s}}(\Lambda_1+\cdots+\Lambda_{l-1}+\Lambda_{l+1}+\cdots+\Lambda_n|p)\\
&\qquad\qquad\times\mathbf{C}_{n-1}(\Lambda_1,\cdots,\Lambda_{l-1},\Lambda_{l+1},\cdots,\Lambda_n|p)\\
&-(n+1)k_L\int_{-k_L/2}^{k_L/2}\mathbf{H}^{\mathrm{s}}(\Lambda_1+\cdots+\Lambda_n+\lambda_n|p)\\
&\qquad\qquad\times\mathbf{C}_{n+1}(\Lambda_1,\cdots,\Lambda_n,\lambda_n|p)d\lambda_n\\
&+\sum_{l=1}^{n}(n+1)\iint_{-k_L/2}^{k_L/2}\mathbf{H}^{\mathrm{s}}(\Lambda_1+\cdots+\Lambda_{l-1}+\Lambda_{l+1}+\cdots+\Lambda_n+\lambda_{n-1}+\lambda_n|p)\\
&\qquad\qquad\times\mathbf{C}_{n+1}(\Lambda_1,\cdots,\Lambda_{l-1},\Lambda_{l+1},\cdots\Lambda_n,\lambda_{n-1},\lambda_n|p)d\lambda_{n-1}d\lambda_n=0. \qquad (5.46)
\end{aligned}
$$

Note that the n-th order relation (5.46) describes ascending coupling [53] between $\mathbf{C}_n(\cdot)$ and the sum of $\mathbf{C}_{n-1}(\cdot)$ and descending coupling between $\mathbf{C}_n(\cdot)$ and the integral terms of $\mathbf{C}_{n+1}(\cdot)$. Since $\mathbf{H}^{\mathrm{s}}(\lambda'|p)$ is of the order of σ^1 by (5.32), however, one finds from these hierarchical equations that $\mathbf{C}_0(p)$ is of the order of σ^0 and $\mathbf{C}_n(\lambda_1,\lambda_2,\cdots,\lambda_n|p)$ is of the order of σ^n for $n\geq 1$ under $k\sigma<1$. Therefore, for a sufficiently small σ, we may solve the hierarchical equations.

5.4.2 Binary kernels by a single scattering approximation

In this section, we discuss binary kernels $\hat{\mathbf{C}}_0(p)$, $\hat{\mathbf{C}}_1(\Lambda|p)$ and $\hat{\mathbf{C}}_n(\Lambda_1,\cdots,\Lambda_n|p)$ obtained by a single scattering approximation, which is the same manner as [8]. Neglecting integral terms in (5.43), (5.44) and (5.46), we may obtain such binary kernels as

$$
\begin{aligned}
\hat{\mathbf{C}}_0(p) &= \mathbf{I}^0, \qquad (5.47)\\
\hat{\mathbf{C}}_1(\Lambda|p) &= \frac{2}{ik_L}[\mathbf{H}^{\mathrm{c}}(\Lambda|p)]^{-1}\mathbf{H}^{\mathrm{s}}(0|p)\mathbf{I}^0, \qquad (5.48)\\
\hat{\mathbf{C}}_n(\Lambda_1,\cdots,\Lambda_n|p) &= \frac{1}{ink_L}\,[\mathbf{H}^{\mathrm{c}}(\Lambda_1+\cdots+\Lambda_n|p)]^{-1}\\
&\qquad\times\sum_{l=1}^{n}\,\mathbf{H}^{\mathrm{s}}(\Lambda_1+\cdots+\Lambda_{l-1}+\Lambda_{l+1}+\cdots+\Lambda_n|p)\\
&\qquad\times\hat{\mathbf{C}}_{n-1}(\Lambda_1,\cdots,\Lambda_{l-1},\Lambda_{l+1},\cdots,\Lambda_n|p), \quad (n\geq 2). \qquad (5.49)
\end{aligned}
$$

(5.47) means that there only occurs a specular reflection of $\mathbf{I}^0$ that stands for the incident plane wave for an average wave field, and (5.48) is written as a "bare" single scattering of the incidence.

(5.49) describes ascending coupling between the n-th and $(n-1)$-th order binary kernels, and could be regarded as an n-tuple "bare" single scattering of the incidence. Since $\det[\mathbf{H}^{\rm c}(\Lambda|p)]$ vanishes for $p+\Lambda=\pm k-k_Lq$ as is mentioned above, (5.48) and (5.49) diverge. This is a drawback of the single scattering approximation. Such a drawback can be overcome by taking multiple scattering effects into account, as is discussed below. Note that the solution in [8] does not diverge, since the ensemble average of the random surface is periodic with average height. However, in the case where the average height becomes zero, such a solution diverges.

5.4.3 Binary kernels by the multiply renormalizing approximation

Let us obtain approximate binary kernels $\mathbf{C}_n(\Lambda_1,\cdots,\Lambda_n|p)$ by use of the multiply renormalizing approximation [53], which is made up of two steps.

First, we get an expression of $\mathbf{C}_n(\Lambda_1,\cdots,\Lambda_n|p)$ by use of a truncation procedure and the diagonal approximation [53]. Neglecting $\mathbf{C}_{N+1}(\cdot)$ in the N-th order relation ($N\geq 2$), we obtain

$$\begin{aligned}
&ik_L\mathbf{H}^{\rm c}(\Lambda_1+\cdots+\Lambda_N|p)\mathbf{C}_N^{(N)}(\Lambda_1,\cdots,\Lambda_N|p)\\
&=\sum_{l=1}^{N}\frac{1}{N}\ \mathbf{H}^{\rm s}(\Lambda_1+\cdots+\Lambda_{l-1}+\Lambda_{l+1}+\cdots+\Lambda_N|p)\\
&\qquad\qquad\times\mathbf{C}_{N-1}^{(N)}(\Lambda_1,\cdots,\Lambda_{l-1},\Lambda_{l+1},\cdots,\Lambda_N|p).
\end{aligned}\tag{5.50}$$

Here, the superscript $^{(N)}$ indicates the truncation number N. Substituting (5.50) into the $(N-1)$-th order relation, we get

$$\begin{aligned}
&ik_L\mathbf{H}^{\rm c}(\Lambda_1+\cdots+\Lambda_{N-1}|p)\mathbf{C}_{N-1}^{(N)}(\Lambda_1,\cdots,\Lambda_{N-1}|p)\\
&-\sum_{l=1}^{N-1}\frac{1}{N-1}\mathbf{H}^{\rm s}(\Lambda_1+\cdots+\Lambda_{l-1}+\Lambda_{l+1}+\cdots+\Lambda_{N-1}|p)\\
&\qquad\times\mathbf{C}_{N-2}^{(N)}(\Lambda_1,\cdots,\Lambda_{l-1},\Lambda_{l+1},\cdots,\Lambda_{N-1}|p)\\
&+i\int_{-k_L/2}^{k_L/2}\mathbf{H}^{\rm s}(\Lambda_1+\cdots+\Lambda_{N-1}+\lambda_{N-1}|p)\\
&\qquad\times[\mathbf{H}^{\rm c}(\Lambda_1+\cdots+\Lambda_{N-1}+\lambda_{N-1}|p)]^{-1}\\
&\qquad\times\mathbf{H}^{\rm s}(\Lambda_1+\cdots+\Lambda_{N-1}|p)d\lambda_{N-1}\mathbf{C}_{N-1}^{(N)}(\Lambda_1,\cdots,\Lambda_{N-1}|p)\\
&+\sum_{l=1}^{N-1}i\int_{-k_L/2}^{k_L/2}\mathbf{H}^{\rm s}(\Lambda_1+\cdots+\Lambda_{N-1}+\lambda_{N-1}|p)\\
&\qquad\times[\mathbf{H}^{\rm c}(\Lambda_1+\cdots+\Lambda_{N-1}+\lambda_{N-1}|p)]^{-1}\\
&\qquad\times\mathbf{H}^{\rm s}(\Lambda_1-\cdots-\Lambda_{l-1}-\Lambda_{l+1}+\cdots+\Lambda_{N-1}+\lambda_{N-1}|p)\\
&\qquad\times\mathbf{C}_{N-1}^{(N)}(\Lambda_1,\cdots,\Lambda_{l-1},\Lambda_{l+1},\cdots,\Lambda_{N-1},\lambda_{N-1}|p)d\lambda_{N-1}\\
&-\sum_{l=1}^{N-1}\frac{iN}{k_L}\iint_{-k_L/2}^{k_L/2}\mathbf{H}^{\rm s}(\Lambda_1+\cdots+\Lambda_{l-1}+\Lambda_{l+1}+\cdots+\Lambda_{N-1}+\lambda_{N-2}+\lambda_{N-1}|p)\\
&\qquad\times[\mathbf{H}^{\rm c}(\Lambda_1+\cdots+\Lambda_{l-1}+\Lambda_{l+1}+\cdots+\Lambda_{N-1}+\lambda_{N-2}+\lambda_{N-1}|p)]^{-1}\\
&\qquad\times\mathbf{H}^{\rm s}(\Lambda_1+\cdots+\Lambda_{l-1}+\Lambda_{l+1}+\cdots+\Lambda_{N-1}+\lambda_{N-1}|p)\\
&\qquad\times\mathbf{C}_{N-1}^{(N)}(\Lambda_1,\cdots,\Lambda_{l-1},\Lambda_{l+1},\cdots,\Lambda_{N-1},\lambda_{N-1}|p)d\lambda_{N-2}d\lambda_{N-1}=0.
\end{aligned}\tag{5.51}$$

Taking the diagonal approximation on (5.51), we obtain $\mathbf{C}_{N-1}^{(N)}(\cdot)$ as

$$\begin{aligned}\mathbf{C}_{N-1}^{(N)}&(\Lambda_1,\cdots,\Lambda_{N-1}|p)\\ &\simeq\sum_{l=1}^{N-1}\frac{1}{ik_L(N-1)}\Big[\mathbf{H}^{\rm c}(\Lambda_1+\cdots+\Lambda_{N-1}|p)+\mathbf{M}^{(1)}(\Lambda_1+\cdots+\Lambda_{N-1}|p)\Big]^{-1}\\ &\qquad\times\mathbf{H}^{\rm s}(\Lambda_1+\cdots+\Lambda_{l-1}+\Lambda_{l+1}+\cdots+\Lambda_{N-1}|p)\\ &\qquad\times\mathbf{C}_{N-2}^{(N)}(\Lambda_1,\cdots,\Lambda_{l-1},\Lambda_{l+1},\cdots,\Lambda_{N-1}|p).\end{aligned}\tag{5.52}$$

Substituting such a relation and applying the diagonal approximation recursively, we get a relation between $\mathbf{C}_n^{(N)}(\cdot)$ and $\mathbf{C}_{n-1}^{(N)}(\cdot)$ as

$$\mathbf{C}_n^{(N)}(\Lambda_1,\cdots,\Lambda_n|p)\simeq\begin{cases}\dfrac{1}{ink_L}\displaystyle\sum_{l=1}^{n}\Big[\mathbf{H}^{\rm c}(\Lambda_1+\cdots+\Lambda_n|p)+\mathbf{M}^{(N-n)}(\Lambda_1+\cdots+\Lambda_n|p)\Big]^{-1}\\ \qquad\times\mathbf{H}^{\rm s}(\Lambda_1+\cdots+\Lambda_{l-1}+\Lambda_{l+1}+\cdots+\Lambda_n|p)\\ \qquad\times\mathbf{C}_{n-1}^{(N)}(\Lambda_1,\cdots,\Lambda_{l-1},\Lambda_{l+1},\cdots,\Lambda_n|p),\quad (N\geq n\geq 2),\\ \dfrac{1}{ik_L}\Big[\mathbf{H}^{\rm c}(\Lambda|p)+\mathbf{M}^{(N-1)}(\Lambda|p)\Big]^{-1}\mathbf{H}^{\rm s}(0|p)\left\{\mathbf{I}^0+\mathbf{C}_0(p)\right\},\quad (n=1),\end{cases}\tag{5.53}$$

where $\mathbf{M}^{(n)}(\Lambda|p)$ is defined as

$$\mathbf{M}^{(n)}(\Lambda|p)=\begin{cases}\dfrac{1}{k_L}\displaystyle\int_{-k_L/2}^{k_L/2}\mathbf{H}^{\rm s}(\Lambda+\lambda'|p)\\ \qquad\times\big[\mathbf{H}^{\rm c}(\Lambda+\lambda'|p)+\mathbf{M}^{(n-1)}(\Lambda+\lambda'|p)\big]^{-1}\mathbf{H}^{\rm s}(\Lambda|p)d\lambda',\quad (n\geq 1),\\ 0,\qquad\qquad (n=0).\end{cases}\tag{5.54}$$

$\mathbf{M}^{(n)}(\Lambda|p)$ is the n-th order iterative mass operator. Since $\mathbf{M}^{(n)}(\Lambda|p)$ has products of $\mathbf{H}^{\rm s}(\Lambda+\lambda'|p)$ and $\mathbf{H}^{\rm s}(\Lambda|p)$ in the integrand, it contains couplings between different orders on q of the harmonic series. Thus, $\mathbf{M}^{(n)}(\Lambda|p)$ may represent effects of diffraction. Also, $\mathbf{M}^{(n)}(\Lambda|p)$ represents multiple scattering effects because it has a component of an inverse matrix of $\mathbf{H}^{\rm c}(\Lambda+\lambda'|p)+\mathbf{M}^{(n-1)}(\Lambda+\lambda'|p)$. Note that $\mathbf{M}^{(n)}(p+\Lambda)$ can be estimated to be proportional to σ^2 under small roughness $k\sigma<1$, since $\mathbf{H}^{\rm s}(\Lambda|p)$ is of the order of σ^1. We note that $\mathbf{M}^{(1)}(p+\Lambda)$ may correspond to the mass operator by the first order smoothing approximation in the multiple scattering theory [62].

Repeating the above procedure, we obtain $\mathbf{C}_0^{(N)}(p)$ as

$$\mathbf{C}_0^{(N)}(p)=\Big[\mathbf{H}^{\rm c}(0|p)+\mathbf{M}^{(N)}(0|p)\Big]^{-1}\Big[\mathbf{H}^{\rm c}(0|p)-\mathbf{M}^{(N)}(0|p)\Big]\,\mathbf{I}^0.\tag{5.55}$$

From (5.53) and (5.55), $\mathbf{C}_n^{(N)}(\cdot)$ $(n\geq 1)$ can be obtained. The N-th order binary kernel $\mathbf{C}_N^{(N)}(\cdot)$, where N is the order of the truncation, does not have descending coupling from the $(N+1)$-th order, thus it inevitably diverges for wavenumbers which satisfy (5.41) owing to the truncation. Moreover, the truncation at the N-th order relation consequently leads a spurious resonance in $1/\det[\mathbf{H}^{\rm c}(\Lambda|p)+\mathbf{M}^{(2)}(\Lambda|p)]$, that is, $\det[\mathbf{H}^{\rm c}(\Lambda|p)+\mathbf{M}^{(2)}(\Lambda|p)]$ vanishes with some Λ which does not satisfy $p+\Lambda=\pm k+k_Lq$, q being integer. Thus, the solution (5.53) and (5.55) may not work well even though the boundary condition is evaluated without approximation. This will be referred below.

In view of this undesirable nature, a case where the truncation number N goes to infinity should be considered in the next step. We may assume the existence of a limit of the iterative mass operator $\mathbf{M}^{(N)}(\Lambda|p)$:

$$\lim_{N\to\infty}\mathbf{M}^{(N)}(\Lambda|p)=\mathbf{M}^{(\infty)}(\Lambda|p)\equiv\mathbf{M}(\Lambda|p).\tag{5.56}$$

Thus, we obtain a non-linear integral equation in a matrix form for $\mathbf{M}(\Lambda|p)$ from (5.54):

$$\mathbf{M}(\Lambda|p)=\frac{1}{k_L}\int_{-k_L/2}^{k_L/2}\mathbf{H}^{\mathrm{s}}(\Lambda+\lambda'|p)\left[\mathbf{H}^{\mathrm{c}}(\Lambda+\lambda'|p)+\mathbf{M}(\Lambda+\lambda'|p)\right]^{-1}\mathbf{H}^{\mathrm{s}}(\Lambda|p)d\lambda', \tag{5.57}$$

which we call the 'multiple renormalized mass operator' [53]. Using the multiple renormalized mass operator $\mathbf{M}(\Lambda|p)$, the expression of the binary kernels (5.55) and (5.53) can be rewritten as

$$\mathbf{C}_0(p) = \left[\mathbf{H}^{\mathrm{c}}(0|p)+\mathbf{M}(0|p)\right]^{-1}\left[\mathbf{H}^{\mathrm{c}}(0|p)-\mathbf{M}(0|p)\right]\mathbf{I}^0, \tag{5.58}$$

$$\begin{aligned}\mathbf{C}_1(\Lambda|p) &= \frac{1}{ik_L}[\mathbf{H}^{\mathrm{c}}(\Lambda|p)+\mathbf{M}(\Lambda|p)]^{-1}\mathbf{H}^{\mathrm{s}}(0|p)\left[\mathbf{I}^0+\mathbf{C}_0(p)\right]\\ &= \frac{1}{ik_L}[\mathbf{H}^{\mathrm{c}}(\Lambda|p)+\mathbf{M}(\Lambda|p)]^{-1}\mathbf{H}^{\mathrm{s}}(0|p)\\ &\qquad\times\left[\mathbf{I}^0+\left[\mathbf{H}^{\mathrm{c}}(0|p)+\mathbf{M}(0|p)\right]^{-1}\left[\mathbf{H}^{\mathrm{c}}(0|p)-\mathbf{M}(0|p)\right]\mathbf{I}^0\right],\end{aligned} \tag{5.59}$$

$$\begin{aligned}\mathbf{C}_2(\Lambda_1,\Lambda_2|p) &= \frac{1}{2ik_L}\left[\mathbf{H}^{\mathrm{c}}(\Lambda_1+\Lambda_2|p)+\mathbf{M}(\Lambda_1+\Lambda_2|p)\right]^{-1}\\ &\qquad\times\left[\mathbf{H}^{\mathrm{s}}(\Lambda_1|p)\mathbf{C}_1(\Lambda_1|p)+\mathbf{H}^{\mathrm{s}}(\Lambda_2|p)\mathbf{C}_1(\Lambda_2|p)\right]\\ &= -\frac{1}{2{k_L}^2}\left[\mathbf{H}^{\mathrm{c}}(\Lambda_1+\Lambda_2|p)+\mathbf{M}(\Lambda_1+\Lambda_2|p)\right]^{-1}\\ &\qquad\times\Big[\mathbf{H}^{\mathrm{s}}(\Lambda_1|p)\left[\mathbf{H}^{\mathrm{c}}(\Lambda_1|p)+\mathbf{M}(\Lambda_1|p)\right]^{-1}\mathbf{H}^{\mathrm{s}}(0|p)\left[\mathbf{I}^0-\mathbf{C}_0(p)\right]\\ &\qquad+\mathbf{H}^{\mathrm{s}}(\Lambda_2|p)\left[\mathbf{H}^{\mathrm{c}}(\Lambda_2|p)+\mathbf{M}(\Lambda_2|p)\right]^{-1}\mathbf{H}^{\mathrm{s}}(0|p)\left[\mathbf{I}^0-\mathbf{C}_0(p)\right]\Big],\end{aligned} \tag{5.60}$$

$$\begin{aligned}\mathbf{C}_n(\Lambda_1,\cdots,\Lambda_n|p) \simeq \frac{1}{ink_L}\sum_{l=1}^{n}&\left[\mathbf{H}^{\mathrm{c}}(\Lambda_1+\cdots+\Lambda_n|p)+\mathbf{M}(\Lambda_1+\cdots+\Lambda_n|p)\right]^{-1}\\ &\times\mathbf{H}^{\mathrm{s}}(\Lambda_1+\cdots+\Lambda_{l-1}+\Lambda_{l+1}+\cdots+\Lambda_n|p)\\ &\times\mathbf{C}_{n-1}(\Lambda_1,\cdots,\Lambda_{l-1},\Lambda_{l+1},\cdots,\Lambda_n|p),\quad (n\geq 2),\end{aligned} \tag{5.61}$$

From (5.58), one finds that the coherent Floquet mode $\mathbf{C}_0(p)$ is excited by the incidence $\mathbf{I}^0$. When the surface has no deformation, $\mathbf{M}(0|p)$ vanishes. This means that the non-zero order Floquet modes vanish and only the specular reflection remains. Thus, we may conclude that the non-zero order Floquet modes are generated by multiple scattering processes in the case of a binary periodic random surface with zero average : $\langle f(x,\omega)\rangle = 0$.

Since (5.59) has $[\mathbf{H}^{\mathrm{c}}(\Lambda|p)+\mathbf{M}(\Lambda|p)]^{-1}$, which we call a "dressed" single scattering factor, $\mathbf{C}_1(\Lambda|p)$ describes a "dressed" single scattering excited by $\mathbf{I}^0$ the incident plane wave and $\mathbf{C}_0(p)$ the coherent Floquet modes. Furthermore, (5.60) has another "dressed" single scattering factor $[\mathbf{H}^{\mathrm{c}}(\Lambda_1+\Lambda_2|p)+\mathbf{M}(\Lambda_1+\Lambda_2|p)]^{-1}$ in addition to such a "dressed" single scattering factor of $\mathbf{C}_1(\Lambda|p)$. Therefore, $\mathbf{C}_2(\Lambda_1,\Lambda_2|p)$ represents a "dressed" double scattering process made up of such "dressed" single scattering processes. Similarly, $\mathbf{C}_n(\Lambda_1,\cdots,\Lambda_n|p)$ by (5.61) expresses a "dressed" n-tuple scattering process made up of such "dressed" single scattering processes.

The resonance factor $|1/\det[\mathbf{H}^{\mathrm{c}}(\Lambda|p)+\mathbf{M}(\Lambda|p)]|$ represents characteristics of the diffraction and scattering. Thus, properties of the resonance factor against wavenumber Λ is illustrated below.

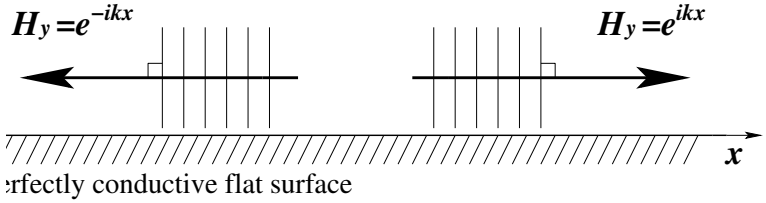

(a) free guided waves along a flat surface

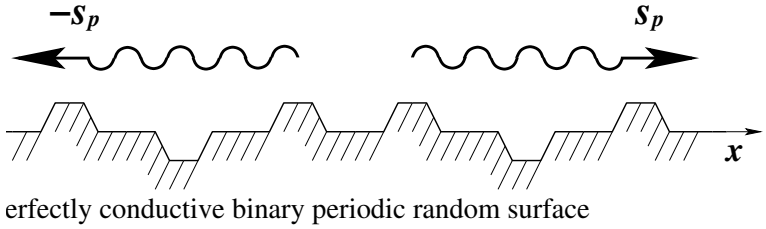

(b) guided surface waves on a binary periodic random surface

Figure 5.2 (a) Free guided waves propagating into the x direction along a perfectly conductive flat surface without any roughness. Such free guided waves have the Rayleigh wavenumber $+k$ and $-k$, and satisfy the Helmholtz equation (3.7) and the Neumann condition $\partial H_y/\partial z = 0$ at $z = 0$. (b) Guided surface waves propagating along the perfectly conductive binary periodic random surface. Guided surface waves have complex propagation constants $\pm s_p$ into the x direction.

5.5 Wood's anomaly and incoherent Wood's anomaly

In this section, we discuss the physical mechanisms of anomalies which appear in the diffraction and scattering.

As is well known, Wood's anomaly appears for critical angles of incidence as rapid variations in the diffraction powers in the perfectly periodic case [28, 29]. On the other hand, another anomaly which occurs in the angular distribution of the scattering has been found in cases of periodic random surfaces [6, 8]. In this paper, we newly show that it takes place in the scattering from a periodic random surface with binary deformations even when the surface is flat on average.

As far as the authors know, there have been few discussions on the physical mechanisms of such anomalies. In this section, we point out that such anomalies are caused by diffraction of the guided surface waves.

As is explained in section 5.3.2, a binary periodic random surface with zero average acts as a periodic surface for the average wave field, and the incident wave is diffracted into discrete directions. When $\mathbf{H}^c(0|p)$ in (5.58) vanishes, the diffraction amplitude $\mathbf{C}_0(p)$ may become large in a shallow case with $\sigma \ll \lambda$. As is well known, this causes Wood's anomaly, which occurs at critical angles of incidence as rapid variations of the diffraction powers against the angle of incidence.

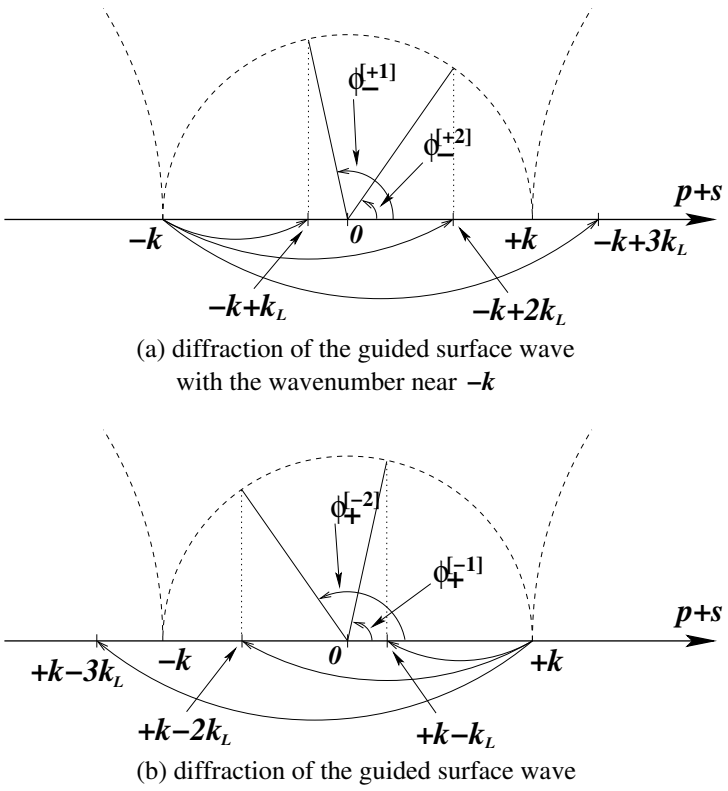

Figure 5.3 Incoherent Wood's anomaly at critical angles of scattering (a) $\phi_-^{[+1]}$ and $\phi_-^{[+2]}$ and (b) $\phi_+^{[-1]}$ and $\phi_+^{[-2]}$ for $L = 1.35\lambda$. (a) Guided surface wave with the wavenumber near $-k$ is diffracted into $-k + k_L$ and $-k + 2k_L$ by the periodic grating. It is also diffracted to $-k+3k_L$ in the evanescent region. (b) Guided surface wave with the wavenumber near $+k$ is diffracted into $+k - k_L$ and $+k - 2k_L$ by the periodic grating. It is also diffracted to $+k - 3k_L$ in the evanescent region.

First, we point out a mathematical fact. In a flat surface case without any roughness, TM plane waves $H_y = e^{\pm ikx \pm i\beta_0(\pm k)z} = e^{\pm ikx}$ are exact solutions of the wave equation (5.10) and satisfy the Neumann condition $\partial H_y/\partial z = 0$ at $z = 0$ (See figure 5.2(a)). Therefore, a plane wave with the Rayleigh wavenumber $+k$ or $-k$ is a free guided wave propagating along the flat surface [20, 58]. Such a free guided wave does not exist in the TE case. When the surface has a periodic structure, such a free guided wave is scattered by the surface roughness and decays exponentially with propagation distance. As a result, it becomes a guided surface wave with a complex propagation constant $+s_p$ or $-s_p$ into the x direction (See figure 5.2(b)). In our case, the surface, which is not periodic but flat on average, works as a periodic surface due to the multiple scattering effects. Mathematically, such $\pm s_p$ should be given as complex roots of the determinant of $[\mathbf{H}^c(0|p) + \mathbf{M}(0|p)]$. When the surface roughness is sufficiently small, however, we may expect that such complex propagation constant s_p exists very close to the Rayleigh wavenumber k. † In the case of a perfectly periodic surface, or when a periodic random surface

†Since this complex propagation constant s_p should exist very close to the Rayleigh wavenumber k in the shallow case, we assume $Re(s_p) \approx k$ and put such complex s_p as real k in the following discussion for simplicity.

acts as a perfectly periodic surface for an average wave field, the surface has a discrete spectrum, and such a guided surface wave is excited by the incident wave. Therefore, such excitation takes place only for the critical angles of incidence $\theta_W^{[l]}$, which are determined by

$$k^2 - (k\cos\theta_W^{[l]} - lk_L)^2 = 0, \quad (l = \pm 1, \pm 2, \cdots). \tag{5.62}$$

When $\theta = \theta_W^{[l]}$ holds, such a guided surface wave is excited due to the diffraction by perfect periodicity and may have a large amplitude. Then, it is diffracted again due to the periodicity. Thus, a multiple scattering takes place for a critical angle of incidence, which causes Wood's anomaly. As a result, Wood's anomaly appears as rapid variations of the coherent diffraction powers. Note that, at $\theta = \theta_W^{[l]}$, the lth order Floquet mode becomes cutoff.

In the case of a periodic random surface with binary fluctuations, another anomaly, which we call incoherent Wood's anomaly, appears at several scattering angles as rapid variations in the angular distribution of the scattering. The surface spectrum has a discrete component effectively and a continuous component due to the binary fluctuations. Because of the scattering by the continuous component, such a guided surface wave is always excited by the incident plane wave with any angle of incidence and then diffracted into discrete directions by the discrete component. To describe these processes, we rewrite a critical wavenumber which satisfies (5.41) as

$$\lambda_\pm^{[l]} = \pm k - p + lk_L, \quad (l = 0, \pm 1, \pm 2, \cdots). \tag{5.63}$$

Let us consider the binary kernel $\mathbf{C}_1(\Lambda|p)$ given by (5.59). When $\Lambda = \lambda_\pm^{[0]} = \pm k - p$ holds, $[\mathbf{H}^{\mathrm{c}}(\Lambda|p) + \mathbf{M}(\Lambda|p)]$ becomes small in (5.59), since $\mathbf{H}^{\mathrm{c}}(\Lambda|p)$ vanishes with such Λ and $\mathbf{M}(\Lambda|p)$ is estimated to be of the order of σ^2 under small roughness $k\sigma < 1$. Thus, the solution $\mathbf{C}_1(\Lambda|p) = \mathbf{C}_1(\lambda_\pm^{[0]}|p)$ has a large amplitude, because $\mathbf{M}(\Lambda|p)$ is small in the shallow case. From (5.17), we regard $\mathbf{C}_1(\lambda_\pm^{[0]}|p)$ as the amplitude of the guided surface wave, which is diffracted into discrete directions $\lambda_\pm^{[l]}$. This means that $\mathbf{C}_1(\lambda_\pm^{[0]}|p) = \mathbf{C}_1(\pm k - p + lk_L|p)$ could have a large amplitude for any integer l, due to the discrete Bragg coupling from $\lambda_\pm^{[0]} = (\pm k - p)$ to $\lambda_\pm^{[l]} = (\pm k - p + lk_L)$. Thus, we may observe rapid variations of the scattering amplitude near a critical scattering angle $\phi_\pm^{[l]}$ (See figure 5.3),

$$p + \lambda_\pm^{[l]} = \pm k + lk_L = k\cos\phi_\pm^{[l]}, \tag{5.64}$$

$$\phi_\pm^{[l]} = \cos^{-1}\left(\pm 1 + l\frac{\lambda}{L}\right), \quad (l = \pm 1, \pm 2, \cdots), \tag{5.65}$$

where the sign $\pm$ goes together in (5.65). It should be noticed that $\lambda_\pm^{[l]}$ and $\phi_\pm^{[l]}$ only depend on the period L and the wavelength λ and are independent of the angle of incidence θ.

Note that incoherent Wood's anomaly has been found in a deterministic case of periodic grooves with single defect [46].

5.6 Numerical examples

Let us discuss the properties of diffraction and scattering of the wave field by determining the binary kernels up to the first order.

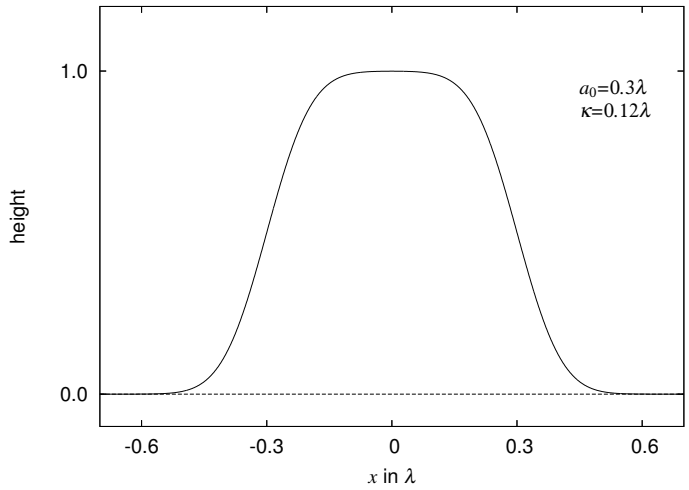

Figure 5.4 Local surface profile $g(x)$, which is a rectangular boss with smooth edge. $\kappa = 0.12\lambda$ and $a_0 = 0.3\lambda$, λ is wavelength.

5.6.1 Parameters of calculation

In this paper, we take the local surface profile $g(x)$ as a trapezoidal boss with smooth edges. We put such a local profile for numerical calculations as

$$g(x) = \frac{1}{2}\left[\mathrm{erf}\left(\frac{x+a_0}{\kappa}\right) - \mathrm{erf}\left(\frac{x-a_0}{\kappa}\right)\right], \quad \mathrm{erf}(x) = \frac{2}{\sqrt{\pi}}\int_0^x e^{-t^2}dt, \tag{5.66}$$

where $\mathrm{erf}(x)$ is the error function with $\mathrm{erf}(\pm\infty) = \pm 1$, a_0 is a width parameter, and κ is a constant which determines the slope angle of the trapezoidal boss. When $a_0/\kappa \gg 1$, it holds that $g(0) \approx 1$ as is shown in figure 5.4. We calculated numerical examples for periods $L = 1.35\lambda$ and 1.7λ, and height parameters $\sigma = 0.025\lambda$, 0.05λ and 0.1λ, λ being wavelength.

In this paper, $\mathbf{C}_0(p)$ and $\mathbf{C}_1(\Lambda|p)$ are used to calculate statistical properties of the diffraction and scattering from the binary periodic random surface. We determine the binary kernels $\mathbf{C}_0(p)$ and $\mathbf{C}_1(\Lambda|p)$ by introducing the truncation number of the order in the spectral domain N_q, which means that we assume

$$\begin{cases} C_0^{(q)}(p) = 0, \\ C_1^{(q)}(\lambda'|p) = 0, \end{cases} \qquad |q| > N_q, \tag{5.67}$$

Thus, the infinite-dimensional matrices and vectors (5.34)-(5.39) are approximated by finite ones : $N_q \times N_q$ matrices and N_q dimensional vectors in the numerical calculations below. N_q should be set so that the first-order band-limited binary kernel $C_1^{(q)}(\cdot)$ enjoys (5.24), however, we take N_q as to make $C_1^{(q)}(\cdot)$ satisfy

$$\begin{aligned} &\left|C_1^{(q)}(k_L/2 - p|p) - C_1^{(q+1)}(-k_L/2 - p|p)\right| \\ &\qquad < \epsilon\left|C_1^{(q)}(k_L/2 - p|p) + C_1^{(q+1)}(-k_L/2 - p|p)\right|. \end{aligned} \tag{5.68}$$

at the band edge on the evaluation of ϵ for $L = 1.35\lambda$ and $\theta = 90^\circ (p = 0)$. In this paper, we set †

$$N_q = \begin{cases} 29, & (\sigma = 0.025\lambda), \\ 43, & (\sigma = 0.05\lambda,\ 0.1\lambda), \end{cases} \qquad \epsilon = \begin{cases} 0.01, & (\sigma = 0.025\lambda), \\ 0.025, & (\sigma = 0.05\lambda). \end{cases} \tag{5.69}$$

5.6.2 Calculation of mass operator

In this section, we present procedures to calculate the multiple renormalized mass operator $\mathbf{M}(\Lambda|p)$ numerically.

To calculate properties of the diffraction and scattering, it is necessary to obtain $\mathbf{M}(\Lambda|p)$ solving the non-linear integral equation (5.57) for $\mathbf{M}(\Lambda|p)$. To calculate $\mathbf{M}(\Lambda|p)$ numerically, the iterative solution with initial guess $\mathbf{M}^{(0)}(\Lambda|p) \equiv 0$ is often employed under the estimation that $\mathbf{M}(\Lambda|p)$ is of the order of σ^2. However, this iterative solution gives the iterative mass operator (5.54) again. Moreover, when the second-order iterative mass operator with the truncation number $N = 2$ is used to calculate the properties of the diffraction and scattering, a serious problem comes out: a spurious peak appears in the Λ-dependence of the resonance factor of the matrix $[\mathbf{H}^{\mathrm{c}}(\Lambda|p) + \mathbf{M}^{(2)}(\Lambda|p)]$ in the zero order binary kernels (5.55), which implies the existence of a complex spurious pole †. Such a spurious pole is similar to those appearing in the corresponding resonance factor of the iterative mass operator in classical random surfaces [53].

To overcome this problem, we estimate the mass operator $\mathbf{M}(\Lambda|p)$ for the binary periodic random surface in the same manner as it is used in the case of the classical random surfaces [53].

Thus, we use the modified iterative mass operator $\tilde{\mathbf{M}}^{(n)}(\Lambda|p)$ as,

$$\tilde{\mathbf{M}}^{(n)}(\Lambda|p) = \begin{cases} \dfrac{1}{k_L}\displaystyle\int_{-k_L/2}^{k_L/2} \mathbf{H}^{\mathrm{s}}(\Lambda+\lambda'|p) \\ \qquad \times\Big[\mathbf{H}^{\mathrm{c}}(\Lambda+\lambda'|p)+\tilde{\mathbf{M}}^{(n-1)}(\Lambda+\lambda'|p)\Big]^{-1}\mathbf{H}^{\mathrm{s}}(\Lambda|p)d\lambda', & (n\geq 1), \\ \mathcal{M}^{(\delta)}(\Lambda|p), & (n=0). \end{cases} \tag{5.70}$$

Here, the initial value matrix $\mathcal{M}^{(\delta)}(\lambda'|p)$ is set as a diagonal matrix and its elements can be calculated as follows ‡ :

$$\mathcal{M}^{(\delta)}(\lambda'|p) = \begin{pmatrix} \mathcal{M}_{-q}(\lambda'|p) & 0 & \cdots & \cdots & 0 \\ 0 & \ddots & & & \vdots \\ \vdots & & \mathcal{M}_n(\lambda'|p) & & \vdots \\ \vdots & & & \ddots & 0 \\ 0 & \cdots & \cdots & 0 & \mathcal{M}_q(\lambda'|p) \end{pmatrix}, \tag{5.71}$$

$$\mathcal{M}_n(\lambda'|p) = -\frac{H^c_{nn}(\lambda'|p)}{2} + \sqrt{\left(\frac{H^c_{nn}(\lambda'|p)}{2}\right)^2 + H^s_{nn}(\lambda'|p)^2}, \quad (n \leq |q|), \tag{5.72}$$

† To obtain an approximate solution with high accuracy, N_q should be sufficiently large, however, it takes a certain amount of calculation time (approximately two weeks for $\tilde{\mathbf{M}}^{(1)}(\Lambda|p)$ with $N_q = 43$ for $\sigma = 0.1\lambda$ on a workstation with dual Quad-core Xeon X5365 3.0GHz CPUs). We set N_q as (5.69), however, for angles very close to critical angles of incidence $\theta_W^{[l]}$, the relative error (5.68) is not as small as that for other θ.

† Such a spurious pole does not appear in the Λ-dependence of the resonance factor of the matrix $[\mathbf{H}^{\mathrm{c}}(\Lambda|p) + \mathbf{M}^{(1)}(\Lambda|p)]$ in the first order binary kernels (5.53).

‡ In the discussion in section 4, we have introduced infinite-dimensional matrices and vectors, however, $\tilde{\mathbf{M}}^{(n)}(\Lambda|p)$ and $\mathcal{M}^{(\delta)}(\Lambda|p)$ are written as $N_q \times N_q$ matrices in (5.70) and (5.71), which is actually used for numerical calculation.

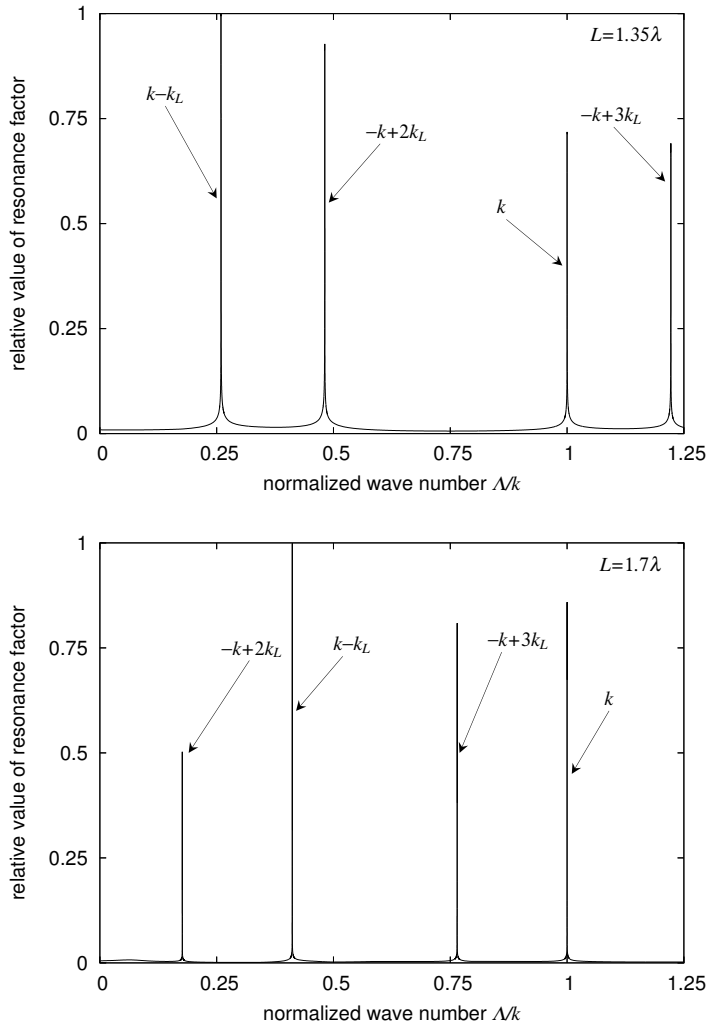

Figure 5.5 Relative value of $\left|1/\det[\mathbf{H}^c(\Lambda|p)+\tilde{\mathbf{M}}^{(2)}(\Lambda|p)]\right|$ against wavenumber Λ for periods $L=1.35\lambda$ (upper figure) and 1.7λ (lower figure) with height $\sigma=0.05\lambda$ ($p=0$). The resonance factor has large value at critical wavenumbers k, $\lambda_+^{[-1]}=k-k_L$, $\lambda_-^{[2]}=-k+2k_L$ and $\lambda_-^{[3]}-k+3k_L$.

where the branch cut of $\sqrt{\ }$ in (5.72) is chosen such that $\lim_{|\lambda'|\to\infty}\mathcal{M}_n(\lambda'|p)=0$ holds.

It was demonstrated in Ref [53], if we take the δ-exact solution as an initial value, the multiple renormalized mass operator can be numerically obtained only by two times of iteration. In our case of the binary periodic random surface, we employ $\tilde{\mathbf{M}}^{(2)}(\Lambda|p)$ instead of the multiple renormalized mass operator $\mathbf{M}(\Lambda|p)$ for numerical calculations below [†], which we write $\mathbf{M}(\Lambda|p)$ in what follows.

[†] $\tilde{\mathbf{M}}^{(2)}(\Lambda|p)$ converges as $\tilde{\mathbf{M}}^{(2)}(\Lambda|p)\approx\tilde{\mathbf{M}}^{(n)}(\Lambda|p)$ ($n\geq 3$) owing to the initial value $\mathcal{M}^{(\delta)}(\Lambda|p)$ under a convergence study up to $\tilde{\mathbf{M}}^{(8)}(\Lambda|p)$ for $p=0$ with $\sigma=0.05\lambda$ and $L=1.35\lambda$.

5.6.3 Properties of diffraction and scattering

Let us start with the property of the resonance factor. Figure 5.5 illustrates relative values of the resonance factor $\left|1/\det[\mathbf{H}^{\mathrm{c}}(\Lambda|0)+\tilde{\mathbf{M}}^{(2)}(\Lambda|0)]\right|$ against wavenumber Λ for periods $L=1.35\lambda$ with height $\sigma=0.05\lambda$ and $L=1.7\lambda$ with height $\sigma=0.025\lambda$ ($p=0$). The resonance factor has steep peaks at critical wave numbers k, $\lambda_{+}^{[-1]}$, $\lambda_{-}^{[2]}$ and $\lambda_{-}^{[3]}$ for both periods $L=1.35\lambda$ and 1.7λ, as is expected [†]. Since the resonance factor commonly appears in the binary kernels, such peaks lead rapid variations both in the diffraction powers and in the angular distributions of differential scattering cross section.

Next, we show relations on powers of diffraction and scattering. Figure 5.6 illustrates the relative coherent diffraction power for $L=1.35\lambda$ and $\sigma=0.05\lambda$ (upper figure) and for $L=1.7\lambda$ and $\sigma=0.025\lambda$ (lower figure) against the angles of incidence. Total coherent diffraction power is normalized to unity. The line '0th order' means the relative power of the 0th order Floquet mode, i.e, $\mathrm{Re}[\beta_0(p)]\left|C_0^{(0)}(p)\right|^2/\beta_0(p)$, and the line '1st order' that of the 1st order Floquet mode, and so on. For $L=1.3\lambda$, the diffraction power rapidly changes near the critical angles of incidence $\theta_W^{[-2]}=61.218^\circ$ and $\theta_W^{[1]}=74.974^\circ$ given by (5.62), at which one particular diffraction mode appears or disappears. This is well-known Wood's anomaly. For $L=1.7\lambda$, such rapid variations appear at critical incident angles $\theta_W^{[-3]}=40.119^\circ$, $\theta_W^{[1]}=65.684^\circ$ and $\theta_W^{[-2]}=79.836^\circ$. Figure 5.7 illustrates the normalized optical theorem (5.20) against the angle of incidence θ for $L=1.35\lambda$ and $\sigma=0.05\lambda$ (upper figure), and for $L=1.7\lambda$ and $\sigma=0.025\lambda$ (lower figure). The incident power is normalized as unity. 'Coherent' means power of coherent diffractions, 'Incoherent' means that of incoherent scattering, and 'Total' means a sum of both powers. When the angle of incidence is close to 90°, the incoherent scattering increases. From the upper figure, it is found that error $|\mathrm{Total}-1|$ is less than 0.05 for any angles of incidence except for low grazing angles of incidence less than 20°, where accuracy of the coherent diffractions is not sufficient. For critical angles of incidence, sharp peaks appear in the power of coherent diffractions, while that of incoherent scattering compensationally decreases sharply. Near $\theta_W^{[1]}=74.974^\circ$ with $L=1.35\lambda$, 'Total' slightly exceeds unity (at most 1.002). From the lower figure, it is found that the error $|\mathrm{Total}-1|$ is less than 0.015 for any angles of incidence except for grazing incident angles less than 15°. For $\sigma=0.025\lambda$, power of incoherent scattering is at most less than 3.4×10^{-2}. In this case, the optical theorem holds better accuracy at grazing angles of incidence than the case for $L=1.35\lambda$ and $\sigma=0.05\lambda$, however, the coherent power rapidly decreases for $\theta<5^\circ$.

In order to grasp characteristics of incoherent Wood's anomaly, we show some exapmles of the differential scattering cross section $\sigma(\phi|\theta)$. Figure 5.8 illustrates $\sigma(\phi|\theta)$ for angles of incidence $\theta=74.98^\circ$ and 90° (upper figure), and $\theta=74.98^\circ$ and $74.9727^\circ\approx\theta_W^{[1]}$ (lower figure) with $L=1.35\lambda$ and $\sigma=0.05\lambda$. As is expected, incoherent Wood's anomaly occurs near critical scattering angles $\phi_{\pm}^{[l]}$ as rapid variations in $\sigma(\phi|\theta)$ associating a peak and a dip together within a narrow range of scattering angles. Such critical scattering angles $\phi_{\pm}^{[l]}$ are calculated by (5.65) with $L=1.35\lambda$ as $\phi_{-}^{[2]}=61.218^\circ$, $\phi_{+}^{[-1]}=74.974^\circ$, $\phi_{-}^{[1]}=105.026^\circ$, $\phi_{+}^{[-2]}=118.782^\circ$. The critical scattering angles are independent of the angles of incidence θ. For $\theta=90^\circ$, only dips appear at critical scattering angles, while a peak and dip are associated together at $\phi_{+}^{[-1]}=74.974^\circ$ and $\phi_{-}^{[1]}=105.026^\circ$ for $\theta=74.98^\circ$. Appearance of peaks and dips vary with parameters, such

[†]Strictly speaking, wavenumber Λ at th peak point near k has small shift from exact k, since s_p is a complex propagation constant and its real part does not correspond to k exactly. Such shift amounts $1.5\times10^{-5}k$ for $\sigma=0.05\lambda$, and varies with the height parameter σ: the shift becomes large ($1.8\times10^{-4}k$) for $\sigma=0.1\lambda$, which suggests that complex s_p moves away from the real x-axis, while it becomes small ($1\times10^{-6}k$) for $\sigma=0.025\lambda$

as the period of the surface, the height of the surface profile or the angle of incidence. Note that $\sigma(\phi|\theta)$ does not decrease until low grazing scattering angles, and then vanishes rapidly at $\phi = 0^\circ$ and $\phi = 180^\circ$, which can be considered as an anomalous scattering [19] due to the existence of the guided surface modes. In the case for $\theta = 90^\circ$ with $\sigma = 0.05\lambda$, $\sigma(\phi|\theta)$ diminishes rapidly for $\phi < 0.2^\circ$ and $\phi > 179.8^\circ$. When $\theta = 74.9727^\circ$, which is very close to $\theta_W^{[1]}$, behavior of $\sigma(\phi|\theta)$ is quite different from that for $\theta = 74.98^\circ$: $\sigma(\phi|\theta)$ decreases around directions of the specular reflection. It can be considered that the component $[\mathbf{I}^0 + \mathbf{C}_0(p)]$ in (5.59) decreases for angles of incidence near $\theta_W^{[l]}$. On the other hand, $\sigma(\phi|\theta)$ becomes large for $\phi > 130^\circ$. Figure 5.9 illustrates $\sigma(\phi|\theta)$ for periods of the surface $L = 1.35\lambda$ and 1.7λ with $\theta = 85^\circ$ and $\sigma = 0.025\lambda$. Incoherent Wood's anomaly appears at different scattering angles for $L = 1.35\lambda$ and 1.7λ, since the critical scattering angles only depend on the wavelength λ and the period of the surface L. With $L = 1.7\lambda$, $\phi_\pm^{[l]}$ are calculated by (5.65) as $\phi_-^{[3]} = 40.119^\circ$, $\phi_+^{[-1]} = 65.684^\circ$, $\phi_-^{[2]} = 79.836^\circ$, $\phi_+^{[2]} = 100.164^\circ$, $\phi_-^{[1]} = 114.316^\circ$, $\phi_+^{[-3]} = 139.881^\circ$. With $\theta = 85^\circ$ and $\sigma = 0.025\lambda$, only dips appear at $\phi_+^{[-l]}$ and $\phi_-^{[l]}$ $(l = 1, 2, 3)$ for both $L = 1.35\lambda$ and $L = 1.7\lambda$. Figure 5.10 illustrates $\sigma(\phi|\theta)$ for height parameters $\sigma = 0.025\lambda$, 0.05λ and 0.1λ. Behavior of $\sigma(\phi|\theta)$ near $\phi_-^{[1]} = 105.026^\circ$ is shown in the lower figure. It can be seen that $\sigma(\phi|\theta)$ is proportional to σ^2 for most angles of scattering, however, near critical scattering angles and low grazing scattering angles $\sigma(\phi|\theta)$ is no longer proportional. It is also found that, in the shallow case with $\sigma = 0.025\lambda$, an anomalous dip becomes narrower and steeper than a dip with $\sigma = 0.05\lambda$ or a peak with $\sigma = 0.1\lambda$. On the other hand, in the case with $\sigma = 0.1\lambda$, $\sigma(\phi|\theta)$ changes gently in comparison with the shallow cases, however, such a peak and dip appear within a range less than one degree. $\sigma(\phi|\theta)$ starts to decrease for $\phi < 2.5^\circ$ and $\phi > 177.0^\circ$ with $\sigma = 0.1\lambda$. When $\sigma = 0.1\lambda$, $\sigma(\phi|\theta)$ increases toward the low grazing angles, which may be because the coupling with the guided surface wave becomes strong due to large σ.

5.7 Conclusion

We have studied the diffraction and scattering of a TM plane wave from a binary periodic random surface generated by a binary sequence using the stochastic functional approach. We have considered the equal probability case of the binary sequence, where the ensemble average of the periodic random surface becomes flat. Assuming that such a binary periodic random surface is mathematically modeled by a periodic stationary process, we wrote the scattered wave in a stochastic Floquet form, which is a product of an exponential phase factor and a periodic stationary process. We expressed such a periodic stationary process in the harmonic series representation, with mutually correlated stationary processes which are represented by a sum of orthogonal binary functional series with band-limited binary kernels. Then, the hierarchical equations for the binary kernels were derived from the Neumann boundary condition without approximation. We have pointed out that the solution obtained by the single scattering approximation diverges unphysically when the periodic random surface is zero on average. Thus, we have obtained expressions for such binary kernels by use of the multiply renormalizing approximation, in which effects of the multiple scattering are involved. Furthermore, the multiple renormalized mass operator should be employed to obtain the binary kernels in order to avoid their unphysical divergence due to the truncation procedure. Then, several statistical properties of the diffraction and scattering were calculated in terms of such binary kernels. It is found that

incoherent Wood's anomaly occurs at critical scattering angles as rapid variations in the angular distribution of the scattering even when a binary periodic random surface has zero average. It is caused by the diffraction of the guided surface wave along the surface. On the other hand, such anomalies do not appear in the TE case [59]. Furthermore, the differential scattering cross section does not diminish until the low grazing scattering angles, which can be considered as an anomalous scattering due to the existence of the guided surface modes.

In the discussion of this chapter, however, accuracy of the optical theorem is not sufficient for grazing angles of incidence. Therefore, more accurate solution should be studied.

Our discussion was limited to the properties on the first-order scattering. In the case of Gaussian fluctuations on height parameter, the diffracted backscattering enhancement in the second-order scattering has been found for TM incidence [8]. On the other hand, the contribution of the second-order scattering becomes small for TE incidence in the binary case. Thus, it may be interesting to study the second-order scattering for TM incidence in the binary case [59]. Furthermore, the discussion was limited to the equal probability case, however, it can be extended to an unequal probability case. Studies on diffraction and scattering for such a case will be left for future study.

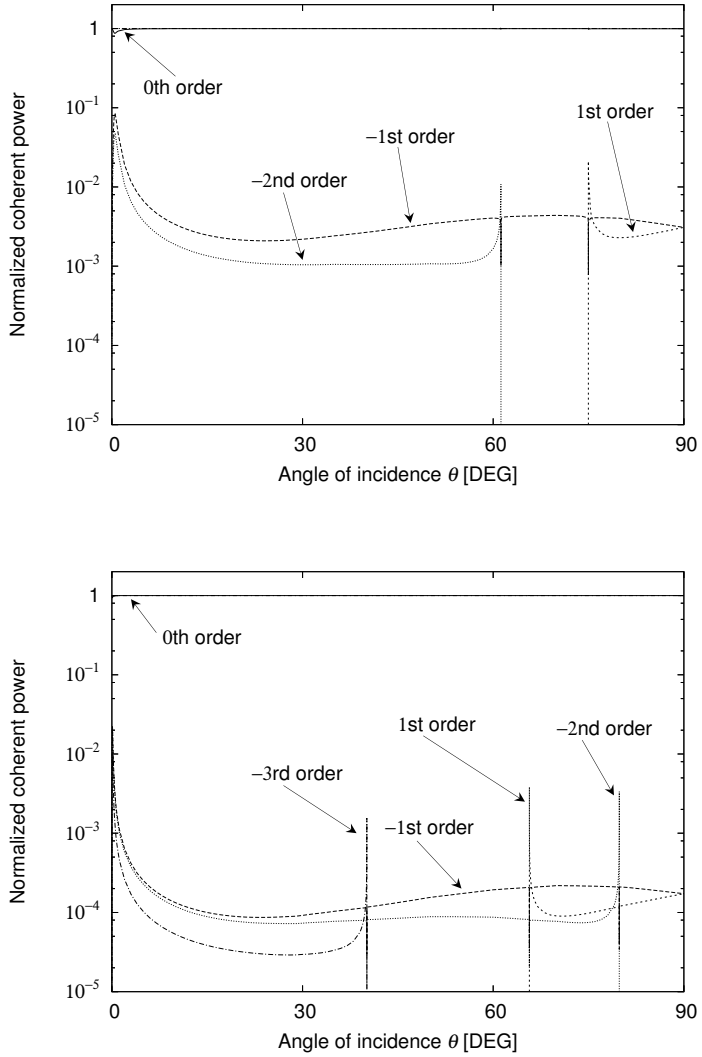

Figure 5.6 Relative coherent power against the angle of incidence θ for periods $L = 1.35\lambda$ with height $\sigma = 0.05\lambda$(upper figure) and periods $L = 1.7\lambda$ with height $\sigma = 0.025\lambda$(lower figure). The line '0th order' means the relative power of the 0th order Floquet mode, i.e, $\mathrm{Re}[\beta_0(p)] \left|C_0^{(0)}(p)\right|^2 / \beta_0(p)$, and the line '1st order' that of the 1st order Floquet mode, and so on. Wood's anomaly occurs at angles where one particular diffraction mode disappears.

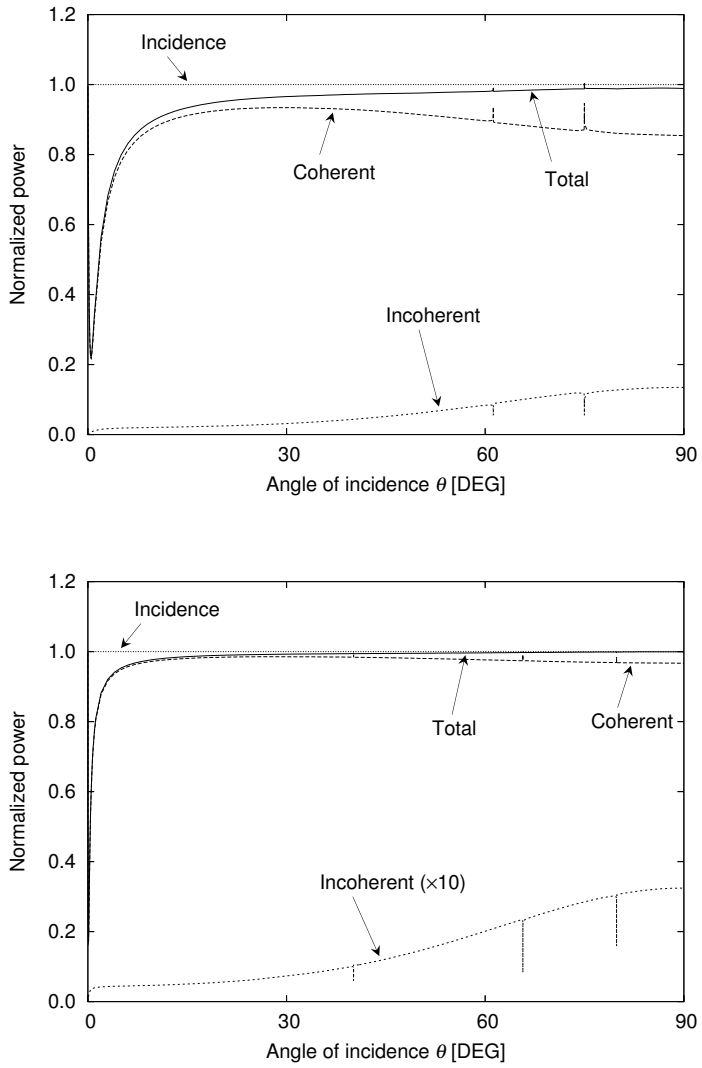

Figure 5.7 Normalized optical theorem against θ for $\sigma = 0.05\lambda$ and $L = 1.35\lambda$ (upper figure), and for $\sigma = 0.025\lambda$ and $L = 1.7\lambda$ (lower figure). The incident power is normalized as unity. 'Coherent' means power of coherent diffractions, 'Incoherent' means that of incoherent scattering, and 'Total' means a sum of both power. When the angle of incidence is close to 90°, the incoherent scattering increases. Error $|\text{Total} - 1|$ is less than 0.05 for $\sigma = 0.05\lambda$ except for grazing incident angles less than 20°. For $\sigma = 0.025\lambda$, it holds better accuracy for grazing angles of incidence, however, the coherent power rapidly decreases for $\theta < 5°$.

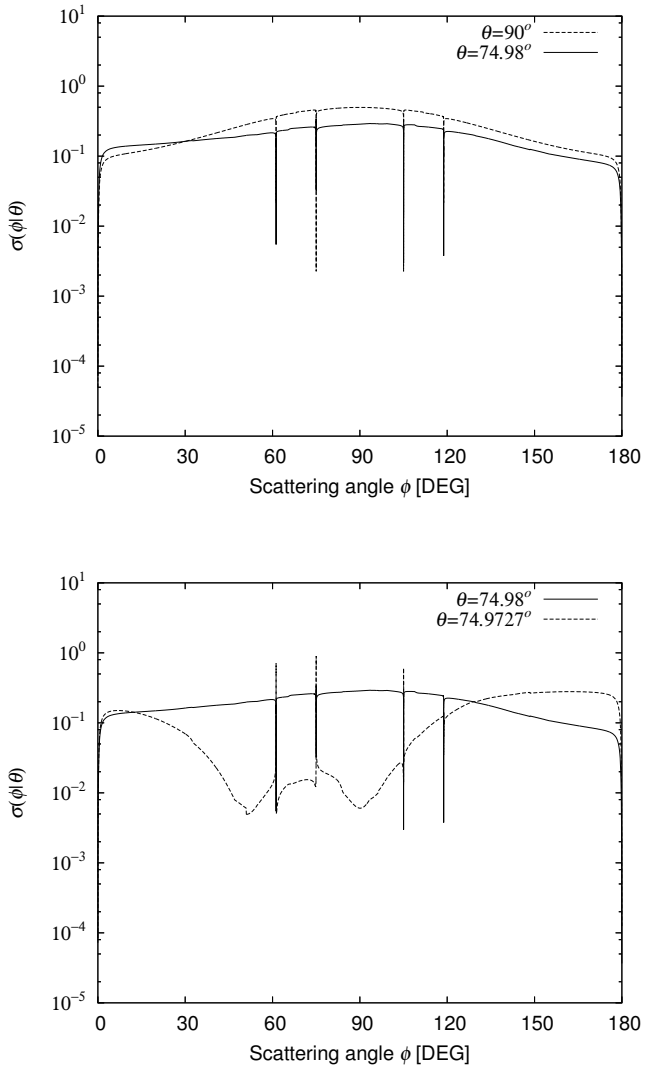

Figure 5.8 Differential scattering cross section $\sigma(\phi|\theta)$ for $\theta = 74.98°$ and $90°$ (upper figure), and $\theta = 74.98°$ and $74.9727° \approx \theta_W^{[1]}$ (lower figure) with $L = 1.35\lambda$, $\sigma = 0.05\lambda$. Incoherent Wood's anomaly occurs near critical scattering angles $\phi_{\pm}^{[l]}$ as rapid variations in $\sigma(\phi|\theta)$ associating a peak and a dip together within a narrow range of scattering angles. $\sigma(\phi|\theta)$ does not decrease until low grazing scattering angles, and vanishes rapidly at $\phi = 0°$ and $\phi = 180°$, which can be considered as an anomalous scattering due to the existence of the guided surface modes. When $\theta = 74.9727°$, behavior of $\sigma(\phi|\theta)$ is quite different from that for $\theta = 74.98° : \sigma(\phi|\theta)$ becomes small around directions of the specular reflection.

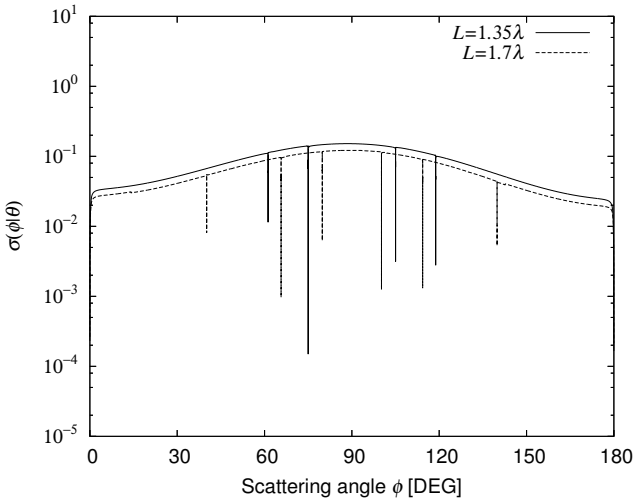

Figure 5.9 Differential scattering cross section $\sigma(\phi|\theta)$ for $L = 1.35\lambda$ and 1.7λ with $\theta = 85^\circ$ and $\sigma = 0.025\lambda$. Incoherent Wood's anomaly appears at different angles of scattering for $L = 1.35\lambda$ and 1.7λ, since the critical angles of scattering only depend on the wavelength λ and the period of the surface L. With $\theta = 85^\circ$ and $\sigma = 0.025\lambda$, only peaks appear at $\phi_-^{[3]}$ and $\phi_+^{[-3]}$ for $L = 1.7\lambda$ and only dips appear at $\phi_-^{[2]}$ and $\phi_+^{[2]}$ for $L = 1.7\lambda$ and at $\phi_+^{[-1]}$ for $L = 1.35\lambda$. In most cases, a peak and a dip are associated together at critical angles of scattering $\phi_\pm^{[l]}$, however, only a peak or a dip appears with some parameters, such as the period of the surface or the angle of incidence.

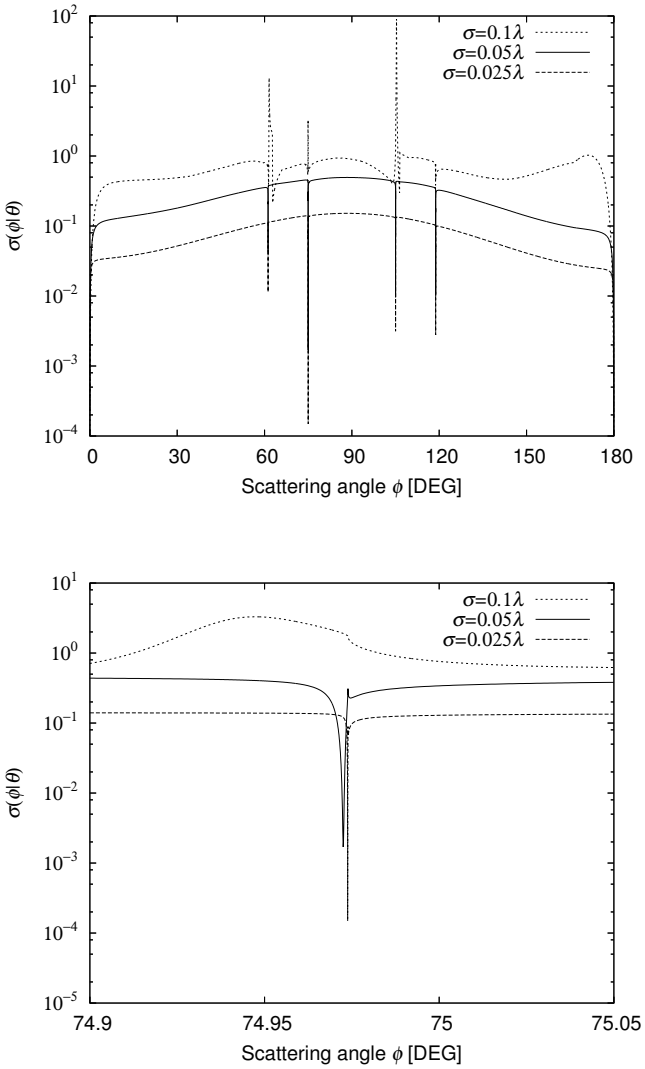

Figure 5.10 Differential scattering cross section $\sigma(\phi|\theta)$ for $\sigma = 0.025\lambda$, 0.05λ and 0.1λ with $L = 1.35\lambda$ and $\theta = 85°$ (upper figure), and behavior of $\sigma(\phi|\theta)$ near $\phi_{-}^{[1]}$ (lower figure). $\sigma(\phi|\theta)$ is proportional to σ^2 for most angles of scattering, however, $\sigma(\phi|\theta)$ is no longer proportional near critical angles of scattering and grazing angles. In the shallow case with $\sigma = 0.025\lambda$, an anomalous peak and dip become narrower and steeper than those with $\sigma = 0.05\lambda$ and 0.1λ. In the case with $\sigma = 0.1\lambda$, $\sigma(\phi|\theta)$ changes gently in comparison with the shallow cases, however, such a peak and dip appear within a range less than one degree.

Chapter 6

Conclusion

In this thesis, diffraction and scattering from periodic surfaces with binary fluctuations have been studied theoretically.

Here are the summaries of each chapter.

Chapter 2 We considered a one-dimensional periodic grating with single defect, of which position is known. We took TE plane wave as an incidence, wrote the wave field above the grooves as a perturbation from the diffracted wave for the perfectly periodic case. We derived two sets of equations to determine the wave field from the boundary condition, and we obtained a new representation of the optical theorem, which relates the total scattering cross section with the reduction of the scattering amplitude. Further, we proposed the single scattering approximation given only by the base components for the perfectly periodic grating.

We found that the differential scattering cross section is determined by the spectrum of the groove. This property may be applicable to the measurement of the condition of surfaces combining with the other polarization. We found that when the guided mode in the grooves becomes resonant, the differential scattering cross section becomes almost symmetric even for oblique incidence. We found the single scattering approximation is useful when the depth of the groove is small.

Chapter 3 We have considered the scattering of a TM plane wave from a periodic grating with single defect. We wrote the scattered wave above the grooves as a variation from the diffracted wave for the perfectly periodic case. Then, we obtained an integral equation for the scattering amplitude, which is solved by the iteration method using the diagonal approximation solution as an initial guess. We found that incoherent Wood's anomaly appears in the differential scattering cross section for the periodic grating with single defect. The critical angles of scattering where incoherent Wood's anomaly appears only depend on the period of the grating and the wavelength, and are independent of the angle of incidence. We pointed out that incoherent Wood's anomaly is caused by the diffraction of the guided surface waves.

When the angle of incidence becomes close to one of the critical angles of incidence or close to a low grazing angle, error with respect to the optical theorem becomes large. This means that our iterative solution is not good enough for such angles of incidence. Therefore, practical methods of approximation must be studied to obtain a highly accurate solution.

Chapter 4 We have studied the scattering of a TE plane wave from a periodic random surface generated by a binary sequence using the stochastic functional approach. Assuming that such

a periodic random surface is mathematically modeled by a periodic stationary process, we have pointed out that the scattered wave has a stochastic Floquet form, which is a product of an exponential phase factor and a periodic stationary process. We reconsider the harmonic series representation used in [44] for such a periodic stationary process. We write such a periodic stationary process by orthogonal binary functionals with binary kernels given by multiple Fourier integrals. We then find that for the binary case it is necessary to divide such Fourier integrals into bands with equal band width. Then, such a periodic stationary process is represented by a harmonic series, of which coefficients are mutually correlated wide sense stationary processes given by binary functionals with band-limited binary kernels. Using the Dirichlet boundary condition, we have determined the band-limited binary kernels up to the second order, from which several statistical properties of the scattering were calculated. It is found that the components of the first order incoherent scattering are relatively large in the diffraction directions of the exciting Floquet modes and have some dips corresponding to the zeros of spectrum of the local profile. We find that, due to the special property of the binary random variable, the second order scattering cross section has a subtractive term and becomes much smaller than the first order one. The second order scattering cross section has dips in the diffraction directions of the Floquet modes. It is also found that the incoherent power begins to decrease when the height parameter gets large, possibly due to the diffraction and multiple scattering effects by the mass operator.

Chapter 5 We have studied the diffraction and scattering of a TM plane wave from a binary periodic random surface generated by a binary sequence using the stochastic functional approach. Assuming that such a binary periodic random surface is mathematically modeled by a periodic stationary process, we wrote the scattered wave in a stochastic Floquet form, which is a product of an exponential phase factor and a periodic stationary process. We expressed such a periodic stationary process in the harmonic series representation, with mutually correlated stationary processes which are represented by a sum of orthogonal binary functional series with band-limited binary kernels. Then, the hierarchical equations for the binary kernels were derived from the Neumann condition, and expressions for such binary kernels were obtained by use of the multiply renormalizing approximation. Several statistical properties of the diffraction and scattering were calculated in terms of such binary kernels. It is found that incoherent Wood's anomaly occurs at critical angles of scattering as rapid variations in the angular distribution of the scattering even when a binary periodic random surface has zero average. It is caused by the diffraction of the guided surface wave along the surface. On the other hand, such anomalies do not appear in the TE case [59]. Furthermore, the differential scattering cross section does not diminish until the low grazing limit, which can be considered as an anomalous scattering due to the existence of the guided surface modes.

Future studies In the discussions of chapter 2 and 3, we have considered the single defect case in the periodic grating of rectangular grooves. However, there are other mathematical models of periodic grating with defects: one is a case with double or finite number of defects which positions are known. Another is a case with random defects, that is, the defect probability is known but their positions are unknown. It is theoretically interesting to consider such periodic gratings with defects.

Although it is also practically important to consider a metallic or dielectric grating with defects for the optical measurement or inspection, it is still difficult to treat the cases with

defects for such materials.

In the discussions of chapter 4 and 5, we have considered the periodic random surfaces with binary fluctuations on height parameter. In the TM case, our discussion was limited to the properties on the first-order scattering. In the case of Gaussian fluctuations on height parameter, the diffracted backscattering enhancement in the second-order scattering has been found for TM incidence [8]. On the other hand, the contribution of the second-order scattering becomes small for TE incidence in the binary case [59]. Thus, it may be interesting to study the second-order scattering for TM incidence in the binary case. Furthermore, the discussion was limited to the equal probability case, however, it can be extended to an unequal probability case.

Studies on diffraction and scattering for such cases will be left for future study.

Appendix A

Multi-variate binary polynomials and orthogonal functional expansion

Here, we summarize some formulae on multi-variate binary polynomials and orthogonal functional expansion called the binary expansion. For mathematical details, see references [49, 63].

Let $b_m(\omega)$ be an independent stationary sequence with (5.3). Then we define binary polynomials $B_n[\,\cdot\,]$ as

$$B_0 = 1, \quad B_1[b_m(\omega)] = b_m(\omega), \quad B_2[b_m(\omega), b_n(\omega)] = b_m(\omega)b_n(\omega) - \delta(m,n), \tag{A.1}$$

$$\begin{aligned} B_n[b_{i_1}, b_{i_2}, \cdots, b_{i_n}] &= \begin{cases} b_{i_1}b_{i_2}\cdots b_{i_n} & (i_1, i_2, \cdots, i_n \text{ are all distinct}) \\ 0 & (\text{any other case}) \end{cases} \\ &= \Delta_n(i_1, i_2, \cdots, i_n) \times b_{i_1}b_{i_2}\cdots b_{i_n}, \end{aligned} \tag{A.2}$$

where ω in $b_m(\omega)$ is dropped to simplify notations in (A.2). Here, $\Delta_n(\,\cdot\,)$ is a binary function defined as

$$\Delta_n(i_1, i_2, \cdots, i_n) = \begin{cases} 1 & (i_1, i_2, \cdots, i_n \text{ are all distinct}) \\ 0 & (\text{any other case}) \end{cases} \tag{A.3}$$

$$\begin{aligned} &= \Big[1 - \sum_{k=1}^{n-1} \delta(i_n, i_k)\Big]\Big[1 - \sum_{k=1}^{n-2} \delta(i_{n-1}, i_k)\Big] \\ &\qquad \times \cdots \times \Big[1 - \delta(i_3, i_2) - \delta(i_3, i_1)\Big]\Big[1 - \delta(i_2, i_1)\Big]. \end{aligned} \tag{A.4}$$

Clearly, $B_n[\,\cdot\,]$ and $\Delta_n(\,\cdot\,)$ are symmetrical and vanishes for any diagonal arguments.

From (A.1), (4.7) and (5.8), one finds the translation property under T,

$$B_n[b_{i_1}(T^m\omega), b_{i_2}(T^m\omega), \cdots, b_{i_n}(T^m\omega)] = B_n[b_{m+i_1}(\omega), b_{m+i_2}(\omega), \cdots, b_{m+i_n}(\omega)] \tag{A.5}$$

The multi-variate binary polynomials have zero average and enjoy the orthogonal relation

$$\langle B_n[b_{i_1}, b_{i_2}, \cdots, b_{i_n}]\rangle = \delta(n, 0), \tag{A.6}$$

$$\langle B_n[b_{i_1}, b_{i_2}, \cdots, b_{i_n}] B_m[b_{j_1}, b_{j_2}, \cdots, b_{j_m}]\rangle = \Delta_n(i_1, i_2, \cdots, i_n)\delta(m,n)\delta^{(n)}(i,j), \tag{A.7}$$

$$\delta^{(n)}(i,j) = \sum_{l_1=1}^{n} \delta(i_1, j_{l_1}) \times \sum_{\substack{l_2=1 \\ l_2 \neq l_1}}^{n} \delta(i_2, j_{l_2}) \times \cdots \times \sum_{\substack{l_n=1 \\ l_n \neq l_1, .., l_{n-1}}}^{n} \delta(i_n, j_{l_n}). \tag{A.8}$$

Here, $\delta^{(n)}(i,j)$ equals to the sum of all distinct product of n-tuple Kronecker deltas of the form $\delta(i_u, j_v)$, which involves $n!$ terms. From (A.4), we find the recurrence relations

$$B_1[b_{i_1}]B_1[b_{i_2}] = B_2[b_{i_1}, b_{i_2}] + \delta(i_1, i_2), \tag{A.9}$$

$$\begin{aligned} B_2[b_{i_1}, b_{i_2}]B_1[b_{i_3}] &= B_3[b_{i_1}, b_{i_2}, b_{i_3}] + B_1[b_{i_2}]\delta(i_3, i_1) + B_1[b_{i_1}]\delta(i_3, i_2) \\ &- B_1[b_{i_2}]\delta(i_3, i_1)\delta(i_2, i_1) - B_1[b_{i_1}]\delta(i_3, i_2)\delta(i_1, i_2), \end{aligned} \tag{A.10}$$

$$\begin{aligned} B_{n-1}[b_{i_1}, \cdots, b_{i_{n-1}}]B_1[b_{i_n}] &= B_n[b_{i_1}, b_{i_2}, \cdots, b_{i_n}] \\ &+ \sum_{l=1}^{n-1} B_{n-2}[b_{i_1}, \cdots, b_{i_{l-1}}, b_{i_{l+1}}, \cdots, b_{i_{n-1}}]\delta(i_n, i_l) \\ &- \sum_{l=1}^{n-1}\sum_{\substack{k=1 \\ k\neq l}}^{n-1} B_{n-2}[b_{i_1}, \cdots, b_{i_{l-1}}, b_{i_{l+1}}, \cdots, b_{i_{n-1}}] \\ &\qquad \times\delta(i_n, i_l)\delta(i_k, i_l). \end{aligned} \tag{A.11}$$

Let $\Phi(\omega) = \Phi(\cdots, b_{-1}, b_0, b_1, \cdots)$ be a stochastic functional of the binary sequence $b_m(\omega)$ with a finite mean square

$$\langle|\Phi(\omega)|^2\rangle < \infty. \tag{A.12}$$

Then, $\Phi(\omega)$ has an orthogonal functional expansion in terms of the binary polynomial as

$$\Phi(\omega) = c_0 + \sum_{m=-\infty}^{\infty} c_1(m)B_1[b_m] + \sum_{m,n=-\infty}^{\infty} c_2(m,n)B_2[b_m, b_n] + \cdots, \tag{A.13}$$

where $c_n(i_1, \cdots, i_n)$ is a deterministic function that we call the binary kernel. Thus, the mean square of $\Phi(\omega)$ is written as

$$\langle|\Phi(\omega)|^2\rangle = |c_0|^2 + 1!\sum_{m=-\infty}^{\infty}|c_1(m)|^2 + 2!\sum_{m,n=-\infty}^{\infty}|c_2(m,n) - \delta(m,n)c_2(m,n)|^2 + \cdots. \tag{A.14}$$

A binary kernel $c_n(i_1, \cdot, i_n)$ is assumed to be symmetrical with respect to its arguments : $i_1, \cdots, i_n$. (A.13) is an orthogonal expansion, because each sum in the right hand side is uncorrelated to any other term by the orthogonality (A.7). By (A.7), the kernel functions are determined by the cross correlations as

$$\langle\Phi(\omega)\cdot B_n[b_{i_1}, b_{i_2}, \cdots, b_{i_n}]\rangle = n!\Delta_n(i_1, i_2, \cdots, i_n)c_n(i_1, i_2, \cdots, i_n). \tag{A.15}$$

Appendix B

Properties of band-limited binary kernels and stationary processes

Here, we discuss some properties of the band-limited kernels and the stationary process $U^{(q)}(x,z,\omega)$ given by (5.17).

Band-limited binary kernels From (4.25) and (4.28), one easily finds the properties of $C_1^{(q)}(\lambda_s), C_2^{(q)}(\lambda_1, \lambda_s - \lambda_1)$:

$$\begin{aligned} C_1^{(q)}(\lambda_s + k_L) &= C_1^{(q+1)}(\lambda_s), && \text{(B.1)} \\ C_2^{(q)}(\lambda_1, \lambda_s - \lambda_1) &= C_2^{(q)}(\lambda_s - \lambda_1, \lambda_1), && \text{(B.2)} \\ C_2^{(q)}(\lambda_1 + k_L, \lambda_s - (\lambda_1 + k_L)) &= C_2^{(q)}(\lambda_1, \lambda_s - \lambda_1), && \text{(B.3)} \\ C_2^{(q)}(\lambda_1, \lambda_s + k_L - \lambda_1) &= C_2^{(q+1)}(\lambda_1, \lambda_s - \lambda_1). && \text{(B.4)} \end{aligned}$$

(B.2) shows that $C_2^{(q)}(\cdot)$ is symmetrical with its wavenumber arguments. A higher order band-limited kernel is defined by

$$\begin{aligned} &C_n^{(q)}(\lambda_1, \cdots, \lambda_{n-1}, \lambda_s - \lambda_{n-1} - \cdots - \lambda_1) \\ &= \sum_{l_1, \cdots, l_{n-1} = -\infty}^{\infty} C_n(\lambda_1 + k_L l_1, \cdots, \lambda_{n-1} + k_L l_{n-1}, \lambda_s - \lambda_1 - \cdots - \lambda_{n-1} + k_L(q - l_1 - \cdots - l_{n-1})), \end{aligned} \quad \text{(B.5)}$$

which satisfies the property

$$C_n^{(q)}(\lambda_1, \ldots, \lambda_{n-1}, \lambda_s + k_L - \lambda_{n-1} - \cdots - \lambda_1) = C_n^{(q+1)}(\lambda_1, \ldots, \lambda_{n-1}, \lambda_s - \lambda_{n-1} - \cdots - \lambda_1). \quad \text{(B.6)}$$

Stationary processes $U^{(q)}(x,z,\omega)$ By (5.17) and the orthogonal property (A.7), we have the average of $U^{(q)}(x,z,\omega)$ as

$$\langle U^{(q)}(x,z,\omega) \rangle = C_0^{(q)} e^{i\beta_q(p)z}, \quad \text{(B.7)}$$

which is independent of x. We also obtain the mutual correlation function $R^U_{q,q'}(x - x', z)$ as

$$\begin{aligned} R^U_{q,q'}(x - x', z) &= \left\langle (U^{(q)}(x,z,\omega) - \langle U^{(q)}(x,z,\omega) \rangle)(U^{(q')}(x',z,\omega) - \langle U^{(q')}(x',z,\omega) \rangle) \right\rangle \\ &= k_L \int_{-k_L/2}^{k_L/2} C_1^{(q)}(\lambda_s) C_1^{(q')*}(\lambda_s) e^{i\lambda_s(x-x') + i\beta_q(p+\lambda_s)z - i\beta'_q(p+\lambda_s)z} d\lambda_s \end{aligned}$$

$$
\begin{aligned}
&+ \quad 2k_L^2 \iint_{-k_L/2}^{k_L/2} C_2^{(q)}(\lambda_1, \lambda_s - \lambda_1) C_2^{(q')*}(\lambda_1, \lambda_s - \lambda_1) \\
&\qquad\qquad \times e^{i\lambda_s(x-x')+i\beta_q(p+\lambda_s)z - i\beta'_q(p+\lambda_s)z} d\lambda_1 d\lambda_s \\
&- \quad 2k_L \int_{-k_L/2}^{k_L/2} e^{i\lambda_s(x-x')+i\beta_q(p+\lambda_s)z - i\beta'_q(p+\lambda_s)z} \\
&\qquad \times \left(\int_{-k_L/2}^{k_L/2} C_2^{(q)}(\lambda_1, \lambda_s - \lambda_1) d\lambda_1 \right) \cdot \left(\int_{-k_L/2}^{k_L/2} C_2^{(q')*}(\lambda'_1, \lambda_s - \lambda'_1) d\lambda'_1 \right) d\lambda_s \qquad \text{(B.8)}
\end{aligned}
$$

which means that $R^U_{q,q'}(x - x', z)$ only depends on the difference $(x - x')$, so that $U^{(q)}(x, z, \omega)$ becomes a wide sense stationary process of x. By (5.16), (5.17) and (B.8), we obtain the correlation function of $U(x, z, \omega)$, $R^U(x, x', z)$ as

$$
\begin{aligned}
R^U(x, x', z) &= \left\langle \left(U(x, z, \omega) - \langle U(x, z, \omega) \rangle \right) \left(U(x', z, \omega) - \langle U(x', z, \omega) \rangle \right) \right\rangle \\
&= \sum_{q,q'=-\infty}^{\infty} e^{ik_L(qx - q'x')} R^U_{q,q'}(x - x', z), \qquad \text{(B.9)}
\end{aligned}
$$

which is a periodic function of x and x' with the period L.

Appendix C

Derivation of optical theorem

Here, we summerize the derivation of the optical theorem for the binary random case and single defect case.

Binary random case Let us consider an area which is surrounded by $ABCD$ and the periodic random surface $z = f(x, \omega)$ shown in figure C.1. We take A and D at $x = -mL - \frac{L}{2}$ and B and C at $x = mL + \frac{L}{2}$, and z_0 is taken as $z_0 \gg \max\{f(x, \omega)\}$. Since $\Psi^*(x, z, \omega)$ satisfies Helmholtz equation (4.11), $\Psi^* \frac{\partial \Psi}{\partial n}$ and $\Psi \frac{\partial \Psi^*}{\partial n}$ satisfies Green's theorem on $ABCDA$:

$$\int_{ABCDA} \left(\Psi^* \frac{\partial \Psi}{\partial n} - \Psi \frac{\partial \Psi^*}{\partial n} \right) = 0 \tag{C.1}$$

The integral along the periphery of $ABCDA$ can be decomposed into four parts:

$$\left(\int_{AB} dx + \int_{BC} dz + \int_{CD} dl + \int_{DA} dz \right) \left(\Psi^* \frac{\partial \Psi}{\partial n} - \Psi \frac{\partial \Psi^*}{\partial n} \right) = 0. \tag{C.2}$$

Now, let us extend the area $ABCDA$ along x-axis with $m \to \infty$. Generally, the integrals along (AB) and (CD) diverge under such extension, while the integrals along (BC) and (DA) in the z direction remain finite. On the other hand, Ψ and Ψ^* satisfy the Dirichlet and Neumann boundary condition on the surface $z = f(x, \omega)$. Thus, the integral along (CD) vanishes. Dividing both sides of (C.2) by $(2m + 1)L$, we obtain

$$\begin{aligned} &\lim_{m \to \infty} \frac{1}{(2m+1)L} \int_{-mL-L/2}^{mL+L/2} \left(\Psi^* \frac{\partial \Psi}{\partial z} - \Psi \frac{\partial \Psi^*}{\partial z} \right) \Big|_{z=z_0} dx \\ &\quad = \lim_{m \to \infty} \frac{1}{(2m+1)L} \sum_{N=-m}^{m} \int_{NL-L/2}^{NL+L/2} \mathrm{Im}[\Psi^* \mathrm{grad} \Psi] \Big|_{z=z_0} dx = 0. \end{aligned} \tag{C.3}$$

Here, we rewrote $\partial n \to \partial z$ along (AB).

Since the total wave field Ψ has the stochastic Floquet form (4.19), $\Psi^* \mathrm{grad} \Psi$ is a periodic stationary process. Furthermore, $\langle \Psi^* \mathrm{grad} \Psi \rangle$ becomes a periodic function of x with the period L. Substituting (4.26) into (C.3) and dividing both sides of (C.3) by k, (C.3) can be rewritten as

$$\lim_{n \to \infty} \frac{1}{(2n+1)L} \sum_{m=-n}^{n} \int_{mL-L/2}^{mL+L/2} \mathrm{Im} \left[\frac{\Psi^*}{k} \mathrm{grad} \Psi \right] \Big|_{z=z_0} dx$$

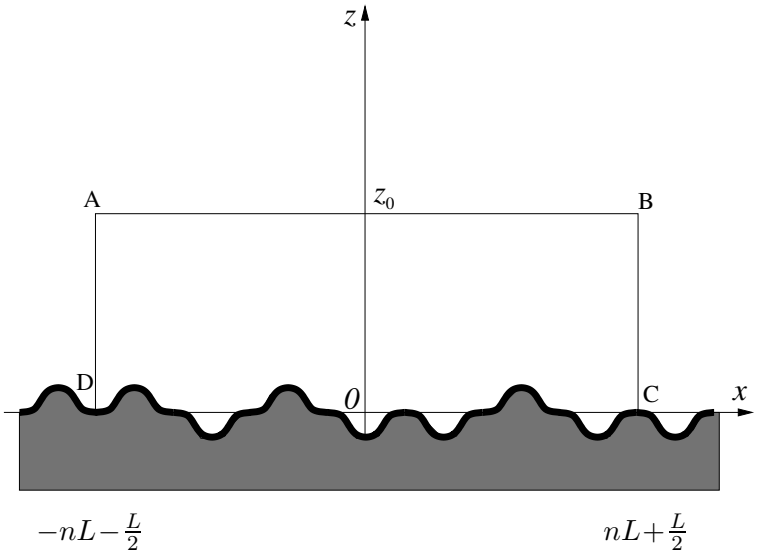

Figure C.1 Area of optical theorem, which is surrounded by $DABC$ and with the periodic random surface.

$$= \frac{1}{L}\int_{-L/2}^{L/2} \mathrm{Im}\left\langle \frac{\Psi^*}{k}\mathrm{grad}\Psi\Big|_{z=z_0}\right\rangle dx = \frac{1}{L}\int_{-L/2}^{L/2} \mathrm{Re}\left\langle \frac{\Psi^*}{ik}\frac{\partial\Psi}{\partial z}\Big|_{z=z_0}\right\rangle dx$$
$$= -\frac{\beta_0(p)}{k} + \frac{1}{L}\int_{-L/2}^{L/2} \mathrm{Re}\left\langle \frac{U^*}{ik}\frac{\partial U}{\partial z}\Big|_{z=z_0}\right\rangle dx = 0. \tag{C.4}$$

The first term of the left hand side of (C.4) is the energy of the incident wave, while the second term expresses the energy of diffracted and scattered waves.

By (5.17) and the orthogonal property of the binary polynomials (A.7), the second term of (C.4) becomes

$$\begin{aligned}
&\frac{1}{L}\int_{-L/2}^{L/2} \mathrm{Re}\left\langle \frac{U^*}{ik}\frac{\partial U}{\partial z}\Big|_{z=z_0}\right\rangle dx \\
&= \frac{1}{L}\int_{-L/2}^{L/2} \mathrm{Re}\left[\frac{1}{k}\Big(\sum_{q,q'=-\infty}^{\infty} e^{ik_L(q'-q)x}\beta_{q'}(p)C_0^{(q')}C_0^{(q)*}\right. \\
&\quad + \sum_{m=-\infty}^{\infty}\sum_{q,q'}^{\infty}\iint_{-k_L/2}^{k_L/2} e^{ik_L(q'-q)x}e^{i(\lambda_s'-\lambda_s)(x-mL)+i(\beta_{q'}(p+\lambda_s')-\beta_q(p+\lambda_s))z_0} \\
&\qquad\qquad \times\beta_{q'}(p+\lambda_s')C_1^{(q')}(\lambda_s')C_1^{(q)*}(\lambda_s)d\lambda_s d\lambda_s' \\
&\quad + \sum_{m,n}^{\infty}\sum_{m',n'}^{\infty}\sum_{q,q'}^{\infty}\iiint\!\!\iint_{-k_L/2}^{k_L/2} e^{ik_L(q'-q)x} \\
&\qquad \times e^{i(\lambda_s'-\lambda_1')(x-m'L)-i(\lambda_s-\lambda_1)(x-mL)+i\lambda_1'(x-n'L)-i\lambda_1(x-nL)} \\
&\qquad \times e^{i(\beta_{q'}(p+\lambda_s')-\beta_q(p+\lambda_s))z_0}(2!\delta(m,m')\delta(n,n') - 2!\delta(m,n)\delta(m,m')\delta(m',n')) \\
&\qquad \left.\times\beta_{q'}(p+\lambda_s')C_2^{(q')}(\lambda_s'-\lambda_1',\lambda_1')C_2^{(q)*}(\lambda_s-\lambda_1,\lambda_1)d\lambda_1 d\lambda_s d\lambda_1' d\lambda_s' + \cdots\Big)\right] dx.
\end{aligned} \tag{C.5}$$

For the zeroth order binary kernels, integrating over one period L, only terms with $q'-q=0$ remain, because all factors on x are periodic functions. For the first order binary kernels, by use

of the identity for δ-pulse series (4.47), $\lambda'_s - \lambda_s = 0$ holds ($-k_L/2 \le \lambda_s, \lambda'_s \le k_L/2$ with $m = 0$), and again only terms with $q' - q = 0$ remain. Thus,

$$\begin{aligned}
&\frac{1}{L}\int_{-L/2}^{L/2} \mathrm{Re}\Big\langle \frac{U^*}{ik}\frac{\partial U}{\partial z}\Big|_{z=z_0}\Big\rangle dx = \\
&= \frac{1}{L}\int_{-L/2}^{L/2} \mathrm{Re}\Big\langle \frac{1}{k}\Big(\sum_{q=-\infty}^{\infty}\Big(\beta_q(p)\left|C_0^{(q)}\right|^2 + 1!k_L\int_{-k_L/2}^{k_L/2}\beta_q(p+\lambda_s)\left|C_1^{(q)}(\lambda_s)\right|^2 d\lambda_s\Big) \\
&+ \sum_{m,n}^{\infty}\sum_{m',n'}^{\infty}\sum_{q,q'}^{\infty}\iiint_{-k_L/2}^{k_L/2} e^{ik_L(q'-q)x} e^{i(\lambda'_s-\lambda'_1)(x-m'L)-i(\lambda_s-\lambda_1)(x-mL)+i\lambda'_1(x-n'L)-i\lambda_1(x-nL)} \\
&\qquad \times e^{i(\beta_{q'}(p+\lambda'_s)-\beta_q(p+\lambda_s))z_0}(2!\delta(m,m')\delta(n,n') - 2!\delta(m,n)\delta(m,m')\delta(m',n')) \\
&\qquad \times \beta_{q'}(p+\lambda'_s)C_2^{(q')}(\lambda'_s-\lambda'_1,\lambda'_1)C_2^{(q)*}(\lambda_s-\lambda_1,\lambda_1)d\lambda_1 d\lambda_s d\lambda'_1 d\lambda'_s + \cdots\Big)\Big\rangle dx.
\end{aligned}$$

For the second order binary kernels, by use of (4.47),

$$\begin{aligned}
&\frac{1}{L}\int_{-L/2}^{L/2} \mathrm{Re}\Big\langle \frac{U^*}{ik}\frac{\partial U}{\partial z}\Big|_{z=z_0}\Big\rangle dx = \\
&= \frac{1}{L}\int_{-L/2}^{L/2} \mathrm{Re}\Big\langle \frac{1}{k}\Big(\sum_{q=-\infty}^{\infty}\Big(\beta_q(p)\left|C_0^{(q)}\right|^2 + 1!k_L\int_{-k_L/2}^{k_L/2}\beta_q(p+\lambda_s)\left|C_1^{(q)}(\lambda_s)\right|^2 d\lambda_s\Big) \\
&\quad + 2!\sum_{m,n}^{\infty}\sum_{q,q'}^{\infty} k_L^2 \iiint_{-k_L/2}^{k_L/2} e^{ik_L(q'-q)x} e^{i((\lambda'_s-\lambda'_1)-(\lambda_s-\lambda_1))x+i(\lambda'_1-\lambda_1)x+i(\beta_{q'}(p+\lambda'_s)-\beta_q(p+\lambda_s))z_0} \\
&\qquad\qquad \times \delta((\lambda_s-\lambda_1)-(\lambda'_s-\lambda'_1)+k_Lm)\delta(\lambda_1-\lambda'_1+k_Ln) \\
&\qquad\qquad \times \beta_{q'}(p+\lambda'_s)C_2^{(q')}(\lambda'_s-\lambda'_1,\lambda'_1)C_2^{(q)*}(\lambda_s-\lambda_1,\lambda_1)d\lambda_1 d\lambda_s d\lambda'_1 d\lambda'_s \\
&\quad - 2!\sum_{m=-\infty}^{\infty}\sum_{q,q'}^{\infty} k_L \iiint_{-k_L/2}^{k_L/2} e^{ik_L(q'-q)x} e^{i(\lambda'_s-\lambda_s)x+i(\beta_{q'}(p+\lambda'_s)-\beta_q(p+\lambda_s))z_0}\delta(\lambda_s-\lambda'_s+k_Lm) \\
&\qquad \times \beta_{q'}(p+\lambda'_s)C_2^{(q')}(\lambda'_s-\lambda'_1,\lambda'_1)C_2^{(q)*}(\lambda_s-\lambda_1,\lambda_1)d\lambda_1 d\lambda_s d\lambda'_1 d\lambda'_s + \cdots\Big)\Big\rangle dx.
\end{aligned}$$

For the first term of the integral for $C_2(\lambda,\lambda')$, $\delta((\lambda_s-\lambda_1)-(\lambda'_s-\lambda'_1)+k_Lm)\delta(\lambda_1-\lambda'_1+k_Ln) = \delta(\lambda_s-\lambda'_s+k_Lm)\delta(\lambda_1-\lambda'_1+k_Ln)$ is satisfied only with $m,n=0$, and for the second term, $\delta(\lambda_s-\lambda'_s+k_Lm)$ only with $m=0$. As a result, only terms with $q'-q=0$ remain for the integration over x, then, the optical theorem up to the second order binary kernels becomes as follows:

$$\begin{aligned}
&\frac{1}{L}\int_{-L/2}^{L/2} \mathrm{Re}\Big\langle \frac{U^*}{ik}\frac{\partial U}{\partial z}\Big|_{z=z_0}\Big\rangle dx \\
&= \frac{1}{L}\int_{-L/2}^{L/2}\Big\langle \frac{1}{k}\sum_{q=-\infty}^{\infty}\Big(\mathrm{Re}\left[\beta_q(p)\right]\left|C_0^{(q)}\right|^2 + 1!k_L\int_{-k_L/2}^{k_L/2}\mathrm{Re}\left[\beta_q(p+\lambda_s)\right]\left|C_1^{(q)}(\lambda_s)\right|^2 d\lambda_s \\
&\qquad + 2!k_L^2\iint_{-k_L/2}^{k_L/2}\mathrm{Re}\left[\beta_q(p+\lambda_s)\right]\left|C_2^{(q)}(\lambda_s-\lambda_1,\lambda_1)\right|^2 d\lambda_1 d\lambda_s \\
&\qquad - 2!k_L\iiint_{-k_L/2}^{k_L/2}\mathrm{Re}\left[\beta_q(p+\lambda_s)\right]C_2^{(q)}(\lambda_s-\lambda'_1,\lambda'_1)C_2^{(q)*}(\lambda_s-\lambda_1,\lambda_1)d\lambda_1 d\lambda'_1 d\lambda_s\Big)\Big\rangle dx
\end{aligned}$$

$$= \frac{1}{L}\int_{-L/2}^{L/2}\Big\langle \frac{1}{k}\sum_{q=-\infty}^{\infty}\Big(\mathrm{Re}\left[\beta_q(p)\right]\left|C_0^{(q)}\right|^2 + 1!k_L\int_{-k_L/2}^{k_L/2}\mathrm{Re}\left[\beta_q(p+\lambda_s)\right]\left|C_1^{(q)}(\lambda_s)\right|^2 d\lambda_s$$
$$+ 2!k_L^2\iint_{-k_L/2}^{k_L/2}\mathrm{Re}\left[\beta_q(p+\lambda_s)\right]\left|C_2^{(q)}(\lambda_s-\lambda_1,\lambda_1)\right|^2 d\lambda_1 d\lambda_s\Big)$$
$$- 2!k_L\int_{-k_L/2}^{k_L/2}\mathrm{Re}\left[\beta_q(p+\lambda_s)\right]\times\left|\sum_{q=-\infty}^{\infty}\int_{-k_L/2}^{k_L/2}C_2^{(q)}(\lambda_s-\lambda,\lambda)d\lambda\right|^2 d\lambda_s\Big\rangle dx. \quad \text{(C.6)}$$

Single defect case Let us consider an area which is surrounded by $ABCD$ and the periodic arrays of rectangular grooves with single defect $z = f(x)$ shown in figure C.2. We take A and D at $x = -(N + \frac{L}{2})L$ and B and C at $x = (N + \frac{L}{2})L$. Now, let us extend the area $ABCDA$ along x-axis with $N \to \infty$. As is mentioned in section 2.4, $\psi_s(x,z)$ decays proportional to $(x^2+z^2)^{-1/4}$. Thus $\hat{\Psi}_1\mathrm{grad}\psi_s^*$, $\psi_s\mathrm{grad}\hat{\Psi}_1^*$ and $\psi_s\mathrm{grad}\psi_s^*$ vanish at $|x| \to \infty$, which means the integrals along (BC) and (DA) in the z direction can be considered to vanish. Further, $\hat{\Psi}_1\mathrm{grad}\hat{\Psi}_1^*$ is a periodic function of x with the period L, and Ψ and Ψ^* satisfy the Dirichlet and Neumann boundary condition on the surface $z = f(x)$. Thus, we obtain from the identity $\mathrm{Im}[\mathrm{div}(\hat{\Psi}_1+\psi_s)\mathrm{grad}(\hat{\Psi}_1+\psi_s)^*] = 0$

$$\lim_{m\to\infty}\int_{-(N+1/2)L}^{(N+1/2)L}\mathrm{Im}\Big[\hat{\Psi}_1(x,z)\frac{\partial}{\partial z}\psi_s^*(x,z)$$
$$+\psi_s(x,z)\frac{\partial}{\partial z}\hat{\Psi}_1^*(x,z)+\psi_s(x,z)\frac{\partial}{\partial z}\psi_s^*(x,z)\Big|_{z=z_0}\Big]dx = 0. \quad \text{(C.7)}$$

On the other hand, from (2.15)(2.16)(2.27)(2.28), we get the integrand of (C.7) as

$$\hat{\Psi}_1(x,z)\frac{\partial}{\partial z}\psi_s^*(x,z)+\psi_s(x,z)\frac{\partial}{\partial z}\hat{\Psi}_1^*(x,z)+\psi_s(x,z)\frac{\partial}{\partial z}\psi_s^*(x,z)$$
$$= -i\left[e^{-i\beta_0(p)z_0}+\sum_{n=-\infty}^{\infty}A_n(p)e^{ink_Lx+i\beta_n(p)z_0}\right]\int_{-\infty}^{\infty}\beta_0^*(p+s)a^*(s)e^{-isx-i\beta_0^*(p+s)z_0}ds$$
$$+\int_{-\infty}^{\infty}a(s)e^{isx+i\beta_0(p+s)z_0}ds\left[i\beta_0(p)e^{i\beta_0(p)z_0}-i\sum_{n=-\infty}^{\infty}\beta_n^*(p)A_n^*(p)e^{-ink_Lx-i\beta_n^*(p)z_0}\right]$$
$$-i\int_{-\infty}^{\infty}\int_{-\infty}^{\infty}\beta_0^*(p+s)a^*(s)a(s)e^{i(s-s')x+i[\beta_0(p+s)-\beta_0^*(p+s')z_0}dsds'. \quad \text{(C.8)}$$

For convenience, we define $U(s|N)$ as

$$U(s|N) = \int_{-(N+1/2)L}^{(N+1/2)L}e^{isx}dx, \quad \text{(C.9)}$$
$$\lim_{N\to\infty}U(s|N) = 2\pi\delta(s), \qquad U(-s|N) = U(s|N). \quad \text{(C.10)}$$

Integrating in terms of x over $[(-(N+1/2)L,(N+1/2)L]$, we rewrite (C.8) as

$$\int_{-(N+1/2)L}^{(N+1/2)L}\hat{\Psi}_1(x,z)\frac{\partial}{\partial z}\psi_s^*(x,z)+\psi_s(x,z)\frac{\partial}{\partial z}\hat{\Psi}_1^*(x,z)+\psi_s(x,z)\frac{\partial}{\partial z}\psi_s^*(x,z)dx$$
$$= -i\int_{-\infty}^{\infty}\beta_0^*(p+s)a^*(s)U(s|N)e^{-i[\beta_0(p)+\beta_0^*(p+s)]z_0}ds$$

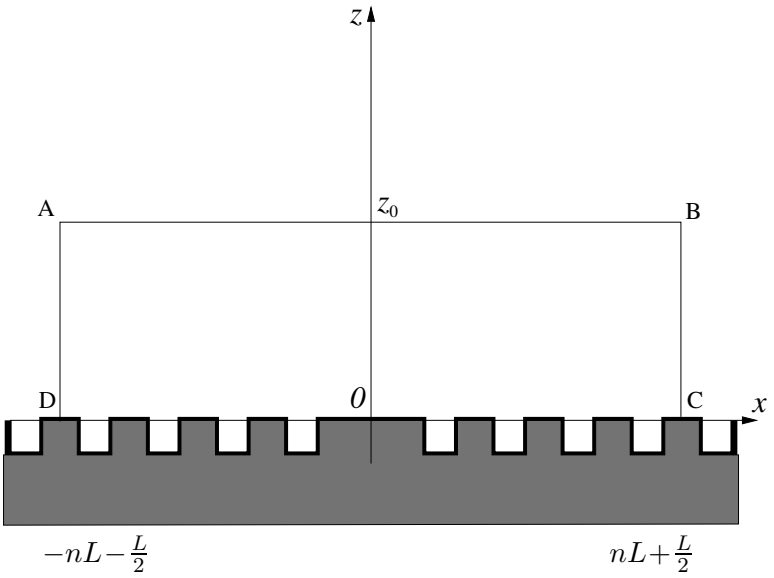

Figure C.2 Area of optical theorem for sigle defect case, which is surrounded by $DABC$ and with the periodic grooves with single defect.

$$
\begin{aligned}
&-i\sum_{n=-\infty}^{\infty}\int_{-\infty}^{\infty}\beta_0^*(p+s)a^*(s)A_n(p)U(s-nk_L|N)e^{i[\beta_n(p)-\beta_0^*(p+s)]z}ds\\
&+i\beta_0\int_{-\infty}^{\infty}a(s)U(s|N)e^{i[\beta_0(p)+\beta_0(p+s)]z_0}ds\\
&-i\sum_{n=-\infty}^{\infty}\beta_n^*(p)A_n^*(p)\int_{-\infty}^{\infty}U(s-nk_L)a(s)e^{i[\beta_0(p+s)-\beta_n^*(p)]z_0}ds\\
&-i\int_{-\infty}^{\infty}\int_{-\infty}^{\infty}\beta_0^*(p+s)a^*(s')a(s)U(s-s'|N)e^{i[\beta_0(p+s)-\beta_0^*(p+s')z}dsds'. \qquad \text{(C.11)}
\end{aligned}
$$

Putting $N\to\infty$ and taking the imaginary part

$$
\begin{aligned}
&\lim_{N\to\infty}\int_{-(N+1/2)L}^{(N+1/2)L}\mathrm{Im}\left[\Psi_1(x,z)\frac{\partial}{\partial z}\Psi_1^*(x,z)\Big|_{z=z_0}\right]dx\\
&\quad=2\pi\mathrm{Im}\Big[-i\beta_0^*(p)a^*(p)e^{-i[\beta_0(p)+\beta_0^*(p)]z_0}\\
&\qquad-i\sum_{n=-\infty}^{\infty}\beta_0^*(p+nk_L)a^*(nk_L)A_n(p)e^{i[\beta_n(p)-\beta_0^*(p+nk_L)]z_0}\\
&\qquad+i\beta_0(p)a(p)e^{i[\beta_0(p)+\beta_0^*(p)]z_0}-i\sum_{n=-\infty}^{\infty}\beta_n^*(p)A_n^*(p)a(nk_L)e^{i[\beta_0(p+nk_L)-\beta_n^*(p)]z_0}\\
&\qquad-i\int_{-\infty}^{\infty}\beta^*(p+s)|a(s)|^2e^{i[\beta_0(p+s)-\beta_0^*(p+s)]z_0}ds\Big]\\
&\quad=-2\pi i\Big[\sum_{n=-\infty}^{\infty}\beta_n^*a^*(nk_L)A_n(p)e^{i[\beta_n(p)-\beta_0^*(p+k_Ln)]z_0}\\
&\qquad+\sum_{n=-\infty}^{\infty}\beta_n^*(p)A_n^*(p)a(nk_L)e^{i[\beta_n(p)-\beta_n^*(p)]z_0}
\end{aligned}
$$

$$+\int_{-\infty}^{\infty}\beta_0^*(p+s)|a(s)|^2e^{i[\beta_0(p+s)-\beta_0^*(p+s)]z_0}ds\Big]=0. \tag{C.12}$$

Then, we finally obtain the optical theorem for the single defect case

$$-2\sum_{n=-\infty}^{\infty}\text{Re }[\beta_n^*(p)]\text{ Re }[a(nk_L)A_n^*(p)]=\int_{-\infty}^{\infty}\text{Re }[\beta_0(p+s)]|a(s)|^2ds \tag{C.13}$$

Here, we have used the facts that $\beta_0(p+nk_L)=\beta_n(p)$, and $-i\beta_0^*(p)a^*(p)e^{-i[\beta_0(p)+\beta_0^*(p)]z_0}+i\beta_0(p)a(p)e^{i[\beta_0(p)+\beta_0^*(p)]z_0}$ and $i[\beta_n(p)-\beta_n^*(p)]$ are real numbers.

Appendix D

Binary kernels by multiply renormalizing approximation for TE incidence

In this appendix, we derive expressions of the binary kernels by the multiply renormalizing approximation for TE plane wave incidence, following the same procedure for TM case in Chapter 5.

From the boundary condition (4.36), the n-th order hierarchical equation is written as

(n-th order) $(n \geq 3)$ $\qquad (m_1, \cdots, m_n = 0, \pm 1, \pm 2, \cdots)$

$$
\begin{aligned}
&\sum_{q=-\infty}^{\infty} e^{ik_L qx} \Big[\int \cdots \int_{-k_L/2}^{k_L/2} \cos[\sigma\beta_q(p+\lambda_s)g(x)] \\
&\qquad \times e^{i(\lambda_s-(\lambda_1+\cdots+\lambda_{n-1}))(x-m_nL)+i\lambda_1(x-m_1L)+\cdots+i\lambda_{n-1}(x-m_{n-1}L)} \\
&\qquad \times C_n^{(q)}(\lambda_s-(\lambda_1+\cdots+\lambda_{n-1}),\lambda_1,\cdots,\lambda_{n-1}|p)d\lambda_1\cdots d\lambda_{n-1}d\lambda_s \\
&+\frac{i}{n}\delta(m_1,0)\int \cdots \int_{-k_L/2}^{k_L/2} \sin[\sigma\beta_q(p+\lambda_s-\lambda_1)g(x)] \\
&\qquad \times e^{i(\lambda_s-(\lambda_1+\cdots+\lambda_{n-1}))(x-m_nL)+i\lambda_2(x-m_2L)+\cdots+i\lambda_{n-1}(x-m_{n-1}L)} \\
&\qquad \times C_{n-1}^{(q)}(\lambda_s-(\lambda_1+\cdots+\lambda_{n-1}),\lambda_2,\cdots,\lambda_{n-1}|p)d\lambda_2\cdots d\lambda_{n-1}d\lambda_s \\
&\quad \vdots \\
&+\frac{i}{n}\delta(m_n,0)\int \cdots \int_{-k_L/2}^{k_L/2} \sin[\sigma\beta_q(p+\lambda_1+\cdots+\lambda_{n-1})g(x)] \\
&\qquad \times e^{i\lambda_1(x-m_1L)+\cdots+i\lambda_{n-1}(x-m_{n-1}L)} C_{n-1}^{(q)}(\lambda_1,\cdots,\lambda_{n-1}|p)d\lambda_1\cdots d\lambda_{n-1} \\
&+(n+1)\ i\int \cdots \int_{-k_L/2}^{k_L/2} \sin[\sigma\beta_q(p+\lambda_s)g(x)] \\
&\qquad \times e^{i(\lambda_s-(\lambda_1+\cdots+\lambda_n))x+i\lambda_1(x-m_1L)+\cdots+i\lambda_n(x-m_nL)} \\
&\qquad \times C_{n+1}^{(q)}(\lambda_s-(\lambda_1+\cdots+\lambda_n),\lambda_1,\cdots,\lambda_n|p)d\lambda_1\cdots d\lambda_n d\lambda_s \\
&-n(n+1)\delta(m_n,0)\ i\int \cdots \int_{-k_L/2}^{k_L/2} \sin[\sigma\beta_q(p+\lambda_s)g(x)] \\
&\qquad \times e^{i(\lambda_s-(\lambda_1+\cdots+\lambda_n))x+i\lambda_1(x-m_1L)+\cdots+i\lambda_{n-1}(x-m_{n-1}L)+i\lambda_n x}
\end{aligned}
$$

$$\times C_{n+1}^{(q)}(\lambda_s-(\lambda_1+\cdots+\lambda_n),\lambda_1,\cdots,\lambda_n|p)d\lambda_1\cdots d\lambda_n d\lambda_s\Big]=0 \tag{D.1}$$

Here, (D.1) holds for any m_n. Expanding the factors of (D.1) by (4.40), introducing the infinite-dimensional matrices (4.41)-(4.46) and applying (4.47) after multiplying $e^{i\Lambda_1 m_1 L+\cdots+i\Lambda_n m_n L}$ and summing up with every m_j $(1\le j\le n)$, we obtain the n-th order hierarchical equation in matrix form,
(n-th order)

$$\begin{aligned}
&k_L\mathbf{\Gamma}^{\rm c}(\Lambda_1+\cdots+\Lambda_n|p)\mathbf{C}_n(\Lambda_1,\cdots,\Lambda_n|p)\\
&+\sum_{l=1}^{n}\frac{i}{n}\,\mathbf{\Gamma}^{\rm s}(\Lambda_1+\cdots+\Lambda_{l-1}+\Lambda_{l+1}+\cdots+\Lambda_n|p)\\
&\qquad\qquad\times\mathbf{C}_{n-1}(\Lambda_1,\cdots,\Lambda_{l-1},\Lambda_{l+1},\cdots,\Lambda_n|p)\\
&+(n+1)\;ik_L\int_{-k_L/2}^{k_L/2}\mathbf{\Gamma}^{\rm s}(\Lambda_1+\cdots+\Lambda_n+\lambda_n|p)\\
&\qquad\qquad\times\mathbf{C}_{n+1}(\Lambda_1,\cdots,\Lambda_n,\lambda_n|p)d\lambda_n\\
&-\sum_{l=1}^{n}(n+1)\;i\iint_{-k_L/2}^{k_L/2}\mathbf{\Gamma}^{\rm s}(\Lambda_1+\cdots+\Lambda_{l-1}+\Lambda_{l+1}+\cdots+\Lambda_n+\lambda_{n-1}+\lambda_n|p)\\
&\qquad\qquad\times\mathbf{C}_{n+1}(\Lambda_1,\cdots,\Lambda_{l-1},\Lambda_{l+1},\cdots\Lambda_n,\lambda_{n-1},\lambda_n|p)d\lambda_{n-1}d\lambda_n=0.
\end{aligned}\tag{D.2}$$

Let us obtain approximate binary kernels $\mathbf{C}_n(\Lambda_1,\cdots,\Lambda_n|p)$ by use of the multiply renormalizing approximation [53], which is made up of two steps.

First, we get an expression of $\mathbf{C}_n(\Lambda_1,\cdots,\Lambda_n|p)$ by use of a truncation procedure and the diagonal approximation [53]. Neglecting $\mathbf{C}_{N+1}(\cdot)$ in the N-th order relation $(N\ge 2)$, we obtain

$$\begin{aligned}
&k_L\mathbf{\Gamma}^{\rm c}(\Lambda_1+\cdots+\Lambda_N|p)\mathbf{C}_N^{(N)}(\Lambda_1,\cdots,\Lambda_N|p)\\
&=-\sum_{l=1}^{N}\frac{i}{N}\,\mathbf{\Gamma}^{\rm s}(\Lambda_1+\cdots+\Lambda_{l-1}+\Lambda_{l+1}+\cdots+\Lambda_N|p)\\
&\qquad\qquad\times\mathbf{C}_{N-1}^{(N)}(\Lambda_1,\cdots,\Lambda_{l-1},\Lambda_{l+1},\cdots,\Lambda_N|p),
\end{aligned}\tag{D.3}$$

where, the superscript $^{(N)}$ indicates the truncation number N. Substituting (D.3) into the $(N-1)$-th order relation, we get

$$\begin{aligned}
&k_L\mathbf{\Gamma}^{\rm c}(\Lambda_1+\cdots+\Lambda_{N-1}|p)\mathbf{C}_{N-1}^{(N)}(\Lambda_1,\cdots,\Lambda_{N-1}|p)\\
&+i\sum_{l=1}^{N-1}\frac{1}{N-1}\mathbf{\Gamma}^{\rm s}(\Lambda_1+\cdots+\Lambda_{l-1}+\Lambda_{l+1}+\cdots+\Lambda_{N-1}|p)\\
&\qquad\times\mathbf{C}_{N-2}^{(N)}(\Lambda_1,\cdots,\Lambda_{l-1},\Lambda_{l+1},\cdots,\Lambda_{N-1}|p)\\
&+\int_{-k_L/2}^{k_L/2}\mathbf{\Gamma}^{\rm s}(\Lambda_1+\cdots+\Lambda_{N-1}+\lambda_{N-1}|p)\\
&\qquad\times[\mathbf{\Gamma}^{\rm c}(\Lambda_1+\cdots+\Lambda_{N-1}+\lambda_{N-1}|p)]^{-1}\\
&\qquad\times\mathbf{\Gamma}^{\rm s}(\Lambda_1+\cdots+\Lambda_{N-1}|p)d\lambda_{N-1}\mathbf{C}_{N-1}^{(N)}(\Lambda_1,\cdots,\Lambda_{N-1}|p)\\
&+\sum_{l=1}^{N-1}\int_{-k_L/2}^{k_L/2}\mathbf{\Gamma}^{\rm s}(\Lambda_1+\cdots+\Lambda_{N-1}+\lambda_{N-1}|p)
\end{aligned}$$

$$
\begin{aligned}
&\times[\mathbf{\Gamma}^{\mathrm{c}}(\Lambda_1+\cdots+\Lambda_{N-1}+\lambda_{N-1}|p)]^{-1}\\
&\times\mathbf{\Gamma}^{\mathrm{s}}(\Lambda_1-\cdots-\Lambda_{l-1}-\Lambda_{l+1}+\cdots+\Lambda_{N-1}+\lambda_{N-1}|p)\\
&\times\mathbf{C}_{N-1}^{(N)}(\Lambda_1,\cdots,\Lambda_{l-1},\Lambda_{l+1},\cdots,\Lambda_{N-1},\lambda_{N-1}|p)d\lambda_{N-1}\\
-\sum_{l=1}^{N-1}\frac{N}{k_L}&\iint_{-k_L/2}^{k_L/2}\mathbf{\Gamma}^{\mathrm{s}}(\Lambda_1+\cdots+\Lambda_{l-1}+\Lambda_{l+1}+\cdots+\Lambda_{N-1}+\lambda_{N-2}+\lambda_{N-1}|p)\\
&\times[\mathbf{\Gamma}^{\mathrm{c}}(\Lambda_1+\cdots+\Lambda_{l-1}+\Lambda_{l+1}+\cdots+\Lambda_{N-1}+\lambda_{N-2}+\lambda_{N-1}|p)]^{-1}\\
&\times\mathbf{\Gamma}^{\mathrm{s}}(\Lambda_1+\cdots+\Lambda_{l-1}+\Lambda_{l+1}+\cdots+\Lambda_{N-1}+\lambda_{N-1}|p)\\
&\times\mathbf{C}_{N-1}^{(N)}(\Lambda_1,\cdots,\Lambda_{l-1},\Lambda_{l+1},\cdots,\Lambda_{N-1},\lambda_{N-1}|p)d\lambda_{N-2}d\lambda_{N-1}=0. \qquad \text{(D.4)}
\end{aligned}
$$

Taking the diagonal approximation on (D.4), we obtain $\mathbf{C}_{N-1}^{(N)}(\cdot)$ as

$$
\begin{aligned}
&\mathbf{C}_{N-1}^{(N)}(\Lambda_1,\cdots,\Lambda_{N-1}|p)\\
&\simeq\sum_{l=1}^{N-1}\frac{-i}{k_L(N-1)}\left[\mathbf{\Gamma}^{\mathrm{c}}(\Lambda_1+\cdots+\Lambda_{N-1}|p)+\mathbf{M}^{(1)}(\Lambda_1+\cdots+\Lambda_{N-1}|p)\right]^{-1}\\
&\qquad\times\mathbf{\Gamma}^{\mathrm{s}}(\Lambda_1+\cdots+\Lambda_{l-1}+\Lambda_{l+1}+\cdots+\Lambda_{N-1}|p)\\
&\qquad\times\mathbf{C}_{N-2}^{(N)}(\Lambda_1,\cdots,\Lambda_{l-1},\Lambda_{l+1},\cdots,\Lambda_{N-1}|p). \qquad \text{(D.5)}
\end{aligned}
$$

Secondly, substituting such a relation and applying the diagonal approximation recursively, we get a relation between $\mathbf{C}_{n}^{(N)}(\cdot)$ and $\mathbf{C}_{n-1}^{(N)}(\cdot)$ as

$$
\mathbf{C}_{n}^{(N)}(\Lambda_1,\cdots,\Lambda_n|p)\simeq\begin{cases}
\dfrac{-i}{nk_L}\displaystyle\sum_{l=1}^{n}\left[\mathbf{\Gamma}^{\mathrm{c}}(\Lambda_1+\cdots+\Lambda_n|p)+\mathbf{M}^{(N-n)}(\Lambda_1+\cdots+\Lambda_n|p)\right]^{-1}\\
\qquad\times\mathbf{\Gamma}^{\mathrm{s}}(\Lambda_1+\cdots+\Lambda_{l-1}+\Lambda_{l+1}+\cdots+\Lambda_n|p)\\
\qquad\times\mathbf{C}_{n-1}^{(N)}(\Lambda_1,\cdots,\Lambda_{l-1},\Lambda_{l+1},\cdots,\Lambda_n|p), \quad (N\geq n\geq 2),\\
\dfrac{i}{k_L}\left[\mathbf{\Gamma}^{\mathrm{c}}(\Lambda|p)+\mathbf{M}^{(N-1)}(\Lambda|p)\right]^{-1}\mathbf{\Gamma}^{\mathrm{s}}(0|p)\left\{\mathbf{I}^0-\mathbf{C}_0(p)\right\}, \qquad (n=1),
\end{cases} \qquad \text{(D.6)}
$$

where $\mathbf{M}^{(n)}(\Lambda|p)$ is defined as

$$
\mathbf{M}^{(n)}(\Lambda|p)=\begin{cases}
\dfrac{1}{k_L}\displaystyle\int_{-k_L/2}^{k_L/2}\mathbf{\Gamma}^{\mathrm{s}}(\Lambda+\lambda'|p)\\
\qquad\times\left[\mathbf{\Gamma}^{\mathrm{c}}(\Lambda+\lambda'|p)+\mathbf{M}^{(n-1)}(\Lambda+\lambda'|p)\right]^{-1}\mathbf{\Gamma}^{\mathrm{s}}(\Lambda|p)d\lambda', & (n\geq 1),\\
0, & (n=0).
\end{cases} \qquad \text{(D.7)}
$$

$\mathbf{M}^{(n)}(\Lambda|p)$ is an n-th order iterative mass operator. Since $\mathbf{M}^{(n)}(\Lambda|p)$ has products of $\mathbf{\Gamma}^{\mathrm{s}}(\Lambda+\lambda'|p)$ and $\mathbf{\Gamma}^{\mathrm{s}}(\Lambda|p)$ in the integrand, it contains couplings between different orders on q of the harmonic series. Thus, $\mathbf{M}^{(n)}(\Lambda|p)$ may represent effects of diffraction. Also, $\mathbf{M}^{(n)}(\Lambda|p)$ represents multiple scattering effects because it has a component of an inverse matrix of $\mathbf{\Gamma}^{\mathrm{c}}(\Lambda+\lambda'|p)+\mathbf{M}^{(n-1)}(\Lambda+\lambda'|p)$. Note that $\mathbf{M}^{(n)}(p+\Lambda)$ can be estimated to be proportional to σ^2 under small roughness $k\sigma<1$, since $\mathbf{\Gamma}^{\mathrm{s}}(\Lambda|p)$ is of the order of σ^1. Repeating the above procedure, we obtain $\mathbf{C}_0^{(N)}(p)$ as

$$
\mathbf{C}_0^{(N)}(p)=-\left[\mathbf{\Gamma}^{\mathrm{c}}(0|p)+\mathbf{M}^{(N)}(0|p)\right]^{-1}\left[\mathbf{\Gamma}^{\mathrm{c}}(0|p)-\mathbf{M}^{(N)}(0|p)\right]\mathbf{I}^0. \qquad \text{(D.8)}
$$

From (D.6) and (D.8), $\mathbf{C}_n^{(N)}(\cdot)$ $(n\geq 1)$ can be obtained.

Next, since the hierarchical equations (4.48)-(D.2) continue to infinite orders, a limit of the truncation number N could be considered. In such a case, we may assume the existence of a limit of the iterative mass operator $\mathbf{M}^{(N)}(\Lambda|p)$:

$$\lim_{N\to\infty}\mathbf{M}^{(N)}(\Lambda|p)=\mathbf{M}^{(\infty)}(\Lambda|p)\equiv\mathbf{M}(\Lambda|p). \tag{D.9}$$

Thus, we obtain a non-linear integral equation in a matrix form for the multiple renormalized mass operator $\mathbf{M}(\Lambda|p)$ from (D.7):

$$\mathbf{M}(\Lambda|p)=\frac{1}{k_L}\int_{-k_L/2}^{k_L/2}\mathbf{\Gamma}^{\rm s}(\Lambda+\lambda'|p)\left[\mathbf{\Gamma}^{\rm c}(\Lambda+\lambda'|p)+\mathbf{M}(\Lambda+\lambda'|p)\right]^{-1}\mathbf{\Gamma}^{\rm s}(\Lambda|p)d\lambda'. \tag{D.10}$$

Using the multiple renormalized mass operator $\mathbf{M}(\Lambda|p)$, the expression of the binary kernels (D.8) and (D.6) can be rewritten as

$$\mathbf{C}_0(p) \quad = -\left[\mathbf{\Gamma}^{\rm c}(0|p)+\mathbf{M}(0|p)\right]^{-1}\left[\mathbf{\Gamma}^{\rm c}(0|p)-\mathbf{M}(0|p)\right]\mathbf{I}^0, \tag{D.11}$$

$$\begin{aligned}\mathbf{C}_1(\Lambda|p) &= \frac{i}{k_L}[\mathbf{\Gamma}^{\rm c}(\Lambda|p)+\mathbf{M}(\Lambda|p)]^{-1}\mathbf{\Gamma}^{\rm s}(0|p)(\mathbf{I}^0-\mathbf{C}_0(p))\\ &= \frac{i}{k_L}[\mathbf{\Gamma}^{\rm c}(\Lambda|p)+\mathbf{M}(\Lambda|p)]^{-1}\mathbf{\Gamma}^{\rm s}(0|p)\\ &\qquad\times\left[\mathbf{I}^0+[\mathbf{\Gamma}^{\rm c}(0|p)+\mathbf{M}(0|p)]^{-1}[\mathbf{\Gamma}^{\rm c}(0|p)-\mathbf{M}(0|p)]\,\mathbf{I}^0\right],\end{aligned} \tag{D.12}$$

$$\begin{aligned}\mathbf{C}_2(\Lambda_1,\Lambda_2|p) &= -\frac{i}{2k_L}[\mathbf{\Gamma}^{\rm c}(\Lambda_1+\Lambda_2|p)+\mathbf{M}(\Lambda_1+\Lambda_2|p)]^{-1}\\ &\qquad\times(\mathbf{\Gamma}^{\rm s}(\Lambda_1|p)\mathbf{C}_1(\Lambda_1|p)+\mathbf{\Gamma}^{\rm s}(\Lambda_2|p)\mathbf{C}_1(\Lambda_2|p))\end{aligned} \tag{D.13}$$

$$\begin{aligned}&= \frac{1}{2k_L{}^2}[\mathbf{\Gamma}^{\rm c}(\Lambda_1+\Lambda_2|p)+\mathbf{M}(\Lambda_1+\Lambda_2|p)]^{-1}\\ &\qquad\times\left[\mathbf{\Gamma}^{\rm s}(\Lambda_1|p)[\mathbf{\Gamma}^{\rm c}(\Lambda_1|p)+\mathbf{M}(\Lambda_1|p)]^{-1}\mathbf{\Gamma}^{\rm s}(0|p)(\mathbf{I}^0-\mathbf{C}_0(p))\right.\\ &\qquad\left.+\mathbf{\Gamma}^{\rm s}(\Lambda_2|p)[\mathbf{\Gamma}^{\rm c}(\Lambda_2|p)+\mathbf{M}(\Lambda_2|p)]^{-1}\mathbf{\Gamma}^{\rm s}(0|p)(\mathbf{I}^0-\mathbf{C}_0(p))\right],\end{aligned} \tag{D.14}$$

$$\begin{aligned}\mathbf{C}_n(\Lambda_1,\cdots,\Lambda_n|p) \simeq \frac{-i}{nk_L}\sum_{l=1}^{n}&[\mathbf{\Gamma}^{\rm c}(\Lambda_1+\cdots+\Lambda_n|p)+\mathbf{M}(\Lambda_1+\cdots+\Lambda_n|p)]^{-1}\\ &\times\mathbf{\Gamma}^{\rm s}(\Lambda_1+\cdots+\Lambda_{l-1}+\Lambda_{l+1}+\cdots+\Lambda_n|p)\\ &\times\mathbf{C}_{n-1}(\Lambda_1,\cdots,\Lambda_{l-1},\Lambda_{l+1},\cdots,\Lambda_n|p),\qquad(n\geq 2).\end{aligned} \tag{D.15}$$

Since (D.12) has a 'dressed' single scattering factor $[\mathbf{\Gamma}^{\rm c}(\Lambda|p)+\mathbf{M}(\Lambda|p)]^{-1}$, $\mathbf{C}_1(\Lambda|p)$ describes a 'dressed' single scattering excited by $\mathbf{I}^0$ the incident plane wave and $\mathbf{C}_0(p)$ the coherent Floquet mode. Furthermore, (D.14) has another 'dressed' single scattering factor $[\mathbf{\Gamma}^{\rm c}(\Lambda_1+\Lambda_2|p)+\mathbf{M}(\Lambda_1+\Lambda_2|p)]^{-1}$ in addition to such a "dressed" single scattering factor of $\mathbf{C}_1(\Lambda|p)$. Therefore, $\mathbf{C}_2(\Lambda_1,\Lambda_2|p)$ representes a double scattering process made up of such 'dressed' single scattering processes. Similarly, $\mathbf{C}_n(\Lambda_1,\cdots,\Lambda_n|p)$ by (D.15) expresses a "dressed" n-tuple scattering process made up of such "dressed" single scattering processes.

Reference

[1] G.L.Dunning and M.L.Minden, "Scattering from high efficiency diffraction gratings", *Applied Optics* **19** 14 pp.2419-2425(1980)

[2] Ye.V.Zamyatin and S.L.Prosvernin, "Diffraction of electromagnetic waves by an array with small random fluctuation of dimensions", *Sov. J. Tech. Electron.* **31** pp.43-50(1986)

[3] S.N.Vorob'ev, E.V.Zamyatin, and S.L.Prosvernin, "Method for solution in wave diffraction by gratings with random fluctuations of the parameters", *Radiophys. Quantum Electron.(USA)* **32** pp.802-807(1989)

[4] D.P.Chrissoulidis, "EM wave scattering from statistically inhomogeneous and periodic random rough surfaces", *IEE Proc. H* **134** pp.209-214(1989)

[5] M.E.Knotts and K.A.O'donnell, "Anomalous light scattering from a perturbed grating", *Optics Letters* **15** pp.1485-1487(1990)

[6] A.D.Arsenieva and A.A.Maradudin, "Scattering of light from random surfaces that are periodic on average", *Optics Letters* **18** 19 pp.1588-1590(1993)

[7] J.Nakayama, L.Gao, and Y.Tamura, "Scattering of a plane wave from a periodic random surface: a probabilistic approach", *Waves in Random Media* **7** pp.65-78(1997)

[8] L.Gao and J.Nakayama, "Scattering of a TM plane wave from periodic random surfaces", *Waves in random media* **9** pp.53-67(1999)

[9] J.A.Sanhez-Gil and A.Maradudin, "Dynamic near-field calculations of surface-plasmon polariton pulses resonantly scattered at sub-micron metal defects", *Optics Express* **12** 5 pp.883-894(2004)

[10] R.Sato and H.Shirai, "Electromagnetic plane wave scattering by a loaded trough on a ground plane", *IEICE Trans. Electron.* **E77-C** 12 pp.1983-1989(1994)

San

[11] R.Sato and H.Shirai, "Electromagnetic plane wave scattering by a gap on a ground plane", *IEICE Trans. Electron.* **J80-C-I** 5 pp.179-185(1997) (in Japanese)

[12] H.Sekiguchi and H.Shirai, "Electromagnetic scattering analysis for crack depth estimation", *IEICE Trans. Electron.* **E86-C** 11 pp.2224-2229(2003)

[13] R.A.Depine and D.C.Skigin, "Scattering from metallic surface having finite number of rectangular grooves", *Journal of Optics. Soc.Am. A* **11** 11 pp.2844-2850(1994)

[14] N.Bruce, "Control of the backscattered intensity in random rectangular-groove surfaces with variations in the groove depth", *Applied Optics* **44** 5 pp.784-791(2005)

[15] A.Ishimaru, *Wave propagation and scattering in random media*, New York: IEEE Press(1997)

[16] J.A.DeSanto, ed., *Ocean acoustics*, Berlin: Springer-Verlag(1979)

[17] S.O.Rice, "Reflection of electromagnetic waves from slightly random surfaces", *Comm.Pure and Appl.Math.* **4** pp.351-378(1951)

[18] F.G.Bass and I.M.Fuks, *Wave Scattering From Statistically Rough Surfaces*, New York: Pergamon(1979)

[19] J.Nakayama, "Anomalous scattering from a slightly random surface", *Radio Sci.* **17** pp.558-564(1982)

[20] J.Nakayama, K.Mizutani and M.Tsuneoka, "Scattering of electromagnetic waves from a perfectly conductive slightly random surface: Depolarization in backscatter", *J. Math. Phys.* **27** pp.1435-1448(1986)

[21] H.Ogura, T.Kawanishi, N.Takahashi and Z.L.Wang, "Scattering of electromagnetic waves from a slightly random surface - reciprocal theorem, cross-polarization and backscattering enhancement", *Waves in random media* **5** pp.461-495(1995)

[22] H.Ogura and Z.L.Wang, "Surface-plasmon mode on a random rough metal surface: Enhanced backscattering and localization", *Physical Review B - Condensed Matter and Materials Physics* **53** pp.10358-10371(1996)

[23] H.Ogura and N.Takahashi, "Scattering of waves from random rough surface –reciprocal theorem and backscattering enhancement", *Waves in random media* **5** pp.223-242(1995)

[24] H.Ogura and N.Takahashi, "Scattering, radiation and propagation over two-dimensional random surface -stochastic functional approach-", *PIER* **14** pp.89-180(1996)

[25] J.Nakayama, H.Ogura and B.Matsumoto, "A probabilistic theory of scattering from a random rough surface", *Radio Science* **15** pp.1049-1057(1980)

[26] H.Ogura and J.Nakayama, "Initial value problem of the one-dimensional wave propagation in a homogeneous random media", *Physical Review A* **11** pp.957-962(1996)

[27] L.Rayleigh, "On the dynamical theory of gratings", *Proceedings of Royal Society A* **79** pp.399-416(1907)

[28] R.W.Wood, periodic"On a remarkable case of uneven distribution of light in a diffraction grating spectrum", *Phil. Mag.* **4** pp.396-402(1902)

[29] A.Hessel and A.A.Olinear, "A new theory of Wood's anomalies on optical gratings", *Applied Optics* **4** 10 pp.1275-1297(1965)

[30] R.Petit, ed., *Electromagnetic theory of gratings*, Berlin: Springer(1980)

[31] K.Yasuura, Y.Okuno and H.Ikuno, "Improved point-matching method with application to scattering from a periodic surface", *IEEE Trans. Antennas and Propagation* **AP-21** 5 pp.657-662(1973)

[32] K.Yasuura, Y.Okuno and H.Ikuno, "Numerical analysis of scattering from echelette grating - smoothing process on mode-matching method", *Electron. Commun. Jpn.* **60** pp.82-90(1977)

[33] M.G.Moharam and T.K.Gaylord, "Rigorous coupled-wave analysis of metallic surface-relief gratings", *Journal of Optics. Soc.Am. A* **3** 11 pp.1780-1787(1986)

[34] P.Sheng, R.S.Stepleman and P.N.Sanda, "Exact eigenfunctions for square-wave gratings: Application to diffraction and surface-plasmon calculations", *Phys. Rev.* **B 26** 6 pp.2907-2917(1982)

[35] J.Nakayama, "Periodic Fourier transformb and its application to wave scattering from a finite periodic surface", *IEICE Trans. Electron.* **E83-C** 3 pp.481-487(2000)

[36] J.Nakayama, T.Moriyama and J.Yamakita, "Wave scattering from a periodic surface with finite extent: A periodic approach", *IEICE Trans. Electron.* **E84-C** 8 pp.1111-1113(2001)

[37] J.Nakayama, T.Moriyama and J.Yamakita, "Wave scattering from a periodic surface with finite extent: A periodic approach for TM wave", *IEICE Trans. Electron.* **E84-C** 10 pp.1615-1617(2001)

[38] J.Nakayama and H.Tsuji, "Wave scattering and diffraction from a finite periodic surface: Diffraction order and diffraction beam", *IEICE Trans. Electron.* **E85-C** 8 pp.1808-1813(2002)

[39] J.Nakayama and Y.Kitada, "Wave scattering from a finite periodic surface: Spectral formalism for TE wave", *IEICE Trans. Electron.* **E86-C** 6 pp.1098-1105(2003)

[40] J.Nakayama and Y.Tamura, "Low grazing scattering from sinusoidal Neumann surface with finite extent: Undersampling approximation", *IEICE Trans. Electron.* **E91-C** 1 pp.9-16(2008)

[41] J.Nakayama and Y.Tamura, "Low grazing scattering from sinusoidal Neumann surface with finite extent: Total scattering cross section", *IEICE Trans. Electron.* **E91-C** 1 pp.56-63(2008)

[42] J.Nakayama, "Wave scattering from an apodised sinusoidal surface", *IEICE Trans. Electron.* **E83-C** 1 pp.1153-1159(2000)

[43] M.Tateiba, "New approach to the problem of wave scattering by many particles", *Radio Science* **22** pp.881-884(1986)

[44] L.Gao and J.Nakayama, "Diffraction and scattering of a plane wave from randomly deformed periodic surface", *IEICE Trans. Electron.* **E80-C** pp.1374-80(1997)

[45] P.Beckmann and A.Sppichichino, *The scattering of Electromagnetic Waves from Rough Surfaces*, New York: Pergamon(1963)

[46] K.Hattori, J.Nakayama and Y.Tamura, "Scattering of TM plane wave from periodic grating with single defect", *IEICE Trans. Electron.* **E91-C** pp.17-25(2008)

[47] J.L.Doob, *Stochastic Processes*, New York: Wiley(1953)

[48] J.Nakayama and Y.Tamura "Wave reflection by surfaces with translation invariance", *IEE Japan* EMT-07-143 pp.29-34(2007)

[49] J.Nakayama and L.Gao, "Formulas on orthogonal functionals of stochastic binary sequence", *IEICE Trans. Fundamentals* **E80-A** pp.782-5(1997)

[50] L.Gao, *Theory of Scattering from periodic Random Surface and Random Media*, Ph.D Thesis: Kyoto Institute of Technology(1998)

[51] H.Ogura, "Spectral representation of a periodic nonstationary random process", *IEEE Trans. Inform. Technol.* **IT17** pp.143-149(1971)

[52] W.A.Gardner, *Cyclostationarity in Communications and Signal Processing*, Piscataway, NJ: IEEE(1993)

[53] Y.Tamura and J.Nakayama, "Mass operator for wave scattering from a slightly random surface", *Waves in random media* **9** pp.341-368(1999)

[54] Y.Tamura, "*Theory of Wave Scattering and Diffraction from Random Surfaces and thin films with volume disorder*", Ph.D Thesis: Kyoto Institute of Technology(2005) (*in Japanese*)

[55] J.Nakayama, "*Theory of Wave Scattering from Random Surfaces*", Ph.D Thesis: Kyoto University(1985) (*in Japanese*)

[56] K.Hattori and J.Nakayama, "Scattering of TE plane wave from periodic grating with single defect", *IEICE Trans. Electron.* **E90-C** 2 pp.312-319(2007)

[57] C.Bohren and D.Huffman, *Absorption and scattering of light by small particles*, New York: Wiley(1983)

[58] Y.Tamura and J.Nakayama, "TM plane wave scattering and diffraction from a randomly rough half-plane: (part II) An evaluation of the diffraction kernel", *Waves in random media* **16** pp.43-67(2006)

[59] K.Hattori, J.Nakayama and H.Matsuoka, "Wave scattering from a periodic random surface generated by a stationary binary sequence", *Waves in Random Media* **11** pp.1-20(2001)

[60] L.Gao and J.Nakayama, "New formulas on orthogonal functionals of stochastic binary sequence with unequal probability", *IEICE Trans. Fundamentals* **E81-A** pp.347-350(1998)

[61] H.A.Yueh, R.T.Shin, and J.A.Kong, (J.A.Kong ed.), "Scattering from randomly perturbed periodic and quasi-periodic surfaces", *Progress in Electromagnetic Research*, New York: Elsevier(1988)

[62] V.D.Freilikher and I.M.Fuks Green's function method for the Helmholtz equation with perturbed boundary conditions *Radiophys. Quantum Electron.* **13** pp.73-79(1970) (*in Russian*)

[63] J.Nakayama and L.Gao, "Stochastic processes derived from stationary binary sequence", *IEE Japan* EMT-96-50 pp.137-146(1996)

[64] K.Hattori, *Scattering of a plane wave from periodic random surface - a functional expansion of a stationary binary sequence* -, M.E Thesis: Kyoto Institute of Technology(2000)

[65] H.Ogura, "The Thoery of Stochastic Process" (in Japanese), Tokyo: Corona(1978)

[66] A.Sommerfeld, *Partial differential equations in physics*, New York: Academic(1947)

[67] L.J.Nickisch and P.M.Franke, "Finite difference time domain tests of random media propagation theory", *Radio Science* **31** pp.955-963(1996)

[68] N.-J.Li and P.-L.Liu, "Numerical analysis of microdisk lasers with rough boundaries", *IEEE Journal of Quantum Electronics* **33** pp.91-795(1997)

[69] J.D.Jackson, *Classical electrodynamics*, New York: Wiley(1925)

Publication in Journal

(1) K.Hattori, J.Nakayama and H.Matsuoka, "Wave scattering from a periodic random surface generated by a stationary binary sequence", *Waves in Random Media* **11** pp.1-20(2001)

(2) K.Hattori and J.Nakayama, "Scattering of TE plane wave from periodic grating with single defect", *IEICE Trans. Electron.* **E90-C** 2 pp.312-319(2007)

(3) K.Hattori, J.Nakayama and Y.Tamura, "Scattering of TM plane wave from periodic grating with single defect", *IEICE Trans. Electron.* **E91-C** 1 pp.17-25(2008)

(4) K.Hattori, J.Nakayama and Y.Tamura, "Diffraction and scattering of TM plane wave from a binary periodic random surface", *Waves in Random and Complex Media* (*in press*)

Aural Presentations in International Conferences

(1) K.Hattori and J.Nakayama, "Coherent diffraction and incohirent scattering from a periodic raodom surface generated by a stationary binary sequence", *Proceedings PIERS2001(Osaka)* p.246(2001)

(2) K.Hattori and J.Nakayama, "Scattering of TE Plane Wave from Periodic Grating with Defects", *Abstract PIERS2005(Hangzhou)* p.517(2005)

(3) K.Hattori and J.Nakayama, "Scattering of TM Plane Wave from Periodic Grating with Single Defect", *Abstract PIERS2006(Tokyo)* p.332(2006)

(4) K.Hattori and J.Nakayama, "Scattering of TE Plane Wave from Periodic Grating with Random Defects", *PIERS2007 Proceedings(Beijing)* p.2073(2007)

Aural Presentations in Domestic Conferences

(1) K.Hattori and J.Nakayama, "Wave scattering from a thin film with random surface", *Technical Meeting on Electromagnetic Theory* EMT-98-166 pp.13-19(1998)

(2) K.Hattori, J.Nakayama and H.Matsuoka, "Waves cattering from a periodic binary raodom surface (II)", *Technical Meeting on Electromagnetic Theory* EMT-99-129 pp.43-54(1999)

(3) K.Hattori and J.Nakayama, "Scattering of TE plane wave from periodic grating with single defect", *Technical Meeting on Electromagnetic Theory* EMT-05-50 pp.117-123(2005)

(4) K.Hattori and J.Nakayama, "Scattering from periodic array of rectangular grooves(II) -TM plane wave incidence-", *Technical Meeting on Electromagnetic Theory* EMT-06-130 pp.77-83(2006)

(5) K.Hattori, J.Nakayama and Y.Tamura, "Scattering of plane waves from periodic grating with single defect", *Radioation Science Society of Japan* RS06-14 pp.1-16(2006)

(6) K.Hattori and J.Nakayama, "Scattering from periodic grating with single defect (III) -TM plane wave incidence-", *IEICE General Conference* CS-1-5 pp.S25-S26(2007)

(7) K.Hattori, J.Nakayama and Y.Tamura, "Scattering of TE plane wave from random grooves", *Radioation Science Society of Japan* RS07-01 pp.1-14(2007)

(8) K.Hattori, J.Nakayama and Y.Tamura, "Scattering of TM plane wave from a binary periodic random surface", *Technical Meeting on Electromagnetic Theory* EMT-07-144 pp.35-40(2007)

(9) K.Hattori, J.Nakayama and Y.Tamura, "Scattering of TM plane wave from periodic grating with single defect", *Technical Meeting on Electromagnetic Theory* EMT-07-145 pp.41-46(2007)

Related Publication in Journal

(1) J.Nakayama, K.Hattori, and Y.Tamura, "Diffraction Amplitudes from Periodic Neumann Surface: Low Grazing Limit of Incidence", *IEICE Trans. Electron.* **E89-C** 5 pp.642-644(2006)

(2) J.Nakayama, K.Hattori, and Y.Tamura, "Diffraction Amplitudes from Periodic Neumann Surface: Low Grazing Limit of Incidence (II)", *IEICE Trans. Electron.* **E89-C** 9 pp.1362-1364(2006)

(3) J.Nakayama, K.Hattori, and Y.Tamura, "Diffraction Amplitude from Periodic Neumann Surface: Low Grazing Limit of Incidence", *IEICE Trans. Electron.* **E90-C** 2 pp.536-538(2007)

(4) J.Nakayama, K.Hattori, and Y.Tamura, "Low Grazing Scattering from Periodic Neumann Surface with Finite Extent", *IEICE Trans. Electron.* **E90-C** 4 pp.903-906(2007)

Related Presentations in International and Domestic Conferences

(1) J.Nakayama, L.Gao and K.Hattori, "A Recursive Solution of a Linear Equation System and Its Application to Wave Scattering", *Abstract PIERS2005(Hangzhou)* p.645(2005)

(2) J.Nakayama, K.Hattori and Y.Tamura, "Low grazing scattering from periodic Neumann surface with finite extent", *IEICE Technical Report (Photonic Network)* PN2006-57 pp.55-60(2006)

(3) J.Nakayama, K.Hattori and Y.Tamura, "Scattering of TM Wave from Conductive Rough Surface : Low Grazing Limit of Incidence", *Abstract PIERS2006(Tokyo)* p.349(2006)

(4) J.Nakayama, K.Hattori and Y.Tamura, "New representation of Floquet solution in the diffraction theory of periodic grating", *Technical Meeting on Electromagnetic Theory* EMT-06-129 pp.71-76(2006)

(5) J.Nakayama, K.Hattori and Y.Tamura, "Low grazing Scattering from Periodic Neumann Surface with Finite Extent", *PIERS2007 Proceedings(Beijing)* p.2064(2007)